Western Graduate&PostdoctoralStudies

Western University
Scholarship@Western

Electronic Thesis and Dissertation Repository

6-14-2017 12:00 AM

Expanding the Scope of the AuNP Toolbox: Development of Interfacial oNQM Photoclick Reaction and Large AuNP Templates

Tommaso Romagnoli
The University of Western Ontario

Supervisor
Dr. Mark S. Workentin
The University of Western Ontario

Graduate Program in Chemistry
A thesis submitted in partial fulfillment of the requirements for the degree in Master of Science
© Tommaso Romagnoli 2017

Follow this and additional works at: https://ir.lib.uwo.ca/etd

Part of the Nanotechnology Commons

Recommended Citation

Romagnoli, Tommaso, "Expanding the Scope of the AuNP Toolbox: Development of Interfacial oNQM Photoclick Reaction and Large AuNP Templates" (2017). *Electronic Thesis and Dissertation Repository*. 4589.
https://ir.lib.uwo.ca/etd/4589

This Dissertation/Thesis is brought to you for free and open access by Scholarship@Western. It has been accepted for inclusion in Electronic Thesis and Dissertation Repository by an authorized administrator of Scholarship@Western. For more information, please contact wlswadmin@uwo.ca.

Abstract

In recent decades, gold nanoparticles (AuNPs) have been pushed to the forefront of nanomaterial research because of their unique size-dependent physical, chemical and biological properties. As a result, proper surface functionalization would enable control over these desirable properties for potential applications in biomedicine, electronics or catalysis. Over the past few years, the Workentin research group has developed a toolbox of sophisticated methods for the functionalization of small (1-5 nm) AuNP systems by designing functional AuNP templates. These templates are easy to synthesize and can be used to effectively incorporate functionality on the AuNP surface using click and bioorthogonal interfacial chemistry. In this thesis the development of a novel *ortho*-naphthoquinone methide (oNQM) modified AuNP template is described that will allow for unprecedented photochemical spatial and temporal control of reactivity. The first steps towards the development of an innovative large AuNP (> 10 nm) template are also presented to expand the scope of interfacial functionalization and exploit their interesting optical properties.

Keywords: Surface modification, gold nanoparticles, photochemistry, click chemistry, bioorthogonal chemistry.

Co-Authorship Statement

Chapter 1 was written by the author and edited by Prof. M. S. Workentin.

Chapter 2 was written by the author and edited by Prof. M. S. Workentin. I performed all of the experimental work including synthesis and characterization of the NQMP modified thiolated ligand. I also synthesized and characterized the NQMP modified AuNPs with the help of W. Luo for TEM characterization.

Chapter 3 was written by the author and edited by Prof M. S. Workentin. A. Prestwich was an undergraduate student under my co-supervision along with P. Gobbo and Prof. M. S. Workentin. A. Prestwich helped with the synthesis and characterization of Fragments A, B and C. I synthesized and characterized the large AuNPs with the help of W. Luo for TEM characterization.

Chapter 4 was written by the author and edited by Prof. M. S. Workentin.

Acknowledgements

First I would like to express my gratitude to my supervisor Prof. Mark Workentin for all of his patience, support and understanding over the years. I learned a lot from you about things both inside and outside the lab that will undoubtedly come in handy as I transition from my chemistry career. I thank you for believing in me and writing Pulitzer Prize worthy reference letters to help me realize my dreams.

I want to thank other faculty members whom I had the pleasure of learning from during lecture in undergraduate and graduate courses including: Prof. Paul Ragogna (you never forget your first), Prof. Robert Hudson, Prof. Michael Kerr, Prof. Len Luyt, Prof. François Lagugné-Labarthet, Prof. Kim Baines, Prof. Richard Puddephatt, Prof. Viktor Staroverov, Prof. Styliani Constas, Prof. Johanna Blacquiere and Prof. Lars Konermann. In particular I would like to acknowledge Prof. Joe Gilroy for also writing fantastic reference letters as well as his co-supervision and pushing me to be my best during my undergraduate thesis project. A special thanks to my M.Sc. thesis examiners for taking the time out of their busy schedules to read my thesis and challenge me as part of my defense committee.

I would also like to thank the staff in the Department of Chemistry for their high-quality work and support. In particular I would like to thank Mathew Willans, Doug Hairsine, Barakat Misk, Darlene McDonald and everyone else who keep things running smoothly.

A huge thank you to all the past and present students that I've had the pleasure of getting to know these past few years. From the Workentin group I would like to give a big abbraccio to my chemistry mentor Pierangelo Gobbo for investing his time and knowledge with me. I also want to thank Praveen Gunawardene and Wilson Luo for their advice and friendship when things just weren't working right. Other members I want to thank are: Alex van Belois, Vaishnavi Somasundaram, Raj Vasdev, Alec Ray Sherman, Alexis Prestwich, Max Weissman, Dr. Sara Chiassian and Dr. Sung Ju Cho. I want to thank other fellow students for always being friendly and ready to help and I invite you all over for another espresso/latte/cappuccino and a game of Briscola or Scopa.

One last big thank you to my family and friends. I am deeply grateful to my mom and dad who have supported me all this way. Saving the best for last (sorry Mama) I want to thank the beautiful Mel. I don’t know how you’ve been able to put up with me all these years but I wouldn’t be where I am today without you. Also, 2 o’clock coffee time would not have been the same without the delicious treats you baked for us. You are simply the best.

Table of Contents

Abstract ii

Co-Authorship Statement iii

Acknowledgements iv

Table of Contents vi

List of Figures viii

List of Schemes xi

List of Tables xi

List of Abbreviations xii

Chapter 1 1

1.1 Introduction 1
1.2 Properties of AuNPs 1
1.3 Synthesis of AuNPs 8
1.4 Functionalization of AuNPs 11
1.5 Interfacial Bioorthogonal Click Chemistry 14
1.6 Characterization of AuNPs 17
1.7 Objectives – Chapter 2 19
1.8 Objectives – Chapter 3 20
1.9 References 22

Chapter 2 26

2.1 Introduction 26
2.2 Results and Discussion 27
2.2.1 Synthesis and Characterization of HS-EG$_4$-NQMP 27
2.2.2 Synthesis and Characterization of AuNP-EG$_4$-NQMP 31
2.3 Conclusion 38
2.4 Experimental 38
2.6 References 47

Chapter 3 48
3.1 Introduction 48
3.2 Results and Discussion 51
3.2.1 Synthesis of Fragment A 51
3.2.2 Synthesis of Fragment B 52
3.2.3 Synthesis of Fragment C 53
3.2.4 Synthesis of Required Ligands 54
3.2.5 Synthesis and UV-Vis Spectra of Citrate-Stabilized AuNPs 57
3.2.6 Stabilization of 20 nm Citrate-Stabilized AuNPs 60
3.3 Conclusion 64
3.4 Experimental 65
3.6 References 73
Chapter 4 74
4.1 Conclusion 74
4.2 Future Work 76
4.3 References 76
Chapter 5 77
5.1 Chapter 2 Appendix 116
5.2 Chapter 3 Appendix 99
5.3 List of Permissions 123
Curriculum Vitae 124

List of Figures

Figure 1.1: A representation of the reduction of a metal from the large bulk material to smaller nanoparticles of varying size to the individual atoms that make up the material. 2

Figure 1.2: Figure 1.2: TEM images of gold (A) nanospheres (B) nanorods (C) nanostars. The scale bar is indicated. Reprinted with permission from reference 11. 3

Figure 1.3: Cartoon representation of a stabilized AuNP depicting the gold core (Au^0), surface (Au^I) and ligand corona. 4

Figure 1.4: (Top) Colors of various sized monodispersed AuNP in solution (Bottom) TEM images of various sized monodispersed AuNP. The diameter increases from left to right. Images from Sigma-Aldrich product information website. 5

Figure 1.5: UV-Vis spectra of various sized AuNPs. Image from Cytodiagnostics product information website. 6

Figure 1.6: Citrate-stabilized AuNPs prepared by the Turkevich method with $HAuCl_4$ and sodium citrate in aqueous solution under reflux conditions where citrate acts as both the reducing agent and stabilizing ligand. 9

Figure 1.7: (Left) Brust-Schriffin two-phase synthesis of AuNPs by reduction of $HAuCl_4$ using alkanethiols as the stabilizing ligands and $NaBH_4$ as the reducing agent. (Right) Modified one-phase Brust reaction scheme using methoxy terminated tri(ethylene glycol) thiol ligands. ...10

Figure 1.8: (Top) Direct synthesis of functional AuNP where the incorporation of a thiolated-ligand possessing a functional substrate through a direct synthetic method can be quite challenging (Bottom) Indirect synthesis of functional AuNP where the incorporation of functional substrates is often possible using an indirect approach through a place exchange reaction...12

Figure 1.9: Example of AuNP template design for the introduction of versatile functional substrates...14

Figure 1.10: The Workentin group AuNP toolbox. Reaction schemes of click and bioorthogonal functional groups incorporated into AuNP templates. 15

Figure 1.11: Retro-synthesis of the model ligand (n = 1) and highlighted features. 21

Figure 1.12: Design of novel ligand with hydrogen bonding shells. The tail may be replaced with bioorthogonal functional groups. 22

Figure 2.1: ^{1}H NMR spectrum of aromatic region of HO-NQMP. 29
Figure 2.2: ^{1}H NMR spectrum of HS-EG$_4$-NQMP in CDCl$_3$. * denotes residual protonated solvent signals or solvent impurities. 30
Figure 2.3: IR spectrum of HS-EG$_4$-NQMP. 31
Figure 2.4: ^{1}H NMR spectra of HS-EG$_4$-NQMP (top) and AuNP-EG$_4$-NQMP (bottom) in CDCl$_3$. The absence of sharp signals in the bottom spectrum indicates that no free ligand is present. * denotes residual protonated solvent signals or solvent impurities. 34
Figure 2.5: IR of AuNP-EG$_3$-OMe (A) and AuNP-EG$_4$-NQMP (B). 35
Figure 2.6: UV-Vis absorption spectra of HS-EG$_4$-NQMP ligand, methoxy terminated AuNPs and NQMP modified AuNPs in CH$_3$OH at different concentrations. 36
Figure 2.7: (A) TGA plot (B) Derivative plot (dotted black line) of AuNP-EG$_4$-NQMP. The green traces represent the fitted peaks and the red trace represents the sum of the fitted peaks. 37
Figure 2.8: TEM images of AuNP-EG$_3$-OMe (A) and AuNP-EG$_4$-NQMP (B). The scale bar is indicated in each image. 37
Figure 3.1: Retro-synthesis of the model ligand (n = 1) and highlighted features (Reprinted from Chapter 1) 50
Figure 3.2: Design of novel ligand with hydrogen bonding shells. The tail may be replaced with bioorthogonal functional groups (Reprinted from Chapter 1). 51
Figure 3.3: ^{1}H NMR spectrum of HS-EG$_4$-EG$_3$-OMe in CDCl$_3$. * denotes residual protonated solvent signals or solvent impurities. 57
Figure 3.4: UV-Vis spectra in nanopure H$_2$O of citrate-stabilized AuNP synthesized by the Turkevich method. 58

Figure 3.5: Cartoon representation of a large AuNP stabilized by a monolayer of OEG ligands. The hydrophobic C$_{11}$-chain provides stability while the hydrophilic EG unit ensures solubility in water (-OH) and both water and organic solvent (-OCH$_3$). 59

Figure 3.6: TEM image of 20 nm citrate-stabilized AuNPs (average size = 20 ± 1 nm). The scale bar is indicated. 60

Figure 3.7: Example of visual discoloration of AuNP solution due to aggregation (left vs. right)..61

Figure 3.8: Colloidal stability of HS-EG$_4$-EG$_3$-OMe stabilized 20 nm AuNPs characterized by UV−vis measurement in nanopure H_2O. The lower absorbance is a result of material loss during purification. The normalized absorbance spectra shown in the inset demonstrates the shift of the surface plasmon resonance band (Δλ = 5 nm) after place exchange. 63

Figure 3.9: TEM image of HS-EG$_4$-EG$_3$-OMe stabilized AuNPs. The scale bar is indicated. 64

Figure 4.1: The Workentin AuNP toolbox reprinted with the addition of the NQMP-functionalized AuNP template developed in this thesis. 75

List of Schemes

Scheme 1.1: Photochemical generation and reactivity of oNQM from NQMP in aqueous solution. 17

Scheme 1.2: Outline of synthetic strategy for the synthesis of oNQM-AuNP and photoreversible interfacial Michael Addition. 19

Scheme 2.1: Reprinted from Chapter 1. Synthetic strategy for synthesis of NQMP functionalized AuNPs and its proposed reactivity as a novel template. 27

Scheme 2.2: Synthesis of HS-EG_4-NQMP. 28

Scheme 2.3: Place exchange of ethylene glycol monomethyl ether AuNPs to NQMP functionalized AuNPs. 32

Scheme 3.1: Example of carbodiimide-mediated protein conjugation to carboxylic acid terminated PEG AuNPs. 49

Scheme 3.2: Synthesis for thiol protection TrS-$(CH_2)_2$-COOH and activated ester TrS-$(CH_2)_2$-NHS. 52

Scheme 3.3: Synthesis of Fragment B. 53

Scheme 3.4: Synthesis of Fragment C. 54

Scheme 3.5: Synthesis of ligand without repeating unit (n = 0) 55

Scheme 3.6: Synthesis of ligand with one repeating unit (n = 1). 56

List of Tables

Table 3.1: Synthesis of large AuNPs by sodium citrate reduction. 58

List of Abbreviations

Å	Angstrom
Ac	Acetate
AuNP	Gold nanoparticle
˚C	Degree Celsius
CI-HRMS	Chemical ionization high resolution mass spectrometry
cm^{-1}	Wavenumber
CT	Computed tomography
DCC	N,N’-Dicyclohexylcarbodiimide
DIPEA	N,N-Diisopropylethylamine
DMAP	4-Dimethylaminopyridine
DMF	Dimethylformamide
EDC	N’-ethylcarbodiimide
EG	Ethylene glycol
EI-HRMS	Electron impact high resolution mass spectrometry
ESI-HRMS	Electrospray ionization high resolution mass spectrometry
Et	Ethyl
FT-IR	Fourier transform infrared
h	Hours

HBTU	*N,N,N′,N′*-Tetramethyl-*O*-(1*H*-benzotriazol-1-yl)uronium hexafluorophosphate
IR	Infrared
LAH	Lithium aluminum hydride
M	Molar (mol/L)
Me	Methyl
MHz	Megahertz
min	Minutes
μL	Microliter
MRI	Magnetic resonance imaging
MS	Mass spectrometry
NHS	N-Hydroxysuccimide
NIR	Near infrared
nm	Nanometer
NMR	Nuclear magnetic resonance
NP	Nanoparticle
NQMP	Naphthoquinone methide precursor
OEG	Oligo(ethylene glycol)
*o*NQM	*ortho*-Naphthoquinone methide

PCC	Pyridinium chlorochromate
Pd/C	Palladium on carbon
PEG	Poly(ethylene glycol)
PTT	Photothermal therapy
QD	Quantum dot
SPAAC	Strain-promoted alkyne-azide cycloaddition
SPANC	Strain-promoted alkyne-nitrone cycloaddition
SPR	Surface plasmon resonance
TEM	Transmission electron microscopy
TFA	Trifluoroacetic acid
TGA	Thermogravimetric analysis
THF	Tetrahydrofuran
TIPS	Triisopropylsilyl ether
TOAB	Tetraoctylammonium bromide
Tr	Trityl
TsCl	*p*-Toluenesulfonyl chloride
TsOH	*p*-Toluenesulfonic acid
UV-Vis	Ultraviolet-visible
XPS	X-ray photoelectron spectroscopy

CHAPTER 1

1.1 Introduction

Surface modification techniques allow for the introduction of novel physical, chemical or biological properties to a material. For potential applications, proper surface functionalization is a perquisite to enable control of the surface interactions with the environment as well as other moieties or molecules. By placing appropriate functional molecules on the surface of a material, the resulting surface interactions play a vital role in directly affecting the stability and subsequent function of the material. As a result, the exploitation of these surface engineered materials has led to great advances in technology and biomedicine. For example, in recent years' quantum dot (QD) televisions have emerged as next generation technology as a result of the unique size-dependent optical properties of the inorganic nanoparticles. Through research into surface modification techniques to make QDs water soluble and targetable to specific biomolecules, QDs have also demonstrated promising applications as *in vitro* and *in vivo* imaging agents.[1] But despite the recent popularity of QDs, perhaps the most studied nanomaterial in literature are gold nanoparticles (AuNPs) owing to their unique and tunable properties. In general, the ability to modify the surface of a material allows for diverse functionalization for use in a wide range of applications. As a result, AuNPs have been used in numerous applications including electronics,[2] catalysis,[3] chemical and biological sensing[4] and drug delivery.[5]

1.2 Properties of AuNPs

AuNPs are commonly defined as a stable colloidal suspension of gold atom clusters ranging in diameter from 1 to 150 nm with properties differing between bulk gold and gold atoms. As described in Figure 1.1, AuNPs normally range in size over a narrow size distribution whereas Au nanoclusters are atomically precise AuNPs. Despite their use for staining glass in Roman times, the chemistry of AuNPs was not investigated until the 1850s by the work of Michael Faraday who observed the difference in optical properties and light scattering ability between colloidal gold solutions and bulk gold.[6] He prepared colloidal gold by reducing an aqueous solution of a gold salt with a solution of phosphorus in carbon disulfide. Interestingly, transmission electron microscopy (TEM) images of Faraday's AuNPs later revealed that he had synthesized AuNPs with an average size of 6 ± 2 nm.[7]

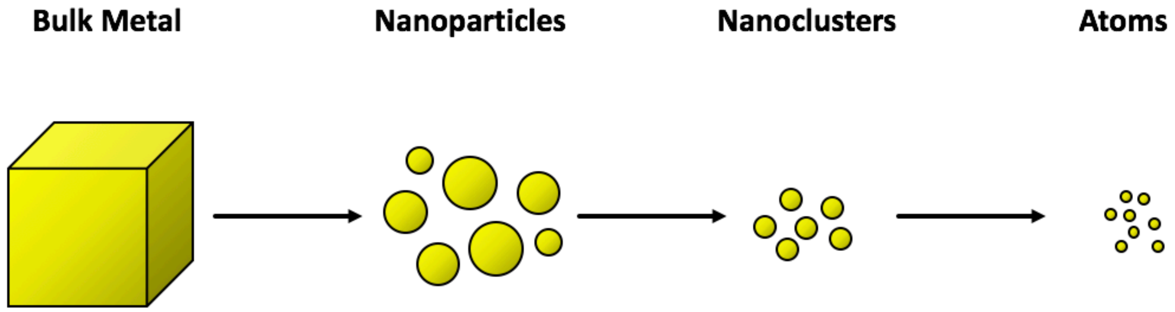

Figure 1.1: A representation of the reduction of a metal from the large bulk material to smaller nanoparticles of varying size to the individual atoms that make up the material.

AuNPs come in many different sizes (1-150 nm) but also many different shapes such as nanospheres, nanorods and nanostars (Figure 1.2). In this thesis, I present work with solutions of gold nanospheres and will refer to them as AuNPs. As described in Figure 1.3, AuNPs are composed of a metal core and usually capped by an organic layer, also known as the ligand corona, which protects the naked AuNPs from aggregation. Among all nanomaterials, AuNPs are often regarded as the most promising template for biomedical applications because of unique physical and chemical properties. AuNPs feature: (i) high chemical stability (ii) high surface area-to-volume ratio (iii) low toxicity (iv) size and shape dependent optical properties. As a result of these properties, AuNPs have been investigated for biomedical applications in medical diagnostics and therapeutics such as drug delivery systems[8] as well as imaging agents for magnetic resonance imaging (MRI)[9] and computed tomography (CT).[10]

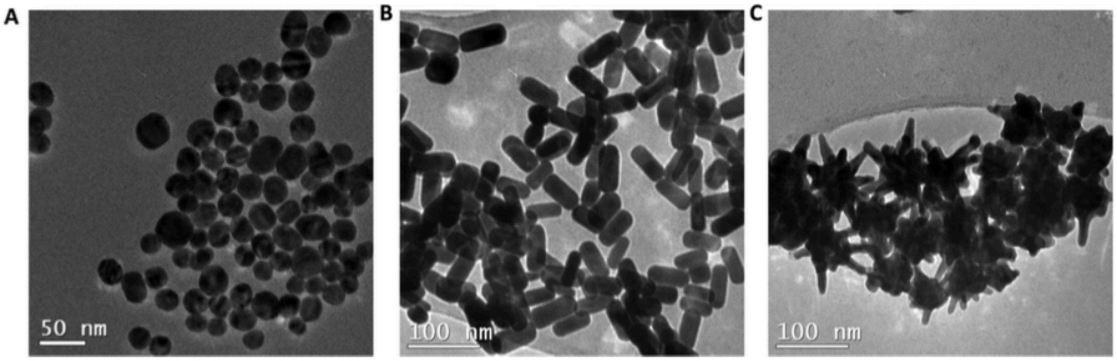

Figure 1.2: TEM images of gold (A) nanospheres (B) nanorods (C) nanostars. The scale bar is indicated. Reprinted with permission from reference 11.[11]

In terms of chemical stability, AuNPs do not oxidize under ambient conditions similar to bulk gold. As a result, AuNPs are easy to work with in a laboratory setting and are regarded as one of the most stable metal nanoparticle. However, what makes gold really special are the remarkable surface properties of the nanoparticles.[12] As a result of the high surface-area-to-volume ratio, at the nanoscale, a large fraction of the gold atoms are concentrated at the surface. Interestingly, these surface atoms seem to exhibit incomplete valence in the sense that they are only bound to the internal atoms and the external sites remain available for interacting with donor-acceptor species, or ligands. Thus, the application of hard and soft acid-base theory (HSAB) can be helpful in understanding the coordination chemistry of AuNPs.[13] In HSAB theory, the Au core is considered a soft acid and therefore would prefer to bind soft bases that contain larger and more polarizable donor atoms. As a result, the surface of AuNPs may be derivatized with thiols[14] (sulfur, S), phosphines[15] (phosphorus, P) as well as amines[16] (nitrogen, N). However, sulfur is more commonly used as the donor atom for decorating Au surfaces as the resulting gold-sulfur bond is similar in strength to that of a covalent bond.[17] This interaction is usually mediated through the sulfhydryl (SH) functional group in thiols (RSH). It is also widely accepted that the covalent interaction at the gold-sulfur interface requires the formation of a gold-thiolate (S^-) bond. This covalent bond in turn gives rise to a very robust, but more importantly, modifiable interaction that provides stabilization and functionalization to the system so that it can be used in a wide range of applications. As a result of the high surface-area-to-volume ratio, it is therefore possible to modify the Au surface to a very large extent which can drastically alter the chemical and physical properties producing a novel functional material. There are three main strategies used for the preparation of functionalized AuNPs that will be discussed in detail later: (i) direct synthesis (ii) place (or ligand) exchange reactions (iii) post-synthetic interfacial reactions. Therefore, functionality can be installed to AuNPs when they are modified with ligands that contain small molecules, polymers, or biomolecules. These appropriately functionalized AuNPs can then be used in biomedical applications.

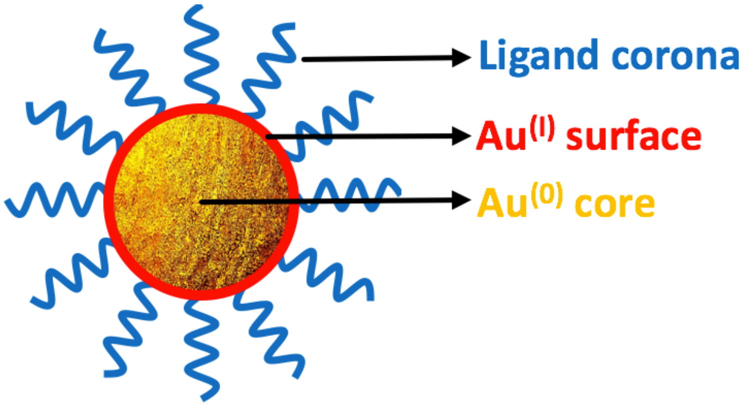

Figure 1.3: Cartoon representation of a stabilized AuNP depicting the gold core (Au^0), surface (Au^I) and ligand corona.

However, in order for AuNPs to be useful in biomedical applications, it is paramount that they do not inhibit or disrupt normal biological processes. Thankfully, AuNPs display great biocompatibility and have emerged as powerful multifunctional agents for anti-cancer treatments. A recent *in vitro* study showed the cytotoxicity profile of NPs based on their surface chemistry, morphology and size.[11] The authors investigated nanospheres, nanorods and nanostars of different sizes and concluded that the morphology and size of the nanoparticles only slightly affected cell viability. The surface chemistry had the most predominant effects on cytotoxicity depending on the type of ligand and functional groups present. It is important to note that PEG modified nanoparticles were determined to be the least toxic of the three ligands studied. Another study by Pan *et al.* revealed that AuNPs in the 1-2 nm range exhibited a size-dependent cytotoxic cellular response but larger nanoparticles were non-toxic.[18] These results support the use of AuNPs in the development of safe and effective nanoparticle based therapies as the gold scaffold is viable for *in vivo* use since the surface chemistry may be easily controlled by installing biocompatible ligands on the surface for further bioconjugation and application.

The size and shape dependent optical properties of AuNPs are exploited the most in nanoparticle research for the design of novel therapeutic and diagnostic systems. AuNPs display surface plasmon resonance (SPR) absorption from collective resonant oscillation of the free electron cloud in the conduction band of the metal resulting in sharp absorption in the visible or near infrared range of the electromagnetic spectrum.[19] This physical property mainly depends on the size and shape of the AuNP but is also influenced by the surface chemistry. For example, in smaller AuNPs (< 10 nm) the SPR causes absorption in the blue-green portion of the spectrum (~450 nm) resulting in a characteristic red wine color. But as the nanoparticle size increases (> 10 nm), the absorption wavelength shifts more to the red and the nanoparticle solution appears more blue in color (Figure 1.4).

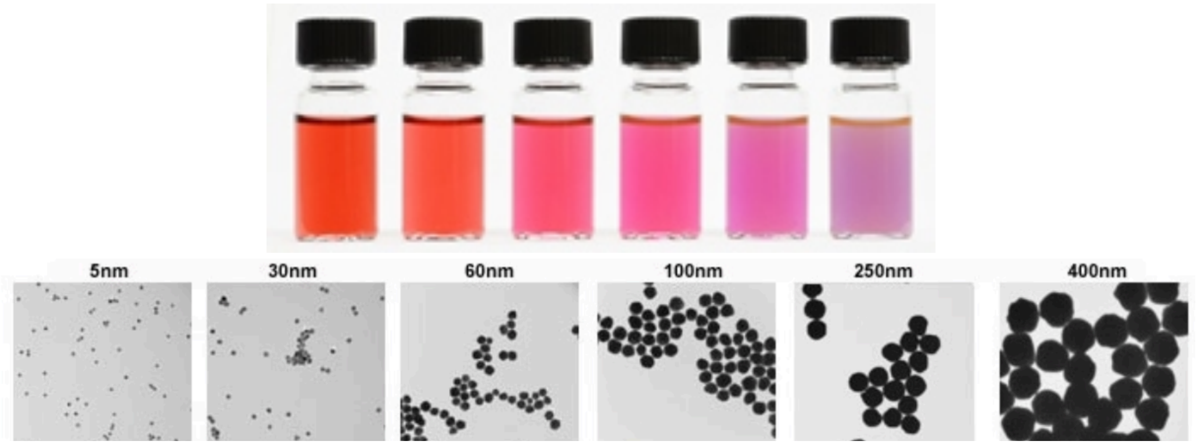

Figure 1.4: (Top) Colors of various sized monodispersed AuNP in solution (Bottom) TEM images of various sized monodispersed AuNP. The diameter increases from left to right. Images from Sigma-Aldrich product information website.[20]

By simply examining the UV-Vis spectrum of AuNP solutions such as the ones in Figure 1.4, the SPR can be readily observed as a sharp absorption in the visible or near infrared range. The size-dependence of the SPR absorption is demonstrated in the UV-Vis spectra below (Figure 1.5). First, it is important to note that small nanoparticles do not exhibit a plasmon because they are better treated as molecular clusters with discrete electronic states.[21] But as the AuNP diameter increases from 20 nm to 100 nm, the wavelength of maximum absorption (the plasmon) also increases. For even larger nanoparticles, the plasmon shifts into the near infrared (NIR) region. In addition, light is not able to polarize the larger particles homogeneously so the plasmon appears quite broad. [21]

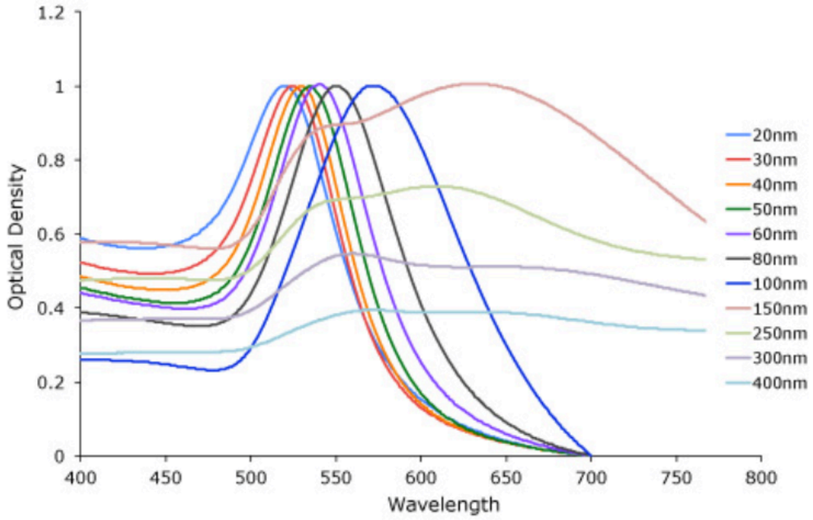

Figure 1.5: UV-Vis spectra of various sized AuNPs. Image from Cytodiagnostics product information website.[22]

Much research has been devoted to exploiting the SPR to serve as a powerful analytical, diagnostic and therapeutic tool. The dependence of the optical properties of spherical AuNPs on particle size and wavelength were analyzed theoretically using multipole scattering theory and compared to experimental results.[23] AuNPs ranging in size from 5 to 100 nm were synthesized and characterized by TEM and UV-Vis and the results were in excellent agreement with the theoretical calculations. As a result, the size and concentration of spherical and monodisperse AuNPs in solution can be simply determined with UV-Vis data. The authors compiled a series of tables to summarize their findings providing a simple and fast method to determine size and concentration of AuNPs. However, this method is limited by the fact that experimental data consists of a distribution of sizes and shapes that are not perfectly spherical or monodisperse. In addition, because the SPR is also influenced by the surface chemistry, a shift in the wavelength of maximum absorption in the UV-Vis spectra indicates successful surface functionalization or conjugation. For spherical AuNPs, a minor red shift of less than 5 nm is typically observed after surface functionalization which can serve as an analytical tool for identifying whether functionalization was successful or not.

AuNPs also have the ability to resonantly scatter visible and near-IR light at frequencies coinciding with the particles' surface plasmon resonances.[24] The light is scattered most strongly at the wavelength of the SPR maximum and is extremely sensitive to the size and shape of the particles. As such, preliminary studies have reported the use of large AuNPs as contrast agents for biomedical imaging. AuNPs also possess several advantages compared to other cellular imaging agents. First, they scatter light intensely and are much brighter than small molecule chemical fluorophores. Also they do not photobleach and can be easily detected at very low concentrations up to 10^{-16} M.[25] El-Sayed *et al.*[26] were able to distinguish between cancerous and non-cancerous cells by conjugating anti-epithelial growth factor receptor (EGFR) antibodies to AuNPs as most cancerous cells express significantly higher amounts of EGFR. The anti-EGFR antibody conjugated AuNPs were able to bind to the surface of cancer cells with 600% greater affinity compared to non-cancerous cells. As a result of the strong resonant light scattering ability, it was possible to image the cells with improved contrast. As a control, non-conjugated AuNPs were also investigated and found to accumulate inside the cells. Anti-EGFR antibody conjugated AuNPs bound specifically to the surface of cancerous cells and non-specifically to noncancerous cells. In addition, upon specific binding to the EGFR on the cell surface of cancerous cells, the plasmon was red-shifted compared to anti-EGFR AuNPs in solution. The magnitude of the plasmon shift was larger and could be differentiated for non-specific binding in non-cancerous cells. As a result, both SPR scattering imaging and SPR absorption spectroscopy could be used as a diagnostic tool in cancer diagnosis for differentiating between cancerous and non-cancerous cells.

In addition to the tunable light absorption and scattering properties useful for imaging, AuNPs can also convert the absorbed light into heat via a series of non-radiative processes leading to an increase in temperature within the lattice on the order of a few tens of degrees.[27] The lattice may then cool off by transferring the thermal energy to the surrounding medium resulting in the heat-up of the surrounding medium. However, depending on the energy source used, it is also possible to induce structural changes or melting to the particle as a result of the heat generated. To avoid this, continuous wave lasers are used to allow for heat dissipation from particles to the surrounding medium. High energy pulsed lasers typically produce unwanted structural changes as a result of the strong excitation in a short amount of time.[28] Thus AuNPs have been investigated in the literature as therapeutic agents for photothermal therapy (PTT) in cancer treatment. In a study by El-Sayed *et al.*, targeted 40 nm AuNPs were able to induce cancer cell damage.[29] However, a disadvantage of spherical particles for use in PTT is that the absorbance peak is in the visible region so it is only suitable for shallow cancers such as skin cancer. For *in vivo* PTT of tumors deep within tissue, NIR light is required because of its deep penetration due to minimal absorption from hemoglobin and water molecules within this spectral region.[27] As a result, gold nanorods have received more attention in the literature as PTT agents because of strong absorption in the NIR region.[30]

1.3 Synthesis of AuNPs

Over the past few decades, many synthetic methods have been developed in order to gain control of the size, shape and surface properties of AuNPs. Their synthesis typically begins in the liquid phase by the reduction of the gold salt tetrachloroauric acid ($HAuCl_4$) leading to nucleation and formation of nanoparticles. In order to prevent aggregation as they form, the nanoparticles are stabilized with a ligand corona. In some syntheses, the stabilizing layer also terminates further growth. Each synthetic approach has its own advantages and limitations in regards to control over the physical properties of the resulting AuNPs. The following methods are best tailored for the synthesis of spherical AuNPs and can be optimally selected to achieve a desired size.[31]

One of the most common methods was developed by Turkevich *et al.* in 1951[32] and later refined by Frens *et al.* in the 1970s[33]. As described in Figure 1.6, it involved the reaction of $HAuCl_4$ with citric acid in boiling water where the citrate ions act as both the reducing and stabilizing agent. Frens was able to refine this method by changing the ratio of gold to citrate in order to control the particle size. This fast and reliable procedure has been widely used to prepare spherical AuNPs with diameters between 10-50 nm but larger AuNPs up to the 100 nm range can also be prepared with good control over the size distribution. During the reaction, the nucleation phase can be visually observed by a change in color from clear to dark blue after ~30 s of boiling after the two reagents have been added. The growth phase can then be seen by a change in color to bright red after ~90 s. But despite being the most common synthetic method, the use of the resulting citrate-stabilized AuNPs is limited. First, it is difficult to isolate them from the aqueous solution so characterization is problematic. Second, the stability of the ligand shell is minimal in regards to changes in pH or ionic strength of the solution. Finally, their functionalization is challenging as larger AuNPs have a higher tendency to irreversibly aggregate due to increased Van der Waals forces and derivatization of the carboxylic acid ligand shell is extremely limited.

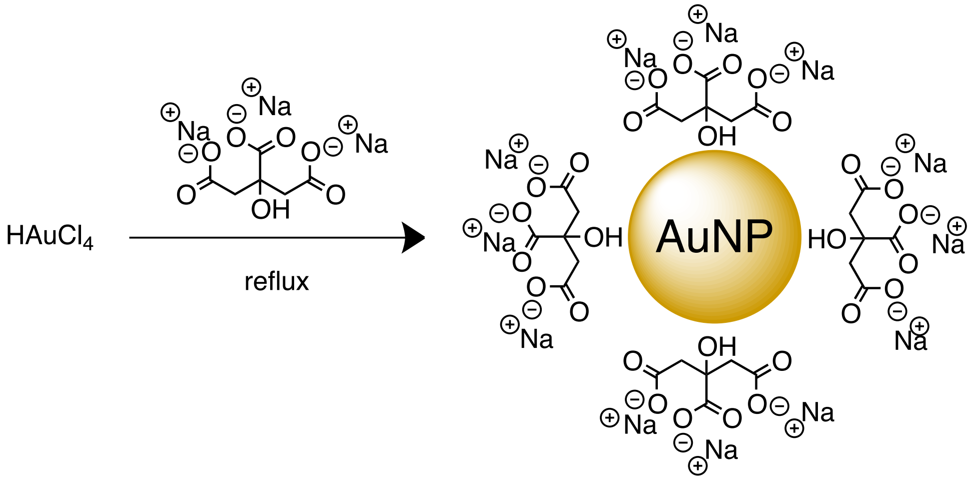

Figure 1.6: Citrate-stabilized AuNPs prepared by the Turkevich method with $HAuCl_4$ and sodium citrate in aqueous solution under reflux conditions where citrate acts as both the reducing agent and stabilizing ligand.

In the early 1990s, Brust and Schriffin developed a direct synthesis method for alkanethiol-stabilized AuNPs.[34] Using a two-phase reaction, aqueous $HAuCl_4$ is transferred to the organic phase (toluene) using the phase transfer reagent tetraoctylammonium bromide (TOAB). Then upon addition of a thiol to the organic phase, the gold (III) salt is reduced to a gold (I)-thiol polymer. This step can be visually observed by a discoloration of the organic phase from orange to clear and colorless. Sodium borohydride ($NaBH_4$) is then added to as the reducing agent to give the final AuNPs where the oxidation state of gold is zero (Figure 1.7, left). This protocol gives spherical AuNPs with low size and shape dispersity in the 1 to 5 nm range depending on the reaction conditions used. The size of the resulting AuNPs can be tuned by varying the molar gold-to-thiol ratio, reaction temperature and reduction rate. For example, a larger thiol to gold ratio thiol results in smaller nanoparticles,[35] lower reaction temperatures decrease size polydispersity[36] and faster addition of the reducing agent gives smaller nanoparticles.[37] The Brust-Schiffrin method yields more stable AuNPs as a result of the strong gold-thiol bond previously described as well as van der Waals attractive forces between neighboring ligands. These AuNPs are also synthetically much easier to work with because they can be thoroughly dried and re-dissolved in common organic solvents without irreversible aggregation or ligand dissociation. This is very important in order to be able to perform post-synthetic modifications on the AuNP surface.

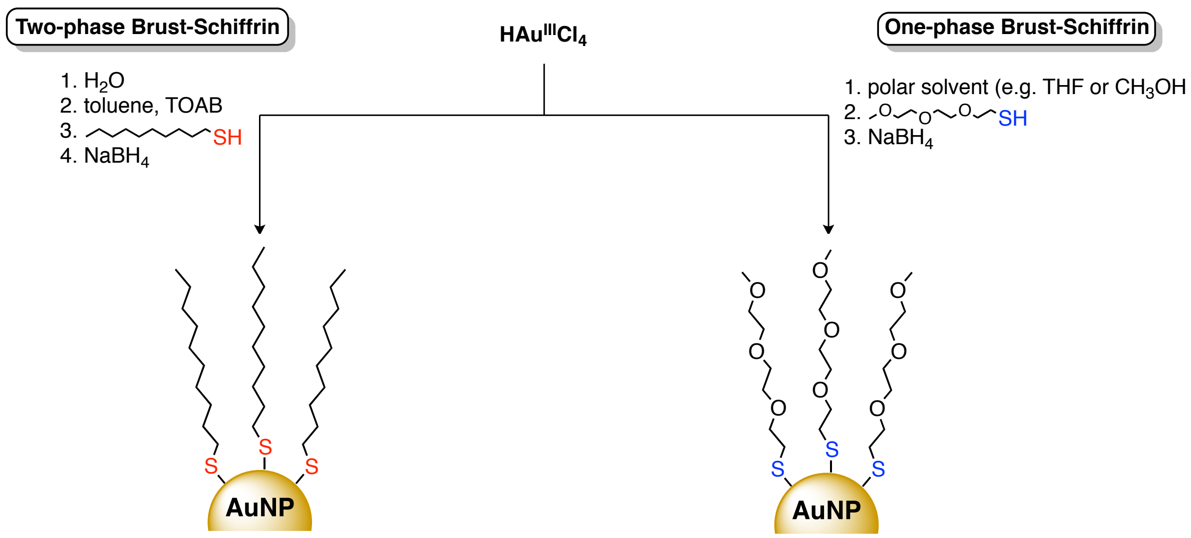
Two-phase Brust-Schiffrin
HAu^{III}Cl$_4$
One-phase Brust-Schiffrin
1. H$_2$O
2. toluene, TOAB
3. SH
4. NaBH$_4$
1. polar solvent (e.g. THF or CH$_3$OH
2. O O O SH
3. NaBH$_4$
S
O
AuNP

Figure 1.7: (Left) Brust-Schriffin two-phase synthesis of AuNPs by reduction of HAuCl$_4$ using alkanethiols as the stabilizing ligands and NaBH$_4$ as the reducing agent. (Right) Modified one-phase Brust reaction scheme using methoxy terminated tri(ethylene glycol) thiol ligands.

Over the years a number of modifications have been made to the Brust-Schiffrin approach to overcome limitations of the alkanethiolate stabilized AuNPs. First, these AuNPs are not soluble in water and therefore incompatible with biological systems. In addition, contamination of residual TOAB can influence potential applications of the AuNPs.[38] Although purification methods were developed, in the end they proved to be costly and time consuming. To overcome these problems, a one-phase method was developed to remove use of the phase transfer reagent and avoid contamination (Figure 1.7, right). To improve solubility in water, PEG based stabilizing ligands replaced the original alkane based ones. The first direct synthesis of oligo(ethylene glycol)-protected AuNPs was reported by Huang *et al*.[39] In recent years, our group has developed improved methodologies for the synthesis of methoxy terminated tri(ethylene glycol) based AuNPs.[40] These ligands contain an –(O-CH$_2$-CH$_2$)- repeating unit and a terminal methoxy (-OCH$_3$) group that decorates the nanoparticle surface and forms a densely packed monolayer in the ligand corona that stabilizes the AuNP. It also produces a more versatile system as the resulting nanoparticles are soluble in both aqueous and organic solvents.

In order to achieve even larger nanoparticles, a seeding growth method is required. This approach was discovered by Perrault and Chan in 2009.[41] It involves using hydroquinone as a mild reducing agent to reduce $HAuCl_4$ in an aqueous solution that contains 15 nm AuNP seeds. Typically, the nanoparticle seeds are produced using the citrate method. This method yields larger AuNPs (> 50 nm) with a greater size range as well as better size and shape dispersity. In summary, along with the other methods previously described, it is possible to synthesize AuNPs with a size range from 1 to 200 nms with homogeneous sizes and shapes for future biomedical applications.

1.4 Functionalization of AuNPs

The development of AuNPs modified with complex ligands containing a functional substrate (small molecule, polymer or biomolecule) is of very high interest. These functional AuNPs may then interact either chemically or physically with other substrates to perform a specific function such as act as a biological or chemical sensors. As previously described, there are three main strategies used for the preparation of functionalized AuNPs including (i) direct synthesis (ii) place (or ligand) exchange reactions (iii) post-synthetic interfacial reactions.

The direct synthesis of functional AuNPs involves the incorporation of a thiol containing complex ligand during AuNP synthesis to simultaneously provide stabilization as well as introduce functionality (Figure 1.8). However, this strategy is challenging as a result of the reaction conditions used for AuNP synthesis. For example, ligands containing functional groups that are easily reduced are incompatible with the sodium borohydride reducing agent used in the Brust-Schriffin method. In addition, the synthesis of such complex thiols can be very difficult and time consuming.

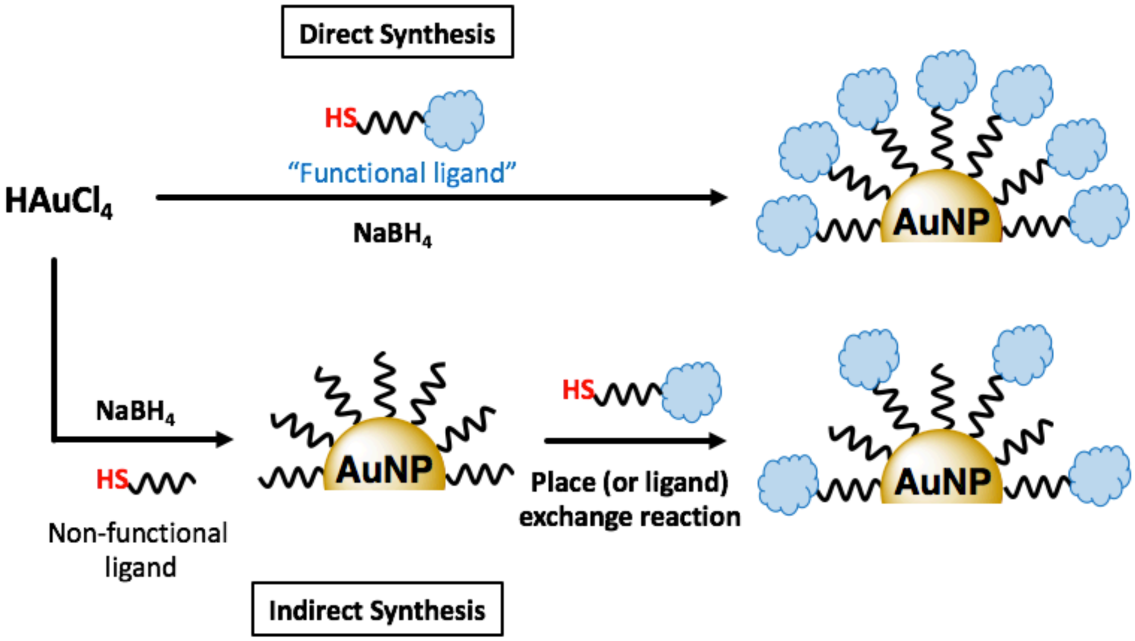
Direct Synthesis
HS
"Functional ligand"
HAuCl$_4$
NaBH$_4$
AuNP
NaBH$_4$
HS
Non-functional ligand
AuNP
HS
Place (or ligand) exchange reaction
AuNP
Indirect Synthesis

Figure 1.8: (Top) Direct synthesis of functional AuNP where the incorporation of a thiolated-ligand possessing a functional substrate through a direct synthetic method can be quite challenging (Bottom) Indirect synthesis of functional AuNP where the incorporation of functional substrates is often possible using an indirect approach through a place exchange reaction.

In order to avoid undesired reactivity with the functional substrate, an intermediate AuNP can be employed as a precursor and then transformed into a functional AuNP system. A versatile method for achieving this transformation is the place or ligand exchange reaction developed by Murray *et al.*[42] In the place exchange reaction, the ligands on the originally synthesized AuNPs may be readily exchanged with another thiolate ligand simply by exposing the AuNPs to a large excess of a thiol with the desired functionality. For example, following place exchange with Brust-Schriffin type AuNPs, the resulting AuNPs contain a mixed monolayer of both the original thiolate and functionalized thiolate ligands. The extent of ligand exchange that takes place can be controlled by the ratio of gold to thiol used as well as the reaction time. Large AuNPs produced by the Turkevich method may also undergo place exchange reactions due to the relatively weak binding between the AuNP surface and carboxyl groups on the citrate ions.

Finally, post-synthetic interfacial reactions may also be used to functionalize AuNPs through an organic reaction with a terminal functional group on the surface of the AuNP. This versatile strategy has led to the development of multifunctional AuNPs as terminal functional groups may react with a multitude of different substrates to introduce novel functionality. Although numerous approaches have been reported in the literature for the conjugation of a molecule of interest to a material surface by reaction with an endogenous[43] or exogenous[44] functional group, no single approach can be broadly adopted due to the vast complexity of substrates for application. As a result, there is a need for a simple and convenient system that allows for material surface functionalization but can also be modified depending on the substrate involved. So over the past few years, the Workentin group has developed a toolbox of sophisticated methods for the systematic functionalization of small (1-5 nm) water-soluble AuNPs through the design of AuNP templates (Figure 1.9). These templates contain a reactive functional group that is introduced to the AuNP surface through the methods previously described, but most commonly via a place exchange reaction. The latter method allows for better control over the loading of the functional ligand. The functional group introduced as a template may then undergo interfacial chemistry with a suitable reaction partner that contains a functional substrate. With this strategy, our group has been able to incorporate various functional groups and create a library of versatile AuNP templates to be able to introduce different structural diversity. For example, using maleimide-functionalized AuNPs as the template our group was able to develop a molecular delivery system via an interfacial glutathione-mediated retro Michael-type addition reaction.[45] Using the same AuNP template, our group was also able to develop an MRI contrast agent via an interfacial Michael addition with a gadolinium(III) chelate.[9]

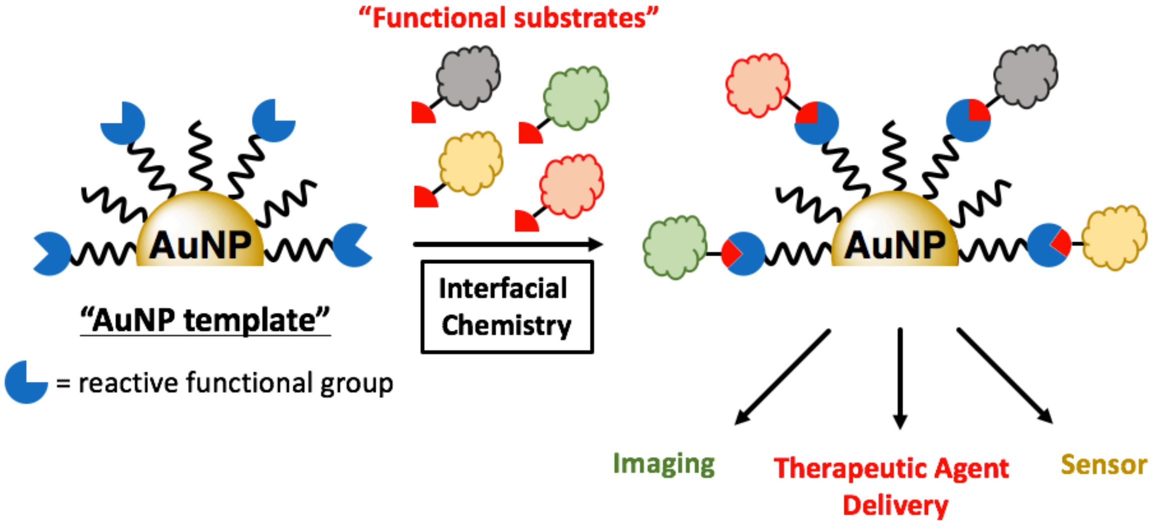

Figure 1.9: Example of AuNP template design for the introduction of versatile functional substrates.

For large AuNPs, carbodiimide-mediated bioconjugation is the most common interfacial reaction used for biofunctionalization but it usually leads to a loss of colloidal stability depending on the polymer used for stabilization. The development of novel carbodiimide reagents has been explored in order to address this issue[46] but the scope of interfacial chemistry for the functionalization of large AuNPs remains quite limited in the present literature.

1.5 Interfacial Bioorthogonal Click Chemistry

The familiar term "click chemistry" was first introduced by Sharpless and describes a set of reactions that are fast, stereo- and chemoselective and high yielding.[47] Most notably, the copper(I)-catalyzed alkyne−azide cycloaddition (CuAAC), has become one of the most reliable click reactions as evidenced by its common practice in materials chemistry[48] and chemical biology[49] for covalently connecting molecules via the formation of a trizaole ring. However, the *in vivo* applications are limited due the cytotoxic nature of the copper catalyst as the presence of the metal ions may damage or destroy oligonucleotides.[50] To overcome these limitations and exploit this class of chemistry in biological systems, a non-cytotoxic subset was developed and termed "bioorthogonal click chemistry". Lately, the strain-promoted alkyne-azide cycloaddition (SPAAC) reaction has emerged and occurs with very fast reaction kinetics as well as high efficiency and chemoselectivity. Strained alkynes can undergo even more rapid strain-promoted cycloaddition with nitrones in the strain-promoted alkyne-nitrone cycloaddition (SPANC) reaction.[51] The driving force of these reactions originates from the strain resulting from the non-linear geometry of the alkyne. The key feature in these strain promoted cycloaddition reactions is the elimination of the metal catalyst that is required for the traditional alkyne-azide click reactions so as a result the SPAAC and SPANC reactions have been viable for use in living systems.[52] The Workentin group has taken advantage of this class of reactions by designing AuNP templates for interfacial bioorthogonal click chemistry (Figure 1.10). Our group was the first to introduce strained alkyne functionality onto AuNPs and demonstrate interfacial SPAAC.[53] The incorporation of a variety of other bioorthogonal functionalities to the AuNP surface has also been achieved such as azides and nitrones. We have also demonstrated an interfacial Staudinger-Bertozzi ligation[54] in addition to 1,4 Michael- type additions[55] and Diels-Alder cycloadditions with maleimides. Our group aims to continue developing new click and bioorthogonal AuNP templates for interfacial functionalization and this is one of the focuses of my thesis.

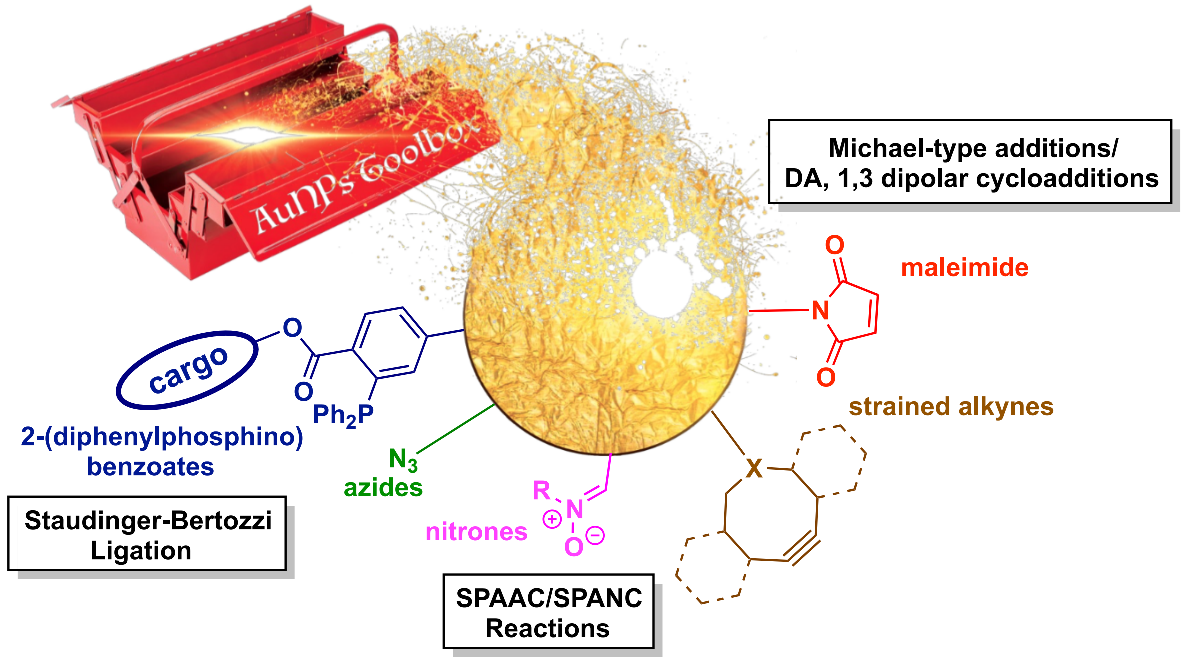
AuNPs Toolbox
Michael-type additions/
DA, 1,3 dipolar cycloadditions
maleimide
O
N
O
strained alkynes
X
cargo
O
O
Ph$_2$P
2-(diphenylphosphino)
benzoates
Staudinger-Bertozzi
Ligation
N$_3$
azides
R
N
O
nitrones
SPAAC/SPANC
Reactions

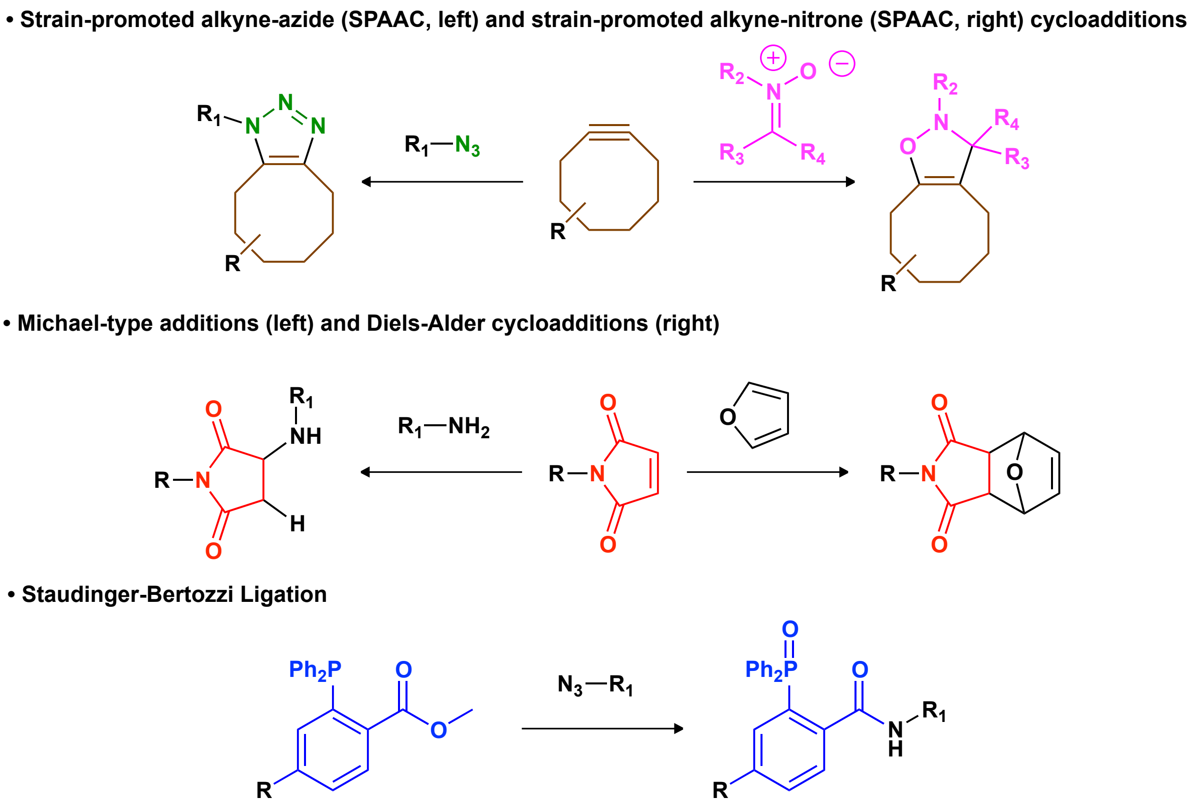
• Strain-promoted alkyne-azide (SPAAC, left) and strain-promoted alkyne-nitrone (SPAAC, right) cycloadditions
R1—N3
R
R1
N
N
N
R2
N
O
R3
R4
• Michael-type additions (left) and Diels-Alder cycloadditions (right)
R1—NH2
R—N
O
NH
H
• Staudinger-Bertozzi Ligation
Ph2P
O
N3—R1
R
H

Figure 1.10: The Workentin group AuNP toolbox. Reaction schemes of click and bioorthogonal functional groups incorporated into AuNP templates.

Recently, the Popik group has developed a photochemically triggered click reaction system for facile and efficient hetero-Diels-Alder as well as Michael addition (Scheme 1.1).[56] Photochemical dehydration of 3-hydroxy-2-naphthalenemethanol derivatives by irradiation with UV light (350 nm) produces *ortho*-naphthoquinone methides (*o*NQMs). The resulting molecule is able to undergo facile cycloaddition to produce photostable Diels-Alder adducts. In aqueous solution, unreacted *o*NQM is rapidly hydrated to regenerate the naphthoquinone methide precursor (NQMP) starting material. The competition between hydration and cycloaddition makes *o*NQMs highly selective as only vinyl ethers and enamines are reactive enough to form the Diels-Alder adduct in aqueous solution. No cycloaddition is observed with other types of alkenes.[57] Instead, the hydration product is recovered demonstrating the selectivity of the reaction. More importantly, *o*NQMs may also undergo Michael addition with various nucleophiles including thiols. The resulting thioether is hydrolytically stable, but it can be quantitatively cleaved photochemically under 300 or 350 nm irradiation back to *o*NQM with a 10% quantum yield.[58] Additionally, although oNQM compounds are reportedly cytotoxic as a result of undesirable side reactivity to alkylate DNA bases, in this system the oNQM functionality is formed photochemically and therefore viable for *in vivo* use.[57] The focus of Chapter 2 in this thesis is the development of a novel AuNP template that contains this highly desirable click and bioorthogonal functionality. The light activation and reversibility will allow for unprecedented temporal and spatial control of reactivity for patterning and delivery.

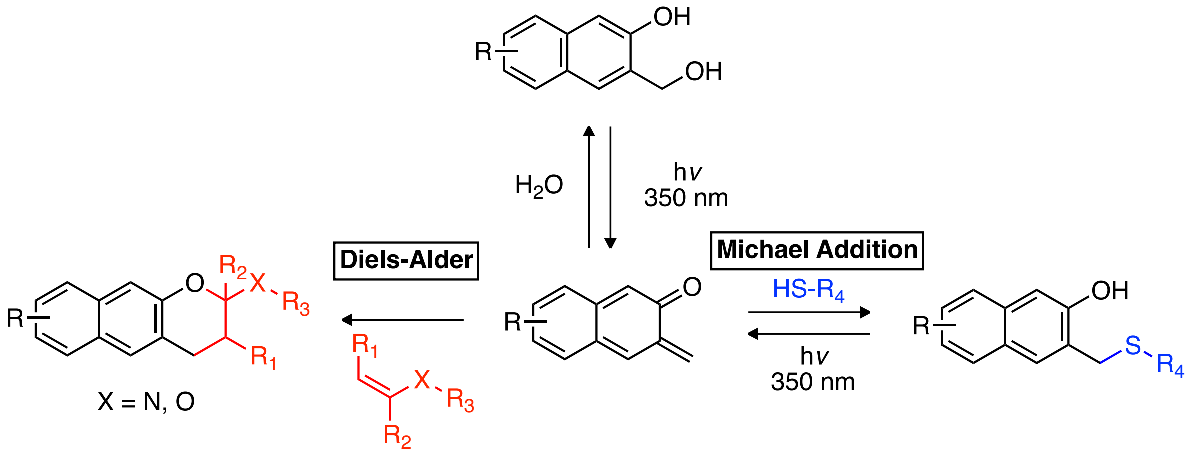

Scheme 1.1: Photochemical generation and reactivity of oNQM from NQMP in aqueous solution.

1.6 Characterization of AuNPs

The characterization of as-synthesized small AuNPs may be completed with a variety of imaging and spectroscopic techniques. Advantageously, the introduction of bioorthogonal functional groups to the AuNP interface may also be characterized by common spectroscopic techniques in order to determine the loading capacity (number of bioorthogonal functionalities incorporated) as well as investigate reactivity. TEM is most commonly used in order to determine the size and shape characteristics of AuNPs. TEM is a microscopy technique in which a beam of electrons is transmitted through a sample of interest to form an image. Using this technique, it is possible to not only directly visualize the AuNP core but also extract information about their shape (spherical, nanorods, nanostars, etc.) as well as their size dispersity through a direct measurement. However, it is not possible to gain information about ligand composition because of the low electron density within the corona. Examples of TEM images of various types of nanoparticles are included in Figure 1.2.

Nuclear magnetic resonance (NMR) spectroscopy is one of the most powerful tools for obtaining significant information about the composition and structure of the ligands on the AuNP surface.[59] The solubility of Brust-Schiffrin type small AuNPs in both organic and aqueous solvent is very amenable to ^{1}H NMR analysis but citrate-stabilized AuNPs are more difficult. The signals in the ^{1}H NMR spectrum of functionalized AuNPs corresponding to ligands on the AuNP surface appear broad. The broadness is due to the inhomogeneous AuNP surfaces and Au-S bonding sites resulting in slightly different chemical shifts. In addition, slow rotation of the thiolates bound to the AuNP core induces a very fast spin-spin relaxation (T_2) that also contributes to broadening.[60] Nevertheless, ^{1}H NMR spectroscopy may still be used to investigate the successful functionalization and purity of AuNPs. For example, after a place exchange reaction, the presence of free ligand appears as sharp signals in the ^{1}H NMR spectrum. On the other hand, ligands bound to the AuNP core will appear at the same chemical shift as their non-bound counterparts, however the signals will be much broader for the reasons previously described. Subsequent interfacial chemistry may also be monitored through ^{1}H NMR spectroscopy in the same manner as conventional small molecule chemistry.

The synthesis of large citrate-stabilized AuNPs in water limits the use of ^{1}H NMR spectroscopy as a characterization tool. However, since the Turkevich method produces larger AuNPs (> 5 nm) that exhibit a surface plasmon, it is possible to take advantage of this unique optical property for characterization. Spherical AuNPs exhibit a strong size-dependent absorption peak in the visible range. As a result, by analyzing the wavelength of maximum absorption it is possible to determine the approximate AuNP core size in excellent agreement with data obtained from imaging techniques such as TEM.[23] The peak absorbance wavelength also shifts to the NIR region for uneven shaped nanoparticles so it is also possible to obtain information about the shape of the nanoparticles. In addition, the plasmon is also influenced by the surface chemistry of the AuNP. A shift in the wavelength of maximum absorption in the UV-Vis spectra can be used to indicate surface functionalization. Typically, a minor red shift of less than 5 nm is observed for spherical AuNPs after surface functionalization.[61]

Finally, after determining the gold core size through microscopic or spectroscopic techniques, the number of ligands with respect to the number of gold atoms on the AuNPs, can be easily determined using thermogravimetric analysis (TGA).[62] TGA measures the changes in the weight of a sample as a function of temperature and/or time under a controlled atmosphere such as nitrogen. As the temperature increases, the organic ligands are removed from the nanoparticle surface and vaporized. The corresponding mass loss associated with this stage indicates the percentage of organic ligands contained on the surface of the AuNPs.

1.7 Objectives – Chapter 2

The goal of this project was to develop a novel photoreactive AuNP-NQMP functionalized template that upon irradiation by UV light undergoes fast, selective and photoreversible Michael addition. The overall synthetic strategy is outlined in Scheme 1.2. First, the introduction of oNQM functionality onto a AuNP template requires the synthesis of a thiolated NQMP ligand. Chapter 2 describes the synthetic strategy for producing this ligand in good yield as well as characterization of all intermediates by ^{1}H NMR, ^{13}C NMR and IR spectroscopy as well as mass spectrometry (MS). Then a place exchange reaction of the proposed ligand using methoxy-terminated AuNPs was accomplished to yield NQMP functionalized AuNPs. This novel AuNP-NQMP template provides a selective and versatile template for interfacial chemistry with spatial and temporal control of reactivity through UV irradiation. My addition to the Workentin AuNP toolbox was fully characterized through ^{1}H NMR, IR, and UV-Vis spectroscopy as well as TGA and TEM. These novel AuNPs will then be able to undergo interfacial Michael addition reactions that are also photoreversible. This unique system will expand the scope of the AuNP toolbox by introducing a novel click and photoreversible functional group with remarkable temporal and spatial control of reactivity for the design of delivery systems.

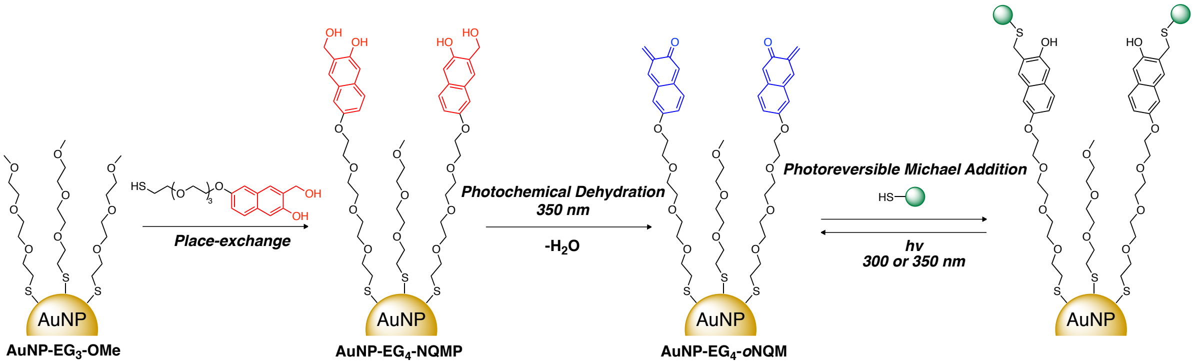

Scheme 1.2: Outline of synthetic strategy for the synthesis of oNQM-AuNP and photoreversible interfacial Michael Addition.

1.8 Objectives – Chapter 3

Another goal of my M.Sc. research was to transpose the toolbox of reactions onto larger AuNPs in order to take advantage of their unique optical properties. Larger AuNPs display SPR absorption resulting from collective resonant oscillation of the free electron cloud of the conduction band of the metal resulting in sharp absorption in the visible[21] or near-infrared[63] range. Large AuNPs also exhibit excellent scattering properties The strongly absorbed light can also be converted to heat so larger AuNPs have been utilized for imaging and PTT[27, 29]. An interesting alternative application of the photothermal effect could be to provide energy for interfacial chemistry to enable faster and more efficient functionalization of the AuNP surface.

However, the synthesis of large AuNPs that are stable and water-soluble remains challenging as they have a higher tendency to aggregate due to increased Van der Waals forces so the ability to further exploit the SPR for *in vivo* applications is limited. In the current literature, polyethylene glycol (PEG) is commonly used for stabilization but as a result of its polydispersity (non-uniform polymer lengths), it is difficult to characterize and functionalize the final AuNP. The dilemma presented in the literature is that high molecular weight PEG provides excellent stability but poor conjugation ability. On the other hand, low molecular weight PEG enables high conjugation ability but provides minimal stability resulting in irreversible aggregation, especially for larger AuNPs. In order to address this issue, Liu *et al*. reported a simple method using mixed PEG layers with specific ratios of low and high molecular weight PEG.[64] Through characterization by X-ray Photoelectron Spectroscopy (XPS), successful bioconjugation of proteins and monoclonal antibodies was then demonstrated without detectable aggregation. However the scope of PEG stabilized AuNPs is limited because the tight PEG-thiol AuNP monolayer inhibits place-exchange reactions with other thiols[65] thereby restricting the introduction of more chemically interesting functional groups for interfacial chemistry.

In order to expand the scope of large AuNPs for biomedical applications, it is necessary to circumvent the PEG dilemma by designing hydrophilic ligands of discrete size that still provide excellent stability to the large gold core as well as a high loading capacity. In this fashion, it will be possible to functionalize and characterize the final large AuNP through conventional small NP techniques such as NMR spectroscopy. The structure of the proposed model ligand is described in Figure 1.11. It is derived from three unique fragments such that the final ligand highlights three important features. First, the gold core may be stabilized through thiol binding at the head. At the tail, the model ligand contains a methoxy-terminus that could be replaced with a bioorthogonal functionality as described in Figure 1.10 to undergo click and biorthogonal interfacial chemistry. Finally, the number of repeating units (n) may be systematically increased to provide further stabilization and account for increased AuNP core size. In addition, it is predicted that these ligands will form a network of hydrogen bonding shells around the gold core for increased stabilization and hydrophilicity[66] as described in Figure 1.12. A major factor in the stability of the AuNPs is the repulsive forces that occur between the ligands, which is induced by electrostatic repulsion and steric effects. To overcome this obstacle, the amide hydrogen bonding pattern will allow for lateral hydrogen bonding between ligands in the AuNP monolayer to further stabilize the corona.

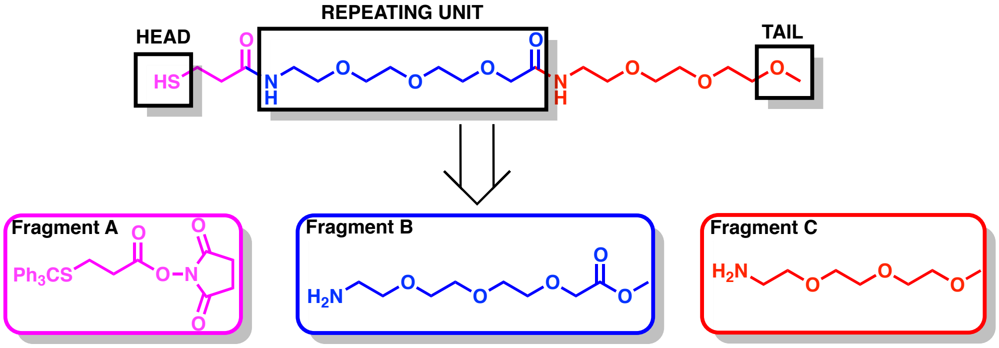

Figure 1.11: Retro-synthesis of the model ligand (n = 1) and highlighted features.

In the end, AuNPs ranging from 20 to 50 nm were synthesized by the Turkevich method and stabilized by these novel ligands to yield functionalizable water-soluble AuNP templates of varying size. The required novel ligand was synthesized through a convergent approach as described in Figure 1.11. The formation of hydrogen bonding shells within the ligand corona will provide sufficient stabilization eliminating the use of polymeric ligands that are conventionally used. By using an oligomeric ligand of discrete size, it will also be possible to achieve a high loading capacity without aggregation. Then once the final AuNP template is made, the synthetic approach can be modified to incorporate the AuNP toolbox and introduce click and bioorthogonal functionalities to the AuNP surface for fast, clean and efficient interfacial chemistry. The overall design is described in Figure 1.11.

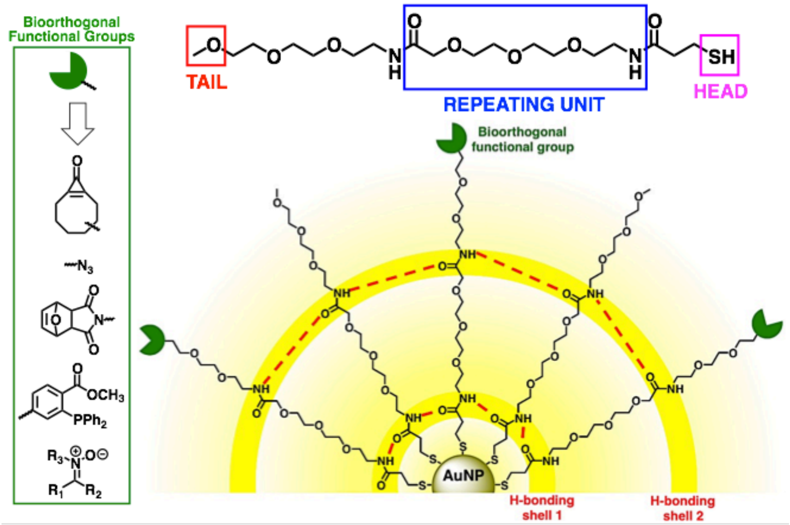
Bioorthogonal Functional Groups
TAIL
REPEATING UNIT
HEAD
SH
Bioorthogonal functional group
AuNP
H-bonding shell 1
H-bonding shell 2

Figure 1.12: Design of novel ligand with hydrogen bonding shells. The tail may be replaced with bioorthogonal functional groups.

1.9 References

[1] S. Jin, Y. X. Hu, Z. J. Gu, L. Liu, H. C. Wu, *Journal of Nanomaterials* **2011**.

[2] M. Homberger, U. Simon, *Phil. Trans. R. Soc. A* **2010**, *368*, 1405-1453.

[3] D. T. Thompson, *Nano Today* **2007**, *2*, 40-43.

[4] K. Saha, S. S. Agasti, C. Kim, X. N. Li, V. M. Rotello, *Chem. Rev.* **2012**, *112*, 2739-2779.

[5] P. Ghosh, G. Han, M. De, C. K. Kim, V. M. Rotello, *Adv. Drug Deliv. Rev.* **2008**, *60*, 1307-1315.

[6] M. Faraday, *Phil. Trans. R. Soc. Lond.* **1857**, *147*, 145-181.

[7] P. P. Edwards, J. M. Thomas, *Angew. Chem. Int. Ed.* **2007**, *46*, 5480-5486.

[8] E. C. Dreaden, L. A. Austin, M. A. Mackey, M. A. El-Sayed, *Ther. Deliv.* **2012**, *3*, 457-478.

[9] M. Milne, P. Gobbo, N. McVicar, R. Bartha, M. S. Workentin, R. H. E. Hudson, *J. Mater. Chem. B* **2013**, *1*, 5628-5635.

[10] T. Reuveni, M. Motiei, Z. Romman, A. Popovtzer, R. Popovtzer, *Int. J. Nanomedicine* **2011**, *6*, 2859-2864.

[11] M. Bhamidipati, L. Fabris, *Bioconjugate Chem.* **2017**, *28*, 449-460.

[12] S. Eustis, M. A. El-Sayed, *Chem. Soc. Rev.* **2006**, *35*, 209-217.

[13] H. E. Toma, V. M. Zamarion, S. H. Toma, K. Araki, *J. Braz. Chem. Soc.* **2010**, *21*, 1158-1176.

[14] M. C. Daniel, D. Astruc, *Chem. Rev.* **2004**, *104*, 293-346.

[15] a) P. M. Shem, R. Sardar, J. S. Shumaker-Parry, *Langmuir* **2009**, *25*, 13279-13283; b) W. W. Weare, S. M. Reed, M. G. Warner, J. E. Hutchison, *J. Am. Chem. Soc.* **2000**, *122*, 12890-12891.

[16] a) D. V. Leff, L. Brandt, J. R. Heath, *Langmuir* **1996**, *12*, 4723-4730; b) K. S. Mayya, F. Caruso, *Langmuir* **2003**, *19*, 6987-6993.

[17] H. Hakkinen, *Nat. Chem.* **2012**, *4*, 443-455.

[18] Y. Pan, S. Neuss, A. Leifert, M. Fischler, F. Wen, U. Simon, G. Schmid, W. Brandau, W. Jahnen-Dechent, *Small* **2007**, *3*, 1941-1949.

[19] V. Amendola, R. Pilot, M. Frasconi, O. M. Marago, M. A. Iati, *J. Phys. Condens. Matter.* **2017**, *29*, 203002.

[20] Gold Nanoparticles: Properties and Applciations. http://www.sigmaaldrich.com/technical-documents/articles/materials-science/nanomaterials/gold-nanoparticles.html (accessed May 9, 2017).

[21] S. Link, M. A. El-Sayed, *Annu. Rev. Phys. Chem.* **2003**, *54*, 331-366.

[22] Gold Nanoparticle Properties. http://www.cytodiagnostics.com/store/pc/Gold-Nanoparticle-Properties-d2.htm (accessed May 9, 2017).

[23] W. Haiss, N. T. K. Thanh, J. Aveyard, D. G. Fernig, *Anal. Chem.* **2007**, *79*, 4215-4221.

[24] K. Sokolov, J. Aaron, B. Hsu, D. Nida, A. Gillenwater, M. Follen, C. MacAulay, K. Adler-Storthz, B. Korgel, M. Descour, R. Pasqualini, W. Arap, W. Lam, R. Richards-Kortum, *Technol. Cancer Res. Treat.* **2003**, *2*, 491-504.

[25] J. Yguerabide, E. E. Yguerabide, *Anal. Biochem.* **1998**, *262*, 137-156.

[26] I. H. El-Sayed, X. H. Huang, M. A. El-Sayed, *Nano Lett.* **2005**, *5*, 829-834.

[27] X. Huang, M. A. El-Sayed, *J. Adv. Res.* **2010**, *1*, 13-28.

[28] N. S. Abadeer, C. J. Murphy, *J. Phys. Chem. C* **2016**, *120*, 4691-4716.

[29] I. H. El-Sayed, X. H. Huang, M. A. El-Sayed, *Cancer Lett.* **2006**, *239*, 129-135.

[30] X. Huang, I. H. El-Sayed, M. A. El-Sayed, *Methods Mol. Biol.* **2010**, *624*, 343-357.

[31] Y. C. Yeh, B. Creran, V. M. Rotello, *Nanoscale* **2012**, *4*, 1871-1880.

[32] J. Turkevich, P. C. Stevenson, J. Hillier, *Discuss. Faraday Soc.* **1951**, 55-75.

[33] G. Frens, *Kolloid-Zeitschrift and Zeitschrift Fur Polymere* **1972**, *250*, 736-741.

[34] M. Brust, M. Walker, D. Bethell, D. J. Schiffrin, R. Whyman, *J. Chem. Soc., Chem. Commun.* **1994**, 801-802.

[35] D. V. Leff, P. C. Ohara, J. R. Heath, W. M. Gelbart, *J. Phys. Chem.* **1995**, *99*, 7036-7041.

[36] M. J. Hostetler, J. E. Wingate, C. J. Zhong, J. E. Harris, R. W. Vachet, M. R. Clark, J. D. Londono, S. J. Green, J. J. Stokes, G. D. Wignall, G. L. Glish, M. D. Porter, N. D. Evans, R. W. Murray, *Langmuir* **1998**, *14*, 17-30.

[37] R. L. Whetten, J. T. Khoury, M. M. Alvarez, S. Murthy, I. Vezmar, Z. L. Wang, P. W. Stephens, C. L. Cleveland, W. D. Luedtke, U. Landman, *Adv. Mater.* **1996**, *8*, 428-433.

[38] C. A. Waters, A. J. Mills, K. A. Johnson, D. J. Schiffrin, *Chem. Commun.* **2003**, 540-541.

[39] M. Zheng, Z. G. Li, X. Y. Huang, *Langmuir* **2004**, *20*, 4226-4235.

[40] P. Gobbo, M. S. Workentin, *Langmuir* **2012**, *28*, 12357-12363.

[41] S. D. Perrault, W. C. W. Chan, *J. Am. Chem. Soc.* **2009**, *131*, 17042-17043.

[42] A. C. Templeton, M. J. Hostetler, C. T. Kraft, R. W. Murray, *J. Am. Chem. Soc.* **1998**, *120*, 1906-1911.

[43] Y. A. Chen, A. Star, S. Vidal, *Chem. Soc. Rev.* **2013**, *42*, 4532-4542.

[44] A. B. Bakhtiari, D. Hsiao, G. Jin, B. D. Gates, N. R. Branda, *Angew. Chem. Int. Ed.* **2009**, *48*, 4166-4169.

[45] M. R. Weissman, K. T. Winger, S. Ghiassian, P. Gobbo, M. S. Workentin, *Bioconjugate Chem.* **2016**, *27*, 586-593.

[46] H. Y. Shen, A. M. Jawaid, P. T. Snee, *ACS Nano* **2009**, *3*, 915-923.

[47] H. C. Kolb, M. G. Finn, K. B. Sharpless, *Angew. Chem. Int. Ed.* **2001**, *40*, 2004-2021.

[48] M. Meldal, C. W. Tornoe, *Chem. Rev.* **2008**, *108*, 2952-3015.

[49] C. W. Tornoe, C. Christensen, M. Meldal, *J. Org. Chem.* **2002**, *67*, 3057-3064.

[50] T. Wang, Z. J. Guo, *Curr. Med. Chem.* **2006**, *13*, 525-537.

[51] C. S. Mckay, J. Moran, J. P. Pezacki, *Chem. Commun.* **2010**, *46*, 931-933.

[52] N. J. Agard, J. A. Prescher, C. R. Bertozzi, *J. Am. Chem. Soc.* **2005**, *127*, 11196-11196.

[53] P. Gobbo, Z. Mossman, A. Nazemi, A. Niaux, M. C. Biesinger, E. R. Gillies, M. S. Workentin, *J. Mater. Chem. B* **2014**, *2*, 1764-1769.

[54] P. Gobbo, W. Luo, S. J. Cho, X. X. Wang, M. C. Biesinger, R. H. E. Hudson, M. S. Workentin, *Org. Biomol. Chem.* **2015**, *13*, 4605-4612.

[55] K. D. Hartlen, H. Ismaili, J. Zhu, M. S. Workentin, *Langmuir* **2012**, *28*, 864-871.

[56] S. Arumugam, V. V. Popik, *J. Am. Chem. Soc.* **2009**, *131*, 11892-11899.

[57] S. Arumugam, V. V. Popik, *J. Am. Chem. Soc.* **2011**, *133*, 5573-5579.

[58] S. Arumugam, V. V. Popik, *J. Am. Chem. Soc.* **2012**, *134*, 8408-8411.

[59] X. Liu, M. Yu, H. Kim, M. Mameli, F. Stellacci, *Nat. Commun.* **2012**, *3*, 1182-1189.

[60] Y. Song, A. S. Harper, R. W. Murray, *Langmuir* **2005**, *21*, 5492-5500.

[61] F. Schulz, T. Vossmeyer, N. G. Bastus, H. Weller, *Langmuir* **2013**, *29*, 9897-9908.

[62] E. Mansfield, K. M. Tyner, C. M. Poling, J. L. Blacklock, *Anal. Chem.* **2014**, *86*, 1478-1484.

[63] X. H. Huang, I. H. El-Sayed, W. Qian, M. A. El-Sayed, *J. Am. Chem. Soc.* **2006**, *128*, 2115-2120.

[64] T. Q. Liu, B. Thierry, *Langmuir* **2012**, *28*, 15634-15642.

[65] W. P. Wuelfing, S. M. Gross, D. T. Miles, R. W. Murray, *J. Am. Chem. Soc.* **1998**, *120*, 12696-12697.

[66] H. L. Zhang, H. Xia, H. L. Li, Z. F. Liu, *Chem. Lett.* **1997**, 721-722.

CHAPTER 2

2.1 Introduction

Functionalized AuNPs have demonstrated promising applications in biomedicine,[1] drug delivery and sensing technology[2] by introducing functionalities through interfacial chemistry. As previously described in Figure 1.10, our group has made significant efforts towards the synthesis of small water-soluble AuNP templates that can undergo click and bioorthogonal interfacial chemistry for post-synthetic modification of the gold core. Among all nanomaterials, AuNPs are often regarded as the most promising template for biomedical applications as they feature low toxicity, chemical stability, and high loading capacity because of high surface area-to-volume ratio. In addition, the optical and chemical properties of AuNPs can be tuned by varying the gold core diameter and composition of the ligand corona, respectively. Chapter 2 presents the synthesis of a novel *ortho*-naphthoquinone methide (oNQM) functionalized small AuNP template that can undergo light-induced Hetero-Diels-Alder cycloadditions[3] and reversible photochemical Michael addition[4] (Scheme 1.1). Popik *et al.* have extensively studied the photochemical properties of 3,5-dihydroxy-2-naphthoic acid[5] and demonstrated its use for the modification of surfaces[6] and proteins.[4] As described in Scheme 2.1, the introduction of oNQM functionality is achieved via place exchange onto methoxy terminated AuNPs which requires the synthesis of a thiol-modified NQMP ligand. Commercially available 3,7-dihydroxy-2-naphthoic acid was selected as the starting material in order to potentially minimize steric crowding within the ligand corona of the final AuNP. The synthetic protocol towards the NQMP modified ligand is described herein as well as the characterization of synthetic intermediates by ^{1}H NMR spectroscopy, ^{13}C NMR spectroscopy, IR spectroscopy and MS. The final ligand was also characterized by UV-Vis spectroscopy to investigate its photochemical properties. This interesting photochemical functional group was then successfully introduced onto a AuNP surface for the first time via a place exchange reaction. The resulting NQMP-functionalized AuNPs were characterized by ^{1}H NMR, IR and UV-Vis spectroscopy as well as TGA and TEM. This novel AuNP template expands the scope of the Workentin AuNP toolbox as a result of its versatile reactivity profile including reversible photochemical reactivity.

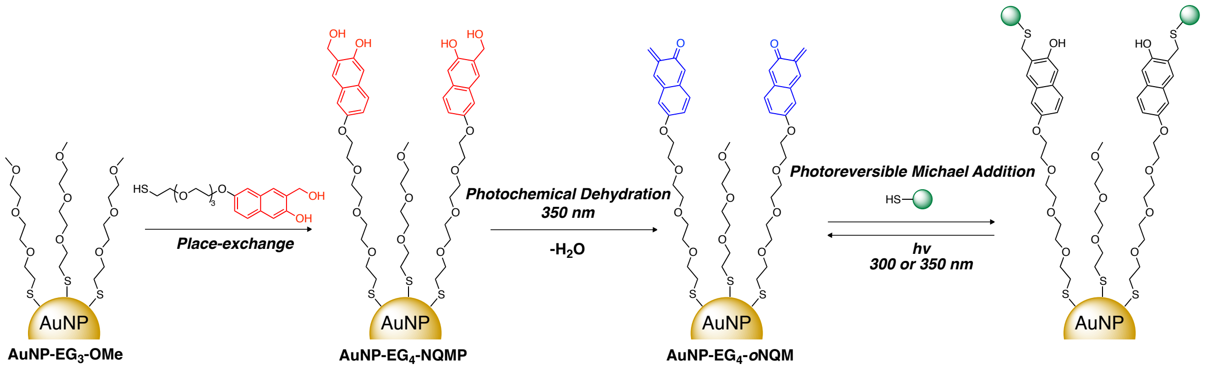

Scheme 2.1: Reprinted from Chapter 1. Synthetic strategy for synthesis of NQMP functionalized AuNPs and its proposed reactivity as a novel template.

2.2 Results and Discussion

2.2.1 Synthesis and Characterization of HS-EG$_4$-NQMP

The synthesis of the thiolated NQMP ligand is outlined in Scheme 2.2. First, tetraethylene glycol (compound **2.1**) was mono-tosylated (compound **2.2**) to provide a better leaving group for subsequent thioacetate substitution (compound **2.3)**. The hydroxyl functional group was then substituted with an iodine to give compound **2.4**. In parallel, the carboxylic acid of the starting material **2.5** was reduced to the corresponding primary alcohol. The resulting diol **2.6** was then protected with an acetonide protecting group to give compound **2.7**. In order to achieve higher yields, 4 Å molecular sieves were used to remove water and methanol formed during the reaction. The resulting compounds **2.4** and **2.7** were then refluxed under basic conditions to give the coupled intermediate **2.8**. The reaction sequence then involved cleavage of the acetonide protecting group to re-form the diol (compound **2.9**). Finally, the thiol functionality was formed by hydrolysis of the thioacetate protecting group to give the final ligand compound **2.10**. It is important to note that all synthetic procedures involving the photosensitive NQMP functionality were performed in the dark to minimize potential photoreactivity.

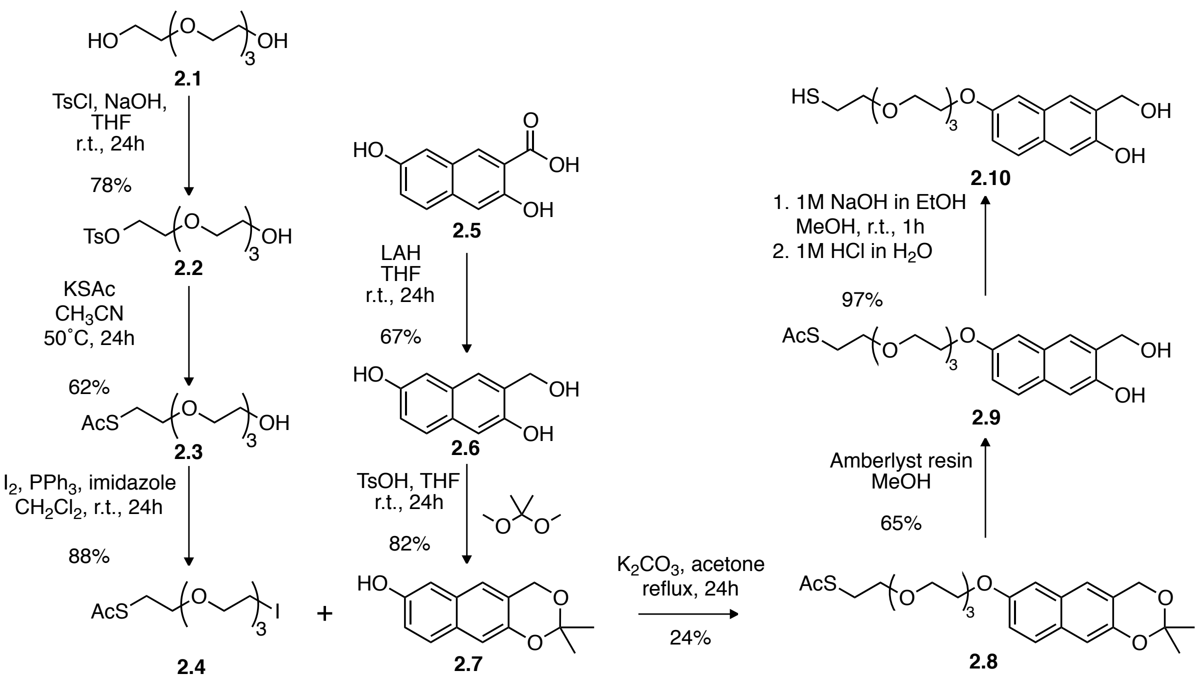
2.1
TsCl, NaOH, THF
r.t., 24h
78%
2.2
KSAc
CH3CN
50˚C, 24h
62%
2.3
I2, PPh3, imidazole
CH2Cl2, r.t., 24h
88%
2.4
2.5
LAH
THF
r.t., 24h
67%
2.6
TsOH, THF
r.t., 24h
82%
2.7
K2CO3, acetone
reflux, 24h
24%
2.8
Amberlyst resin
MeOH
65%
2.9
1. 1M NaOH in EtOH
MeOH, r.t., 1h
2. 1M HCl in H2O
97%
2.10

Scheme 2.2: Synthesis of HS-EG$_4$-NQMP.

The characterization of all compounds in Scheme 2.2 was completed with ^{1}H NMR, ^{13}C NMR and IR spectroscopy as well as mass spectrometry. The characterization of compound **2.2** was in agreement with previously reported data. Subsequent thioacetate substitution in compound **2.3** could be tracked by ^{1}H NMR spectroscopy through the appearance of a singlet at 2.34 ppm (3H) corresponding to the terminal methyl group. The ^{13}C NMR spectrum also revealed a carbonyl signal at 195.6 ppm. Following iodination to give compound **2.4**, the protons alpha to the iodine experienced an upfield shift to 3.27 ppm. The IR spectrum of compound **2.4** also revealed the disappearance of a large OH stretch. In parallel, 3,7-dihydroxy-naphthoic acid (compound **2.5**) was reduced to the corresponding primary alcohol to give compound **2.6** and fully characterized. The ^{1}H NMR spectrum showed five signals in the aromatic region in addition to a diagnostic singlet at 4.77 ppm corresponding to the benzylic protons. Although compound **2.6** has been previously synthesized through a different synthetic route,[7] it is still interesting to inspect the complex splitting pattern observed in the aromatic region. All five protons can be assigned by simply calculating the coupling constants and analyzing resonance structures (Figure 2.1). The doublet of doublets at 6.98 ppm (H_A) is the most interesting signal in the spectrum as it is easy to extract two coupling constants of different magnitudes. The larger coupling constant may be assigned to the $^3J_{A\text{-}C}$ interaction whereas the smaller coupling constant must therefore arise from the $^4J_{A\text{-}B}$ interaction. The remaining singlets can be assigned by resonance. H_E is shielded by resonance so consequently H_D must be the more downfield signal.

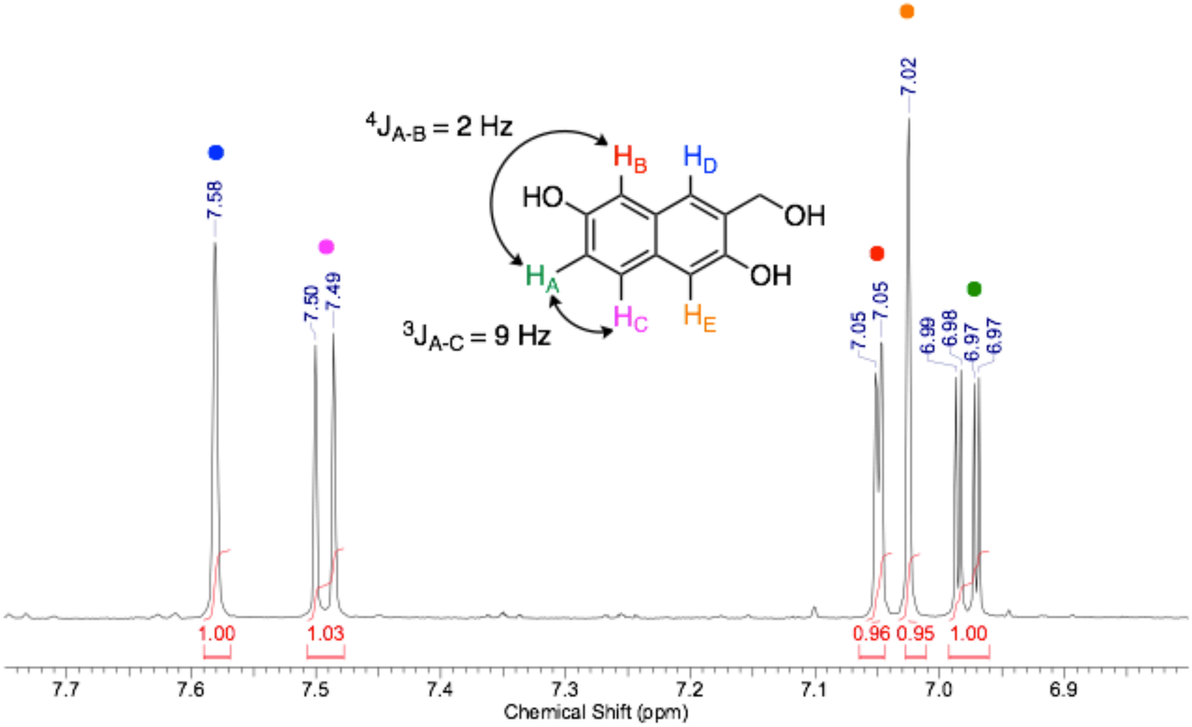

Figure 2.1: ^{1}H NMR spectrum of aromatic region of HO-NQMP.

The photosensitive diol in intermediate **2.6** was then protected with an acetonide protecting group by reaction with 2,2-dimethoxypropane in acetone. It is interesting to note that in the mechanism of this reaction, either the reagent or the solvent may be used to form the protecting group. To aid the progress of the reaction, 4 Å molecular sieves were added to remove excess water and methanol released during the reaction. The acetal could be characterized by the appearance of a large singlet at 1.54 ppm integrating to 6H. Compounds **2.5** and **2.7** were then coupled together through a substitution reaction to give compound **2.8**. In the ^{1}H NMR spectrum of compound **2.8**, the expected ethylene glycol and NQMP aromatic signals were observed. Once the thiol functionality was installed onto the NQMP, the acetal protecting group could be cleaved by treatment with an acidic Amberlyst resin to give compound **2.9** in good yield. Upon reformation of the diol, the chemical shift of the benzylic NQMP protons shifted upfield and the large singlet corresponding to the acetal protons disappeared. Finally, the thioacetate protecting group could be removed by treatment with base to give the final ligand **2.10**. It is important to note that in order to avoid formation of disulfide, the hydrolysis must be performed in the absence of oxygen. As a result, all reagents were carefully placed under a positive pressure of argon gas prior to reaction. The thiol **2.10** was successfully characterized by ^{1}H NMR spectroscopy by the disappearance of the terminal acetate signals as well as the appearance of a triplet at 1.58 ppm corresponding to the SH. The protons alpha to the thiol functionality are also diagnostic of the presence of a thiol as the signal is split into a doublet of triplets.

The synthesis of ligand **2.10** was also attempted using a trityl protecting group for the thiol but it was unsuccessful. The synthesis was carried through to the trityl analogue of compound **2.9** but it was not possible to isolate the thiol. All experimental results and spectral data are included in the Experimental and Appendix sections of this chapter.

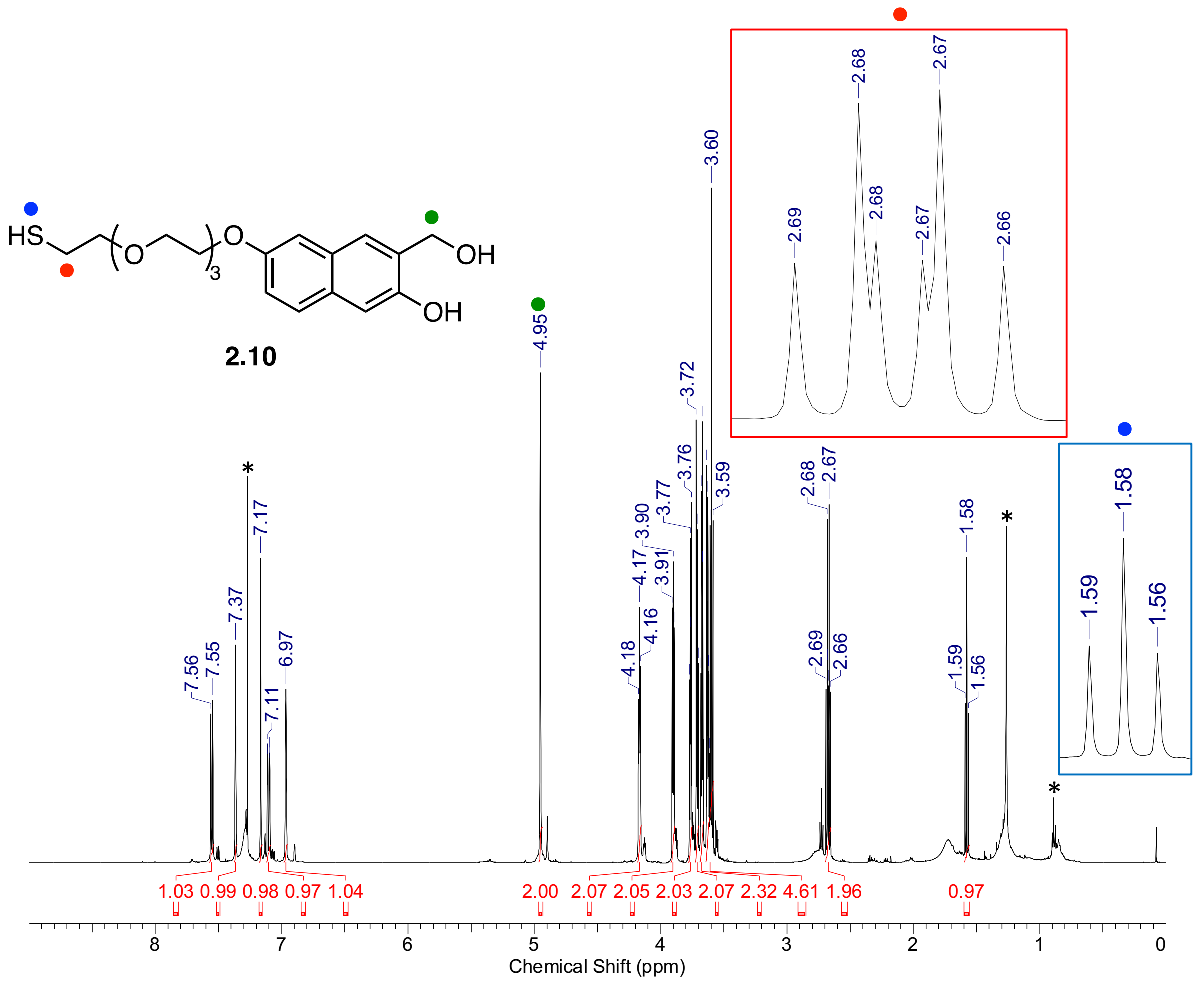

Figure 2.2: ^{1}H NMR spectrum of HS-EG$_4$-NQMP in CDCl$_3$. * denotes residual protonated solvent signals or solvent impurities.

Compound **2.10** was also characterized by IR spectroscopy (Figure 2.3). First, the thiol SH gave a very weak signal at 2550 cm^{-1}. Then in addition to the C_{sp3}-H stretch, the IR spectrum also revealed two broad signals above 3000 cm^{-1}, characteristic of OH stretches.

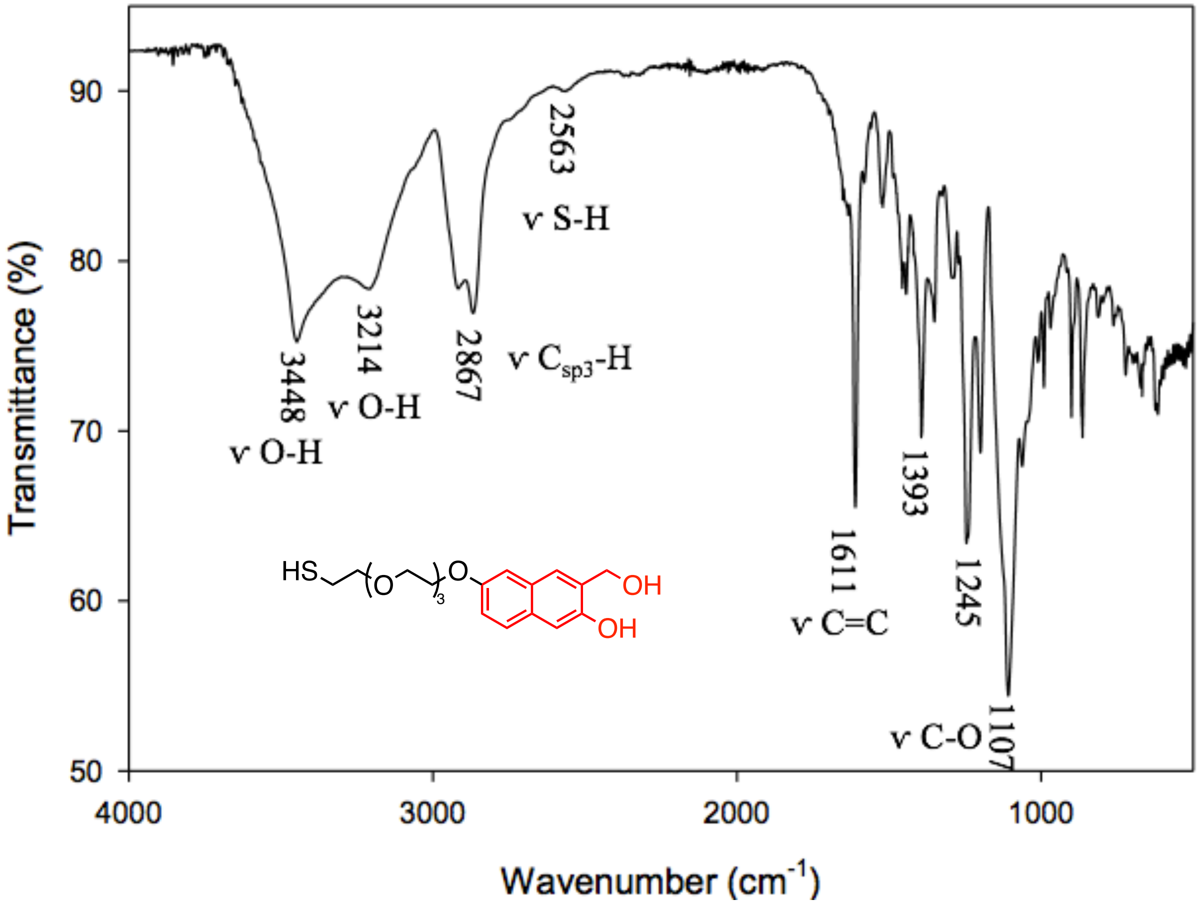

Figure 2.3: IR spectrum of HS-EG_4-NQMP.

2.2.2 Synthesis and Characterization of AuNP-EG_4-NQMP

AuNP-EG_4-NQMP were prepared through a place-exchange reaction of NQMP modified thiol **2.10** onto triethylene glycol monomethyl ether AuNPs (AuNP-EG_3-OMe) in CH_2Cl_2 at room temperature (Scheme 2.3). AuNP-EG_3-OMe were synthesized according to a protocol previously developed by our group to afford AuNPs with a gold core diameter of 3 ±1 nm as determined by TEM measurements.[8] The composition of the ethylene glycol ligand corona also provides both organic solvent and water solubility. In addition, these AuNPs are resistant to both acidic and basic conditions, can be heated to over 100 °C, and can be repeatedly dried and redissolved in solvent with little to no aggregation. As a result, they are very resilient substrates for further modification including place exchange and subsequent interfacial organic chemistry.

After 2 h of place exchange under vigorous stirring in the dark, the solvent was evaporated and the NQMP modified-AuNPs were purified from excess thiol by re-dissolving in ethyl ether (Et_2O) in which the AuNPs are not soluble. The supernatant containing excess thiols and disulfides was removed and the entire washing procedure was repeated six times overall to afford clean AuNP-EG_4-NQMP. These AuNPs were characterized by ^1H NMR, infrared (IR) and UV-Vis spectroscopy as well as by transmission electron microscopy (TEM) and thermogravimetric analysis (TGA).

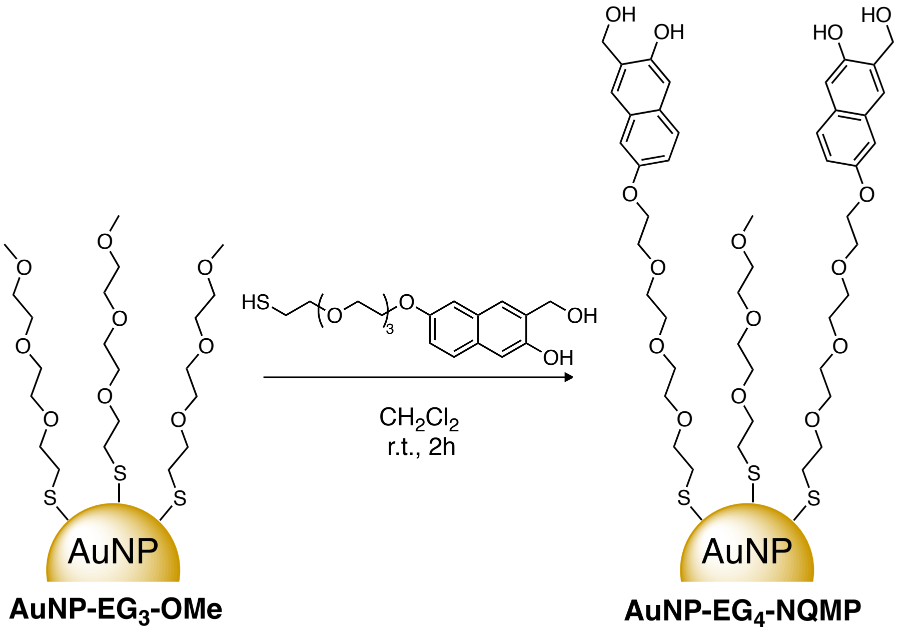

Scheme 2.3: Place exchange of ethylene glycol monomethyl ether AuNPs to NQMP functionalized AuNPs.

The ^1H NMR spectrum of AuNP-EG_4-NQMP showed the presence of broad peaks corresponding to incorporation of NQMP thiol ligand **2.10** as well as the triethylene glycol monomethyl ether ligand (Figure 2.4). As previously described in Chapter 1, the broadening of signals in the ^1H NMR spectrum is commonly observed in AuNP surface analysis by NMR spectroscopy. The ^1H NMR spectrum of AuNP-EG_4-NQMP also indicates that the washing procedure was effective in removing unbound thiols and disulfides as there are no sharp signals present. After only three washes with Et_2O, the ^1H NMR spectrum revealed sharp signals overlaying the broad signals so a total of six washes were required to completely remove excess thiol. It is worth noting that the removal of unbound thiols is important in successfully synthesizing oNQM functionalized AuNPs as any remaining thiol could undergo nucleophilic attack of the Michael acceptor following the photochemical dehydration step. This would result in a loss of control over the desired reactivity. Comparison of ^{1}H NMR spectra of thiol **2.10** and AuNP-EG$_4$-NQMP showed good correspondence of peaks at 7.55, 7.13, 4.91, 4.17 ppm, which confirmed successful synthesis of AuNP-EG$_4$-NQMP. In particular, the signal at 4.91 ppm corresponding to the benzylic protons of NQMP is well-resolved diagnostic of successful NQMP introduction.

The approximate amount of NQMP ligand incorporated after place exchange may also be calculated from the ^{1}H NMR spectrum. Aside from the methylene protons that produce a broad signal at approximately 3.62 ppm, the characteristic peak of AuNP-EG$_3$-OMe is at 3.36 ppm corresponding to the terminal methoxy group. In the ^{1}H NMR spectrum of AuNP-EG$_4$-NQMP, by setting the integral at 3.36 ppm (-OCH$_3$) to 100 and then integrating the signal at 4.91 ppm (-CH$_2$-OH) it is possible to determine the relative amount of NQMP modified ligand vs. triethylene glycol monomethyl ether ligand as follows:

$$Integral\ of\ 3.36\ ppm\ signal\ (-OCH_3) = 100$$
$$Integral\ of\ 4.91\ ppm\ signal\ (-CH_2) = 22$$

Therefore,

$$\frac{100\ (integral\ of\ 3.36\ ppm\ signal)}{3\ (-OCH_3)} \approx 33$$
$$and$$
$$\frac{22\ (integral\ of\ 4.91\ ppm\ signal)}{2\ (-CH_2)} \approx 11$$

Under the reaction conditions used for the place exchange reaction, the ratio of OMe terminated ligand to NQMP functionalized ligand is 3:1 or approximately 25% NQMP incorporation.

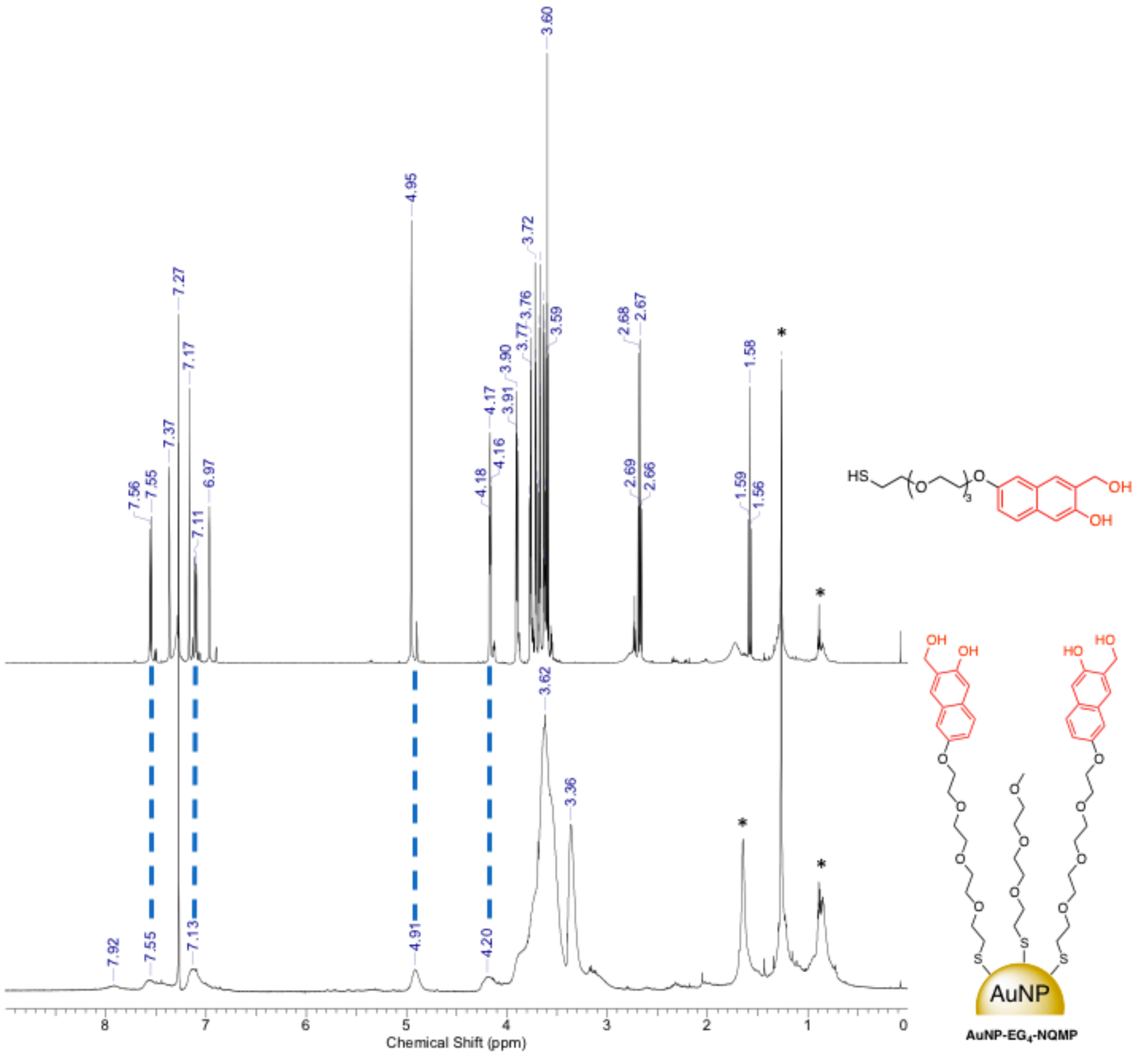

Figure 2.4: ^{1}H NMR spectra of HS-EG$_4$-NQMP (top) and AuNP-EG$_4$-NQMP (bottom) in CDCl$_3$. The absence of sharp signals in the bottom spectrum indicates that no free ligand is present. * denotes residual protonated solvent signals or solvent impurities.

The IR spectrum of AuNP-EG$_4$-NQMP revealed a broad OH stretch at 3362 cm^{-1} corresponding to the two hydroxyl functional groups in the NQMP functionality as described in Figure 2.3. In comparison to the IR spectrum of AuNP-EG$_3$-OMe in Figure 2.5, it is clear that the ligand **2.10** was successfully incorporated onto the AuNP surface.

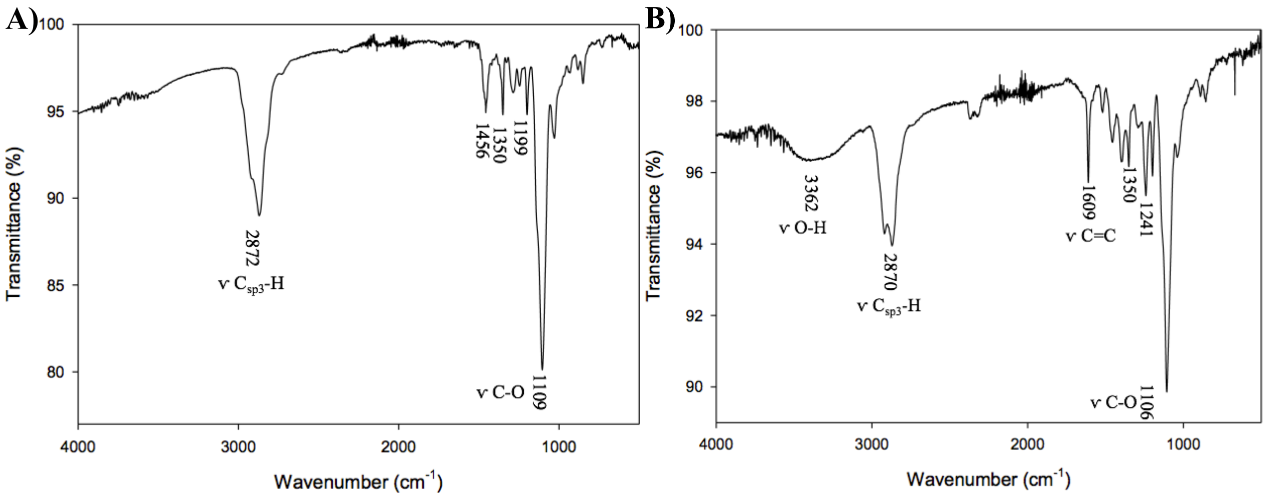

Figure 2.5: IR of AuNP-EG$_3$-OMe (A) and AuNP-EG$_4$-NQMP (B).

The UV-Vis spectrum of HS-EG$_4$-NQMP was also in agreement with previously reported results.[4] The 3-hydroxy-2-naphthalenemethanol chromophore has two major absorption bands in the UV region at $\lambda_{max} = 275\, nm$ and $\lambda_{max} = 324\, nm$. The introduction of an alkoxy substituent at the 7-position of the chromophore (compound **1.10**) resulted in a shift for both bands to $\lambda_{max} = 260\, nm$ and $\lambda_{max} = 342\, nm$. Successful incorporation of NQMP onto the AuNP surface could also be characterized by UV-Vis spectroscopy as described in Figure 2.6. In comparison to the UV-Vis absorption trace of AuNP-EG$_3$-OMe, the NQMP functionalized AuNPs exhibited absorbance at similar wavelengths as the free ligand **2.10**. As a result, the AuNP-EG$_4$-NQMP template is suitable for activation to AuNP-EG$_4$-oNQM by irradiation using a 350 nm fluorescent lamp.

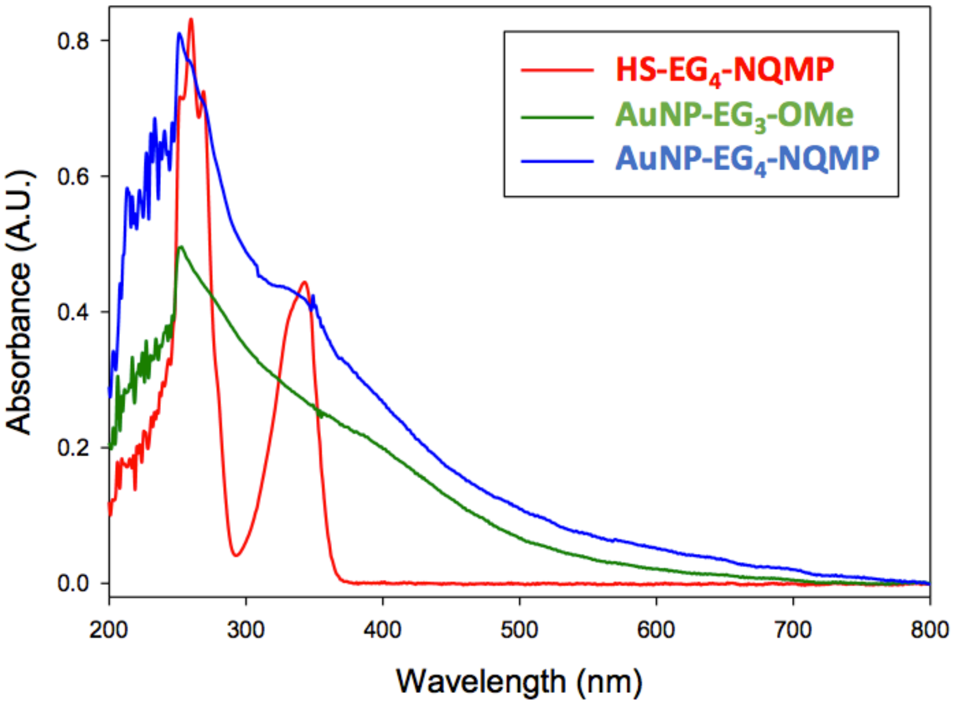

Figure 2.6: UV-Vis absorption spectra of HS-EG_4-NQMP ligand, methoxy terminated AuNPs and NQMP modified AuNPs in CH_3OH at different concentrations.

Thermogravimetric analysis of AuNP-EG_4-NQMP showed an overall 39.7% mass loss corresponding to the organic corona of the AuNPs, i.e. MeO-EG_3-S- and NQMP-EG_4-S- (Figure 2.7, left). In addition, the derivative of the TGA curve showed that there are two ligands present that decompose at distinctly different temperatures (Figure 2.7, right). As in previously reported systems by our group, the MeO-EG_3-S- ligand decomposes at 280 °C.[8] Therefore, the component at 380 °C was assigned to the NQMP-EG_4-S- ligand. By integrating the area under each curve in the derivative plot, it is also possible to determine the relative amounts of each ligand present. Through conversion to a molar ratio, it was found that under the reaction conditions used for the place exchange reaction (see Experimental), the AuNP surface was made up of approximately 20% of the NQMP ligand. This value is in close agreement in comparison to the value previously determined by ^{1}H NMR analysis. The amount of ligand incorporated onto the AuNP surface may be improved by increasing the of ratio thiol to gold used as well as increasing the reaction time. Conversely, decreasing the ratio of thiol to gold or decreasing the reaction time would decrease the relative amount of NQMP ligand introduced to the AuNP surface. Further investigations into the place exchange reaction of this AuNP system would enable for tuning of the solubility properties.

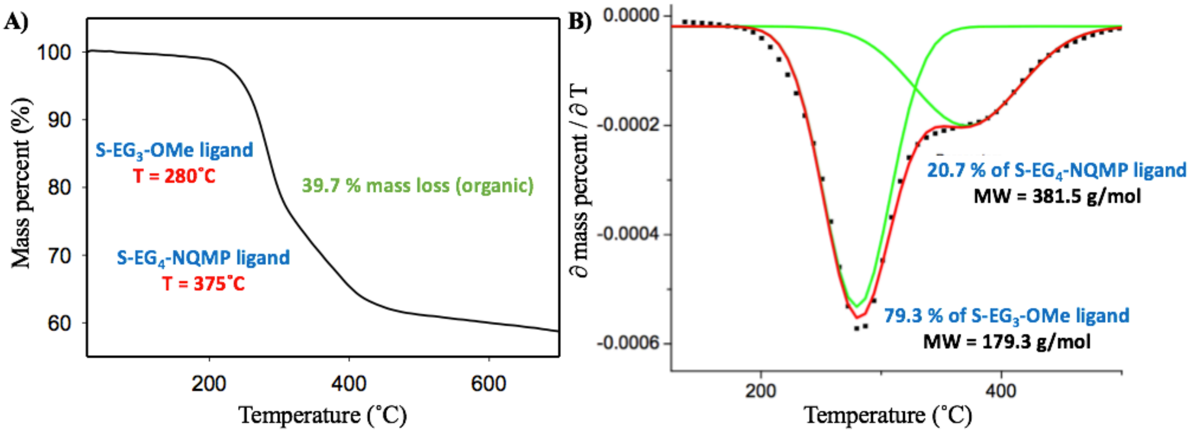

Figure 2.7: (A) TGA plot (B) Derivative plot (dotted black line) of AuNP-EG$_4$-NQMP. The green traces represent the fitted peaks and the red trace represents the sum of the fitted peaks.

The TEM analysis of AuNP-EG$_4$-NQMP compared to AuNP-EG$_3$-OMe also showed no significant change in regards to the size or shape of the gold core following the place exchange reaction. As seen in Figure 2.8, there does not appear to be any significant difference between images of AuNP-EG$_3$-OMe and AuNP-EG$_4$-NQMP. This is an indication that the NQMP functionalized nanoparticles are stable and do not aggregate under the reaction conditions used.

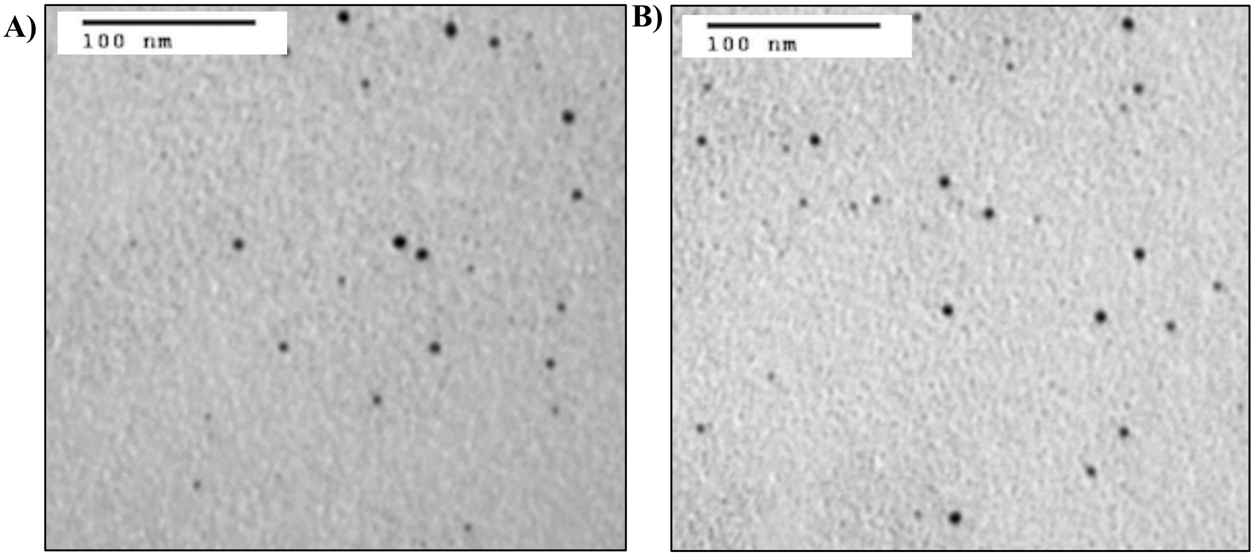

Figure 2.8: TEM images of AuNP-EG$_3$-OMe (A) and AuNP-EG$_4$-NQMP (B). The scale bar is indicated in each image.

2.3 Conclusion

The goal of the work presented in Chapter 2 was to expand the scope of the Workentin AuNP toolbox (Figure 1.12) by the addition of a photoreversible click reaction. A thiolated NQMP ligand with a tetra(ethylene glycol) spacer was synthesized through a selective deprotection strategy in good yield. All synthetic intermediates were characterized by NMR and IR spectroscopy as well as MS. The novel ligand was then introduced onto a small AuNP surface through a place exchange reaction with methoxy terminated AuNPs. The novel NQMP functionalized AuNPs were then characterized by ^{1}H NMR and IR spectroscopy as well as TGA and TEM. The amount of NQMP-modified ligand incorporated under the place exchange reaction conditions used within the ligand corona was also determined to be approximately 20%. Finally, the photochemical properties of this novel template were investigated by UV-Vis spectroscopy. The UV-Vis absorption spectrum revealed absorption maxima at 260 nm and 342 nm that are suitable for photochemical dehydration to the corresponding oNQM functionality by UV irradiation. Therefore, the next steps are to investigate the photochemistry of this novel system towards Diels-Alder cycloaddition and Michael addition substrates. In addition, the photochemical reversibility of this novel template can be explored. In the reaction between a thiol and oNQM, the resulting thioether linkage is stable under ambient conditions but can be cleaved by UV irradiation to regenerate the thiol. This interesting feature allows for the design of photochemically triggered delivery systems.

2.4 Experimental

Materials and Methods

All reagents used were obtained from commercially available sources and used without further purification. 3,7-Dihydroxynapthoic acid, lithium aluminum hydride (LAH), 2,2-dimethoxypropane, *p*-toluenesulfonic acid, tetra(ethylene glycol), *p*-toluenesulfonyl chloride, potassium thioacetate, imidazole, triphenylphosphines, potassium carbonate, Amberlyst 15 hydrogen form wet and 4 Å molecular sieves were purchased from Sigma Aldrich. Iodine was purchased from Alfa Aesar. All common dry solvents were obtained from Caledon. Solvents were dried using an Innovative Technologies solvent purification system, collected under vacuum, and stored under an argon atmosphere over 4 Å molecular sieves.

^{1}H NMR spectra were recorded on a Varian Inova 600 MHz spectrometer and ^{13}C spectra were recorded on a Mercury 400 MHz spectrometer**.** ^{1}H NMR spectra are reported as δ in units of parts per million (ppm) relative to residual chloroform proton (δ 7.27, s). Multiplicities are reported as follows: s (singlet), d (doublet), t (triplet), q (quartet), quin (quintuplet), dd (doublet of doublets), m (multiplet), and bs (broad signal). Coupling constants are reported as *J* values in Hertz (Hz). The number of protons (*n*) for a given resonance is indicated as *n*H, and is based on spectral integration values. ^{13}C NMR spectra are reported as δ in units of parts per million (ppm) relative to $CDCl_3$ (δ 77.0, t)**.** Spectra were analyzed using ACD/SpecManager software v11.01. The spectra were baselined and integrated manually.

Mass spectrometry data were recorded in positive-ion mode with a Bruker micOTOF II instrument using electrospray ionization or other ionization techniques as described.

Transmission electron microscopy (TEM) images were recorded from a TEM Philips CM10 microscope. The TEM grids (Formvar carbon film on 400 mesh copper grids) were purchased from Electron Microscopy Sciences and prepared by dropcasting a drop of nanoparticles solution directly onto the grid surface. The drop was then carefully removed after 30 s with a soft tissue.

UV-Visible spectra were recorded using a Varian Cary 100 bio spectrometer and 1 mm plastic cuvettes. The nanoparticle samples were dissolved in distilled methanol. The background was automatically subtracted from each spectrum.

FT-IR spectra were recorded using a PerkinElmer Spectrum Two FT-IR spectrometer using an attenuated total reflectance accessory. The background was subtracted from each spectrum.

Synthesis of HO-NQMP

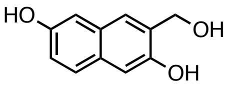

Lithium aluminum hydride (0.16 g, 4.2 mmol) was suspended in anhydrous THF (25 mL) under argon atmosphere then 3,7-dihydroxynaphthoic acid (0.45 g, 2.1 mmol) dissolved in anhydrous THF (10 mL) was added dropwise with vigorous stirring. The reaction was stirred at room temperature for 3 h, quenched with 10% $HCl_{(aq)}$, filtered and extracted with Et_2O. The organic layer was washed with brine (3 x 10 mL), dried with Na_2SO_4, filtered and concentrated under vacuum to give the product as a light yellow solid (0.26 g, 67% yield). ^{1}H NMR (600 MHz, CD_3OD): δ 7.56 (s, 1H), 7.48 (d, J = 8.7 Hz, 1H), 7.03 (d, J = 2.3 Hz, 1H), 7.01 (s, 1H), 6.96 (dd, J = 8.8 Hz, 2.4 Hz, 1H), 4.77 (s, 2H). $^{13}C\{^1H\}$ NMR (75 MHz, CD_3OD): δ 154.3, 152.7, 131.9, 131.1, 130.5, 128.3, 126.1, 119.2, 110.3, 110.0, 61.7. EI-HRMS: Calculated for $C_{11}H_{10}O_3^+$ $[M]^+$: 190.0630, found 190.0632.

Synthesis of HO-NQMP-pt

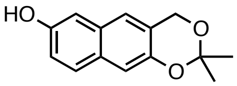

2,2-Dimethoxypropane (1.5 mL, 12 mmol) and a catalytic amount of TsOH (100 mg) were added to a solution of HO-NQMP (0.65 g, 3.4 mmol) dissolved in acetone (50 mL) with 4 Å molecular sieves. The reaction mixture was stirred overnight at room temperature. The solvent was removed under vacuum and the crude reaction mixture was purified by silica gel column chromatography using EtOAc/hexane (1:1) to give the product as a white solid (0.64 g, 82% yield). ^{1}H NMR (600 MHz, CD_3OD): δ 7.55 (d, J = 8.7 Hz, 1H), 7.32 (s, 1H), 7.07 (s, 1H), 7.00-6.98 (m, 2H), 5.02 (s, 2H), 1.54 (s, 6H). $^{13}C\{^1H\}$ NMR (75 MHz, CD_3OD): δ 155.0, 149.1, 131.5, 130.2, 129.1, 123.1, 122.9, 119.8, 112.8, 109.6, 100.9, 62.3, 25.4. IR (cm^{-1}): 3369, 3002, 2926, 2856, 1615, 1523, 1392, 1355, 1253, 1216, 1195, 1110, 1040, 896, 873, 821, 809, 751. EI-HRMS: Calculated for $C_{14}H_{14}O_3^+$ $[M]^+$: 230.0943, found 230.0942.

Synthesis of TsO-EG$_4$-OH

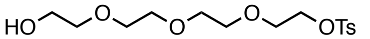

To a solution of tetraethylene glycol (100 mL, 0.579 mol) in THF (150 mL) was added NaOH (3.4 g dissolved in 10 mL H_2O) and the reaction mixture was stirred vigorously for 15 min. At 0°C, *p*-toluenesulfonyl chloride (10.5 g, 0.061 mol) was then slowly added to give a yellow solution. The reaction was left overnight at room temperature then H_2O (150 mL) was added. The reaction mixture was then extracted with CH_2Cl_2 (3 x 80 mL), dried over Na_2SO_4, filtered and concentrated under vacuum to give the mono-tosylated product as a yellow oil (16.57 g, 78% yield). ^{1}H NMR (600 MHz, $CDCl_3$): δ 7.81 (d, J = 12 Hz, 2H), 7.35 (d, J = 12 Hz, 2H), 4.17 (t, J = 6 Hz, 2H), 3.73-3.60 (m, 14H), 2.45 (s, 3H). $^{13}C\{^1H\}$ NMR (75 MHz, $CDCl_3$): δ 144.7, 132.8, 129.7, 127.8, 72.4, 70.6, 70.5, 70.3, 70.2, 69.2, 68.6, 21.5. IR (cm^{-1}): 3440, 2871, 1598, 1452, 1351, 1175, 1096, 1012, 918, 816, 774, 662, 553. CI-HRMS: Calculated for $C_{15}H_{24}O_7S^+$ $[M+1]^+$: 348.1243, found 348.1242.

Synthesis of AcS-EG$_4$-OH

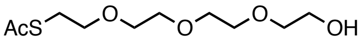

Under argon atmosphere, to a solution of TsO-EG$_4$-OH (7.37 g, 21.1 mmol) dissolved in dry CH_3CN (100 mL) was added KSAc (3.03 g, 26.5 mmol) to give a cloudy white solution. The reaction mixture was stirred overnight at 50°C to give a yellow precipitate. The solution was filtered, concentrated under vacuum then purified by column chromatography using EtOAc to give the product as a light yellow oil (3.3091 g, 62 % yield). ^{1}H NMR (600 MHz, $CDCl_3$): δ 3.74-3.73 (m, 2H), 3.68-3.60 (m, 12H), 3.10 (t, J = 6.4 Hz, 2H), 2.34 (s, 3H). $^{13}C\{^1H\}$ NMR (75 MHz, $CDCl_3$): δ 195.6, 72.5, 70.7, 70.5, 70.4, 70.3, 69.8, 61.8, 30.6, 28.8. IR (cm^{-1}): 3430, 2868, 1688, 1354, 1097, 952, 886, 625. CI-HRMS: Calculated for $C_{10}H_{20}O_5S^+$ $[M+H]^+$: 253.1104, found 253.1108.

Synthesis of AcS-EG$_4$-I

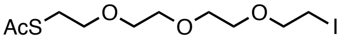

To a solution of AcS-EG$_4$-OH (1.62 g, 6.42 mmol) dissolved in CH_2Cl_2 (60 mL) was sequentially added PPh_3 (2.1694 g, 8.27 mmol), I_2 (2.1102 g, 8.31 mmol) then imidazole (0.565 g, 8.30 mmol) to give a yellow-orange solution. The reaction mixture was left overnight to give a cloudy yellow solution. The reaction mixture was quenched with 10% aqueous $NaHSO_3$ (20 mL) to give a clear solution, extracted with CH_2Cl_2 (3 x 50 mL), dried with Na_2SO_4 and filtered. The resulting white solid was suspended in pentane (100 mL) and stirred for 45 minutes then filtered. The filtrate was evaporated and purified by silica gel column chromatography using EtOAc to give the iodinated product as a light yellow oil (2.0365 g, 88% yield). ^{1}H NMR (600 MHz, $CDCl_3$): δ 3.77 (t, J = 7.0 Hz, 2H), 3.67-3.60 (m, 10H), 3.27 (t, J = 7.0 Hz, 2H), 3.11 (t, J = 6.4 Hz, 2H), 2.35 (s, 3H). $^{13}C\{^1H\}$ NMR (75 MHz, $CDCl_3$): δ 195.5, 72.0, 70.7, 70.6, 70.3, 70.2, 69.8, 30.6, 28.8, 2.9. IR (cm^{-1}): 2866, 1688, 1352, 1100, 1034, 954, 625. CI-HRMS: Calculated for $C_{10}H_{19}IO_5S^+$ $[M+H]^+$: 363.0121, found 363.0116.

Synthesis of AcS-EG$_4$-NQMP-pt

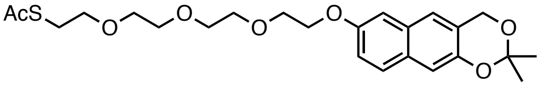

To a solution of HO-NQMP-pt (0.274 g, 0.119 mmol) dissolved in acetone (15 mL) was added K_2CO_3 (0.420 g, 0.30 mmol) followed by AcS-EG$_4$-I (0.520 g, 0.143 mmol). The reaction mixture was refluxed overnight then the solvent was removed under reduced pressure and re-dissolved in ethyl ether (100 mL), washed with brine (3 x 50 mL), dried with Na_2SO_4, filtered and concentrated under vacuum. The crude mixture was purified by silica gel column chromatography using hexanes/EtOAc (1:1) to give the desired product as a light yellow oil (130 mg, 24% yield). ^{1}H NMR (600 MHz, $CDCl_3$): δ 7.59 (d, 8.8 Hz, 1H), 7.34 (s, 1H), 7.16 (s, 1H), 7.12 (dd, J = 8.8 Hz, 2.4 Hz, 1H), 7.03 (d, J = 2.3 Hz, 1H), 5.05 (s, 2H), 4.21 (t, J = 5.3 Hz, 2H), 3.92 (t, J = 5.2 Hz, 2H), 3.77-3.75 (m, 2H), 3.71-3.69 (m, 2H), 3.67-3.65 (m, 4H), 3.63-3.61 (m, 2H), 3.10-3.08 (m, 2H), 2.32 (s, 3H), 1.59 (s, 6H). $^{13}C\{^1H\}$ NMR (75 MHz, $CDCl_3$): δ 195.5, 155.4, 148.1, 129.23, 129.18, 128.0, 122.1, 121.5, 119.3, 112.0, 106.2, 99.6, 70.8, 70.7, 70.5, 70.3, 69.8, 69.7, 67.4, 61.2, 30.5, 28.8, 24.9. IR (cm^{-1}): 2938, 2867, 1739, 1690, 1614, 1512, 1349, 1257, 1201, 1116, 959, 886, 628. EI-HRMS: Calculated for $C_{24}H_{32}O_7S^+$ $[M]^+$: 464.1869, found 464.1863.

Synthesis of AcS-EG$_4$-NQMP

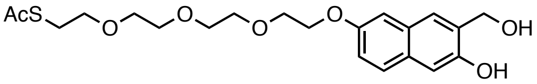

To a solution of AcS-EG$_4$-NQMP-pt (125 mg, 0.27 mmol) dissolved in CH_3OH (5 mL) was added Amberlyst resin (200 mg) and stirred for 2 h. The resin was removed by filtration with a cotton plug then the solvent was removed under reduced pressure and the reaction mixture was purified by silica gel column chromatography using EtOAc/hexanes (3:1) to give the diol as a white solid (74 mg, 65% yield). ^{1}H NMR (600 MHz, $CDCl_3$): δ 7.55 (d, J = 8.8 Hz, 1H), 7.35 (s, 1H), 7.35 (s, 1H), 7.16 (s, 1H), 7.10 (dd, J = 8.8 Hz, 2.3 Hz, 1H), 6.96 (d, J = 2.3 Hz, 1H), 4.94 (s, 2H), 4.17-4.16 (m, 2H), 3.90-3.89 (m, 2H), 3.77-3.75 (m, 2H), 3.71-3.69 (m, 2H), 3.66-3.64 (m, 2H), 3.62-3.60 (m, 2H), 3.57 (t, J = 6.4 Hz, 2H), 3.06 (t, J = 6.5 Hz, 2H), 2.87 (s, 1H), 2.31 (s, 3H). $^{13}C\{^1H\}$ NMR (75 MHz, $CDCl_3$): δ 195.8, 155.2, 152.3, 129.9, 129.0, 127.8, 127.6, 125.9, 119.3, 111.0, 107.0, 70.8, 70.7, 70.5, 70.3, 69.8, 69.7, 67.4, 64.5, 30.5, 28.8. EI-HRMS: Calculated for $C_{21}H_{28}O_7S^+$ $[M]^+$: 424.1556, found 424.1544.

Synthesis of HS-EG$_4$-NQMP

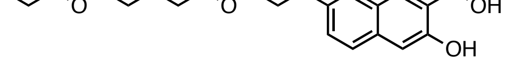

In the reaction flask, AcS-EG$_4$-NQMP-pt (74 mg, 0.17 mmol) was dissolved in CH_3OH (10 mL) and purged with argon for 30 min. In separate flasks, 0.85 mL of 1 M NaOH in EtOH and 1.7 mL of 1 M HCl in H_2O were also purged with argon for 30 min. The base was added to the reaction flask first and let stir for 1 h then the acid was added and stirred for 15 min. The thiol was then extracted using CH_2Cl_2 (3 x 10 mL). The resulting organic solution was then dried with

Na_2SO_4, filtered and concentrated under reduced pressure to give the thiol as a white solid (63 mg, 97% yield). ^1H NMR (600 MHz, $CDCl_3$): δ 7.55 (d, J = 8.8 Hz, 1H), 7.37 (s, 1H), 7.17 (s, 1H), 7.12 (dd, J = 8.8 Hz, 2.3 Hz, 1H), 6.93 (d, J = 2.3 Hz, 1H), 4.95 (s, 2H), 4.18-4.16 (m, 2H), 3.91-3.89 (m, 2H), 3.77-3.75 (m, 2H), 3.72-3.70 (m, 2H), 3.69-3.67 (m, 2H), 3.64-3.60 (m, 4H), 2.68 (dq, J = 8.2 Hz, J = 6.4 Hz, 2H), 1.58 (t, J = 8.2 Hz, 1H). $^{13}C\{^1H\}$ NMR (75 MHz, $CDCl_3$): δ 155.2, 152.3, 129.9, 129.1, 127.8, 127.7, 125.9, 119.4, 111.0, 107.0, 72.9, 70.8, 70.7, 70.6, 70.2, 69.8, 67.4, 64.5, 24.2. IR (cm^{-1}): 3448, 3214, 2867, 1611, 1394, 1245, 1200, 1107, 990, 863. EI-HRMS: Calculated for $C_{19}H_{26}O_5S^+$ $[M]^+$: 382.1450, found 382.1452.

Synthesis of TrS-EG$_4$-OH

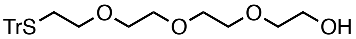

To a solution of triphenylmethanethiol (4.02 g, 14.5 mmol) dissolved in a EtOH/benzene (1:1, 30 mL) was added NaOH (0.90 g, 23 mmol) dissolved in H_2O (8 mL). TsO-EG$_4$-OH (5.02 g, 14.4 mmol) was also dissolved in EtOH/benzene (1:1, 30 mL) and added to the reaction mixture and let stir overnight. The reaction mixture was then washed with aqueous $NaHCO_3$ (3 x 30 mL), brine (3 x 30 mL), dried with Na_2SO_4, filtered and concentrated under vacuum. The crude mixture was purified by silica gel column chromatography using hexane/EtOAc (1:1) to give the product as a clear and colorless oil (5.09 g, 77% yield). ^1H NMR (600 MHz, $CDCl_3$): δ 7.43 (d, J = 12 Hz, 6H), 7.29 (t, J = 12 Hz, 6H), 7.22 (t, J = 12 Hz, 3H), 3.73-3.70 (t, J = 6 Hz, 2H), 3.66-3.58 (m, 8H), 3.48-3.45 (m, 2H), 3.31 (t, J = 6Hz, 2H), 2.45 (t, J = 6 Hz, 2H). $^{13}C\{^1H\}$ NMR (75 MHz, $CDCl_3$): δ 144.8, 129.6, 127.9, 126.6, 72.4, 70.6, 70.4, 70.3, 70.1, 69.6, 66.6, 61.8, 31.6. IR (cm^{-1}): 3453, 3065, 2922, 2866, 1488, 1444, 1100, 743, 700. ESI-HRMS: Calculated for $C_{27}H_{32}O_4S^+$ $[M+Na]^+$: 475.1914, found 475.1914.

Synthesis of TrS-EG$_4$-I

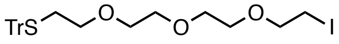

To a solution of TrS-EG$_4$-OH (0.48 g, 1.1 mmol) dissolved in CH_2Cl_2 (20 mL) was sequentially added PPh_3 (0.38 g, 1.4 mmol), I_2 (0.360 g, 1.4 mmol) then imidazole (0.116 g, 1.7 mmol) to give a yellow-orange solution. The reaction mixture was left overnight to give a cloudy white solution. The reaction mixture was quenched with 10% aqueous $NaHSO_3$ (20 mL) to give a clear solution, extracted with CH_2Cl_2 (3 x 50 mL), dried with Na_2SO_4 and filtered. The resulting white solid was suspended in pentane (100 mL) and stirred for 45 minutes then filtered. The volatile components of the filtrate were evaporated then the crude mixture was purified by silica gel column chromatography using hexane/EtOAc (2:1) to give the iodinated product as a light yellow oil (452 mg, 75% yield). ^{1}H NMR (600 MHz, CDCl$_3$): δ 7.44 (d, J = 12 Hz, 6H), 7.29 (t, J = 12 Hz, 6H), 7.22 (t, J = 12 Hz, 3H), 3.74 (t, J = 6 Hz, 2H), 3.64 (m, 4H), 3.61-3.58 (m, 2H), 3.49-3.46 (m, 2H), 3.32 (t, J = 6 Hz, 2H), 3.24 (t, J = 6 Hz, 2H), 2.46 (t, J = 6 Hz, 2H). ^{13}C{^{1}H} NMR (75 MHz, CDCl$_3$): δ 144.7, 129.5, 127.8, 126.5, 71.9, 70.5, 70.4, 70.1, 70.0, 69.5, 66.5, 31.6, 3.00. IR (cm^{-1}): 3054, 2922, 2864, 1597, 1488, 1443, 1106, 1034, 743, 700. ESI-HRMS: Calculated for $C_{27}H_{31}IO_3S^+$ [M+Na]$^+$: 585.0931, found 585.0941.

Synthesis of TrS-EG$_4$-NQMP-pt

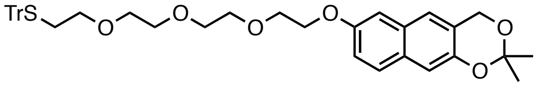

To a solution of HO-NQMP-pt (0.101 g, 0.44 mmol) in acetone (15 mL) was added K$_2$CO$_3$ (0.138 g, 1.1 mmol) followed by TrS-EG$_4$-I (0.273 g, 0.49 mmol). The reaction mixture was refluxed overnight then the solvent was removed under reduced pressure and re-dissolved in ethyl ether (100 mL), washed with brine (3 x 50 mL), dried with Na$_2$SO$_4$, filtered and concentrated under vacuum. The crude mixture was purified by silica gel column chromatography using hexanes/EtOAc (3:2) to give the desired product as a light yellow oil (130 mg, 44% yield). ^{1}H NMR (600 MHz, CDCl$_3$): δ 7.59 (d, J = 8.7 Hz, 1H), 7.44 (d, J = 7.6 Hz, 6H), 7.33 (s, 1H), 7.28 (t, J = 7.6 Hz, 6H), 7.21 (t, J = 7.6 Hz, 3H), 7.18 (s, 1H), 7.12 (dd, J = 8.7 Hz, 2.3 Hz, 1H), 7.02 (d, J = 2.3 Hz), 5.02 (s, 2H), 4.21 (t, J = 7.0 Hz, 2H), 3.90 (t, J = 7.0 Hz, 2H), 3.75-3.74 (m, 2H), 3.69-3.67 (m, 2H), 3.61-3.60 (m, 2H), 3.48-3.47 (m, 2H), 3.33 (t, J = 7.0 Hz, 2H), 2.46 (t, J = 7.0 Hz, 2H), 1.61 (s, 6H). ^{13}C{^{1}H} NMR (75 MHz, CDCl$_3$): δ155.4, 148.1, 144.8, 129.6, 129.3, 129.2, 128.0, 127.9, 126.6, 122.1, 121.5, 119.3, 112.0, 106.3, 99.6, 70.8, 70.7, 70.2, 69.8, 69.6, 67.4, 66.6, 61.2, 31.7, 25.0. IR (cm^{-1}): 3057, 1991, 2922, 2965, 1613, 1512, 1488, 1444, 1372, 1348, 1246, 1257, 1136, 1116, 959, 885, 744, 702. ESI-HRMS: Calculated for $C_{41}H_{44}O_6S^+$ [M+Na]$^+$: 687.2756, found 687.2776.

Synthesis of TrS-EG$_4$-NQMP

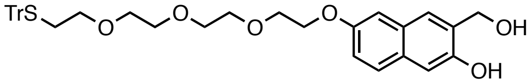

To a solution of TrS-EG$_4$-NQMP-pt (0.318 g, 0.48 mmol) dissolved in CH$_3$OH (5 mL) was added Amberlyst resin (600 mg) and stirred for 2 h. The resin was removed by filtration with a cotton plug then the solvent was removed under reduced pressure and the reaction mixture was purified by silica gel column chromatography using EtOAc/hexanes (2:1) to give the diol as a white solid (0.23 g, 77% yield). ^{1}H NMR (600 MHz, $CDCl_3$): δ 7.53 (d, J = 8.7 Hz, 1H), 7.41 (d, J = 7.6 Hz, 6H), 7.35 (m, 2H), 7.27 (t, J = 7.6 Hz, 6H), 7.20 (t, J = 7.6 Hz, 3H), 7.16 (s, 1H), 7.09 (dd, J = 8.7 Hz, J = 2.3 Hz, 1H), 6.95 (d, J = 2.4 Hz, 1H), 4.93 (s, 2H), 4.15-4.13 (m, 2H), 3.88-3.97 (m, 2H), 3.74-3.72 (m, 2H), 3.67-3.66 (m, 2H), 3.59-3.58 (m, 2H), 3.46-3.44 (m, 2H), 3.30 (t, J = 7.0 Hz, 2H), 2.43 (t, J = 7.0 Hz, 2H). $^{13}C\{^1H\}$ NMR (75 MHz, $CDCl_3$): δ 155.2, 152.3, 144.8, 129.8, 129.6, 129.0, 127.9, 127.6, 126.6, 125.9, 119.3, 110.9, 107.0, 70.8, 70.7, 70.5, 70.1, 69.8, 69.6, 67.4, 66.6, 64.4, 31.6. ESI-HRMS: Calculated for $C_{38}H_{40}O_6S^+$ $[M+Na]^+$: 647.2438, found 647.2434.

Synthesis of AuNP-EG$_3$-OMe

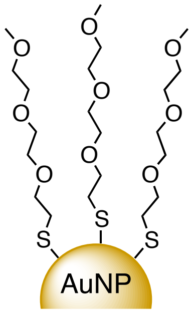

AuNP-EG$_3$-OMe were synthesized according to our previously established procedure.[8] Briefly, $HAuCl_4 \cdot 3H_2O$ (1.5 g, 3.7 mmol, 1.0 eq.) was dissolved in a mixture of distilled CH_3OH (500 mL) and glacial acetic acid (86 mL) to give a yellow solution then HS-EG$_3$-OMe (2.0 g, 11 mmol, 3.0 eq.). The solution darkened slightly in color and was stirred vigorously for two hours at room temperature until the solution color slightly faded. A solution of $NaBH_4$ (1.4 g, 38 mmol, 10.0 eq.) dissolved in Millipore quality H_2O (98 mL) was added dropwise to the reaction mixture under vigorous stirring. The mixture turned dark brown immediately. The resulting solution was stirred overnight at room temperature then the solution was concentrated under vacuum and redissolved with brine (200 mL). The AuNP-EG$_3$-OMe nanoparticles were extracted with toluene (6 x 50 mL) while adding sodium chloride to the aqueous phase after each extraction to maintain the saturation. The aqueous phase was eventually colorless. The combined organic phases were then concentrated in vacuo. Evaporation of the solvent left a thin film of nanoparticles which was then rinsed with hexanes to remove the excess free thiol. The crude Me-EG3-AuNPs were dissolved in nanopure H_2O and further purified by overnight dialysis. The solvent was then removed under reduced pressure and thoroughly dried in vacuo to give AuNP-EG$_3$-OMe. ^{1}H NMR (600 MHz, $CDCl_3$) δ 3.58, 3.66 ($-CH_2-$), 3.36 ($-OCH_3$).

Synthesis of AuNP-EG_4-NQMP

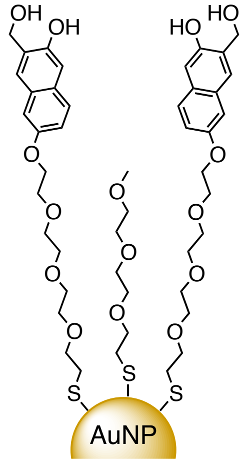

To a solution of AuNP-EG_3-OMe (42 mg) in CH_2Cl_2 (4 mL) was added a solution of HS-EG_4-NQMP (19 mg, 0.18 mmol) in CH_2Cl_2 (1 mL) under an argon atmosphere while stirring vigorously. After 2 h of stirring, the solution was concentrated under reduced pressure to give a thin film of nanoparticles. The residue was washed with Et_2O (20 mL) to remove excess thiol. The nanoparticles were then re-dissolved in 1:1 CH_2Cl_2/CH_3OH (20 mL) and the solvent was removed under reduced pressure to reform the thin film. This washing procedure was performed five more times (six total) and the resulting AuNP-EG_4-NQMP were dried in vacuo. ^1H NMR (600 MHz, $CDCl_3$): δ 7.92, 7.55, 7.13, 4.91, 4.17, 3.62, 3.36.

2.6 References

[1] N. R. Panyala, E. M. Pena-Mendez, J. Havel, *J. Appl. Biomed.* **2009**, *7*, 75-91.

[2] F. Lu, T. L. Doane, J. J. Zhu, C. Burda, *Inorg. Chim. Acta.* **2012**, *393*, 142-153.

[3] S. Arumugam, V. V. Popik, *J. Am. Chem. Soc.* **2011**, *133*, 5573-5579.

[4] S. Arumugam, J. Guo, N. E. Mbua, F. Friscourt, N. N. Lin, E. Nekongo, G. J. Boons, V. V. Popik, *Chem. Sci.* **2014**, *5*, 1591-1598.

[5] S. Arumugam, V. V. Popik, *J. Am. Chem. Soc.* **2009**, *131*, 11892-11899.

[6] S. Arumugam, V. V. Popik, *J. Am. Chem. Soc.* **2012**, *134*, 8408-8411.

[7] R. Johnsson, K. Mani, F. Cheng, U. Ellervik, *J. Org. Chem.* **2006**, *71*, 3444-3451.

[8] P. Gobbo, M. S. Workentin, *Langmuir* **2012**, *28*, 12357-12363.

CHAPTER 3

3.1 Introduction

In recent decades, AuNPs have attracted significant attention because of unique size-dependent physical, chemical and biological properties. In particular, large AuNPs display a surface plasmon resonance (SPR) phenomenon resulting in sharp absorption in the visible[1] or NIR[2] range. The strongly absorbed light is also converted to heat so larger AuNPs have been utilized in thermal ablation therapy.[3] However, the stabilization and functionalization of large AuNPs that are stable and water-soluble is challenging so the ability to further exploit the SPR for *in vivo* applications such as imaging or PTT is limited. In the literature, PEG is most commonly used to stabilize large citrate-stabilized AuNPs through a ligand exchange reaction but it presents a dilemma as described in Chapter 1. High molecular weight PEG provides excellent stability but poor conjugation ability. On the other hand, low molecular weight PEG enables high conjugation ability but provides minimal stability resulting in irreversible aggregation. In addition, the functionalization of large AuNPs is mainly limited to carbodiimide-mediated conjugation to carboxylic acid terminated PEG AuNPs (Figure 3.1). It is also reported that PEG forms a tight monolayer around the large AuNP core that inhibits place-exchange reactions with other thiols.[4] Therefore, the scope of large AuNP functionalization is very limited as a result of stability concerns and poor ability to perform interfacial chemistry. As described in Chapter 1, the Workentin AuNP toolbox contains a wide variety of templates for the functionalization of small (1-5 nm) water-soluble AuNPs via click and bioorthogonal interfacial chemistry. The goal of the work presented in Chapter 3 was to develop a method prepare larger AuNPs (> 10 nm) that are stable and allow for the introduction of functional groups from the click and bioorthogonal toolbox.

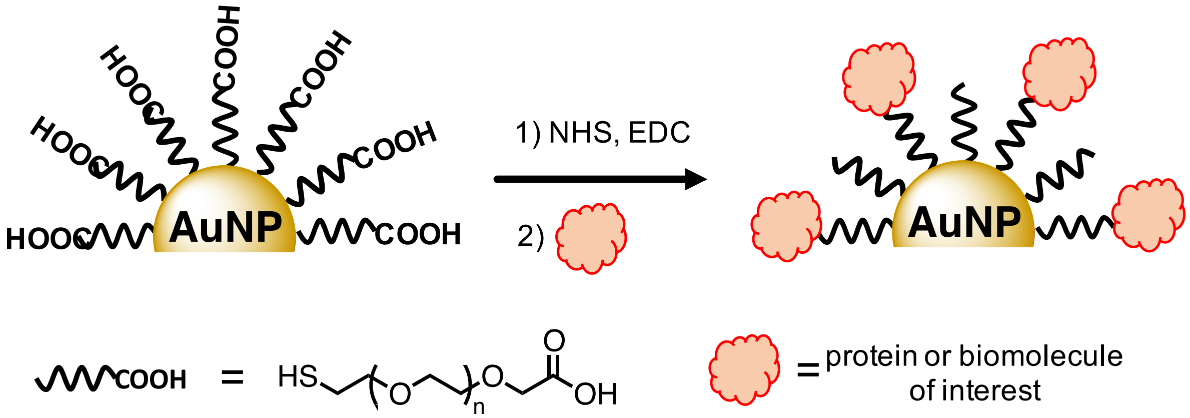

Scheme 3.1: Example of carbodiimide-mediated protein conjugation to carboxylic acid terminated PEG AuNPs.

Our design was to synthesize larger AuNPs by the Turkevich method[5] to yield AuNPs ranging in size from 15-40 nm then introduce functionality through a place exchange reaction with citrate-stabilized AuNPs using an appropriately designed ligand. Figure 3.1 is presented again from Chapter 1 to help describe the synthetic strategy. Through a convergent approach, hydrophilic ligands of discrete size were designed that stabilize the gold core through thiol binding at the head but can also undergo interfacial chemistry at the tail to impart functionality (Figure 3.1). An –OCH_3 terminus was used as a model to impart solubility in both organic media and water to the system. In addition, the ligand contains an ethylene glycol based repeating unit that is conjugated to the head and tail through amide bonds. It is predicted that as a result of the amide conjugation, these ligands will form a network of hydrogen bonding shells around the gold core for increased stabilization and hydrophilicity[6] (Figure 3.2). Also, the ligand length may be systematically adapted by increasing the number of repeating units to account for increased AuNP core size. All synthetic intermediates were characterized by ^1H NMR, ^{13}C NMR and IR spectroscopy as well as MS. The AuNPs synthesized were also characterized by UV-Vis spectroscopy and TEM.

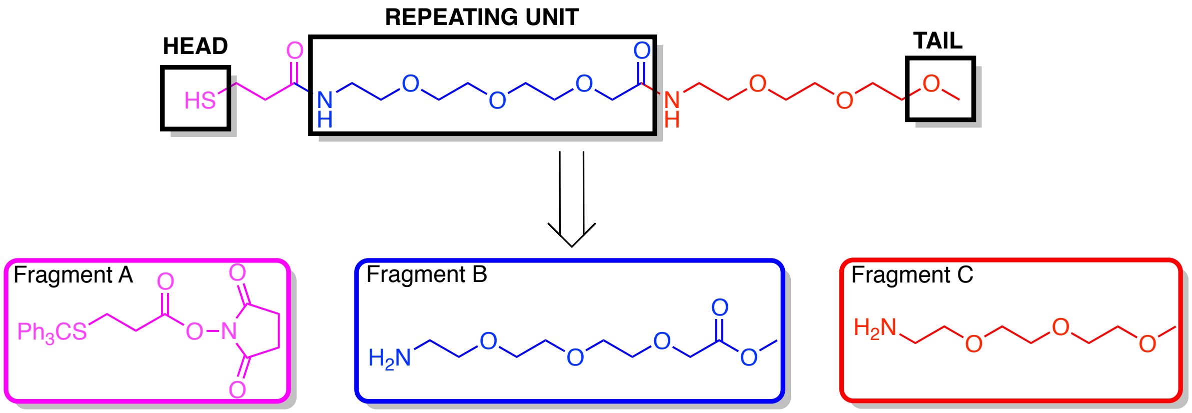

Figure 3.1: Retro-synthesis of the model ligand (n = 1) and highlighted features (Reprinted from Chapter 1)

The novel ligands were then used to stabilize the citrate-stabilized large AuNPs through a place exchange reaction. To the best of our knowledge, this is a demonstration of the smallest molecular weight ligand used to successfully stabilize larger AuNPs (>10 nm). This novel large AuNP template was then characterized by the standard techniques used for large NP characterization including UV-Vis spectroscopy and TEM. Once stabilized, the synthetic approach may be easily modified in order to develop versatile AuNP templates with click and bioorthogonal functional groups from the Workentin AuNP toolbox. Through the synthesis of a modified Fragment C, it is possible to introduce a variety of click and bioorthogonal functional groups to the large AuNP surface through a place exchange reaction with the template presented in this chapter. Figure 3.2 is presented again from Chapter 1 to showcase the overall design including the hydrogen bonding stabilization pattern as well as the introduction of click and bioorthogonal functional groups for the development of novel large AuNP templates.

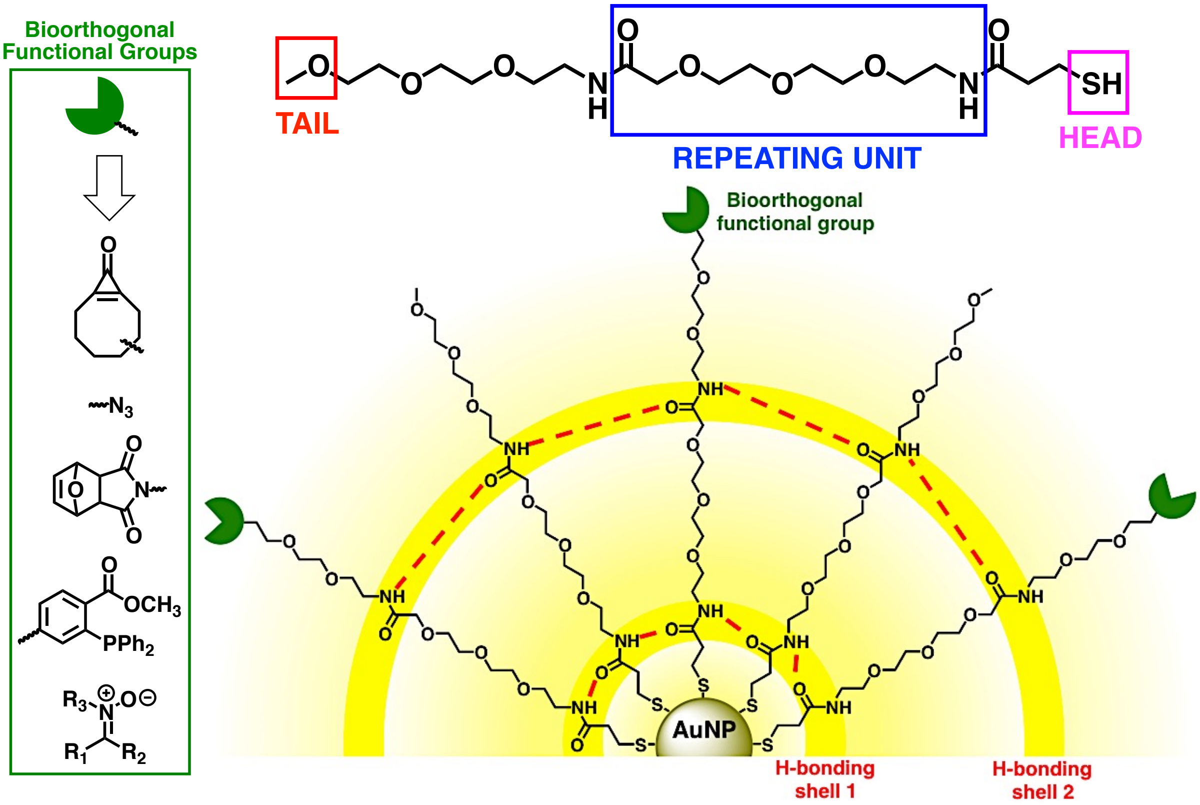
Bioorthogonal Functional Groups
TAIL
REPEATING UNIT
HEAD
SH
Bioorthogonal functional group
AuNP
H-bonding shell 1
H-bonding shell 2

Figure 3.2: Design of novel ligand with hydrogen bonding shells. The tail may be replaced with bioorthogonal functional groups (Reprinted from Chapter 1).

3.2 Results and Discussion

3.2.1 Synthesis of Fragment A

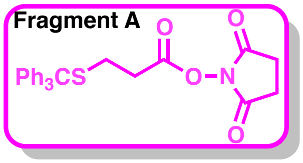
Fragment A
Ph3CS

In order to synthesize the ligands described in Scheme 3.1, a convergent approach was used by assembling three individual fragments together. Fragment A was synthesized according to a procedure reported in the literature[7]. It was selected as a result of its facile synthesis and bifunctional nature. On one end, the trityl-protected thiol is very resilient to a variety of reaction conditions and can be readily removed upon treatment with acid. At the other end, the NHS-activated carboxylic acid provides an excellent leaving group for subsequent amide conjugation (Scheme 3.2).

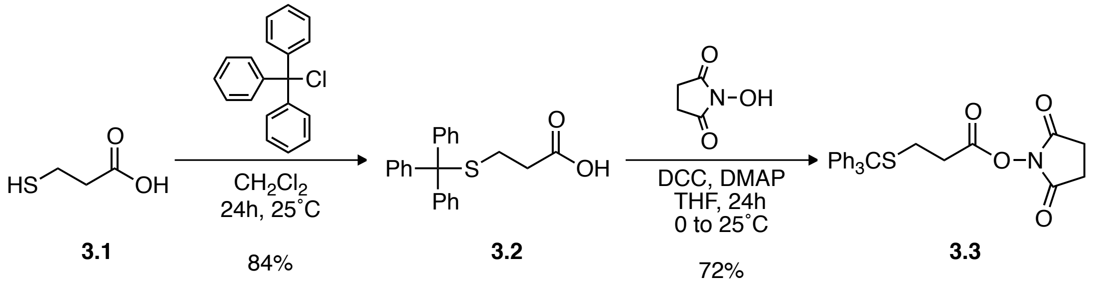

Scheme 3.2: Synthesis for thiol protection TrS-$(CH_2)_2$-COOH and activated ester TrS-$(CH_2)_2$-NHS.

Fragment A was characterized by mass spectrometry (MS) as well as ^{1}H and ^{13}C NMR spectroscopy. Through a nucleophilic substitution reaction, the thiol in compound **3.1** was protected as evidenced by three characteristic signals in the ^{1}H NMR spectra of **3.2**. A doublet at 7.42 ppm, triplet at 7.29 ppm and another triplet at 7.22 ppm indicate the benzylic hydrogens and successful incorporation of the protecting group. Subsequently, activation of the carboxylic acid with NHS gave rise to a strong singlet at 2.81 ppm with an integration of 4H. In the ^{13}C NMR spectrum of compound **3.3** there was also an appearance of a signal relating to the addition of the second chemically equivalent carbonyl groups in NHS.

3.2.2 Synthesis of Fragment B

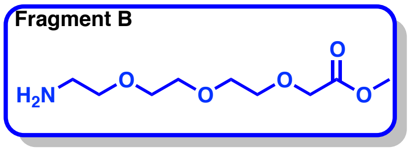

In Fragment B, tetraethylene glycol (compound **3.4**) was selected as the backbone of the repeating unit to impart both organic and water solubility to the final ligand. In this fashion, it is possible to perform interfacial chemistry on the AuNP in organic media as well as biological solutions. As described in Scheme 3.3, commercially available tetraethylene glycol was tosylated to give the mono-tosylated compound **3.5**. The tosylate was selected as it is a good leaving group and also acts as a hydroxyl protecting group in subsequent reactions. Next, the primary alcohol was oxidized to the corresponding carboxylic acid using a catalytic amount of pyridinium chlorochromate (PCC). The intermediate **3.6** was extracted to remove excess acid and carried through to the next step without further purification. An esterification reaction was then performed by simply dissolving **3.6** in an acidic solution of methanol and refluxing for two hours. The intermediate **3.7** was characterized with ^{1}H NMR spectroscopy by the appearance of a strong singlet at 3.76 ppm with an integration of 3H consistent with the formation of a methyl ester. Finally, sodium azide was reacted with **6** through a nucleophilic substitution reaction to afford the azido compound **3.8**. The ^{1}H NMR spectrum revealed a triplet at 3.39 ppm relating to the protons alpha to the azide functionality. Additionally, there was a disappearance of the aromatic signals in both the ^{1}H and ^{13}C NMR spectra resulting from substitution of the tosyl group. Compound **3.8** was not reduced to the corresponding amine because of difficulties encountered when attempting to isolate the product. It was believed that the methyl ester may have been susceptible to nucleophilic attack from amines so Fragment B was carried through as the azide compound **3.8**. Instead I developed a one-pot reaction where the amine was formed *in situ* in Scheme 3.6. I later realized that the Pd/C catalyst was actually no longer active but the one-pot protocol had already yielded good results. The infrared (IR) spectrum of compound **3.8** included intense signals at 2107 cm^{-1} and 1739 cm^{-1} characteristic of azide and carbonyl stretching frequencies, respectively.

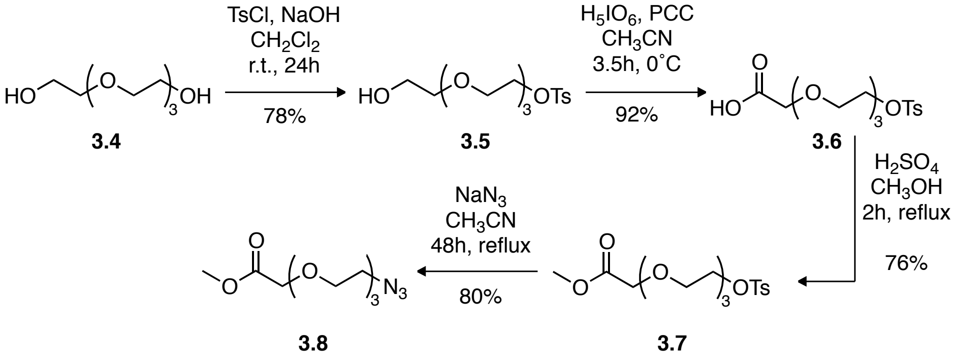

Scheme 3.3: Synthesis of Fragment B.

3.2.3 Synthesis of Fragment C

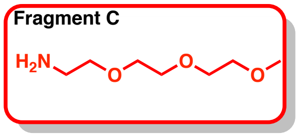

Fragment C was also synthesized according to a modified procedure reported in the literature.[8] As described in Scheme 3.4, the final fragment includes an amino functionality for amide conjugation. It also includes a terminal methoxy group (compound **3.9**) in order to provide the desired solubility in both organic and aqueous media to the final AuNP as previously demonstrated by our group. This group may also be easily replaced by biorthogonal functional groups that can be installed in future investigations. Briefly, triethylene glycol monomethyl ether was tosylated prior to reaction with sodium azide to install the azido functionality. Next, reduction of the azide was catalyzed by palladium on carbon to give the final amino functionalized fragment in very high yield.

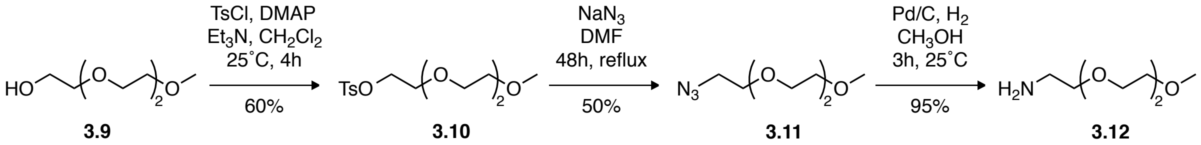

Scheme 3.4: Synthesis of Fragment C.

The characterization of the compounds described in Scheme 3.4 was completed by ^{1}H and ^{13}C NMR spectroscopy as well as MS. In the ^{1}H NMR spectrum of compound **3.10**, an appearance of two doublets at 7.70 and 7.26 ppm with a total integration of 4H confirmed the introduction of the tosyl group. The corresponding azido compound **3.11** was then characterized by the disappearance of the previously mentioned signals. Finally, upon catalyzed reduction of the azide to give compound **3.12**, in the ^{1}H NMR spectrum there was an appearance of a broad singlet at 2.16 ppm with an integration of 2 corresponding to the amine protons.

3.2.4 Synthesis of Required Ligands

In order to synthesize the desired ligands, the individual fragments A, B and C were coupled together through the formation of amide bonds where: Fragment A contains the thiol for binding to the gold core, Fragment B is the repeating unit represented by *n*, and Fragment C contains a terminal methoxy group as a model for bioorthogonal functionalities. It is predicted that the amide bonds will provide additional stabilization to the large AuNP through lateral hydrogen bonding in hydrogen bonding shells. In addition, all three fragments were synthesized in good yield on a gram scale.

The desired ligand was first synthesized without Fragment B, or the repeating unit (Scheme 3.5). Consequently, the ligand only contains one hydrogen bonding shell. Briefly, Fragment C (compound **3.12**) was reacted with Fragment B (compound **3.3**) in high yield to give the amide coupled intermediate **3.13**. The thiol was then deprotected by treatment with trifluoroacetic acid (TFA) in the presence of triisopropylsilyl ether (TIPS) to give the ligand with n = 0.

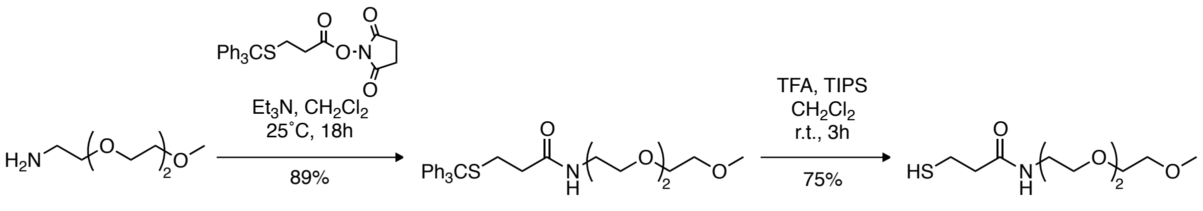

3.12 **3.13** **3.14**

Scheme 3.5: Synthesis of ligand without repeating unit (n = 0)

The ligand **3.14** was fully characterized by ^{1}H and ^{13}C NMR spectroscopy as well as MS. Upon coupling through amide bond formation, in the ^{1}H NMR spectrum there was an appearance of a broad singlet at 6.45 ppm indicative of successful coupling. As well, removal of the trityl group resulted in the disappearance of the corresponding aromatic protons. Additionally, a triplet appeared at 1.63 ppm highlighting the reformation of the SH bond.

The desired ligand was then synthesized with one repeating unit contained within the structure such that two hydrogen bonding shells would provide increased stabilization (Scheme 3.6). In a one pot reaction, Fragment B was formed *in situ* by reduction of compound **3.8** catalyzed by Pd/C and coupling with Fragment A (compound **3.3**) through amide bond formation was also achieved. The intermediate **3.15** was isolated in high yield demonstrating the feasibility of the one pot reaction. Next, the methyl ester was hydrolyzed to give the corresponding carboxylic acid intermediate **3.16**. Through an HBTU mediated coupling, the acid intermediate was coupled with Fragment C to give compound **3.17** with two amide bonds contained within the molecular structure. Initial efforts to activate the carboxylic acid with NHS prior to coupling were not successful. Finally, the trityl protecting group could be cleaved by treatment with TFA in good yield to give ligand **3.18**.

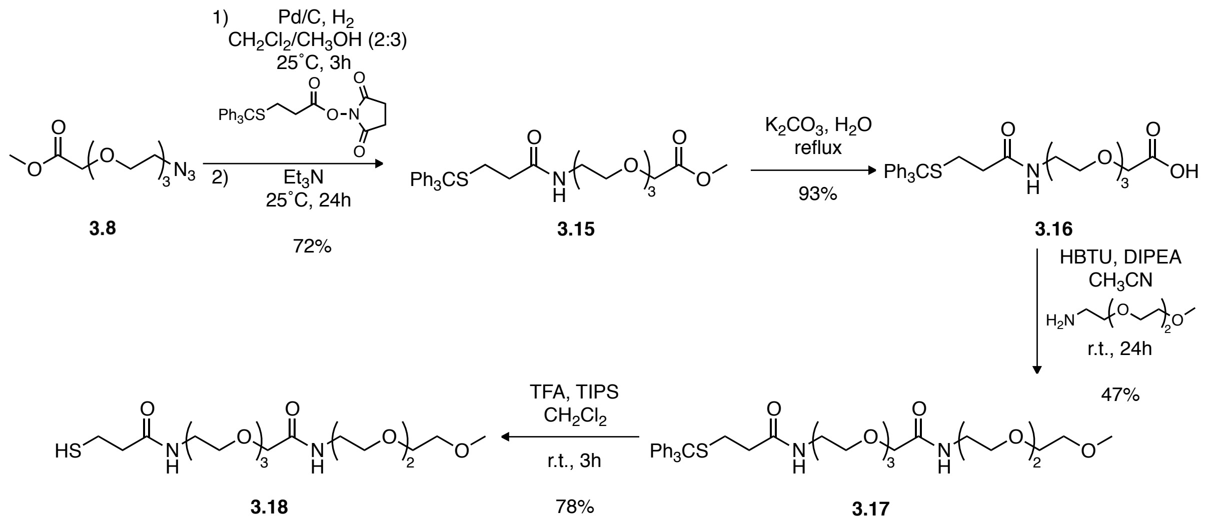

Scheme 3.6: Synthesis of ligand with one repeating unit (n = 1).

The intermediates described in Scheme 6 were characterized by ^{1}H and ^{13}C NMR spectroscopy as well MS. After the one-pot reaction, successful coupling to give compound **3.15** was noted by the appearance of a broad singlet at 5.93 ppm in the ^{1}H NMR spectrum indicating the presence of an amide proton. As well, ethylene protons in Fragment A shifted upfield. In the ^{13}C NMR spectrum, appearance of a carbonyl signal confirmed successful coupling. Next, the hydrolyzed product **3.16** was characterized by the disappearance of a singlet integrating to 3H in the ^{1}H NMR spectrum at 3.70 ppm. Interestingly, the ethylene glycol protons were also more well resolved following hydrolysis. The next HBTU mediated amide coupling step could be tracked very well by ^{1}H & ^{13}C NMR spectroscopy. In the ^{1}H NMR spectrum of **3.17**, integration of ethylene glycol signals corresponded to the expected 29H. The appearance of a second amide bond could also be observed in the ^{1}H NMR spectrum but it was difficult to resolve from the aromatic protons. The ^{13}C NMR spectrum also revealed the formation of a second amide bond through a carbonyl signal at 170.1 ppm. However, upon removal of the trityl protecting group, both amide protons were beautifully well-resolved in the ^{1}H NMR spectrum of **3.18** (Figure 3.3). The SH signal also appeared as a triplet at 1.62 ppm. The methylene protons adjacent to the sulfhydryl functional group appeared as a false quartet. It should be a doublet of triplets but the difference in magnitude of the coupling constants was too small to clearly resolve the complex splitting pattern. In addition, as a result of the gram scale synthesis of each fragment and good yield in the ligand synthesis, the ability to scale the synthesis and develop large quantities of the ligands is straightforward.

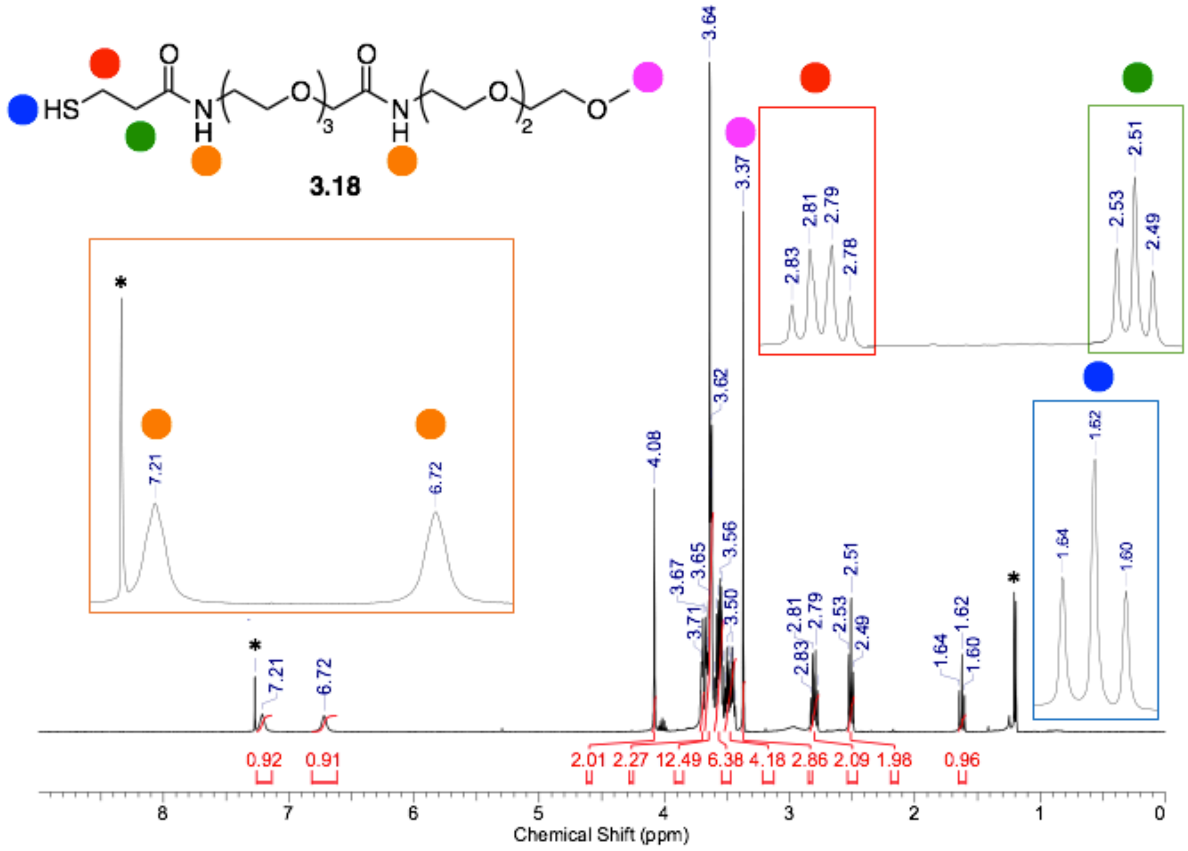

Figure 3.3: ^{1}H NMR spectrum of HS-EG$_4$-EG$_3$-OMe in CDCl$_3$. * denotes residual protonated solvent signals or solvent impurities.

3.2.5 Synthesis and UV-Vis Spectra of Citrate-Stabilized AuNPs

AuNPs were synthesized by reducing gold chloride using the standard sodium citrate method. Briefly, to a solution of H_2O (10 mL) with a stir bar was added 0.2 mL of $HAuCl_4 \bullet H_2O$ stock solution (1% w/v in H_2O) diluted to 10 mL H_2O to give a 0.01% Au solution. The solution was brought to boiling with vigorous stirring prior to adding the desired volume of sodium citrate stock solution (1% w/v). After the solution turned red in color, boiling was continued for 5 minutes then the solution was cooled to room temperature. By varying the sodium citrate to gold ratio, it was possible to control the size of the AuNPs. UV−vis absorption spectra were acquired to determine the characteristic plasmon resonance absorption peak of the AuNPs (Figure 3.4) and identify the approximate size. The results are summarized in Table 3.1. The plasmon bands red-shifted and broadened with increase in size, in good agreement with previously reported results.[9]

Table 3.1: Synthesis of large AuNPs by sodium citrate reduction.

$HAuCl_4 \cdot H_2O$ (µL)	100	100	100	100
Sodium citrate (µL)	100	125	150	200
λ_{max} (nm)	529	526	524	519
Size (nm)	40	30	20	15

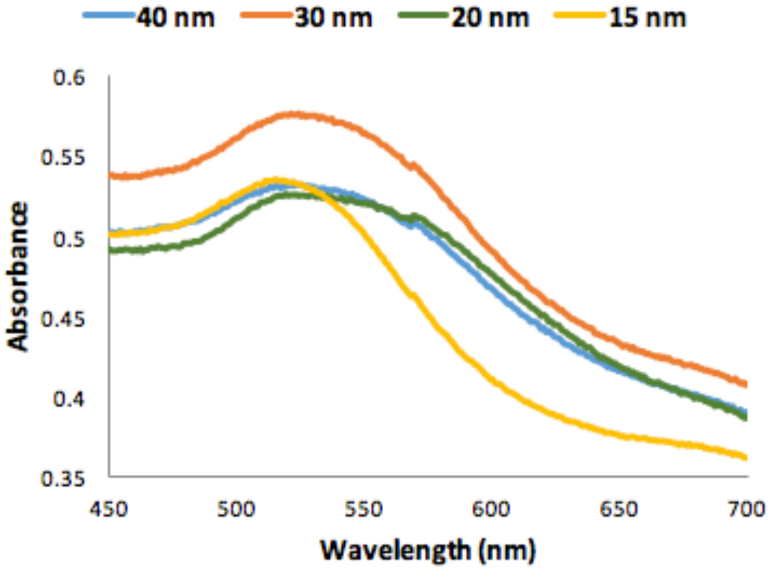

Figure 3.4: UV-Vis spectra in nanopure H_2O of citrate-stabilized AuNP synthesized by the Turkevich method.

Interestingly, the smaller AuNPs (15-20 nm) could be centrifuged and redispersed in water without detectable aggregation. However, centrifugation and redispersion in water of the larger citrate-stabilized AuNPs (30-40 nm) resulted in irreversible aggregation as demonstrated by drastic discoloration of the solution from red to blue and broadening of the plasmon in the UV−vis absorption spectra. In order to prepare concentrated solutions of the larger AuNPs, it has been demonstrated that Tween 20 surfactant is able to prevent aggregation upon centrifugation and redispersion. Tween surfactants are able to weakly physisorb on the surface of AuNPs with diameters from 20 to 175 nm to provide steric stabilization and prevent aggregation.[9] Importantly, the surfactant layer can still be displaced and undergo place exchange reactions with thiols such as PEG-SH. Schollbach *et al.*, also investigated the ability of OEG thiols to stabilize AuNPs.[10] It is reported that short chain OEG with 2-4 EG units can only stabilize AuNPs less than 3 nm in diameter. However long chain $HSC_{11}EG_6$ ligands were able to stabilize AuNPs larger than 10 nm (Figure 3.5). So to investigate the stabilizing efficiency of the ligands **3.14** and **3.18**, 20 nm citrate-stabilized AuNPs were selected.

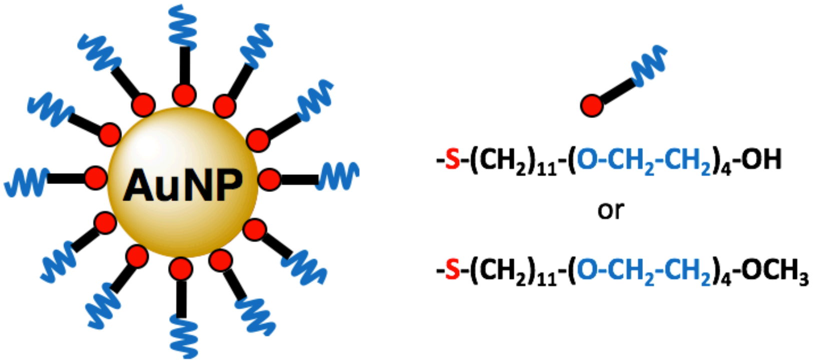
AuNP
$-S-(CH_2)_{11}-(O-CH_2-CH_2)_4-OH$
or
$-S-(CH_2)_{11}-(O-CH_2-CH_2)_4-OCH_3$

Figure 3.5: Cartoon representation of a large AuNP stabilized by a monolayer of OEG ligands. The hydrophobic C_{11}-chain provides stability while the hydrophilic EG unit ensures solubility in water (-OH) and both water and organic solvent ($-OCH_3$).

For the 20 nm AuNPs, the approximate size was first calculated from the UV-Vis spectrum using the ratio of the absorbance at the surface plasmon resonance peak (A_{spr}) to the absorbance at 450 nm (A_{450}) based on a linear fit between theoretical and experimental data:[11]

$$d = \exp\left(B_1 \frac{A_{spr}}{A_{450}} - B_2\right)$$

B_1 is the inverse of the slope (m) of the linear fit between theoretical and experimental data and $B_2 = \frac{B_0}{m}$ where B_0 is the intercept. For AuNPs less than 35 nm, the A_{spr} is increasingly damped relative to absorbance at other wavelengths. As a result, it is necessary to use a ratio of absorbances to determine the AuNP size. Using wavelengths higher than the plasmon was not suitable because of small amounts of aggregates that would absorb at these higher wavelengths. Instead, good agreement was found using the absorbance ratio of wavelengths below 600 nm due to less interference. In the end, strong agreement was found between theoretical and experimental data using the absorbance ratio of the surface plasmon resonance peak and the absorbance at 450 nm. Thankfully, the authors compiled a table of the numerical data from Equation 1 enabling the size determination of AuNPs without the need to perform any calculations. The average size (20 ± 1 nm) and spherical shape was then confirmed by TEM (Figure 3.6). These results are in excellent agreement with the calculated results highlighting the dynamic power of the surface plasmon in the determination of AuNP size.

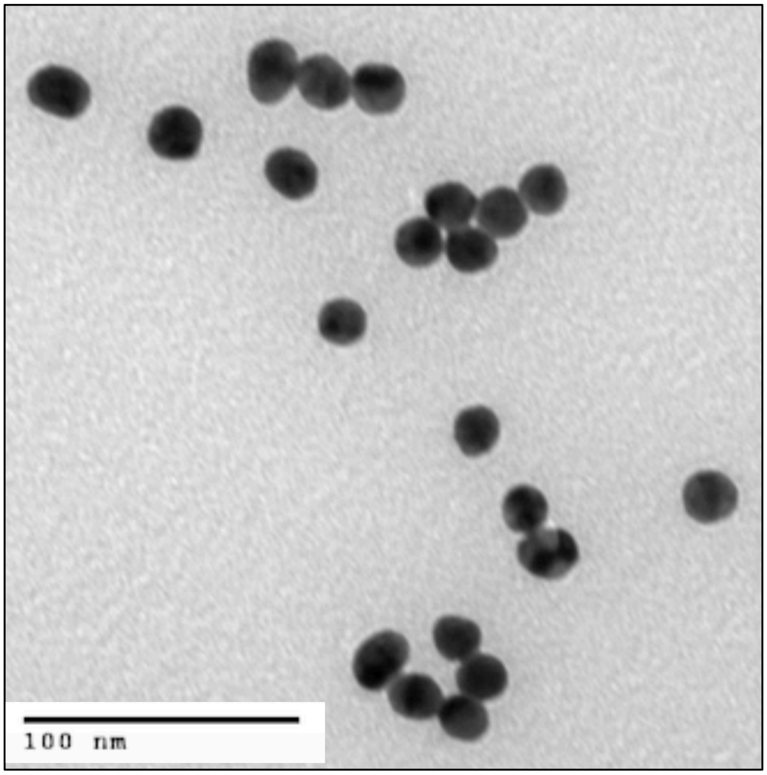

Figure 3.6: TEM image of 20 nm citrate-stabilized AuNPs (average size = 20 ± 1 nm). The scale bar is indicated.

3.2.6 Stabilization of 20 nm Citrate-Stabilized AuNPs

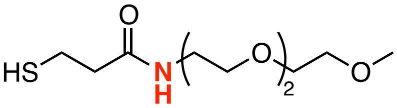

3.14

Initial attempts at stabilizing the 20 nm AuNP core using ligand **3.14** proved unsuccessful as demonstrated by drastic fading in the color of the solution from red to blue (Figure 3.7) and broadening of the plasmon in the UV−vis absorption spectra. This is an indication of irreversible aggregation and that **3.14** was not able to provide sufficient stabilization. This result also highlighted the challenge of stabilizing AuNPs larger than 10 nm as methoxy terminated triethylene glycol ligands are routinely used to stabilize small AuNPs.

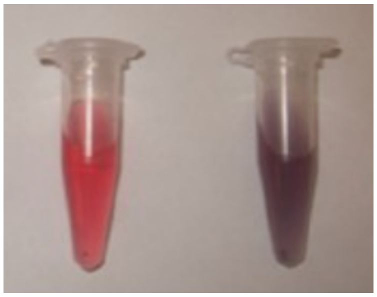

Figure 3.7: Example of visual discoloration of AuNP solution due to aggregation (left vs. right).

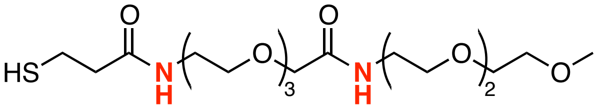

3.18

However, the successful stabilization of the 20 nm AuNPs was accomplished with ligand **3.18** and characterized with UV-Vis absorption spectra as well as TEM images. First, the concentration of AuNPs dissolved in 1.0 mL of water was determined using the methodology developed by Haiss *et al*. In addition to being able to determine the size of AuNPs with UV-Vis spectra, it is also possible to determine the concentration of the AuNP solution. The authors calculated the molar extinction coefficients of AuNPs with diameters ranging from 2 to 100 nm based on the absorbance at 450 nm.[11] Using the Beer-Lambert equation it is possible to calculate the AuNP concentration:

$$A_{450} = \varepsilon_{450} \ell c$$

In the above equation, A_{450} is the absorbance and ε_{450} is the molar extinction coefficient at 450 nm. With a standard path length (ℓ) of 1 cm, the concentration (c) can be determined according to:

$$c = \frac{A_{450}}{\varepsilon_{450}}$$

Next, using a simple calculation considering the total AuNP surface area and the cross sectional area of the thiol molecule it is possible to determine the idealized maximum coverage, or number of ligands required to encapsulate the AuNP surface. For example, in an ideal monolayer of long chain alkanethiolates on a Au surface, a thiolate possesses a footprint[12] of

$$0.214\ \frac{nm^2}{thiolate}$$

Thus, a 20 nm AuNP with a surface area of

$$SA = 4\pi r^2 = 1256\frac{nm^2}{AuNP}$$

requires

$$1256\frac{nm^2}{AuNP}\times\frac{thiolate}{0.214\,nm^2} = 5869\frac{thiolates}{AuNP}$$

in order to provide maximum coverage. The AuNP concentration was found to be $2.65 \times 10^{-10}\ M$ in 1.0 mL of water then 32 µL of a $2.65 \times 10^{-10}\ M$ solution of **3.18** was added and vigorous shaking was applied. It is important to note that relative to the idealized maximum coverage a 10-fold excess of ligands was used. Then 1.5 h after place exchange, the AuNPs were centrifuged four times (30 min at 6000 rpm), including replacement of the supernatant with water to remove excess ligand. After place exchange, the AuNPs could be centrifuged and redispersed in water without detectable aggregation. There was no discoloration of the solution observed unlike the previous attempt using the smaller ligand. Successful place exchange could be confirmed through UV-vis absorption spectroscopy (Figure 3.8). As the plasmon is influenced by the surface chemistry, replacement of the citrate layer results in a shift of the wavelength of maximum absorption by a few nanometers. This expected shift was observed. Additionally, a lower absorbance was observed after place exchange due to some AuNPs being removed with the supernatant during purification. However, the plasmon was not significantly broadened indicating little to no aggregation after place exchange.

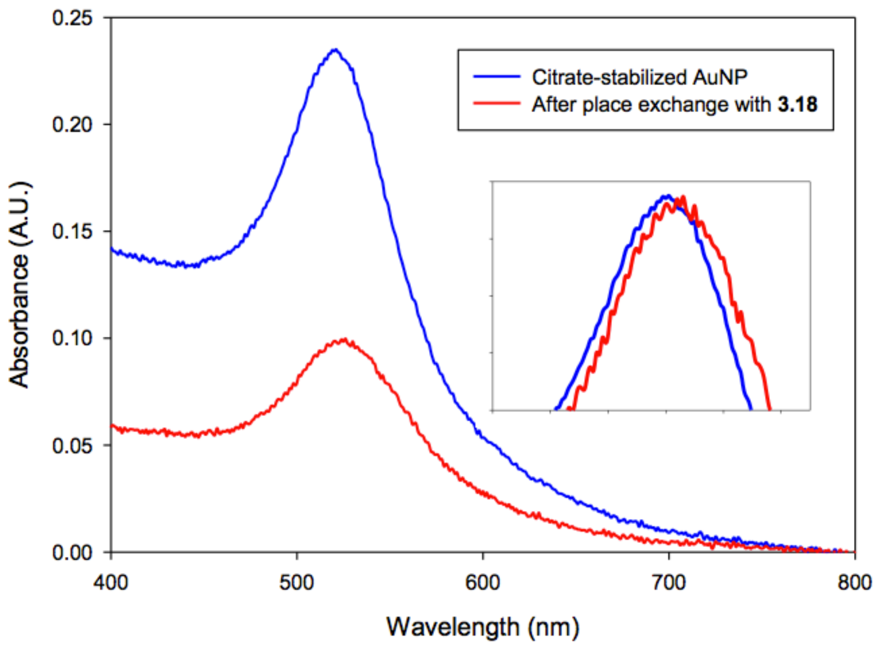

Figure 3.8: Colloidal stability of HS-EG$_4$-EG$_3$-OMe stabilized 20 nm AuNPs characterized by UV−vis measurement in nanopure H_2O. The lower absorbance is a result of material loss during purification. The normalized absorbance spectra shown in the inset demonstrates the shift of the surface plasmon resonance band ($\Delta\lambda = 5$ nm) after place exchange.

TEM images were also collected after place exchange (Figure 3.9). The average size was found to be 21 ± 2 nm in good agreement with the citrate-stabilized AuNP precursor. Therefore, the shift in the surface plasmon observed in Figure 3.8 can be attributed to successful place exchange as there was no significant change in size or shape following displacement of the citrate ions.

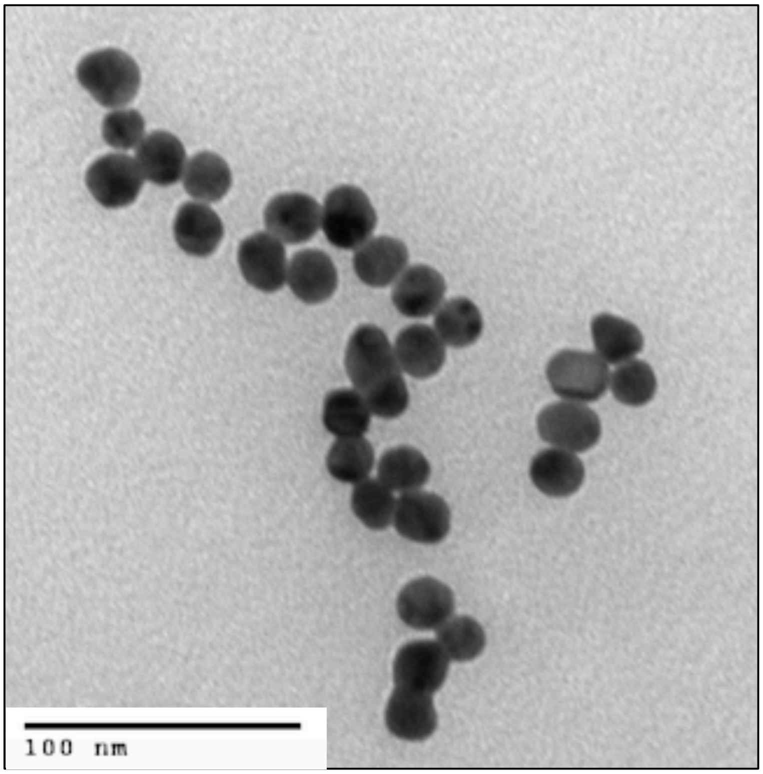

Figure 3.9: TEM image of HS-EG_4-EG_3-OMe stabilized AuNPs. The scale bar is indicated.

3.3 Conclusion

In the literature, PEG-SH has displayed a poor balance between colloidal stability and functionalization so the ability to exploit the optical properties of large AuNPs remains elusive. In addition, common spectroscopic techniques such as NMR spectroscopy are not applicable for characterization. These polymer-AuNP systems are also unable to undergo place exchange reactions so conjugation is typically achieved through carbodiimide chemistry limiting the scope of interfacial chemistry. The ligand designed in this project addresses these issues as a result of its discrete size and ability to form hydrogen bonding shells. The ligand was successfully synthesized in high yield and incorporated onto the surface of 20 nm AuNPs. It is the lowest molecular weight thiolated ethylene glycol based ligand to be shown to stabilize large AuNPs. Successful place exchange was characterized by UV-Vis spectroscopy and the size was confirmed by TEM. The synthetic strategy may now be modified to incorporate click and bioorthogonal functional groups from the Workentin AuNP toolbox. The synthesis may be repeated on a multi gram scale and with a modified Fragment C that contains one of the versatile functional groups previously described. In this manner it will be possible to develop novel click and biorthogonal large AuNP templates on a large scale to investigate their interfacial chemistry for *in vivo* applications. In conclusion, the work presented in this chapter are the first steps towards transposing the vast knowledge in our group obtained from designing small AuNP templates onto larger AuNP systems. Preliminary results indicate that stabilization was successful but characterization by ^{1}H NMR spectroscopy would provide further confirmation as well as the ability to follow the interfacial chemistry. This will enable us to take advantage of the SPR and its interesting absorption, scattering and photothermal properties through more versatile functionalization routes using click and bioorthogonal interfacial chemistry.

3.4 Experimental

Materials and Methods

All reagents used were obtained from commercially available sources and used without further purification. Tritylchloride, *N*-hydroxysuccinimide (NHS), dicyclohexylcarbodiimide (DCC), tetra(ethylene glycol), *p*-toluenesulfonyl chloride, pallidum on carbon (Pd/C), sodium azide and pyridinium chlorochromate (PCC) were purchased from Sigma Aldrich. 4-Dimethylaminopyridine (DMAP) was purchased from Alfa Aesar. All common dry solvents were obtained from Caledon. Solvents were dried using an Innovative Technologies solvent purification system, collected under vacuum, and stored under an argon atmosphere over 4 Å molecular sieves.

^{1}H NMR spectra were recorded on a Varian Inova 600 MHz spectrometer and ^{13}C spectra were recorded on a Mercury 400 MHz spectrometer**.** ^{1}H NMR spectra are reported as δ in units of parts per million (ppm) relative to residual chloroform proton (δ 7.27, s). Multiplicities are reported as follows: s (singlet), d (doublet), t (triplet), q (quartet), quin (quintuplet), dd (doublet of doublets), m (multiplet), and bs (broad signal). Coupling constants are reported as *J* values in Hertz (Hz). The number of protons (*n*) for a given resonance is indicated as *n*H, and is based on spectral integration values. ^{13}C NMR spectra are reported as δ in units of parts per million (ppm) relative to $CDCl_3$ (δ 77.0, t)**.** Spectra were analyzed using ACD/SpecManager software v11.01. The spectra were baselined and integrated manually.

Mass spectrometry data were recorded in positive-ion mode with a Bruker micOTOF II instrument using electrospray ionization or other ionization techniques as described.

Transmission electron microscopy (TEM) images were recorded from a TEM Philips CM10 microscope. The TEM grids (Formvar carbon film on 400 mesh copper grids) were purchased from Electron Microscopy Sciences and prepared by dropcasting a drop of nanoparticles solution directly onto the grid surface. The drop was then carefully removed after 30 seconds with a soft tissue.

UV-Visible spectra were recorded using a Varian Cary 100 bio spectrometer and 1 mm plastic cuvettes. The nanoparticle samples were dissolved in Millipore quality H_2O. The background was automatically subtracted from each spectrum.

FT-IR spectra were recorded using a PerkinElmer Spectrum Two FT-IR spectrometer using an attenuated total reflectance accessory. The background was subtracted from each spectrum.

Synthesis of TrS-COOH (3.2)

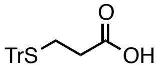

As reported in the literature, under argon atmosphere, 3-mercaptopropionic acid (1.50 mL, 17.2 mmol) was added to a solution of tritylchloride (3.6 g, 12.8 mmol) in anhydrous CH_2Cl_2 (500 mL). The reaction was left overnight at room temperature and then concentrated to give a yellow solid. The crude yellow solid was washed with a cold mixture of hexanes/Et_2O (1:1) to give a white solid that was collected by vacuum filtration. The resulting white solid was then dissolved in a minimum amount of CH_3OH with boiling, cooled to room temperature, added H_2O (30 mL) then cooled on ice. The recrystallized white solid was collected by vacuum filtration to give the purified acid compound (3.17 g, 84% yield). ^1H NMR (600 MHz, $CDCl_3$): δ 7.42 (d, J = 6 Hz, 6H), 7.29 (t, J = 6Hz, 6H), 7.22 (t, J = 6 Hz, 3H), 2.47 (t, J = 6 Hz, 2H), 2.25 (t, J = 6 Hz, 2H). $^{13}C\{^1H]$ NMR (75 MHz, $CDCl_3$): δ 174.1, 144.5, 129.3, 127.7, 126.5, 66.6, 33.1, 26.7. IR (cm^{-1}): 3057, 3035, 2928, 1709, 1595, 1489, 1444, 1249, 1083, 1034, 934, 743, 700, 676, 622, 507, 488, 465. ESI-HRMS: Calculated for $C_{22}H_{20}O_2S^+$ $[M+Na]^+$: 371.1076, found 371.1087.

Synthesis of TrS-NHS (3.3)

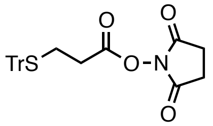

As reported in the literature, to a solution of *N*-hydroxysuccinimide (0.41 g, 3.56 mmol), DCC (0.76 g, 3.68 mmol) and a catalytic amount of DMAP (13.2 mg, 0.11 mmol) in anhydrous THF (30 mL) was added $Ph_3CS-(CH_2)_2-COOH$ (1.07 g, 3.07 mmol) at 0˚C under argon atmosphere. The reaction was cooled for one hour and then left at room temperature overnight. The solution was filtered to remove the dicyclohexylurea and concentrated under vacuum. The crude reaction mixture was purified by silica gel column chromatography using CH_2Cl_2 to give the purified ester compound as a white solid (0.98 g, 72% yield). ^1H NMR (600 MHz, $CDCl_3$): δ 7.44 (d, J = 6 Hz, 6H), 7.31 (t, J = 6Hz, 6H), 7.23 (t, J = 6 Hz, 3H), 2.81 (s, 4H), 2.56 (t, J = 6 Hz, 2H), 2.41 (t, J = 6 Hz, 2H). $^{13}C\{^1H\}$ NMR (75 MHz, $CDCl_3$): δ 168.8, 167.0, 144.3, 129.5, 128.0, 126.8, 67.1, 30.5, 26.1, 25.5. IR (cm^{-1}): 3080, 3024, 2937, 1809, 1775, 1745, 1485, 1441, 1356, 1207, 1153, 1088, 1065, 991, 907, 845, 809, 743, 703, 648, 625, 506. ESI-HRMS: Calculated for $C_{26}H_{23}NO_4S^+$ $[M+Na]^+$: 468.1240, found 468.1230.

Synthesis of TsO-EG₄-OH (3.5)

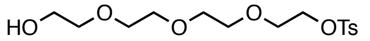

To a solution of tetraethylene glycol (100 mL, 0.51 mol) in THF (150 mL) was added NaOH (3.4 g dissolved in 10 mL H_2O) and the reaction mixture was stirred vigorously for 15 min. At 0˚C, *p*-toluenesulfonyl chloride (10.5 g, 0.061 mol) was then slowly added to give a yellow solution. The reaction was left overnight at room temperature then H_2O (150 mL) was added. The reaction mixture was then extracted with CH_2Cl_2 (3 x 80 mL), dried over Na_2SO_4, filtered and concentrated under vacuum to give the mono-tosylated product as a yellow oil (16.57 g, 78% yield). ^1H NMR (600 MHz, $CDCl_3$): δ 7.81 (d, J = 12 Hz, 2H), 7.35 (d, J = 12 Hz, 2H), 4.17 (t, J = 6 Hz, 2H), 3.73-3.60 (m, 14H), 2.45 (s, 3H). $^{13}C\{^1H\}$ NMR (75 MHz, $CDCl_3$): δ 144.7, 132.8, 129.7, 127.8, 72.4, 70.6, 70.5, 70.3, 70.2, 69.2, 68.6, 21.5. IR (cm^{-1}): 3440, 2871, 1598, 1452, 1351, 1175, 1096, 1012, 918, 816, 774, 662, 553. CI-HRMS: Calculated for $C_{15}H_{24}O_7S^+$ $[M+1]^+$: 348.1243, found 348.1242.

Synthesis of TsO-EG₄-COOH (3.6)

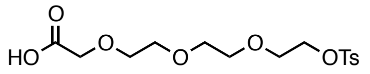

As reported in the literature, under argon atmosphere, to a solution of periodic acid (9.5 g, 42.7 mmol) dissolved in anhydrous CH_3CN (250 mL) was added TsO-EG₄-OH (6.6 g, 18.9 mmol). The reaction mixture was cooled to 0˚C then a catalytic amount of PCC (83 mg, 0.4 mmol) was added. The reaction was left at room temperature for 3.5h to give a yellow-green solution. EtOAc (500 mL) was added and the organic layer was separated and then successively washed with 1:1 brine/H_2O (3 x 500 mL), $NaHSO_3$ (3 x 500mL) and brine (3 x 500 mL). The organic layer was then dried over Na_2SO_4, filtered and concentrated under vacuum to give the desired acid as a light yellow oil (6.3 g, 92% yield). No further purification was performed.

Synthesis of TsO-EG$_4$-COOMe (3.7)

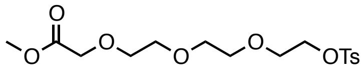

To a solution of TsO-EG4-COOH dissolved in CH_3OH (400 mL) was added H_2SO_4 (40 mL). The solution was then heated at reflux for 2 hours. The solution was concentrated under vacuum then re-dissolved in EtOAc (200 mL) and neutralized by the addition of a solution of 10% $NaHCO_3$ (400 mL). The aqueous layer was extracted with EtOAc (3 x 200 mL). The combined organic layers were dried over Na_2SO_4, filtered and concentrated under vacuum. The solution was purified by silica gel column chromatography using EtOAc to give the desired methyl ester as a light yellow oil (3.7 g, 56% yield). ^{1}H NMR (600 MHz, $CDCl_3$): δ 7.81 (d, J = 12 Hz, 2H), 7.35 (d, J = 12 Hz, 2H), 4,17 (s, 2H), 3.76-3.61 (m, 15H), 2.46 (s, 3H). ^{13}C{^{1}H} NMR (75 MHz, $CDCl_3$): δ 170.9, 144.8, 133.0, 129.8, 128.0, 70.9, 70.7, 70.6, 70.5, 69.2, 68.7, 68.6, 51.2, 21.6. ESI-HRMS: Calculated for $C_{16}H_{24}O_8S^+$ [M+Na]$^+$: 399.1084, found 399.1086.

Synthesis of N$_3$-EG$_4$-COOMe (3.8)

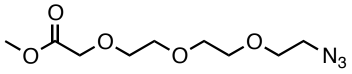

To a solution of TsO-EG$_4$-COOMe (1.06 g, 2.82 mmol) dissolved in CH_3CN (20 mL) was added NaN_3 (0.36 g, 5.54 mmol) and heated at reflux for 48 h. A white precipitate formed. The reaction mixture was filtered and concentrated under vacuum. The crude mixture was purified by silica gel column chromatography using EtOAc to give the desired azido compound as a light yellow oil (553 mg, 80% yield). ^{1}H NMR (600 MHz, $CDCl_3$): δ 4.18 (s, 2H), 3.78-3.67 (m, 13H), 3.39 (t, J = 12 Hz, 2H). ^{13}C{^{1}H} NMR (75 MHz, $CDCl_3$): δ 170.7, 70.7, 70.5, 70.45, 70.44, 69.8, 68.4, 51.6, 50.5. IR (cm^{-1}): 2069, 2098, 1753, 1439, 1348, 1283, 1210, 1116, 937, 852, 706. CI-HRMS: Calculated for $C_9H_{18}N_3O_5^+$ [M+1]$^+$: 248.1241, found 248.1246.

Synthesis of MeO-EG$_3$-OTs (3.10)

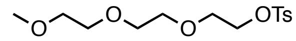
As reported in the literature, to a solution of triethylene glycol monomethyl ether (10 mL, 62 mmol) in CH_2Cl_2 (400 mL) was added triethylamine (20 mL) and DMAP (1.8 g, 15 mmol). At 0°C, *p*-toluenesulfonyl chloride (14.5 g, 76 mmol) was then slowly added to give a yellow solution. The reaction was for 4 hours at room temperature and then concentrated under vacuum. The crude mixture was redissolved in acetone to give a white precipitate, filtered and concentrated under vacuum. The solution was then purified by silica gel column chromatography using EtOAc to give the tosylated product as a yellow oil (11.8 g, 60% yield). $^{13}C\{^1H\}$ NMR (75 MHz, $CDCl_3$): δ 175.1, 144.7, 133.0, 129.8, 127.9, 71.9, 70.7, 70.5, 69.3, 68.6, 59.0, 21.6. ^{13}C $\{^1H\}$ NMR (75 MHz, $CDCl_3$): δ 144.7, 132.9, 129.8, 127.9, 71.8, 70.7, 70.51, 70.49, 69.2, 68.6, 59.0, 21.6. IR (cm^{-1}): 2876, 1598, 1452, 1353, 1175, 1096, 1017, 918, 816, 774, 663, 554. EI-HRMS: Calculated for $C_{14}H_{22}O_6S^+$ $[M]^+$: 318.1137, found 318.1143.

Synthesis of MeO-EG$_3$-N$_3$ (3.11)

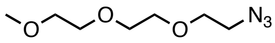
As reported in the literature, to a solution of NaN_3 (1.70 g, 26.15 mmol) dissolved in DMF (100 mL) was added MeO-EG$_3$-OTs (4.09 g, 12.85 mmol). The reaction was heated at reflux for 48 hours. H_2O (100 mL) was then added to the reaction mixture and performed an extraction with EtOAc (100 mL). The organic layer was washed with H_2O (3 x 30 mL). The combined organic layers were dried over Na_2SO_4, filtered and concentrated under vacuum. The solution was purified by silica gel column chromatography using 1:1 EtOAc/hexanes to give the desired azido compound as a light yellow oil (1.22 g, 50% yield). ^1H NMR (600 MHz, $CDCl_3$): δ 3.69-3.65 (m, 8H), 3.57-3.55 (m, 2H), 3.41-3.39 (m, 5H). $^{13}C\{^1H\}$ NMR (75 MHz, $CDCl_3$): δ 71.9, 70.7, 70.6, 70.5, 70.0, 59.0, 50.6. IR (cm^{-1}): 2872, 2097, 1452, 1347, 1285, 1199, 1106, 1029, 934, 851, 646, 557. CI-HRMS: Calculated for $C_9H_{18}N_3O_5^+$ $[M+1]^+$: 190.1192, found 190.1189.

Synthesis of MeO-EG$_3$-NH$_2$ (3.12)

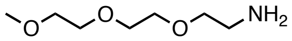
Under hydrogen atmosphere, Pd/C (0.060 mg) was suspended in MeOH (5 mL) purged with hydrogen. Then MeO-EG$_3$-N$_3$ (0.011 g, 0.58 mmol) dissolved in MeOH (5 mL) was added to the reaction flask. The reaction was left for 3 h. Then the solution was filtered with celite to give the final amino compound (0.09 mg, 95% yield). ^1H NMR (600

MHz, $CDCl_3$): δ 3.67-3.53 (m, 10H), 3.39 (s, 3H), 2.91-2.89 (m, 2H), 2.16 (bs, 2H). $^{13}C\{^1H\}$ NMR (75 MHz, $CDCl_3$): δ 71.3, 71.0, 70.0, 69.9, 69.9, 58.4, 50.8. CI-HRMS: Calculated for $C_9H_{18}NO_3^+$ $[M+1]^+$: 164.1287, found 164.1283.

Synthesis of TrS-EG$_3$-OMe (3.13)

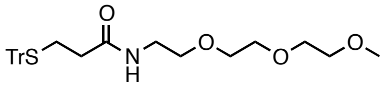

To a solution of TrS-NHS (27.5 mg, 0.17 mmol) in anhydrous CH_2Cl_2 (7 mL) was added MeO-EG$_3$-NH_2 (50.0 mg, 0.11 mmol) and a few drops of Et_3N. The reaction was left at room temperature for 18h then concentrated under vacuum. The crude reaction mixture was purified by silica gel column chromatography using EtOAc to give the purified compound as a light yellow oil (48.7 mg, 89% yield). ^1H NMR (600 MHz, $CDCl_3$): δ 7.42 (d, J = 6Hz, 6H), 7.28 (t, J = 6Hz, 6H), 7.21 (t, J = 6Hz, 3H), 5.99 (bs, 1H), 3.62-3.60 (m, 6H), 3.55-3.54 (m, 2H), 3.52-3.51 (m, 2H), 3.40-3.37 (m, 5H), 2.50 (t, J = 6Hz, 2H), 2.05 (t, J = 6Hz, 2H). $^{13}C\{^1H\}$ NMR (75 MHz, $CDCl_3$): δ 170.9, 144.7, 129.5, 127.9, 126.6, 71.9, 70.5, 70.4, 70.1, 69.7, 59.0, 39.2, 35.4, 27.7.

Synthesis of HS-EG$_3$-OMe (3.14)

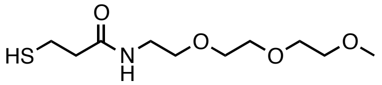

To a solution of TrS-EG$_3$-OMe (110 mg, 0.22 mmol) dissolved in anhydrous CH_2Cl_2 (5 mL) was added TIPS (0.2 mL) then TFA (0.5 mL). The reaction was left at room temperature for 3 hours and then concentrated under vacuum. The crude reaction mixture was purified by silica gel column chromatography using 5:1 CH_2Cl_2/*i*-PrOH to give the final product as a light yellow oil. ^1H NMR (600 MHz, $CDCl_3$): δ 6.45 (bs, 1H), 3.66-3.64 (m, 6H), 3.59-3.58 (m, 4H), 3.50-3.48 (m, 2H), 3.40-3.39 (m, 3H), 2.84-2.80 (m, 2H), 2.54-2.50 (m, 2H), 1.63 (t, 1H). $^{13}C\{^1H\}$ NMR (75 MHz, $CDCl_3$): δ 172.6, 71.9, 70.4, 70.3, 70.2, 69.8, 59.0, 40.3, 39.3, 20.5. EI-HRMS: Calculated for $C_{37}H_{50}N_2O_8S^+$ $[M-H]^+$: 250.1119, found 250.1104.

Synthesis of TrS-EG$_4$-COOMe (3.15)

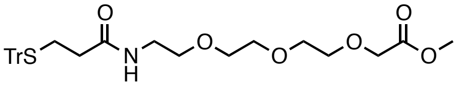

Under hydrogen atmosphere, to a suspension of Pd/C (60 mg) in 2:3 CH_2Cl_2/MeOH (15 mL) purged with hydrogen was added TrS-NHS (0.25 g, 0.56 mmol). Then N_3-EG$_4$-COOMe (0.10 g, 0.40 mmol) dissolved in MeOH (5 mL) was added to the reaction flask. The reaction was stirred at room temperature for 3 h under hydrogen atmosphere. A small amount of Et_3N was then added and the reaction was left to stir overnight under an argon atmosphere. The solution was then filtered with celite and concentrated under vacuum. The solution was purified by silica gel column chromatography using EtOAc to give the desired amide coupled compound (0.158 mg, 72% yield). ^{1}H NMR (600 MHz, $CDCl_3$): δ 7.38 (d, J = 12 Hz, 6H), 7.25 (t, J = 12 Hz, 6H), 7.17 (t, J = 12 Hz, 3H), 5.93 (bs, 1H), 4.12 (s, 2H), 3.70-3.57 (m, 5H), 3.64-3.62 (m, 2H), 3.58-3.54 (m, 4H), 3.49-3.46 (m, 2H), 3.37-3.33 (m, 2H), 2.46 (t, J = 12 Hz, 2H), 2.02 (t, J = 12 Hz, 2H). $^{13}C\{^1H\}$ NMR (75 MHz, $CDCl_3$): δ 171.0, 170.8, 144.7, 129.5, 127.9, 126.6, 70.8, 70.5, 70.4, 70.1, 69.8, 68.5, 66.7, 51.8, 39.2, 35.4, 27.7. IR (cm^{-1}): 3314, 3056, 2870, 1753, 1651, 1537, 1488, 1443, 1350, 1211, 1118, 1034, 853, 745, 701, 622. ESI-HRMS: Calculated for $C_{31}H_{37}NO_6S^+$ [M+Na]$^+$: 574.2234, found 574.2234.

Synthesis of TrS-EG$_4$-COOH (3.16)

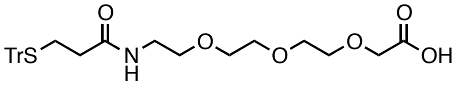

To a solution of TrS-EG$_4$-COOMe (439.6 mg, 0.80 mmol) dissolved in H_2O (30 mL) was added K_2CO_3 (1.0 g). The reaction was heated at reflux for two hours. The reaction mixture was then cooled to room temperature and acidified to pH = 1 using 1M HCl. The acidified solution was then extracted using CH_2Cl_2 (4 x 20 mL). The combined organic layers were dried over Na_2SO_4, filtered and concentrated under vacuum to give the desired acid compound as a clear and colorless oil (0.40 g, 93 % yield). ^{1}H NMR (600 MHz, $CDCl_3$): δ 7.42 (d, J = 12 Hz, 6H), 7.29 (t, J = 12 Hz, 6H), 7.21 (t, J = 12 Hz, 3H), 6.26 (bs, 1H), 4.16 (s, 2H), 3.78-3.75 (m, 2H), 3.69-3.66 (m, 4H), 3.62-3.60 (m, 2H), 3.54-3.50 (m, 2H), 3.44-3.40 (m, 2H), 2.49 (t, J = 12 Hz, 2H), 2.18 (t, J = 12 Hz, 2H). $^{13}C\{^1H\}$ NMR (75 MHz, $CDCl_3$): δ 171.44, 171.39, 144.7, 129.6, 127.9, 126.6, 71.6, 70.6, 70, 69.8, 69.1, 66.7, 39.2, 35.2, 27.8. ESI-HRMS: Calculated for $C_{30}H_{35}NO_6S^+$ [M+Na]$^+$: 560.2077, found 560.2073.

Synthesis of TrS-EG$_4$-EG$_3$-OMe (3.17)

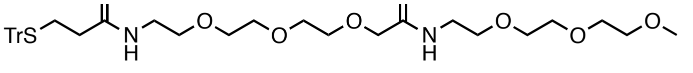

Under argon atmosphere, to a solution of TrS-EG$_4$-COOH (338 mg, 0.63 mmol) and HBTU (334 mg, 0.88 mmol) dissolved in anhydrous CH_3CN (15 mL) was added MeO-EG$_3$-NH_2 (120 mg, 0.74 mmol) and DIPEA (0.3 mL, 1.7 mmol). The reaction was left overnight and then concentrated under vacuum. The crude reaction mixture was purified by silica gel column chromatography using 5% MeOH in CH_2Cl_2 to give the desired product (209

mg, 47% yield). ^{1}H NMR (600 MHz, $CDCl_3$): δ 7.41 (d, J = 6 Hz, 6H), 7.28 (t, J = 6 Hz, 6H), 7.21 (t, J = 6 Hz, 3H), 7.16 (bs, 1H), 6.30 (bs, 1H), 4.04 (s, 2H), 3.68-3.67 (m, 2H), 3.65-3.49 (m, 20H), 3.40-3.37 (m, 5H), 2.49 (t, J = 12 Hz, 2H), 2.09 (t, J = 12 Hz, 2H). $^{13}C\{^1H\}$ NMR (75 MHz, $CDCl_3$): δ 171.1, 170.1, 144.7, 129.6, 127.9, 126.6, 71.9, 70.6, 70.49, 70.45, 70.43, 70.36, 70.2, 70.1, 69.9, 69.8, 66.6, 59.0, 39.2, 38.6, 35.2, 27.7. IR (cm^{-1}): 3422, 3317, 3058, 2971, 1658, 1536, 1489, 1444, 1349, 1250, 1107, 1034, 744, 702. ESI-HRMS: Calculated for $C_{37}H_{50}N_2O_8S^+$ $[M+Na]^+$: 705.3180, found 705.3187.

Synthesis of HS-EG$_4$-EG$_3$-OMe (3.18)

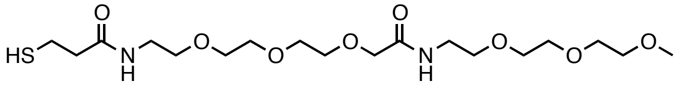

To a solution of TrS-EG$_4$-EG$_3$-OMe (124.9 mg, 0.18 mmol) dissolved in anhydrous CH_2Cl_2 (5 mL) was added TIPS (0.2 mL) then TFA (0.5 mL). The reaction was left at room temperature for 2 hours and then concentrated under vacuum. The crude reaction mixture was purified by silica gel column chromatography using 4:1 CH_2Cl_2/*i*-PrOH to give the final ligand as a clear and colorless oil (62 mg, 78% yield). ^{1}H NMR (600 MHz, $CDCl_3$): 7.21 (bs, 1H), 6.72 (bs, 1H), 4.08 (s, 2H), 3.71-3.69 (m, 2H), 3.67-3.62 (m, 12H), 3.60-3.53 (m, 6H), 3.52-3.45 (m, 4H), 3.37 (s, 3H), 2.80 (q, J = 12 Hz, 2H), 2.51 (t, J = 12 Hz, 2H), 1.62 (t, J = 12 Hz, 1H). $^{13}C\{^1H\}$ NMR (75 MHz, $CDCl_3$): 171.0, 170.4, 71.8, 70.7, 70.6, 70.44, 70.43, 70.34, 70.2, 70.1, 69.9, 69.7, 59.0, 40.1, 39.3, 38.6, 20.5. IR (cm^{-1}): 3515, 3313, 3084, 2872, 2550, 1651, 1543, 1452, 1349, 1286, 1251, 1200, 1101, 940, 850, 576. EI-HRMS: Calculated for $C_{18}H_3N_2O_8S^+$ $[M+H]^+$: 441.2265, found 441.2284.

3.6 References

[1] S. Link, M. A. El-Sayed, *Annu. Rev. Phys. Chem.* **2003**, *54*, 331-366.

[2] X. H. Huang, I. H. El-Sayed, W. Qian, M. A. El-Sayed, *J. Am. Chem. Soc.* **2006**, *128*, 2115-2120.

[3] X. Huang, M. A. El-Sayed, *J. Adv. Res.* **2010**, *1*, 13-28.

[4] W. P. Wuelfing, S. M. Gross, D. T. Miles, R. W. Murray, *J. Am. Chem. Soc.* **1998**, *120*, 12696-12697.

[5] J. Turkevich, P. C. Stevenson, J. Hillier, *Discuss. Faraday Soc.* **1951**, 55-75.

[6] H. L. Zhang, H. Xia, H. L. Li, Z. F. Liu, *Chem. Lett.* **1997**, 721-722.

[7] K. V. Gujraty, R. Ashton, S. R. Bethi, S. Kate, C. J. Faulkner, G. K. Jennings, R. S. Kane, *Langmuir* **2006**, *22*, 10157-10162.

[8] T. Wei, J. H. Jung, T. F. Scott, *J. Am. Chem. Soc.* **2015**, *137*, 16196-16202.

[9] T. Q. Liu, B. Thierry, *Langmuir* **2012**, *28*, 15634-15642.

[10] M. Schollbach, F. J. Zhang, F. Roosen-Runge, M. W. A. Skoda, R. M. J. Jacobs, F. Schreiber, *J. Colloid Interface Sci.* **2014**, *426*, 31-38.

[11] W. Haiss, N. T. K. Thanh, J. Aveyard, D. G. Fernig, *Anal. Chem.* **2007**, *79*, 4215-4221.

[12] F. Schulz, T. Vossmeyer, N. G. Bastus, H. Weller, *Langmuir* **2013**, *29*, 9897-9908.

CHAPTER 4

4.1 Conclusion

The Workentin AuNP toolbox was developed in order to allow for tuning and application of the unique size-dependent physical, chemical and biological properties of AuNPs by designing functional templates with click and bioorthogonal functional groups. For example, our group was the first to introduce strained alkyne functionality onto AuNPs and demonstrate its interfacial SPAAC reactivity.[1] We then expanded the scope of strained alkyne chemistry by developing a protection-deprotection strategy via the formation of a dicobalthexacarbonyl complex.[2] As part of my undergraduate thesis project, we reported the functionalization of a $CO_2(CO)_6$-protected bicyclononyne complex that could be subsequently deprotected to regenerate the strained alkyne functionality. Although this was an excellent protection-deprotection strategy for small molecule chemistry, our group transitioned towards photoreactive cyclopropenone-based strategies for the modification of nanomaterials as a result of the undesirable reactivity of alkyne-$Co_2(CO)_6$ complexes towards nucleophiles, including thiols. By preparing photoDIBO-AuNP precursors that upon irradiation by UV light could generate strained alkyne functionalized AuNPs, our group expanded the AuNP toolbox by the addition of photochemical spatial and temporal control of reactivity.[3]

In Chapter 2, I described my addition to the AuNP click and bioorthogonal toolbox through a light activated and photo-reversible click and bioorthogonal functional group that will allow for unprecedented temporal and spatial control of photo-reactivity. The introduction of oNQM functionality was achieved via place exchange reaction onto methoxy-terminated AuNPs to provide an organic and water-soluble template. This required the synthesis of a complex thiol-modified NQMP ligand. The challenging synthetic protocol and characterization of all synthetic intermediates by ^{1}H NMR, ^{13}C NMR and IR spectroscopy as well as MS was reported in Chapter 2. The final ligand was synthesized in good yield through a selective deprotection strategy using acid/base sensitive protecting groups. The NQMP functional group was then successfully introduced onto a AuNP surface via place exchange with an approximate 20% loading that can be controlled by altering the reaction conditions such as a ratio of thiol to gold and reaction time. The novel template was characterized by ^{1}H NMR spectroscopy, IR spectroscopy, TGA and TEM. The spectral data confirmed the presence the NQMP ligand and TEM images revealed no significant change in regards to the size or shape of the gold core following place exchange when compared to the precursor AuNP. The photochemical properties were also investigated by UV-Vis spectroscopy revealing absorption maxima at 260 nm and 342 nm suitable for activation to the corresponding oNQM functionality. Figure 4.1 describes the introduction of this novel click and bioorthogonal functional group into the Workentin AuNP toolbox.

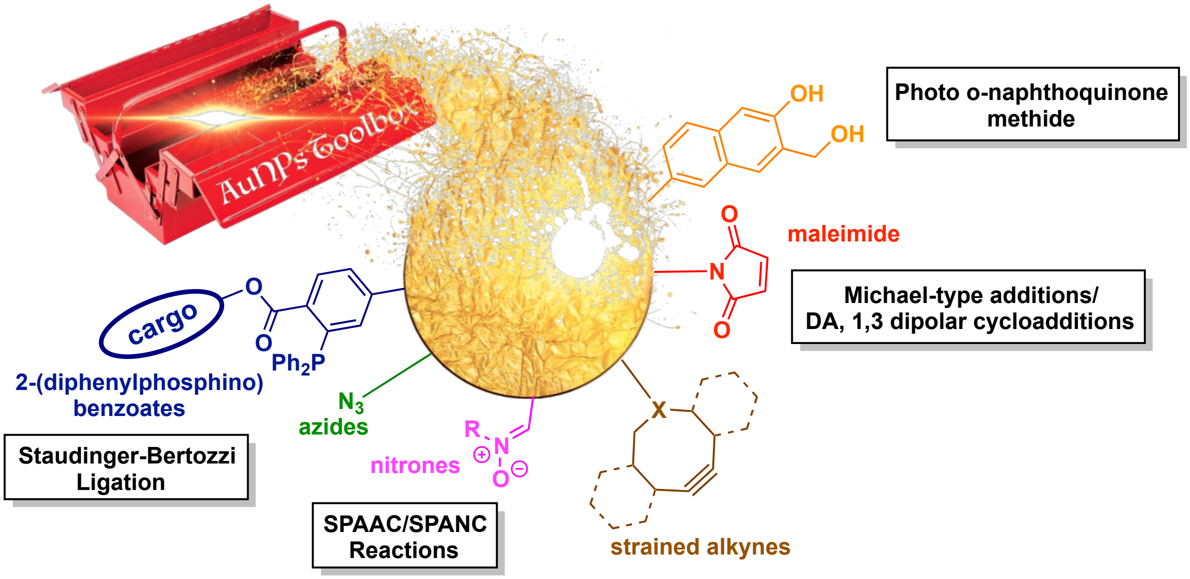
AuNPs Toolbox
OH
OH
Photo o-naphthoquinone methide
O
maleimide
N
O
Michael-type additions/ DA, 1,3 dipolar cycloadditions
cargo
O
O
Ph_2P
2-(diphenylphosphino) benzoates
Staudinger-Bertozzi Ligation
N_3
azides
R
N
O
nitrones
SPAAC/SPANC Reactions
X
strained alkynes

Figure 4.1: The Workentin AuNP toolbox reprinted with the addition of the NQMP-functionalized AuNP template developed in this thesis.

In Chapter 3, my aim was to develop a method to transfer the methods we have developed for the functionalization of small AuNPs onto larger AuNP systems in order to take advantage of the SPR. However, large AuNPs are much more difficult to stabilize than their small counterpart and subsequent functionalization is quite limited. In this chapter I described the synthesis of a novel ligand through a convergent approach by conjugating three different fragments through the formation of amide bonds. The design of this ligand included an amide bond pattern to provide additional stabilization as well as a repeating unit to increase the size of the ligand to account for larger AuNP core sizes. All three fragments were successfully synthesized in good yield so it is feasible to scale up the synthesis and generate large amounts of whatever ligand length is desired. In this chapter, the ligand was synthesized with one repeating unit and incorporated onto 20 nm AuNPs through a place exchange reaction with citrate-stabilized AuNPs. Through UV-Vis spectroscopy, preliminary results indicated that the place exchange reaction was successful. No discoloration of the solution was observed and TEM images indicated that no aggregation occurred following place exchange.

4.2 Future Work

Future developments with the novel NQMP-functionalized AuNP template developed in Chapter 2 will be to investigate the photochemical generation of oNQM and subsequent photochemical reactivity towards hetero-Diels-Alder cycloaddition and Michael Addition substrates. In particular, the resulting thioether linkage in the Michael Addition adduct between oNQM and a thiol may be photochemically cleaved to regenerate both starting materials for applications such as patterning and delivery systems.

The work presented in Chapter 3 detailed the first steps towards the stabilization and functionalization of large AuNPs via click and bioorthogonal chemistry. Future developments include a phase transfer protocol into organic media to for characterization via ^{1}H NMR spectroscopy. The synthetic strategy may then be modified to incorporate click and bioorthogonal functional groups from our AuNP toolbox and investigate the interfacial chemistry properties of this novel system.

4.3 References

[1] P. Gobbo, Z. Mossman, A. Nazemi, A. Niaux, M. C. Biesinger, E. R. Gillies, M. S. Workentin, *J. Mater. Chem. B* **2014**, *2*, 1764-1769.

[2] P. Gobbo, T. Romagnoli, S. M. Barbon, J. T. Price, J. Keir, J. B. Gilroy, M. S. Workentin, *Chem. Commun.* **2015**, *51*, 6647-6650.

[3] W. Luo, P. Gobbo, C. D. McNitt, D. A. Sutton, V. V. Popik, M. S. Workentin, *Chem. Eur. J.* **2017**, *23*, 1052-1059.

5.1 Chapter 2 Appendix

Table of Contents

2.A Characterization of HO-NQMP (compound **2.6**)........78
2.B Characterization of HO-NQMP-pt (compound **2.7**)........79
2.C Characterization of TsO-EG$_4$-OH (compound **2.2**)........81
2.D Characterization of AcS-EG$_4$-OH (compound **2.3**)........83
2.E Characterization of AcS-EG$_4$-I (compound **2.4**)........85
2.F Characterization of AcS-EG$_4$-NQMP-pt (compound **2.8**)........87
2.G Characterization of AcS-EG$_4$-NQMP (compound **2.9**)........89
2.H Characterization of HS-EG$_4$-NQMP (compound **2.10**)........90
2.I Characterization of TrS-EG$_4$-OH........92
2.J Characterization of TrS-EG$_4$-I........94
2.K Characterization of TrS-EG$_4$-NQMP-pt........96
2.L Characterization of TrS-EG$_4$-NQMP........98

2.A Characterization of HO-NQMP

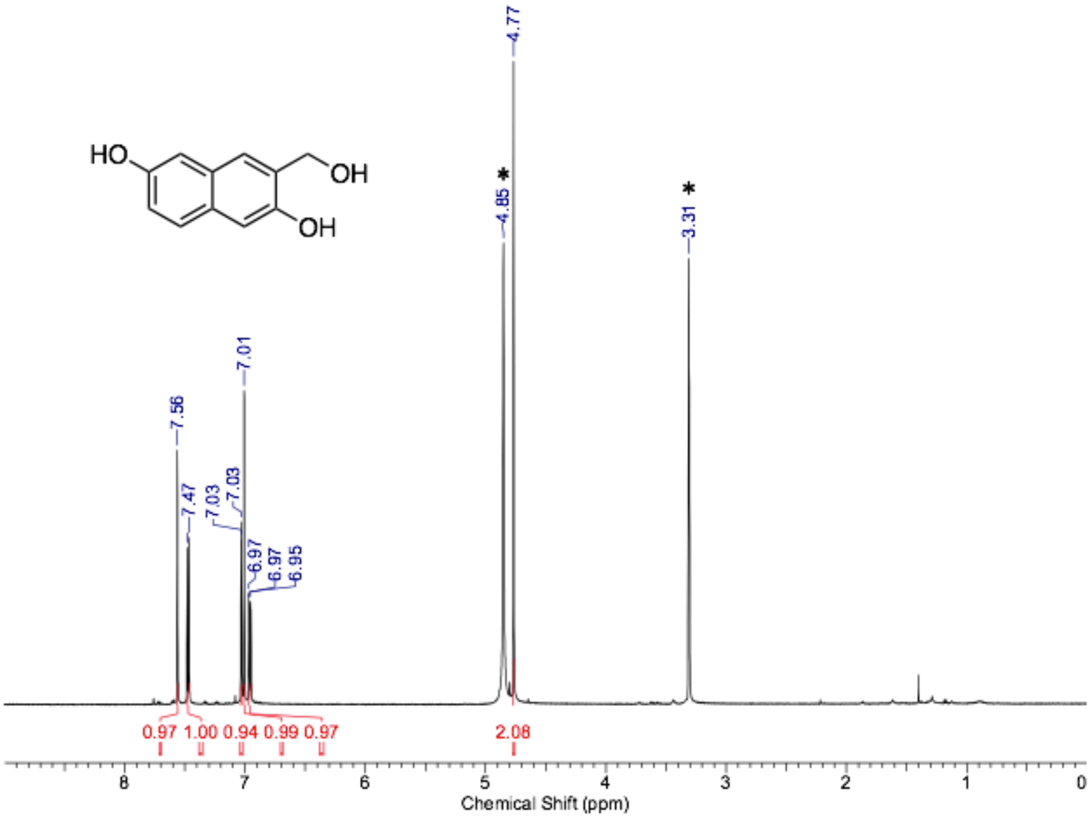

Figure 2.A1: ^{1}H NMR spectrum of HO-NQMP in CD$_3$OD. * denotes solvent signals.

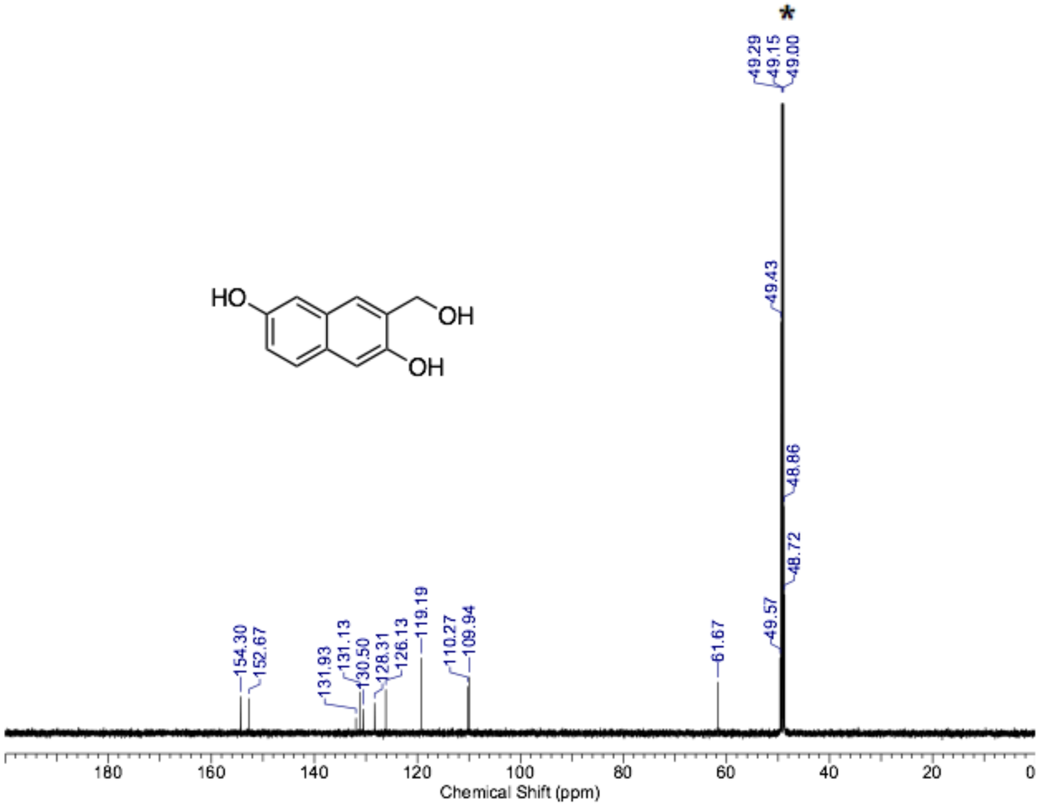

Figure 2.A2: ^{13}C{^{1}H} spectrum of HO-NQMP in CD$_3$OD. * denotes solvent signal(s).

2.B Characterization of HO-NQMP-pt

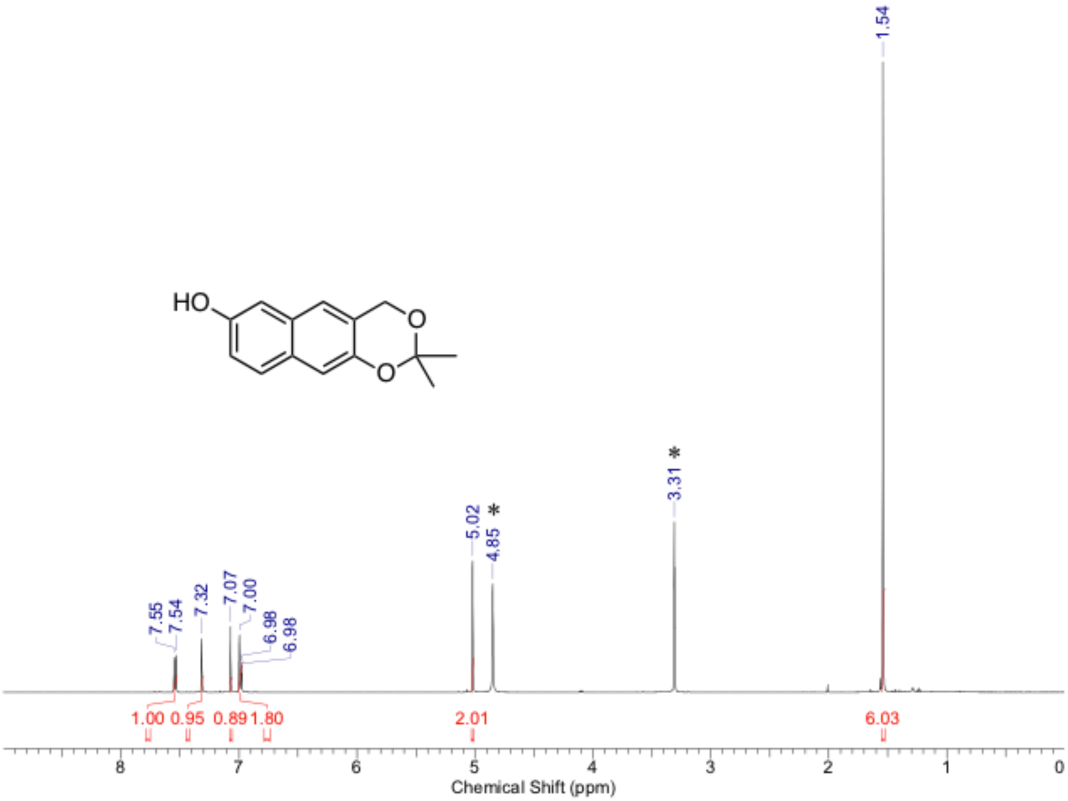

Figure 2.B1: ^{1}H NMR spectrum of HO-NQMP-pt in CD_3OD. * denotes solvent signal(s).

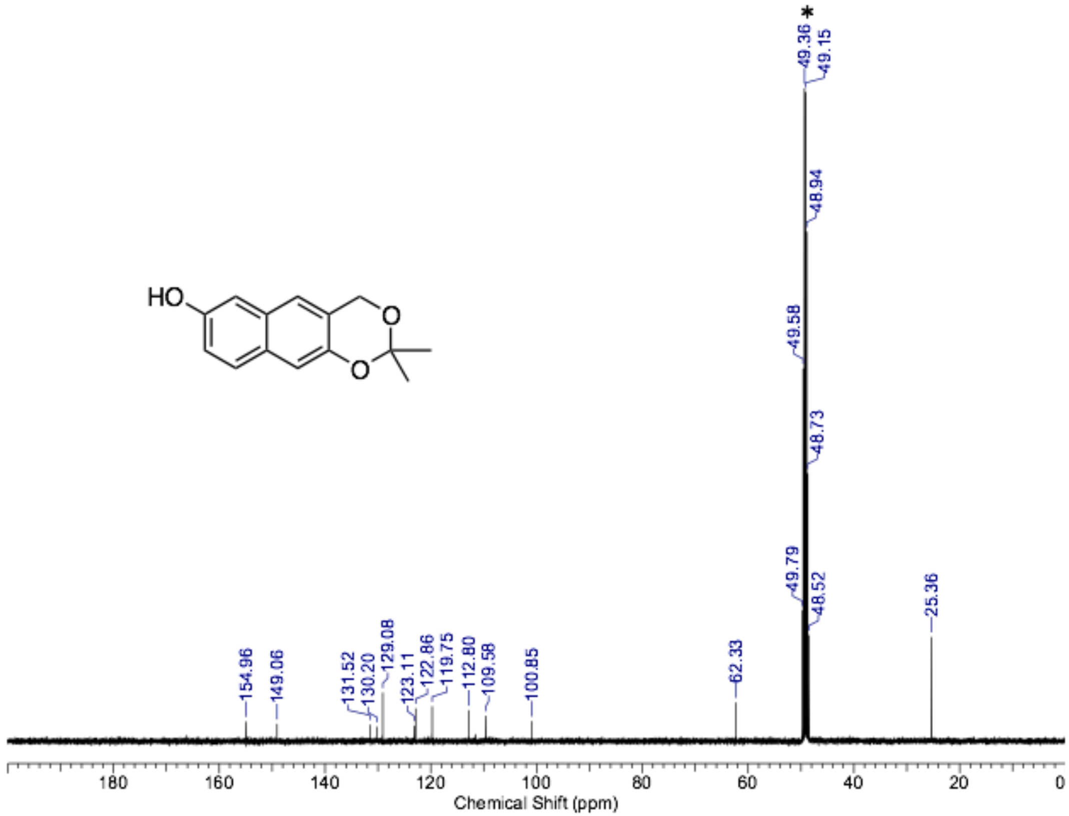

Figure 2.B2: $^{13}C\{^1H\}$ spectrum of HO-NQMP-pt in CD_3OD. * denotes solvent signal(s).

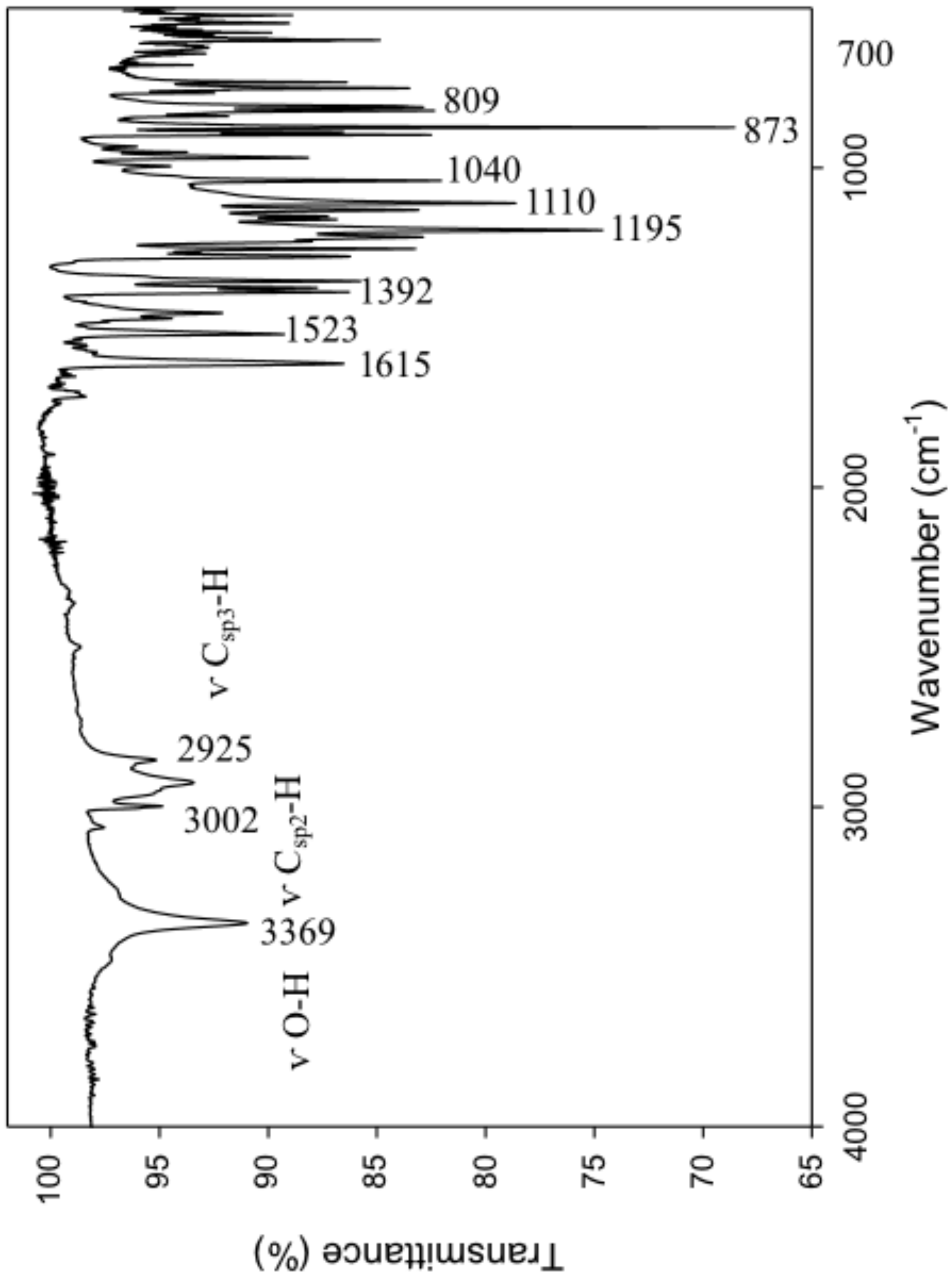

Figure 2.B3: IR absorption spectrum of HO-NQMP-pt.

2.C Characterization of TsO-EG$_4$-OH

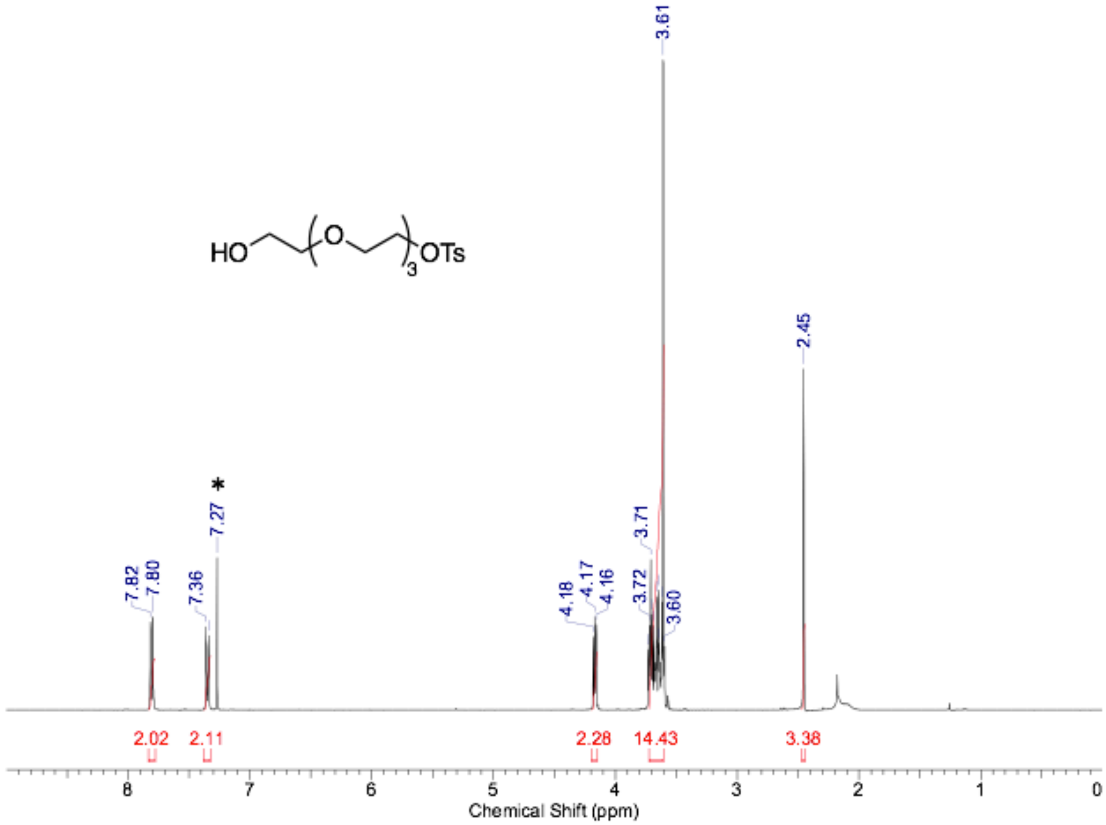

Figure 2.C1: ^{1}H NMR spectrum of TsO-EG$_4$-OH in CDCl$_3$. * denotes solvent signal(s).

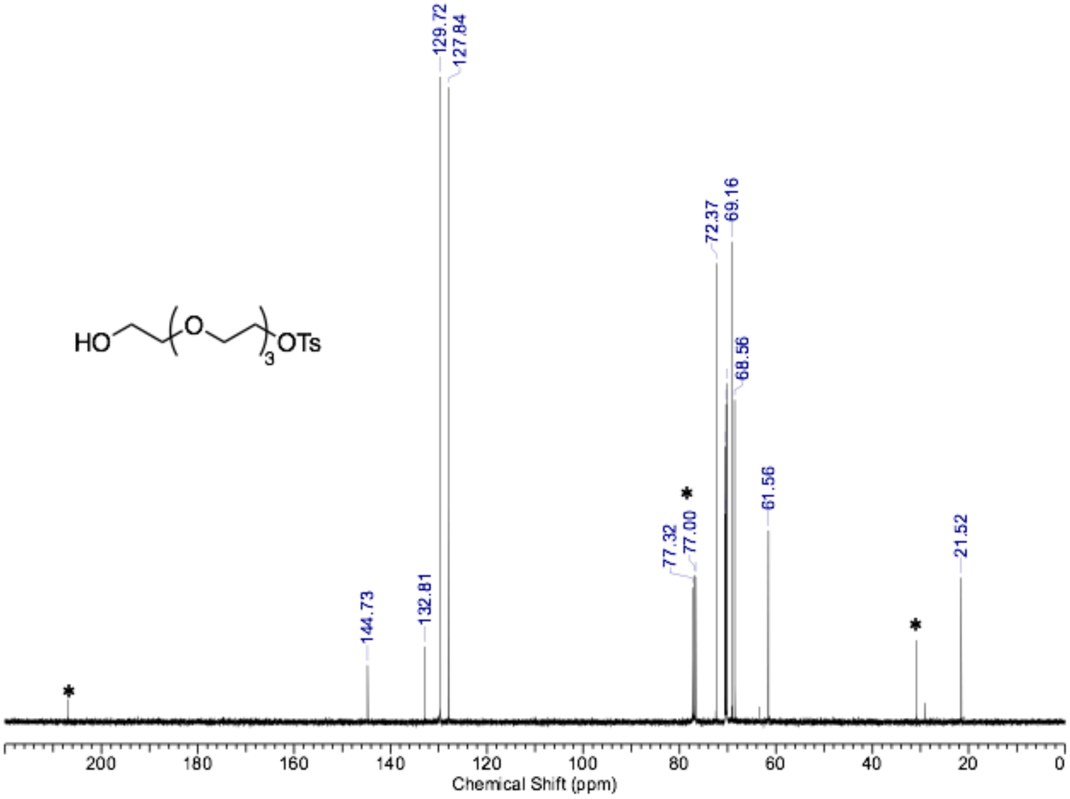

Figure 2.C2: ^{13}C{^{1}H} spectrum of TsO-EG$_4$-OH in CDCl$_3$. * denotes solvent signal(s).

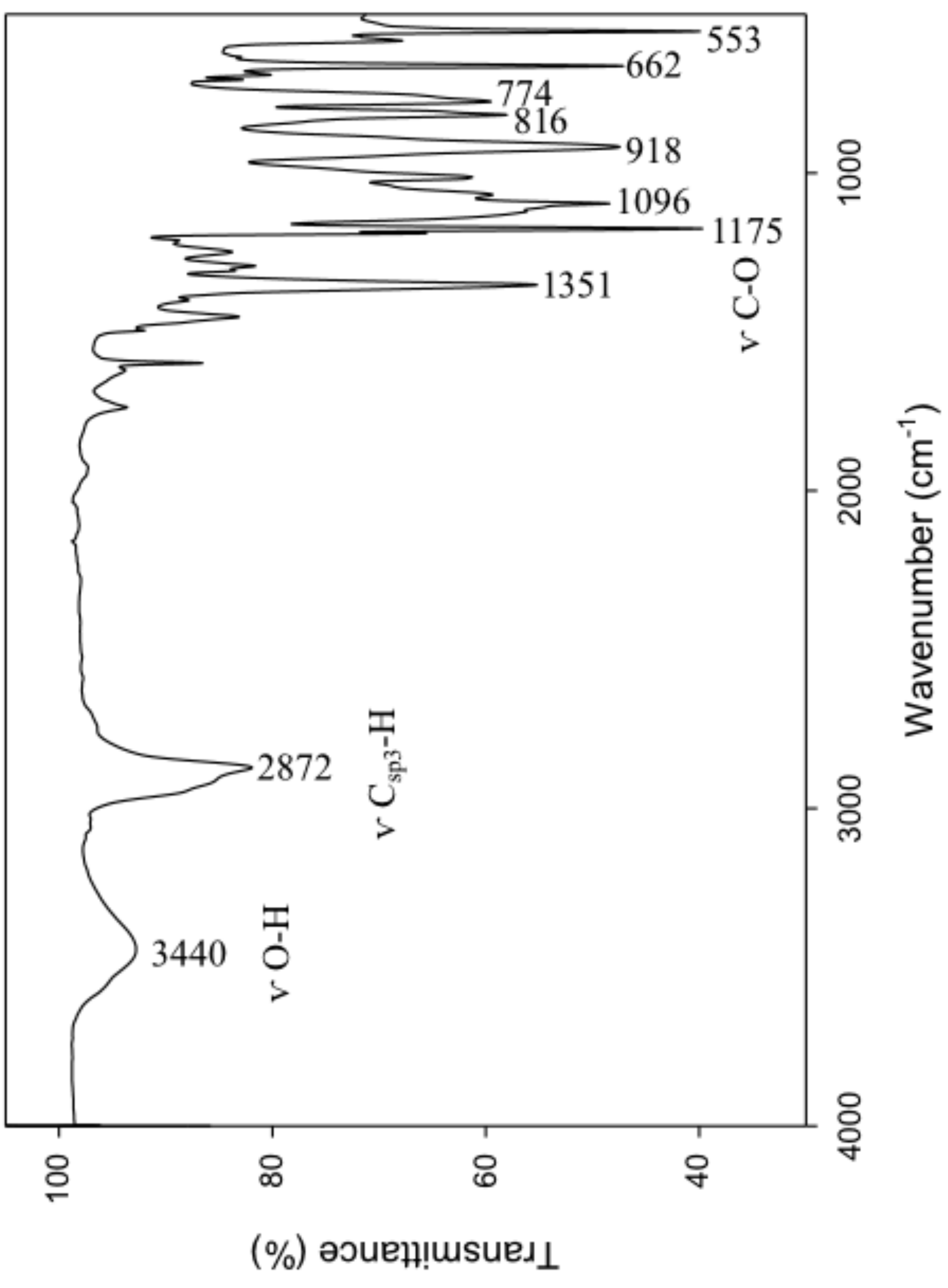

Figure 2.C3: IR absorption spectrum of TsO-EG$_4$-OH.

2.D Characterization of AcS-EG$_4$-OH

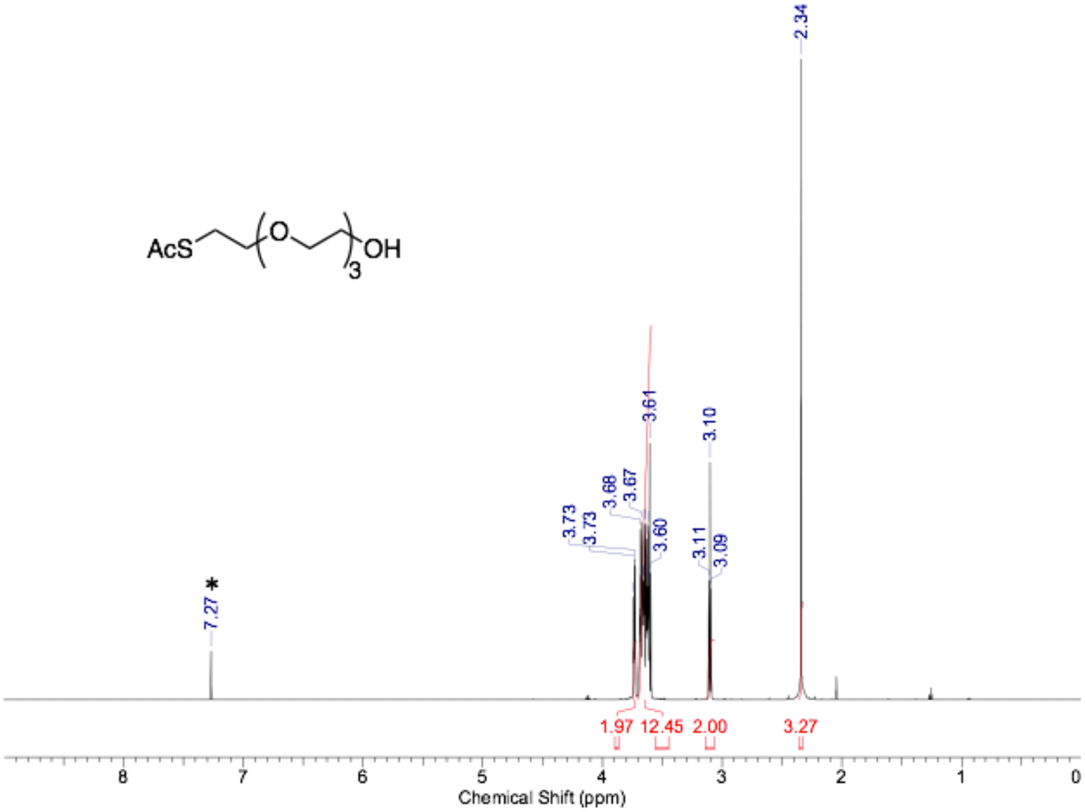

Figure 2.D1: ^{1}H NMR spectrum AcS-EG$_4$-OH in CDCl$_3$. * denotes solvent signal(s).

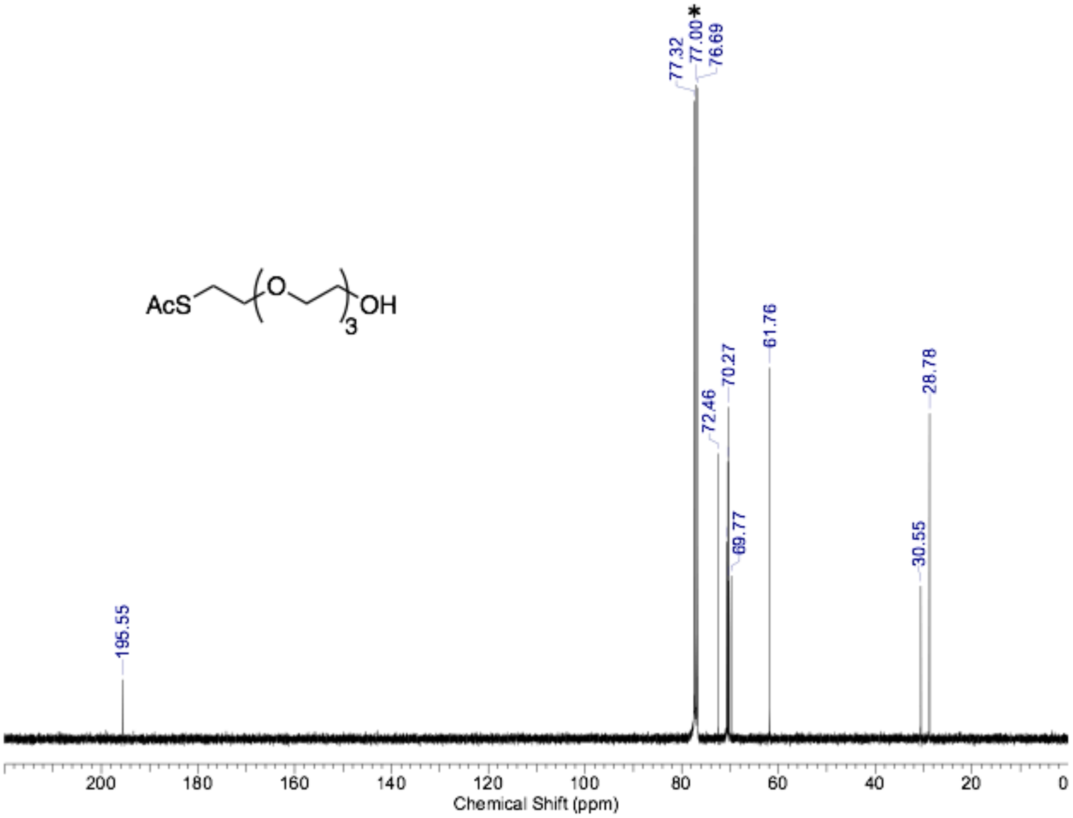

Figure 2.D2: ^{13}C{^{1}H} spectrum of AcS-EG$_4$-OH in CDCl$_3$. * denotes solvent signal(s).

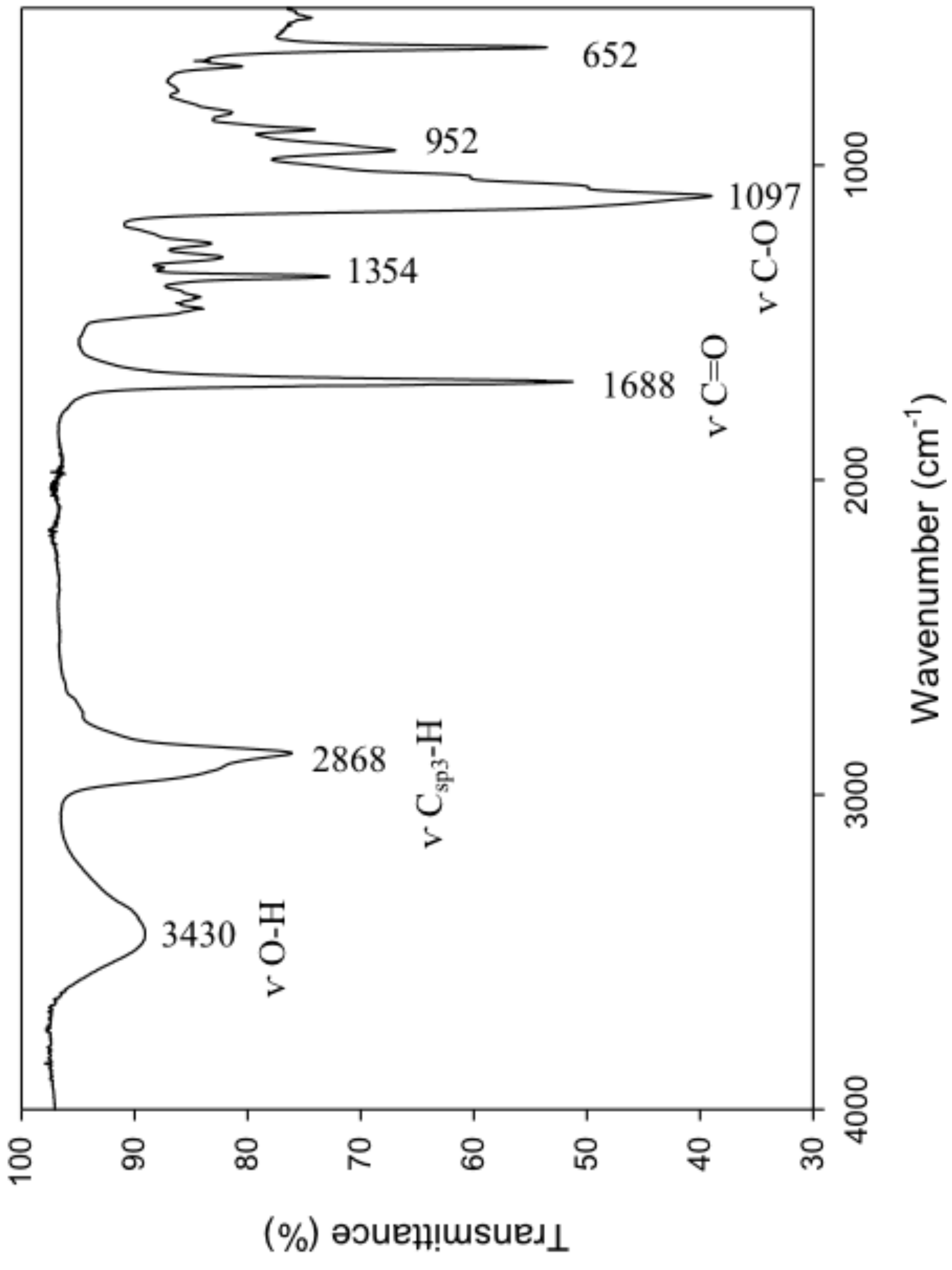

Figure 2.D3: IR absorption spectrum of AcS-EG$_4$-OH.

2.E Characterization of AcS-EG$_4$-I

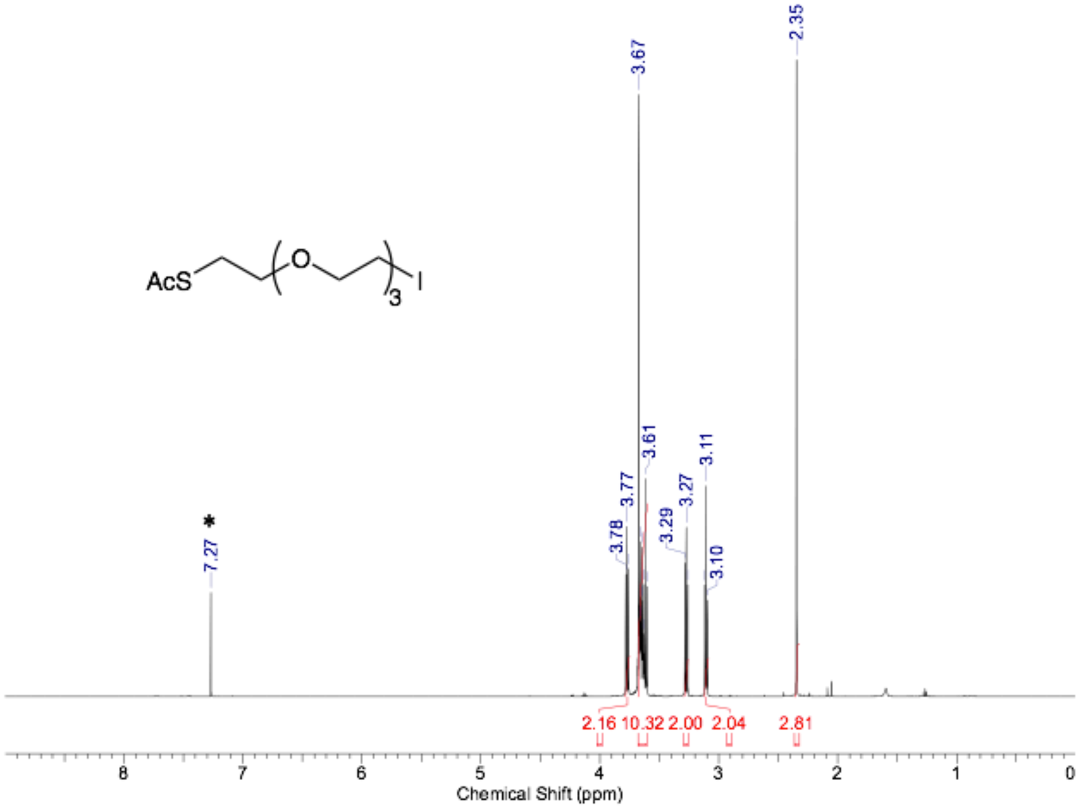

Figure 2.E1: ^{1}H NMR spectrum of AcS-EG$_4$-I in CDCl$_3$. * denotes solvent signal(s).

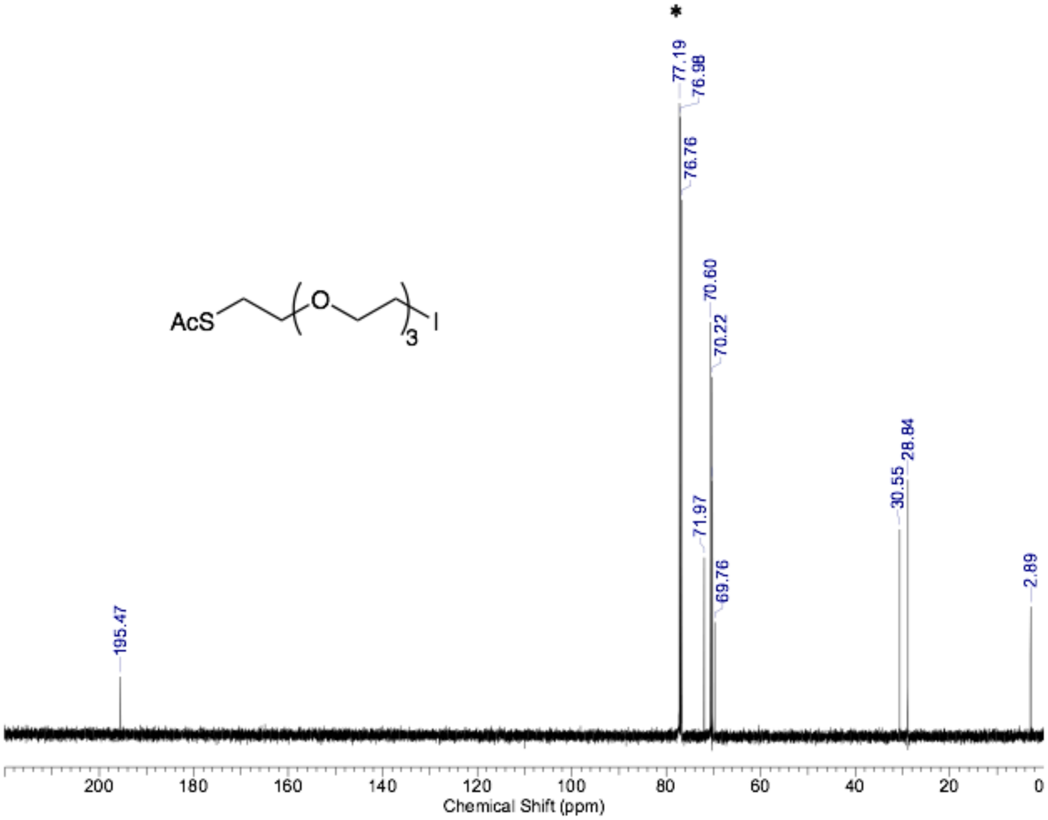

Figure 2.E2: ^{13}C{^{1}H} spectrum of AcS-EG$_4$-I. * denotes solvent signal(s).

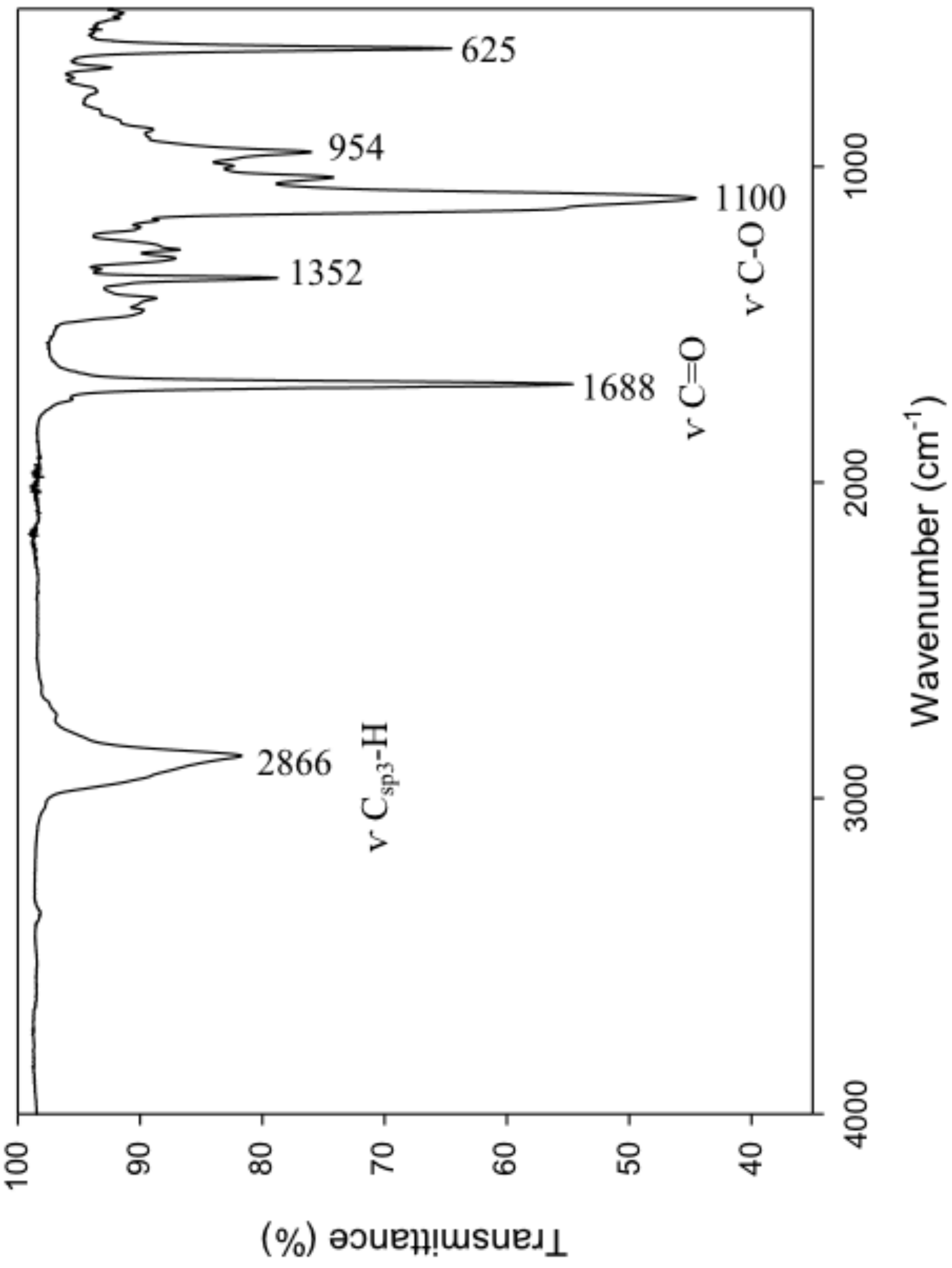

Figure 2.E3: IR absorption spectrum of AcS-EG$_4$-I.

2.F Characterization of AcS-EG$_4$-NQMP-pt

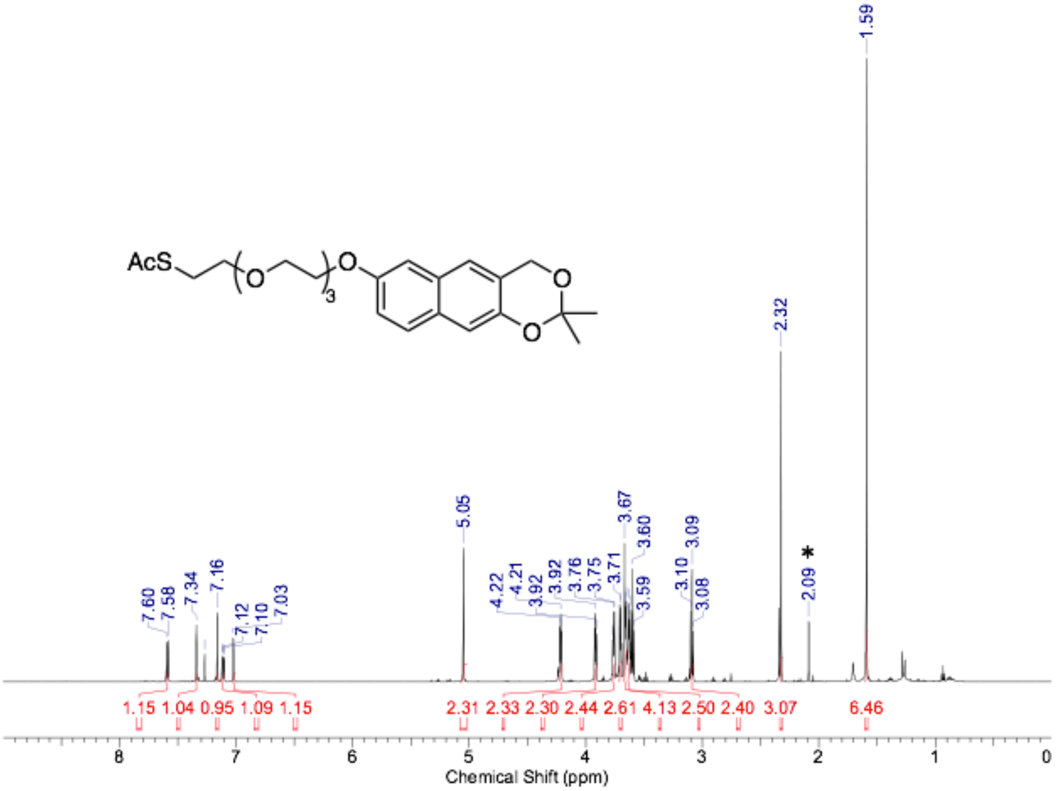

Figure 2.F1: ^{1}H NMR spectrum of AcS-EG$_4$-NQMP-pt in CDCl$_3$. * denotes solvent signal(s).

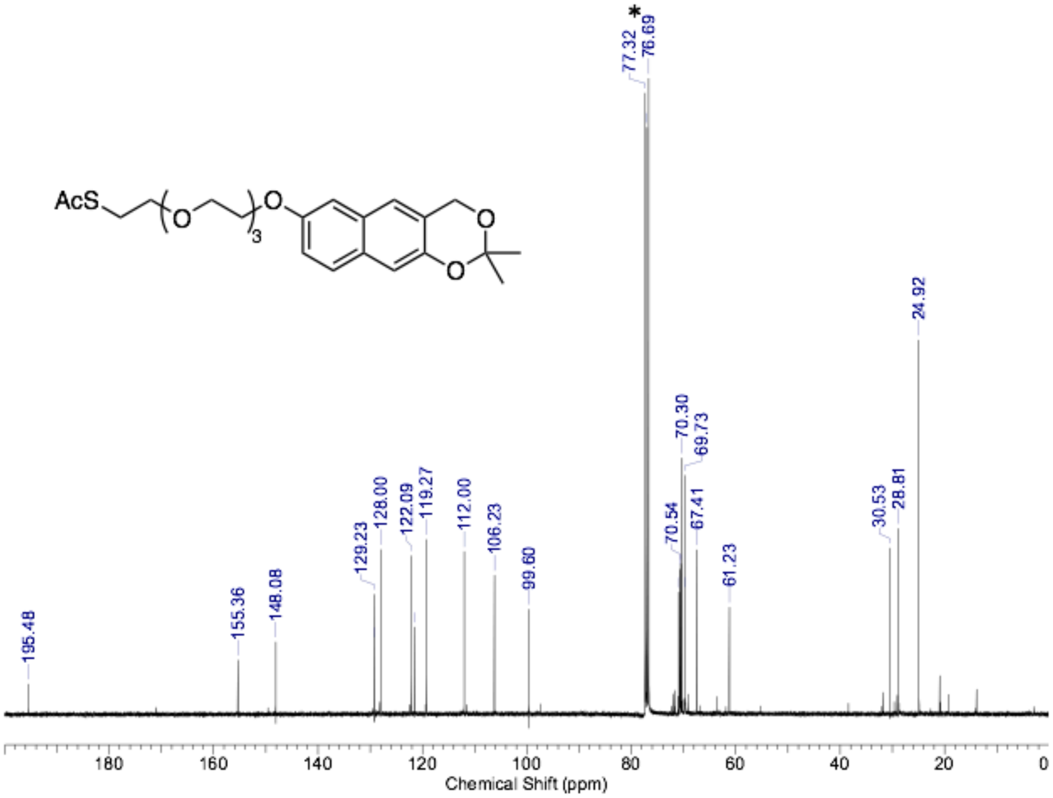

Figure 2.F2: ^{13}C{^{1}H} spectrum of AcS-EG$_4$-NQMP-pt in CDCl$_3$. * denotes solvent signal(s).

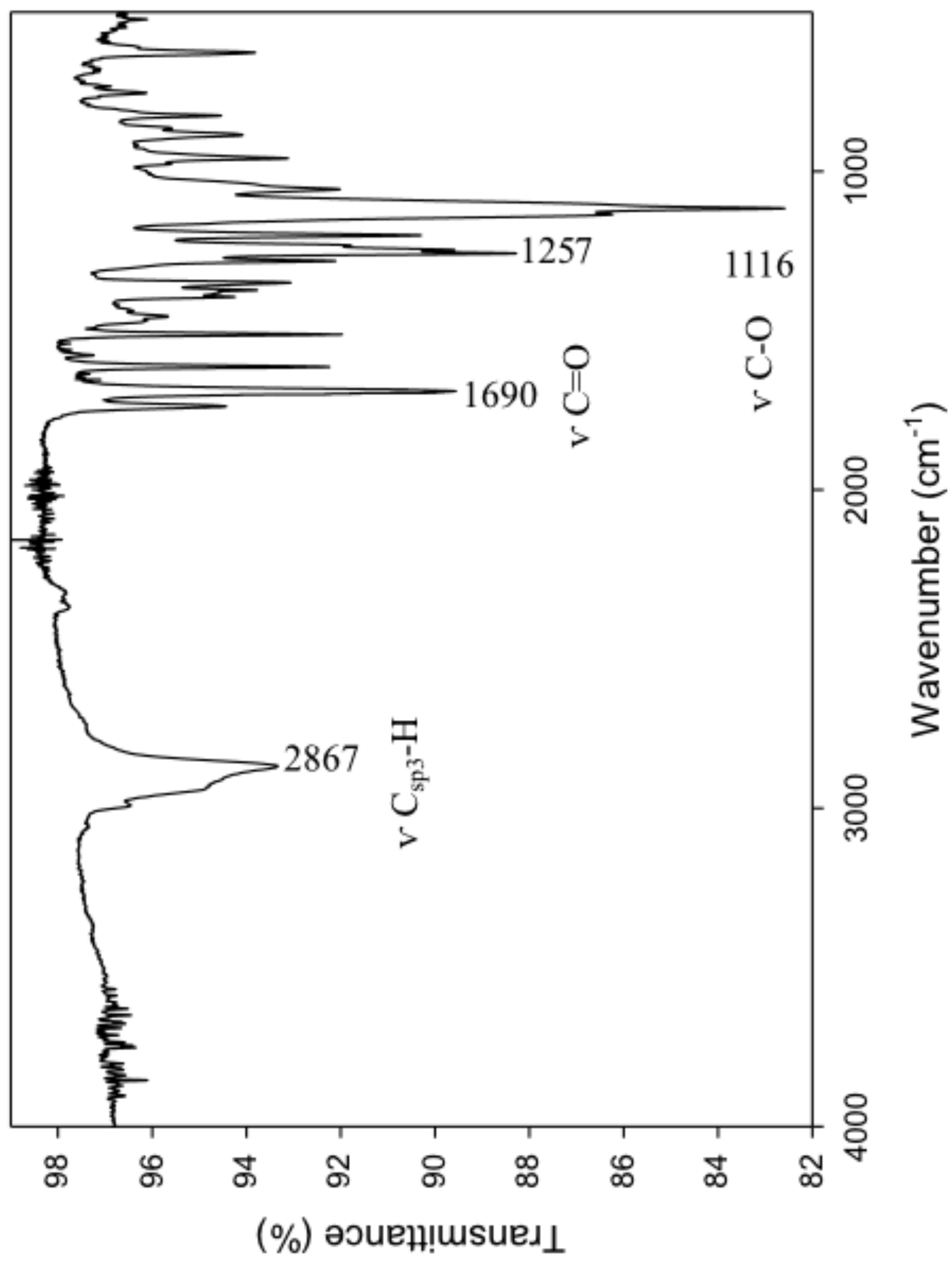

Figure 2.F3: IR absorption spectrum of AcS-EG$_4$-NQMP-pt.

2.G Characterization of AcS-EG$_4$-NQMP

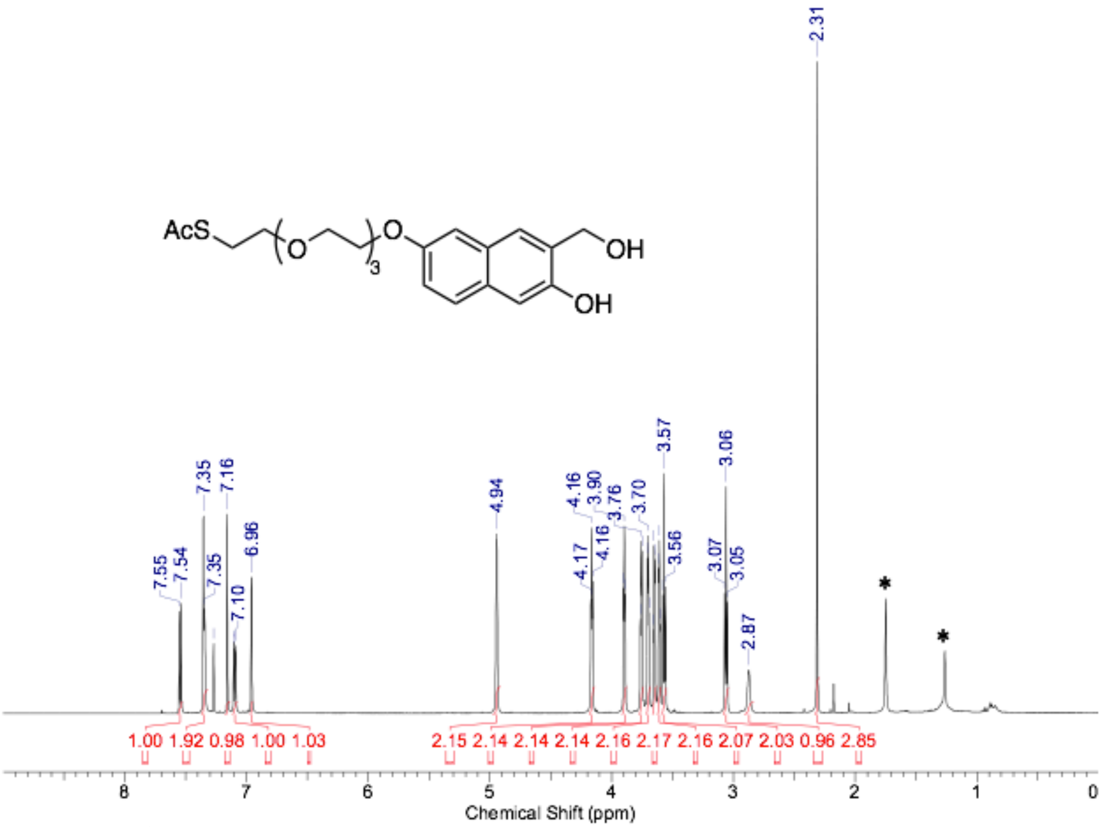

Figure 2.G1: ^{1}H NMR spectrum of AcS-EG$_4$-NQMP in CDCl$_3$. * denotes solvent signal(s).

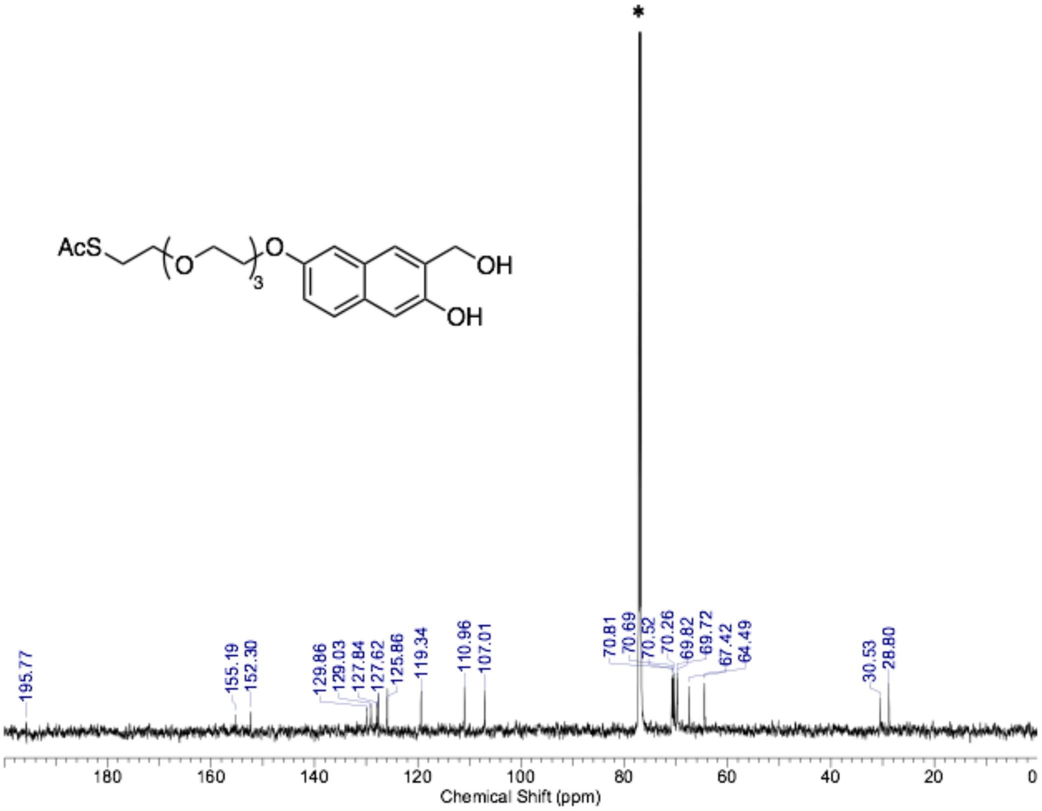

Figure 2.G2: ^{13}C{^{1}H} spectrum of AcS-EG$_4$-NQMP in CDCl$_3$. * denotes solvent signal(s).

2.H Characterization of HS-EG$_4$-NQMP

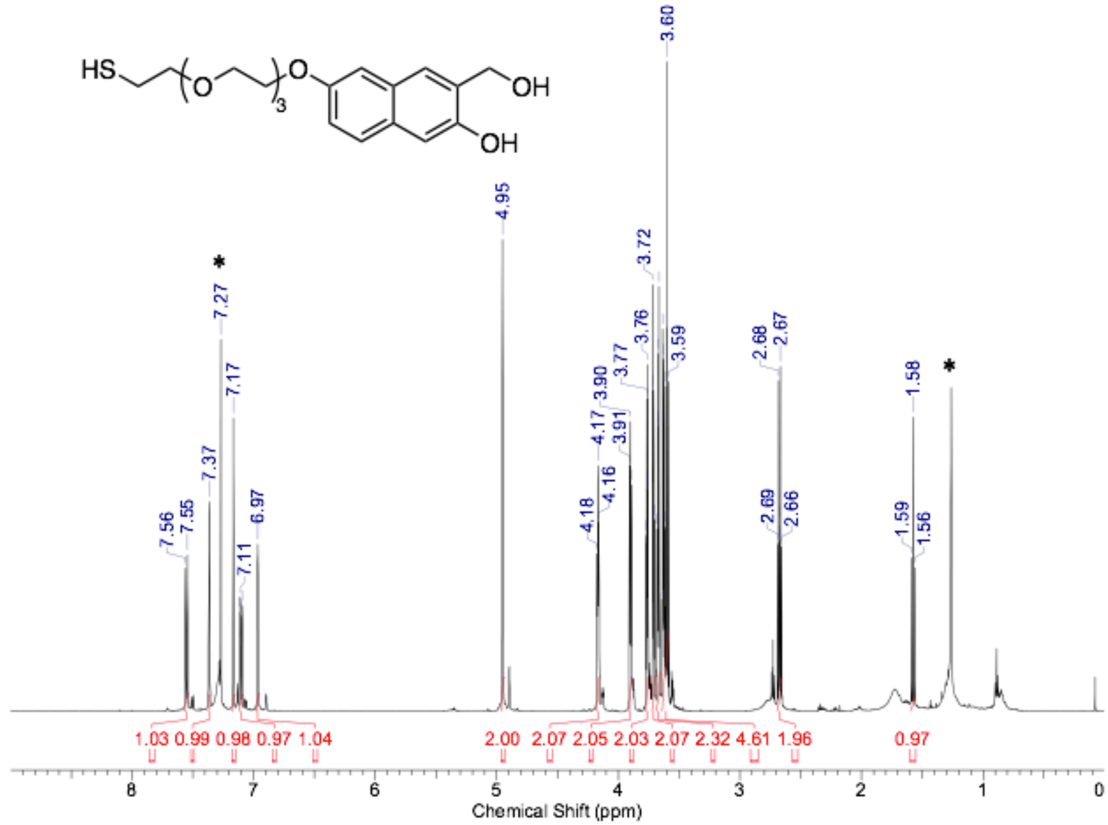

Figure 2.H1: ^{1}H NMR spectrum of HS-EG$_4$-NQMP in CDCl$_3$. * denotes solvent signal(s).

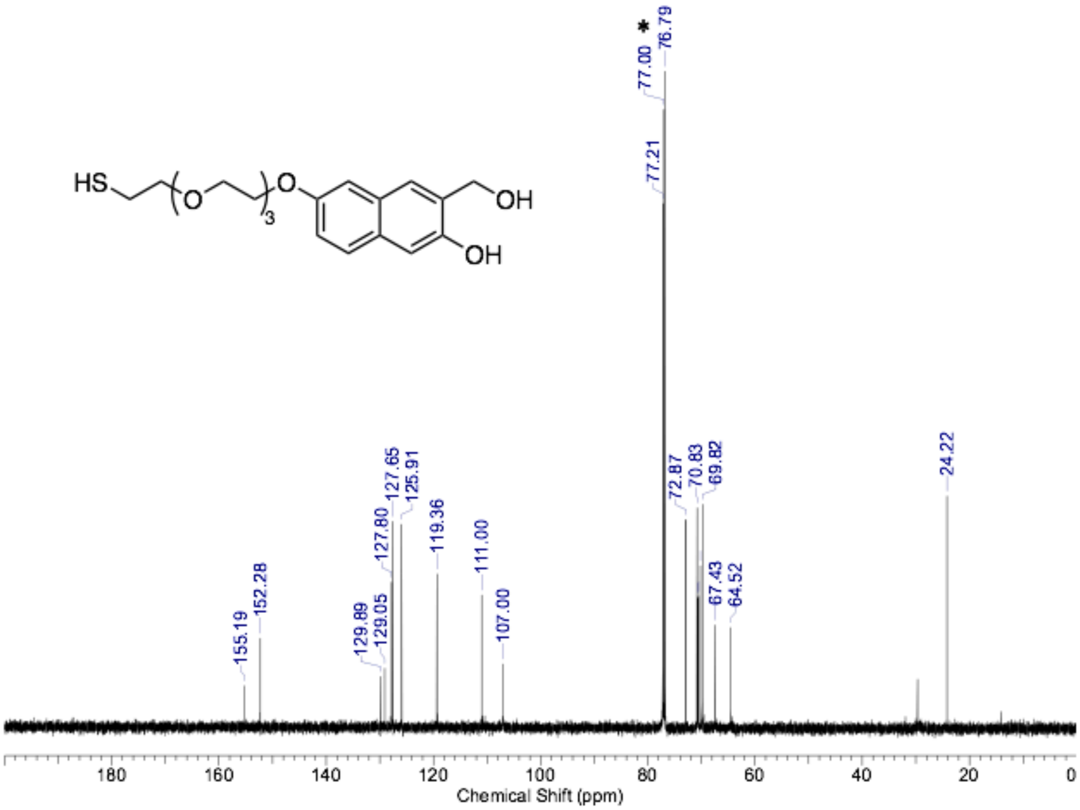

Figure 2.H2: ^{13}C{^{1}H} spectrum of HS-EG$_4$-NQMP in CDCl$_3$. * denotes solvent signal(s).

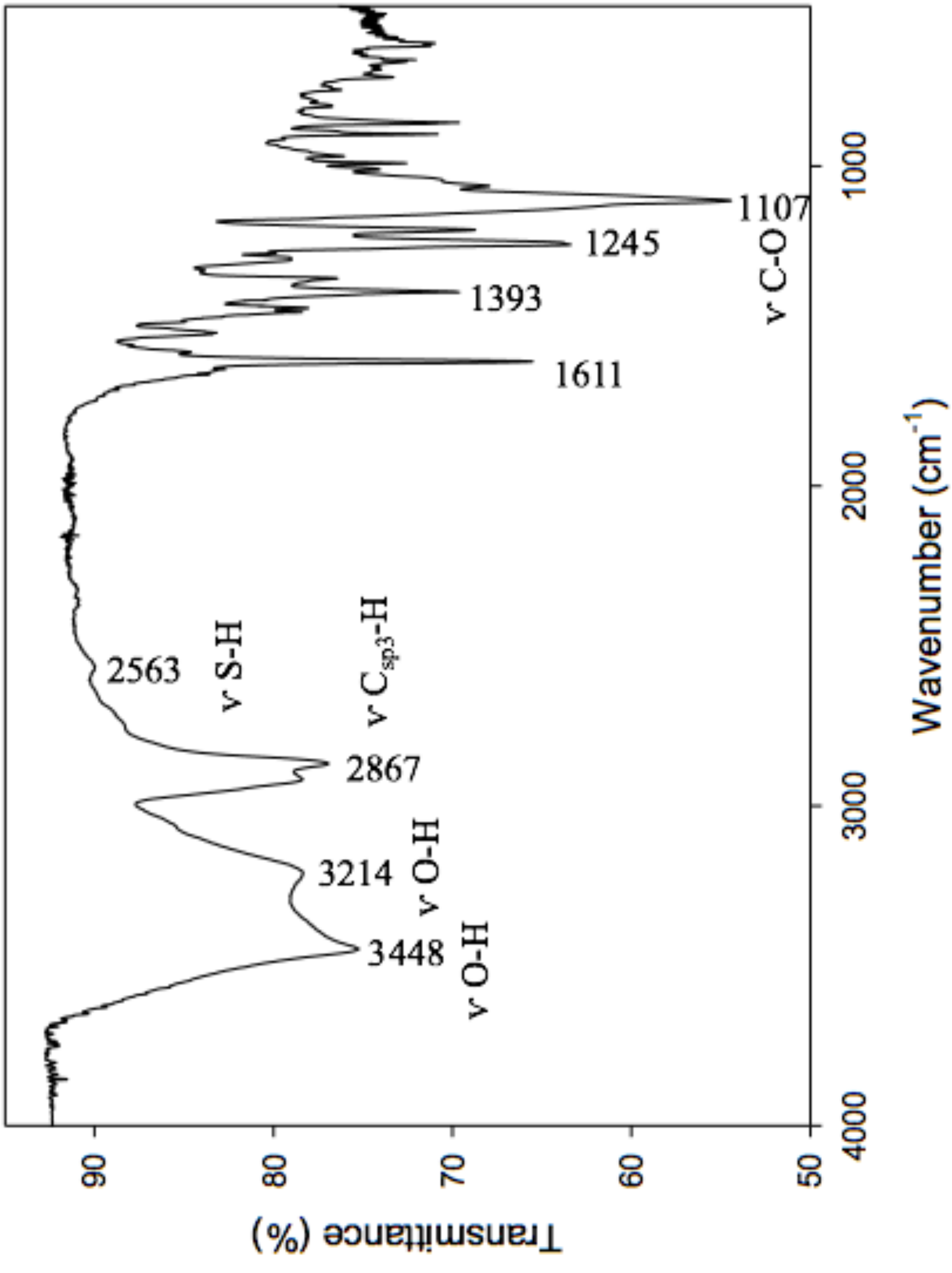

Figure 2.H3: IR absorption spectrum of HS-EG$_4$-NQMP.

2.I Characterization of HO-EG$_4$-TrS

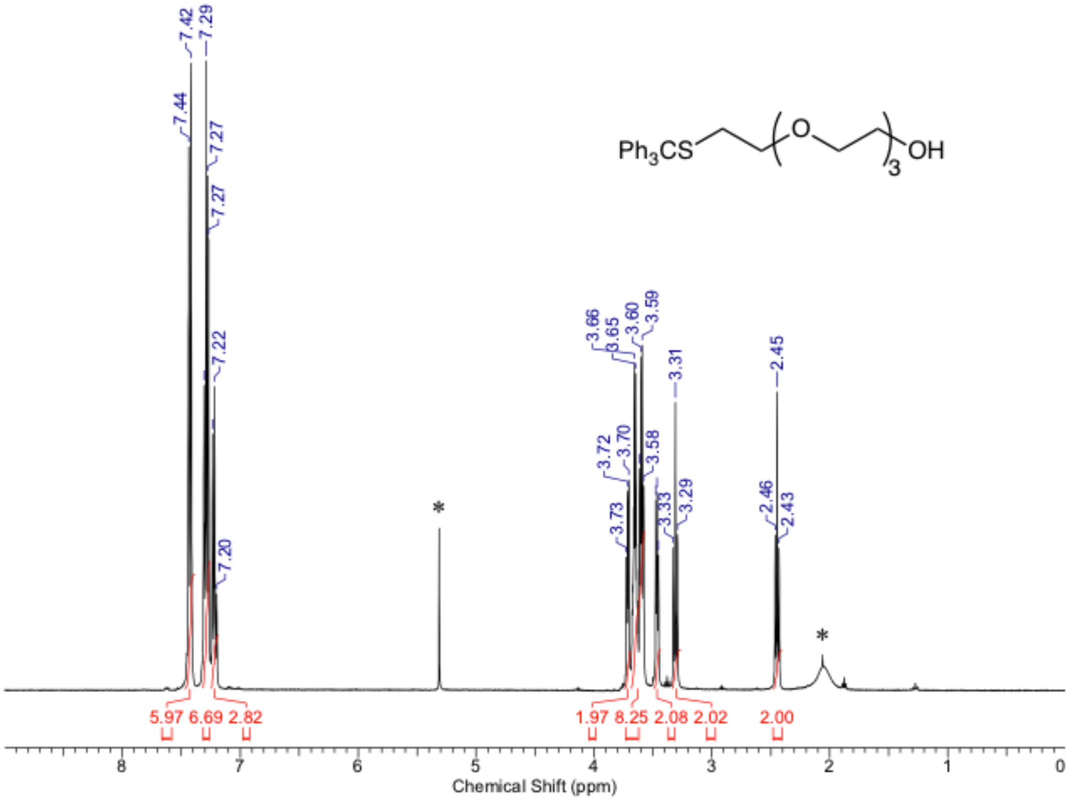

Figure 2.I1: ^{1}H NMR spectrum of HO-EG$_4$-TrS in CDCl$_3$. * denotes solvent signal(s).

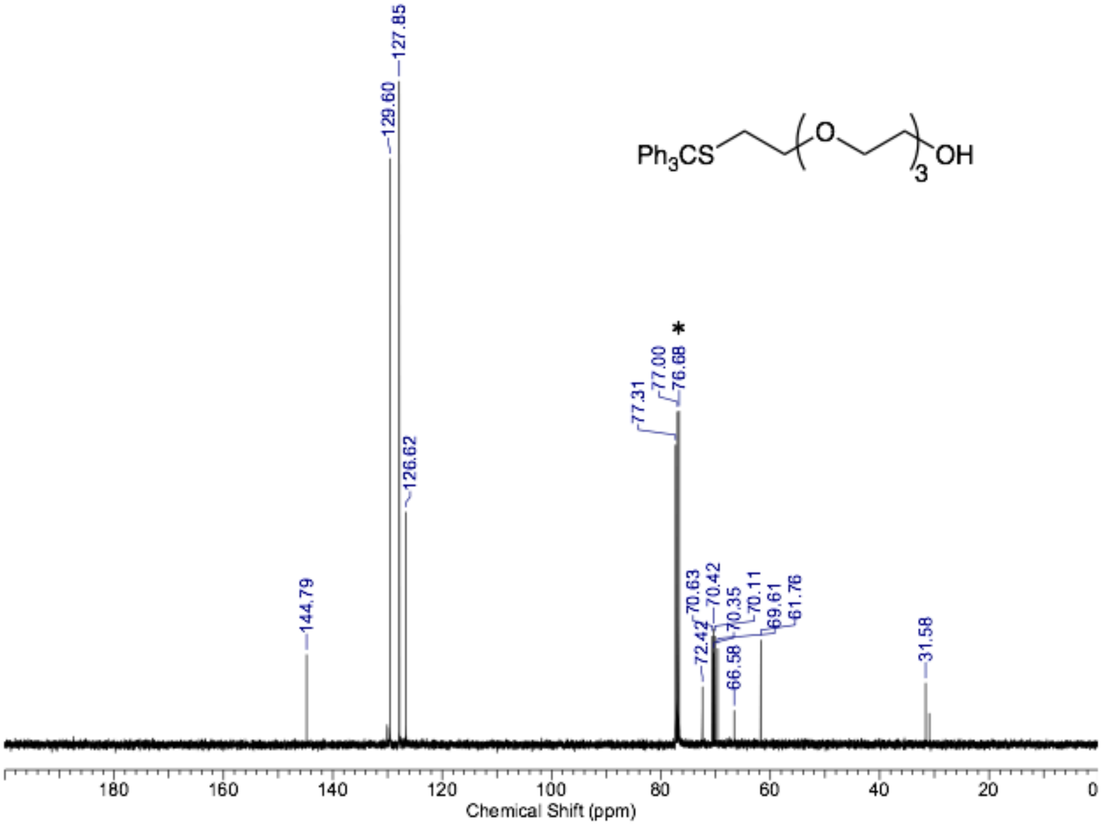

Figure 2.I2: ^{13}C{^{1}H} spectrum of HO-EG$_4$-TrS in CDCl$_3$. * denotes solvent signal(s).

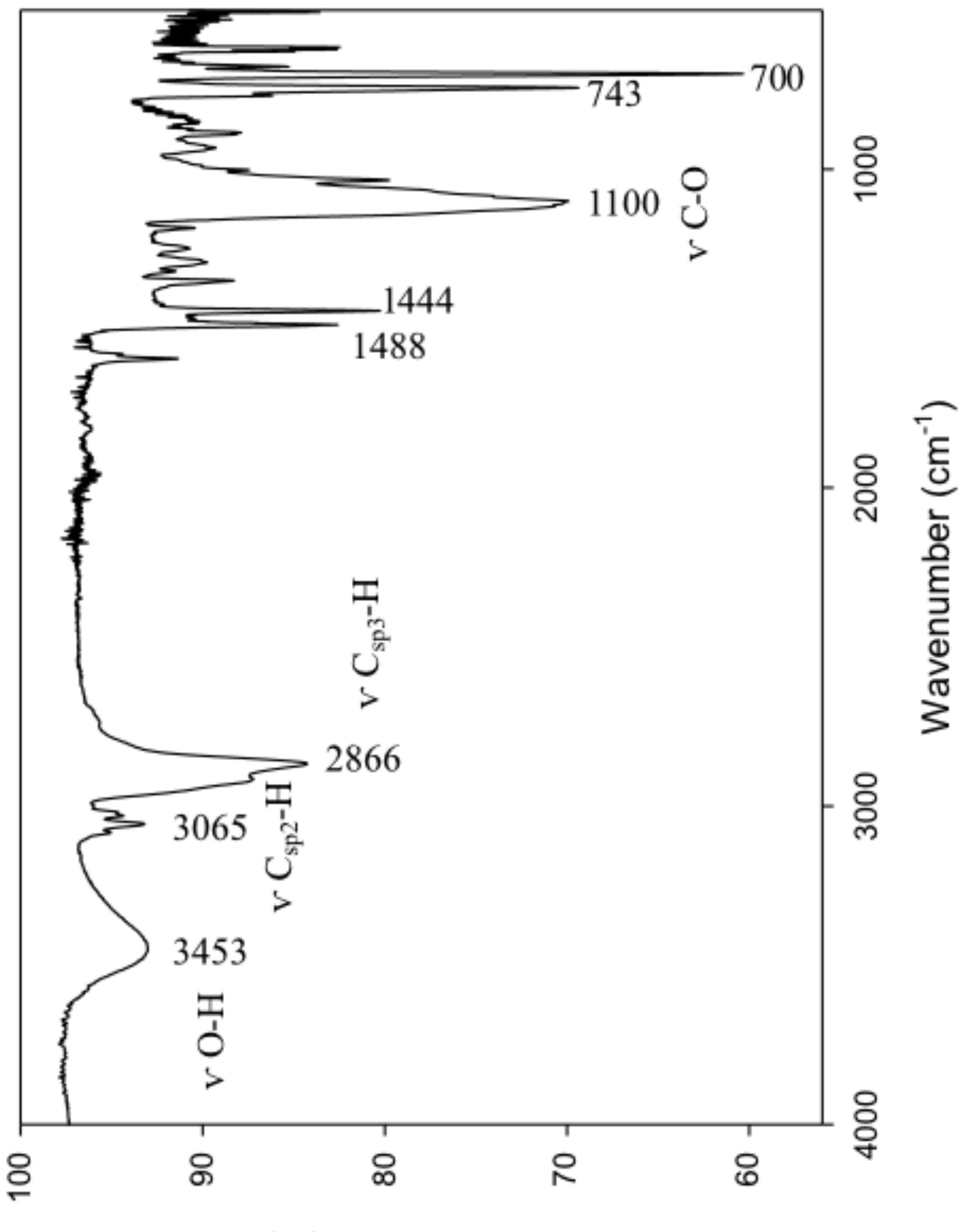

Figure 2.I3: IR absorption spectrum of HO-EG_4-TrS.

2.J Characterization of I-EG$_4$-TrS

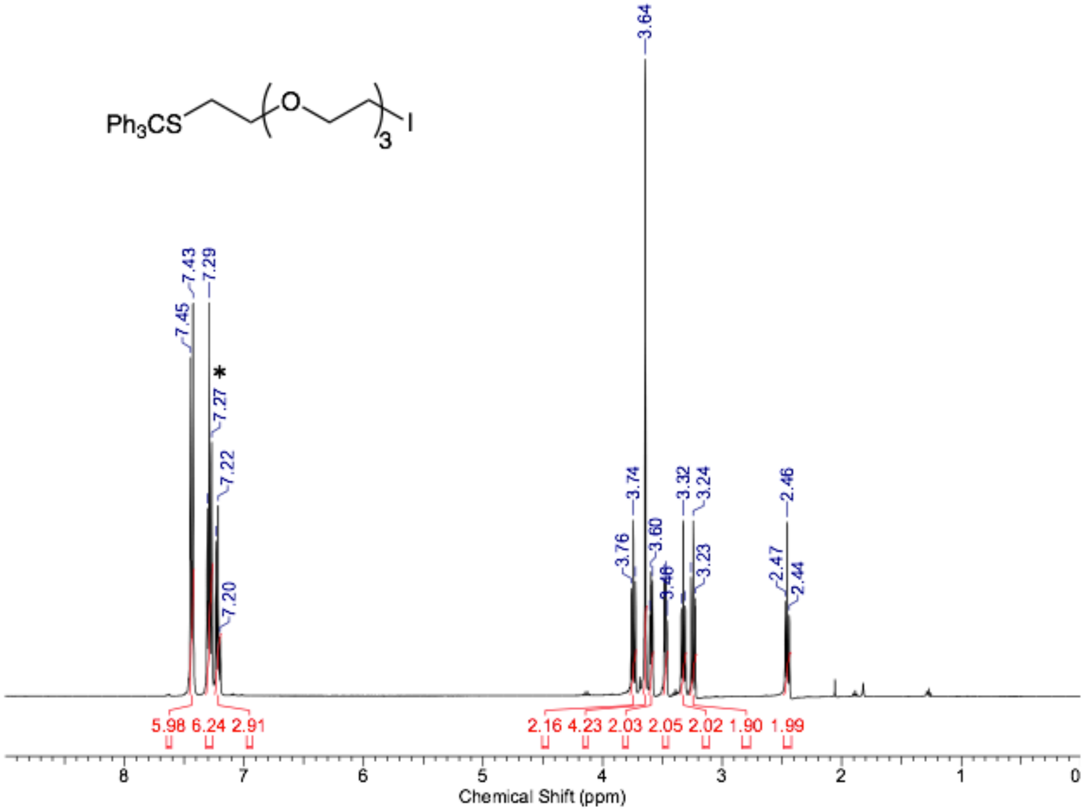

Figure 2.J1: ^{1}H NMR spectrum of I-EG$_4$-TrS in CDCl$_3$. * denotes solvent signal(s).

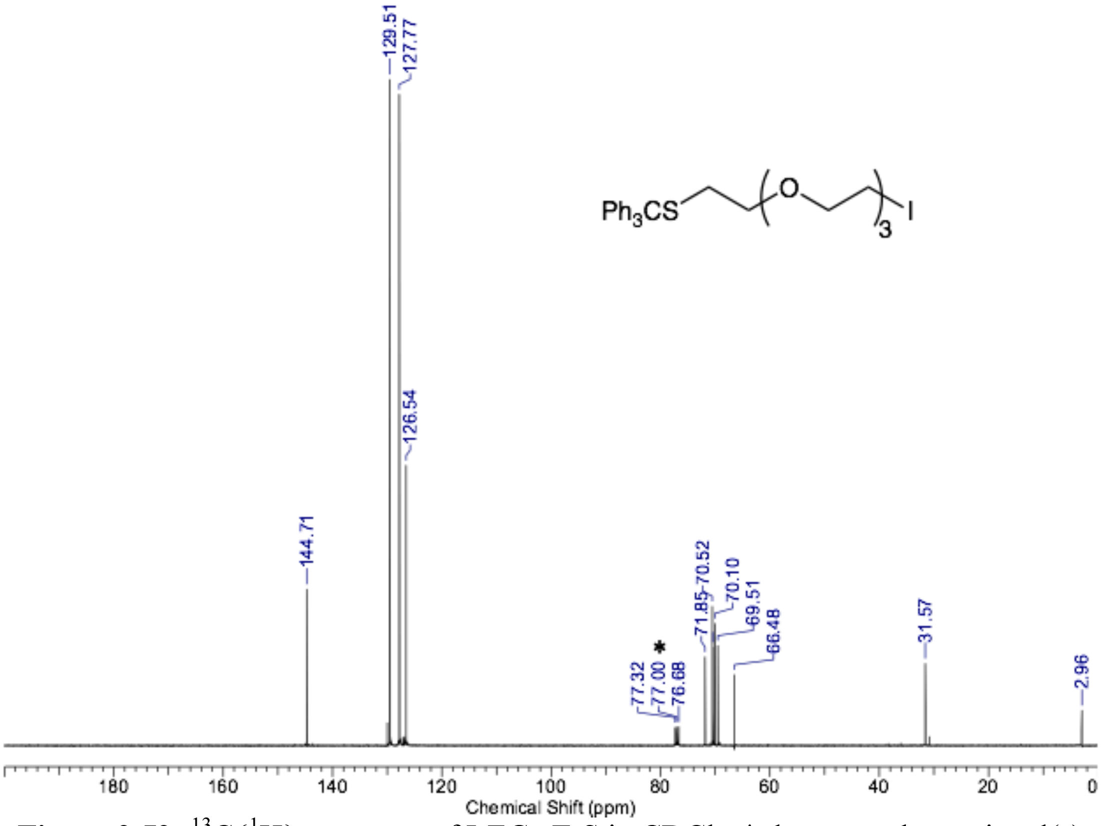

Figure 2.J2: ^{13}C{^{1}H} spectrum of I-EG$_4$-TrS in CDCl$_3$. * denotes solvent signal(s).

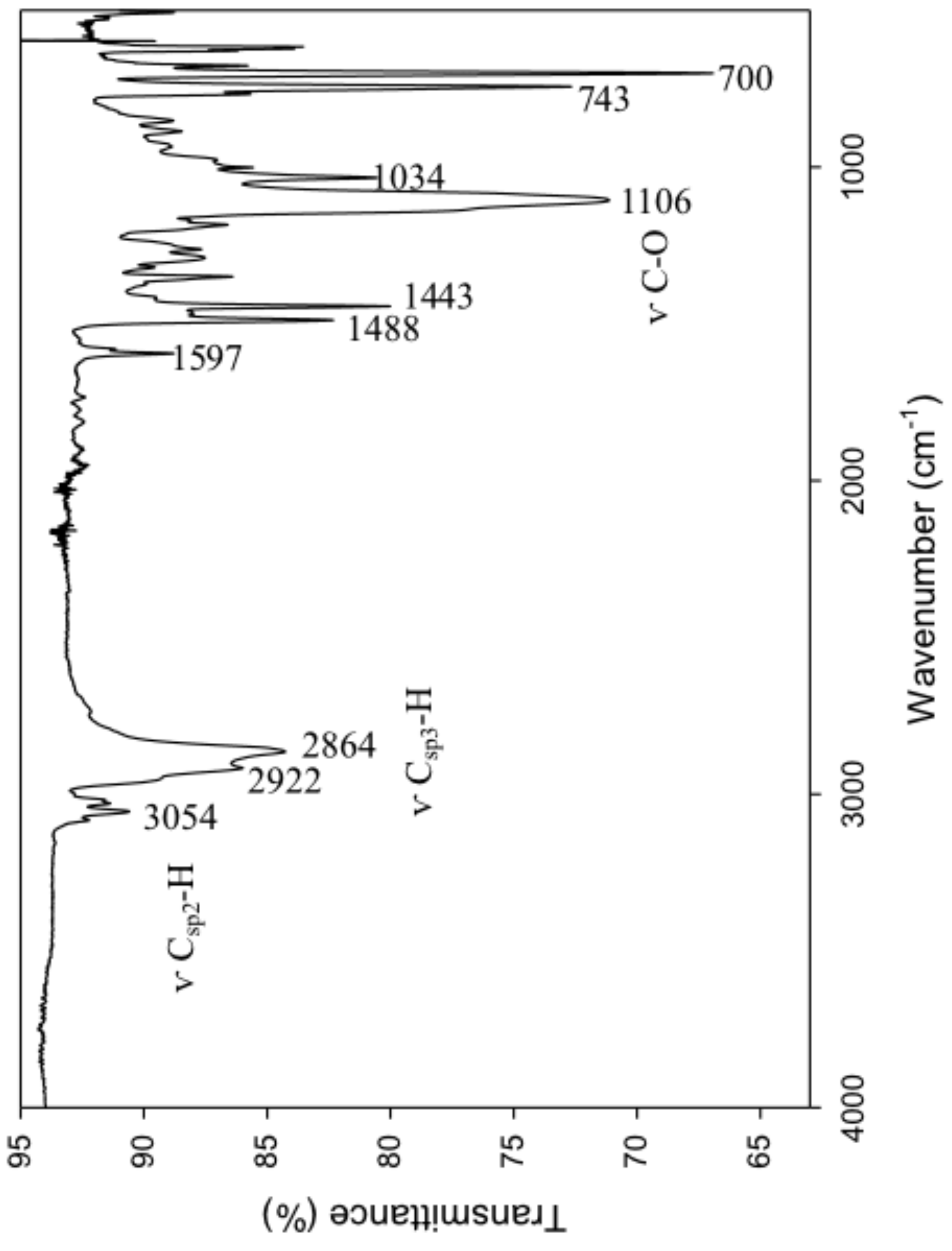

Figure 2.J3: IR absorption spectrum of I-EG$_4$-TrS.

2.K Characterization of TrS-EG$_4$-NQMP-pt

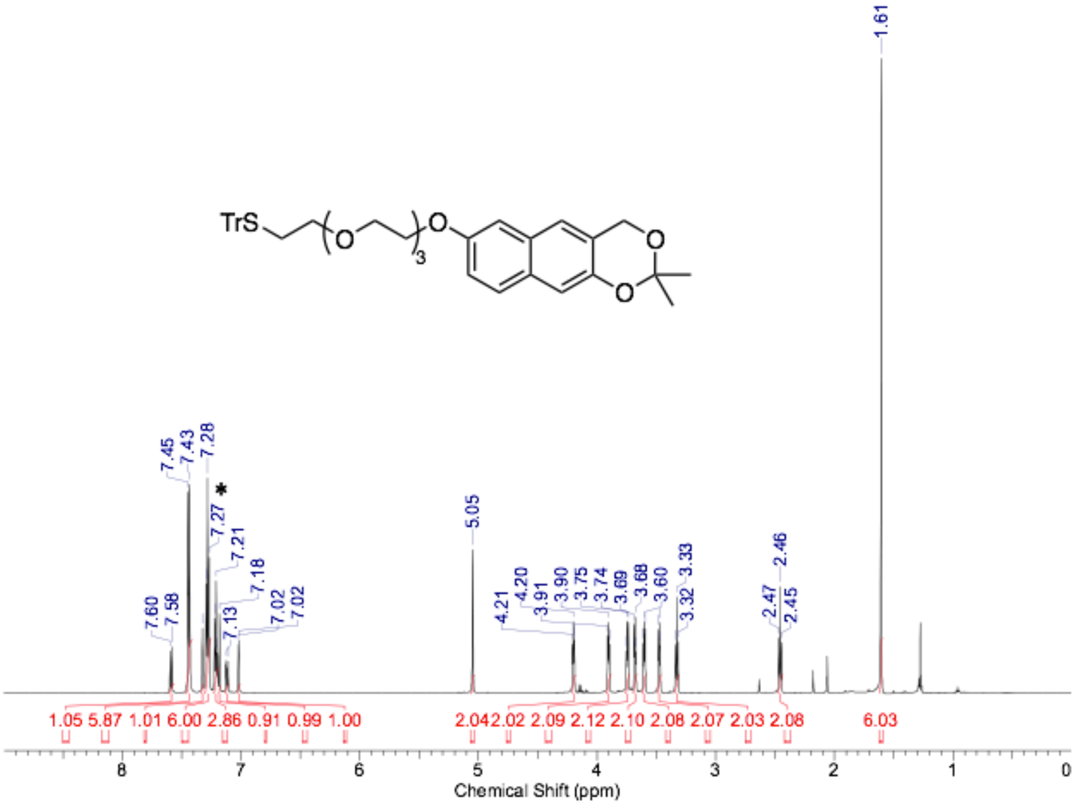

Figure 2.K1: ^{1}H NMR spectrum of TrS-EG$_4$-NQMP-pt in CDCl$_3$. * denotes solvent signal(s).

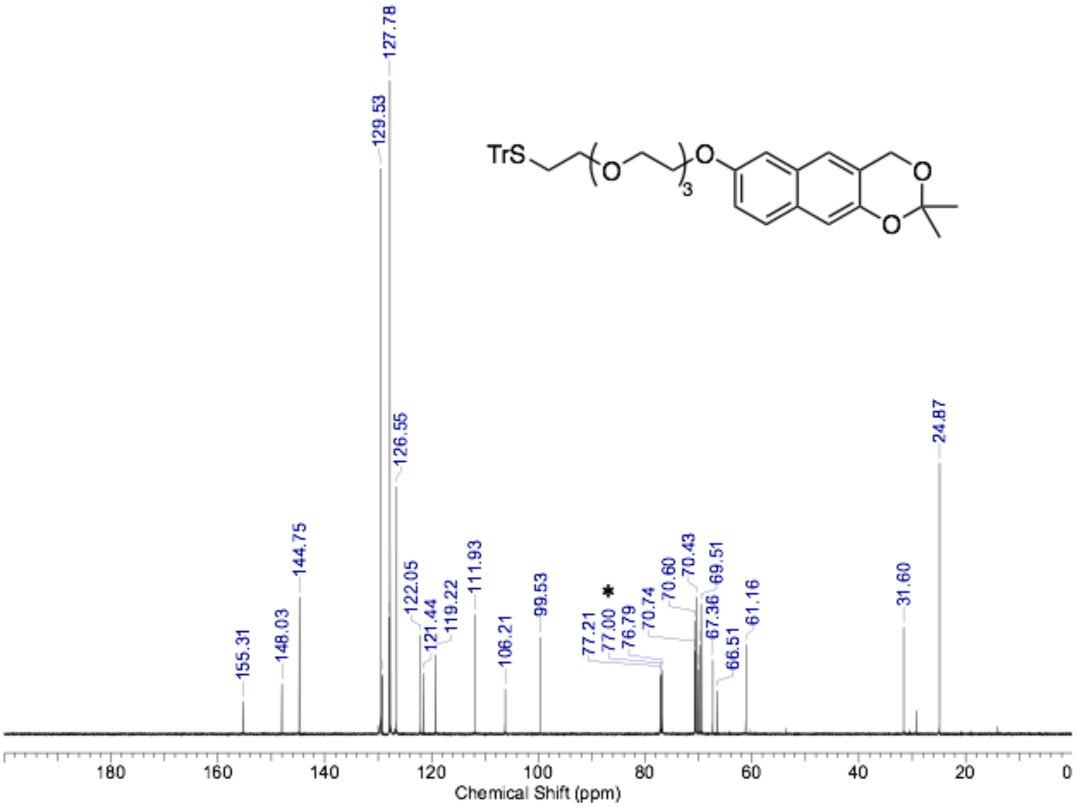

Figure 2.K2: ^{13}C{^{1}H} spectrum of TrS-EG$_4$-NQMP-pt in CDCl$_3$. * denotes solvent signal(s).

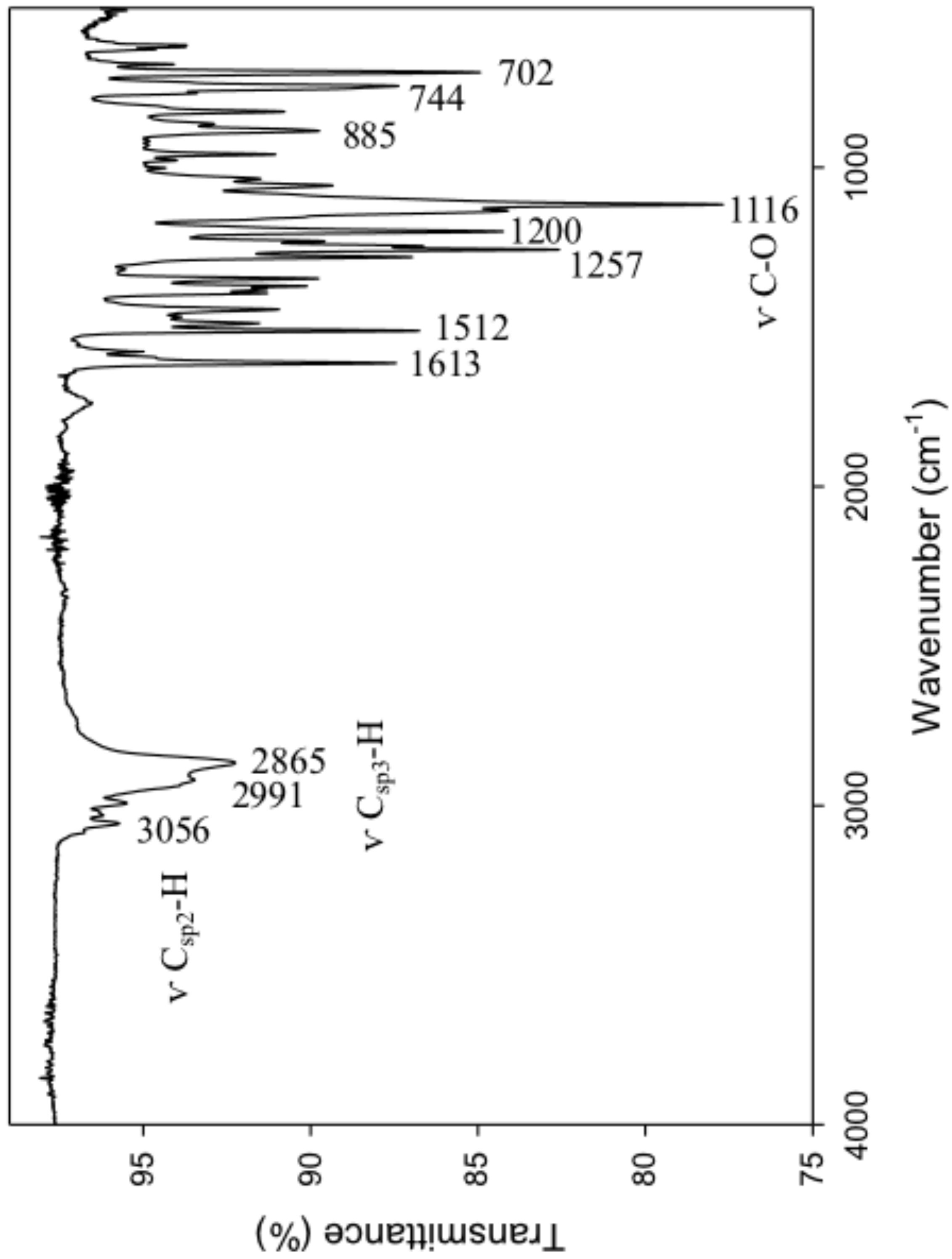

Figure 2.K3: IR absorption spectrum of TrS-EG_4-NQMP-pt.

2.L Characterization of TrS-EG$_4$-NQMP

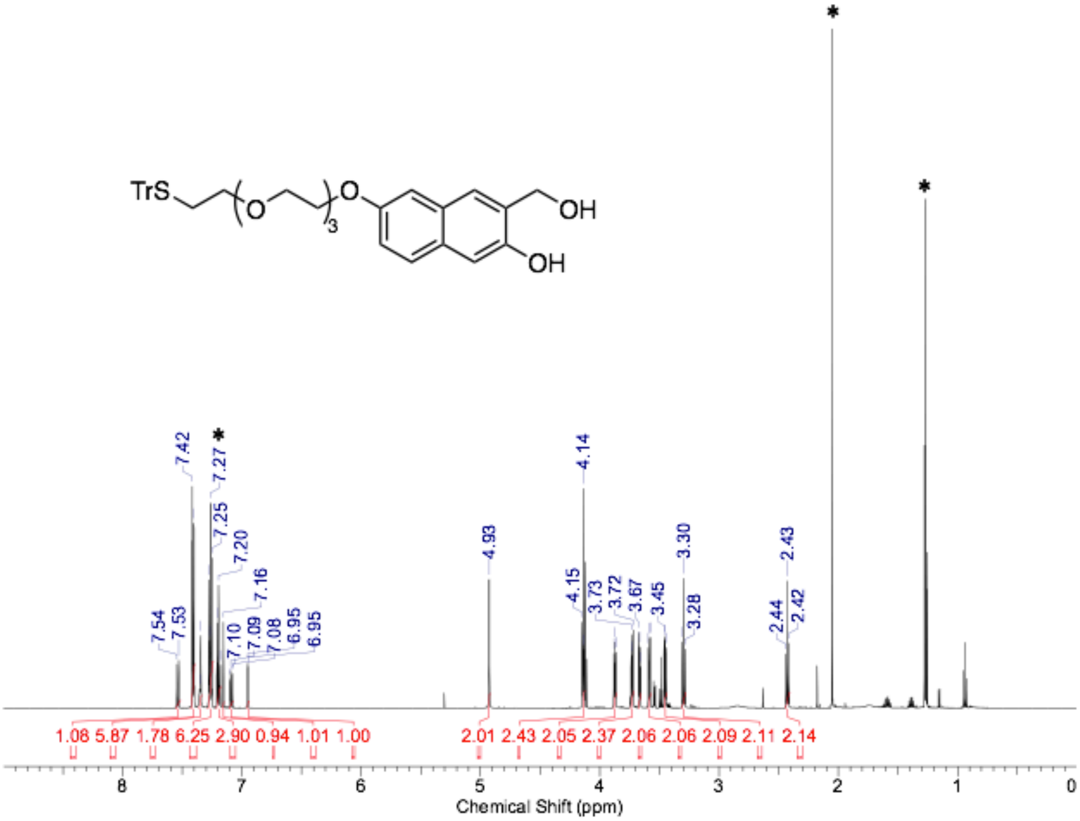

Figure 2.L1: ^{1}H NMR spectrum of TrS-EG$_4$-NQMP in CDCl$_3$. * denotes solvent signal(s).

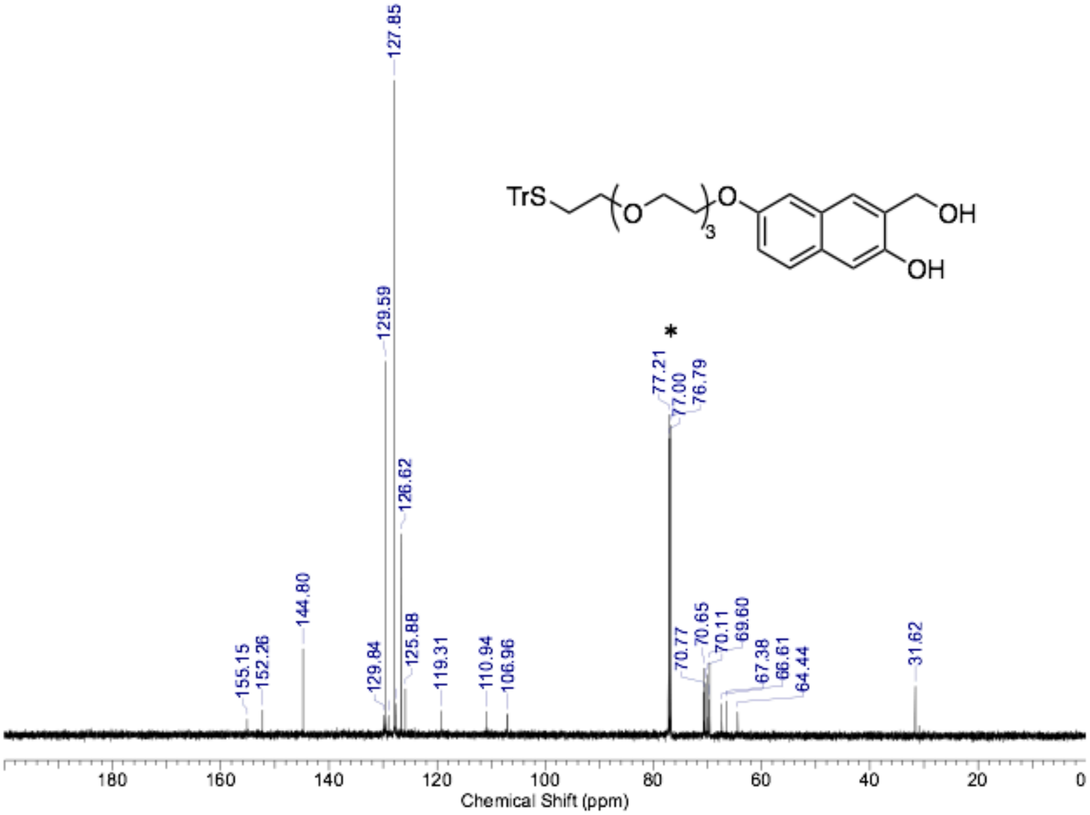

Figure 2.L2: ^{13}C{^{1}H} spectrum of TrS-EG$_4$-NQMP in CDCl$_3$. * denotes solvent signal(s).

5.2 Chapter 3 Appendix

Table of Contents

3.A Characterization of $Ph_3CS-(CH_2)_2-COOH$ (compound **3.2**)........100
3.B Characterization of $Ph_3CS-(CH_2)_2-NHS$ (compound **3.3**)........102
3.C Characterization of TsO-EG_4-OMe (compound **3.5**)........104
3.D Characterization of TsO-EG_4-COOMe (compound **3.7**)........106
3.E Characterization of N_3-EG_4-COOMe (compound **3.8**)........107
3.F Characterization of MeO-EG_3-OTs (compound **3.20**)........109
3.G Characterization of MeO-EG_3-N_3 (compound **3.11**)........111
3.H Characterization of MeO-EG_3-NH_2 (compound **3.12**)........113
3.I Characterization of Ph_3CS-EG_3-OMe (compound **3.13**)........114
3.J Characterization of HS-EG_3-OMe (compound **3.14**)........115
3.K Characterization of Ph_3CS-EG_4-COOMe (compound **3.15**)........116
3.L Characterization of Ph_3CS-EG_4-COOH (compound **3.16**)........118
3.M Characterization of Ph_3CS-EG_4-EG_3-OMe (compound **3.17**)........119
3.N Characterization of HS-EG_4-EG_3-OMe (compound **3.18**)........121

3.A Characterization of $Ph_3CS\text{-}(CH_2)_2\text{-}COOH$

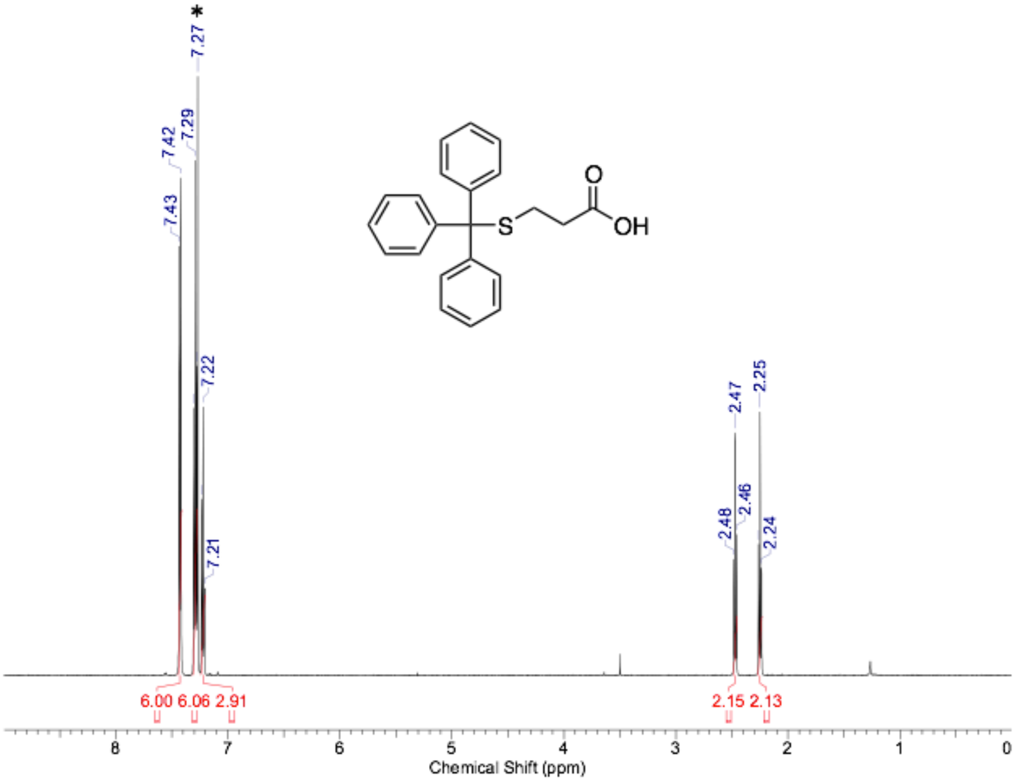

Figure 3.A1: ^1H NMR spectrum of $Ph_3CS\text{-}(CH_2)_2\text{-}COOH$ in $CDCl_3$. * denotes solvent signal(s).

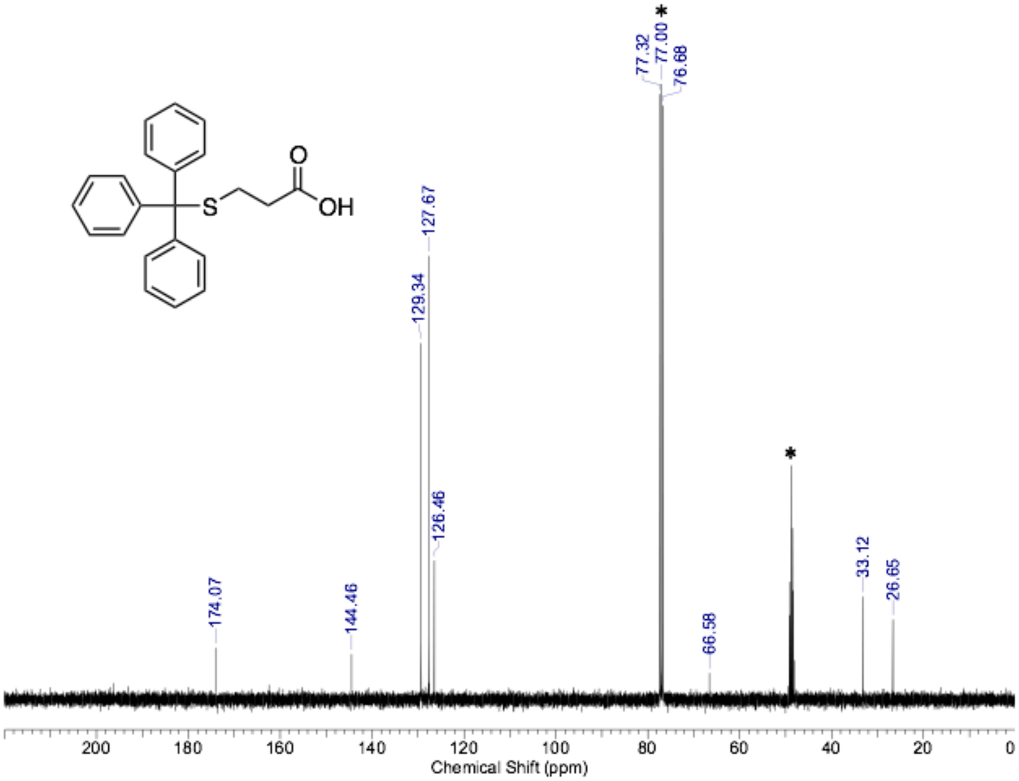

Figure 3.A2: $^{13}C\{^1H\}$ spectrum of $Ph_3CS\text{-}(CH_2)_2\text{-}COOH$ in $CDCl_3$. * denotes solvent signal(s).

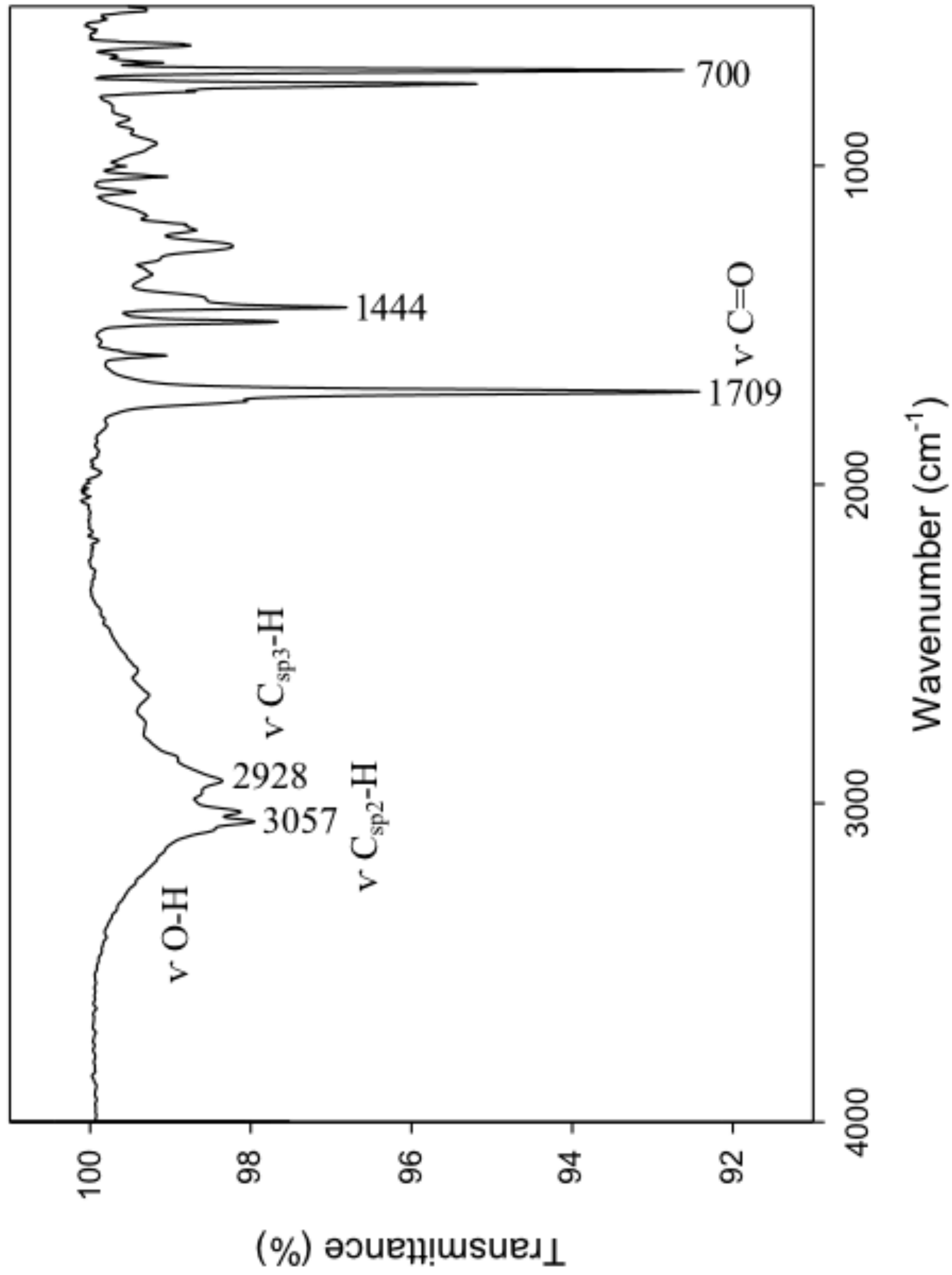

Figure 3.A3: IR absorption spectrum of Ph_3CS-$(CH_2)_2$-COOH.

3.B Characterization of Ph_3CS-$(CH_2)_2$-NHS

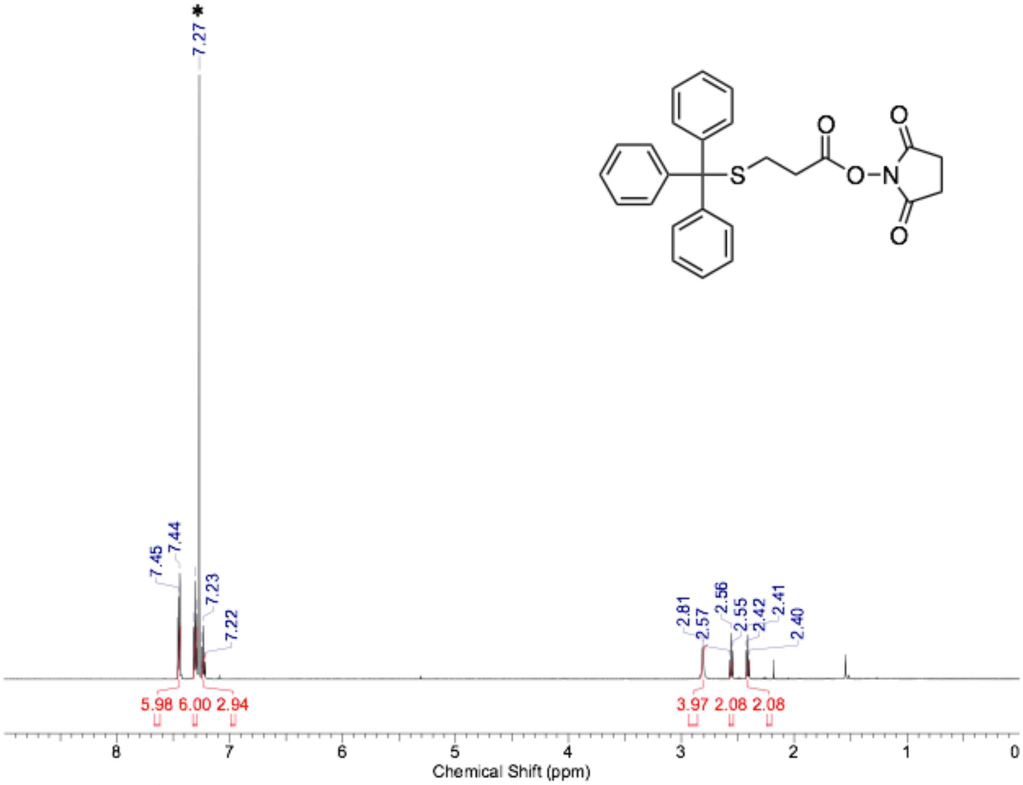

Figure 3.B1: ^{1}H NMR spectrum of Ph_3CS-$(CH_2)_2$-NHS in $CDCl_3$. * denotes solvent signal(s).

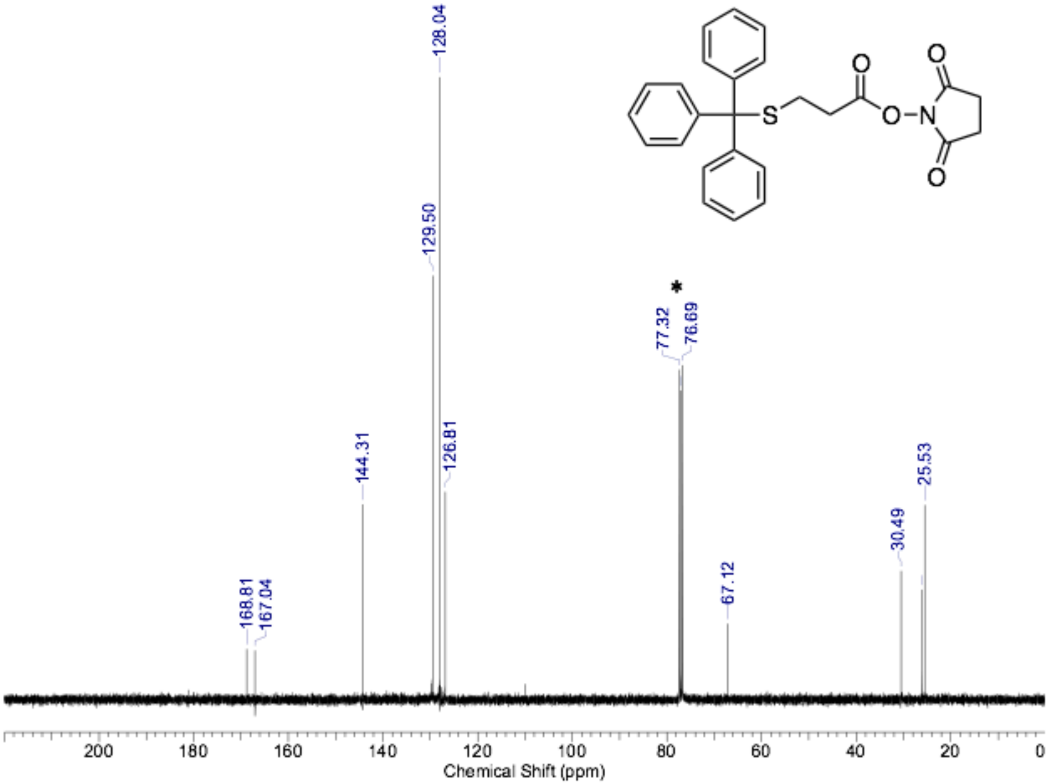

Figure 3.B2: $^{13}C\{^1H\}$ spectrum of Ph_3CS-$(CH_2)_2$-NHS in $CDCl_3$. * denotes solvent signal(s).

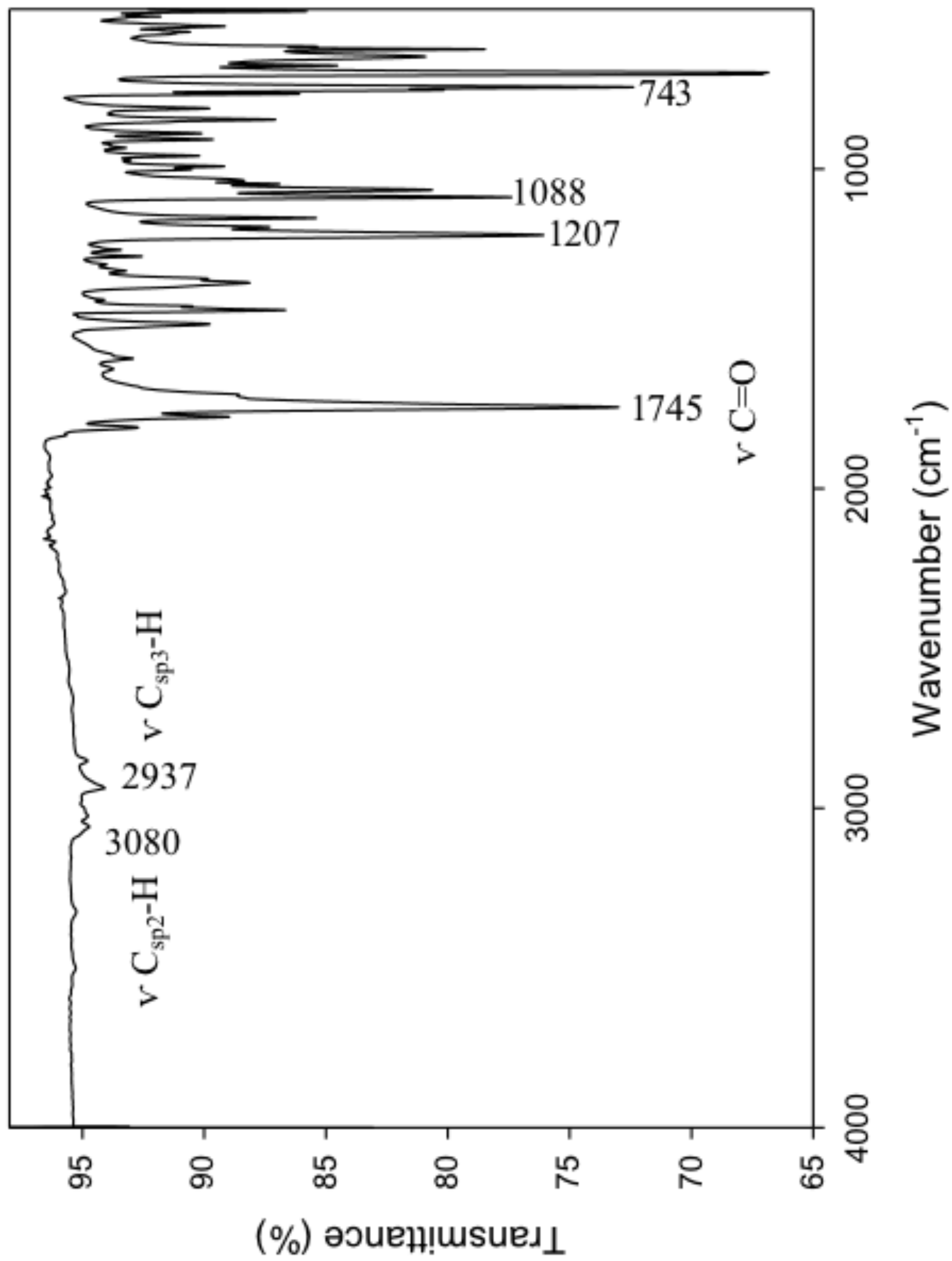

Figure 3.B3: IR absorption spectrum of Ph_3CS-$(CH_2)_2$-NHS.

3.C Characterization of TsO-EG$_4$-OH

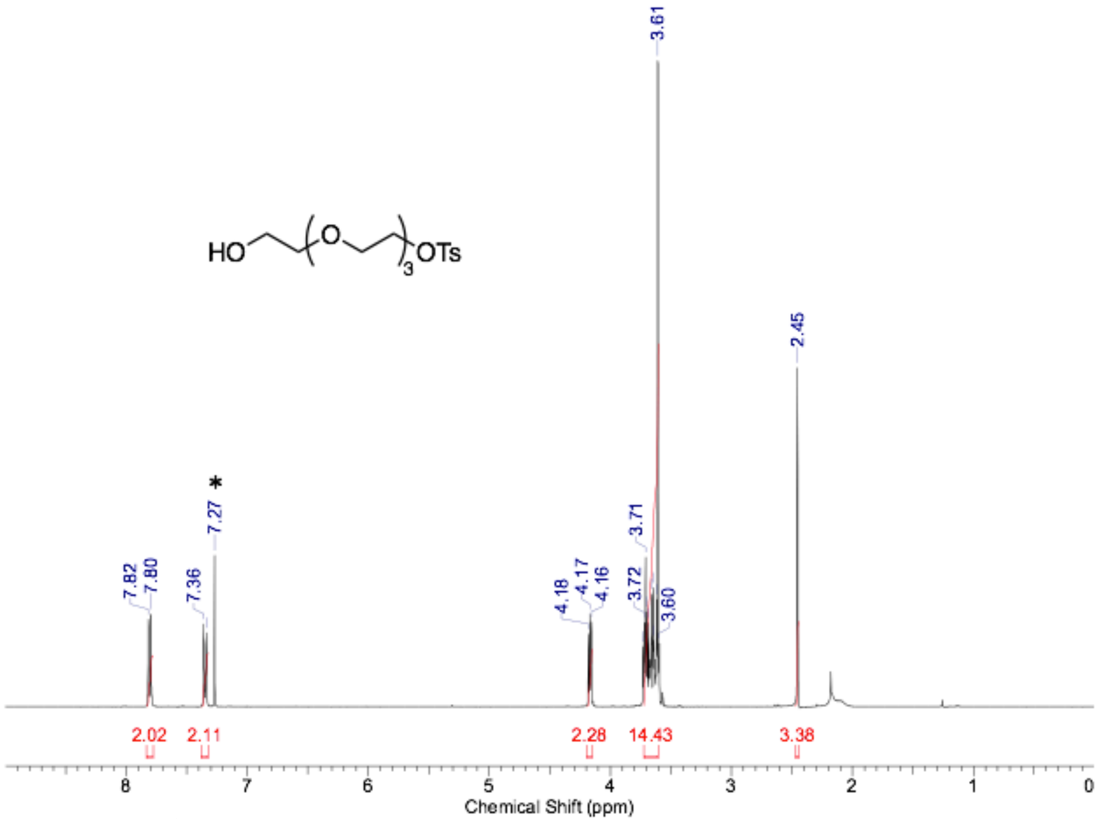

Figure 3.C1: ^{1}H NMR spectrum of TsO-EG$_4$-OH in CDCl$_3$. * denotes solvent signal(s).

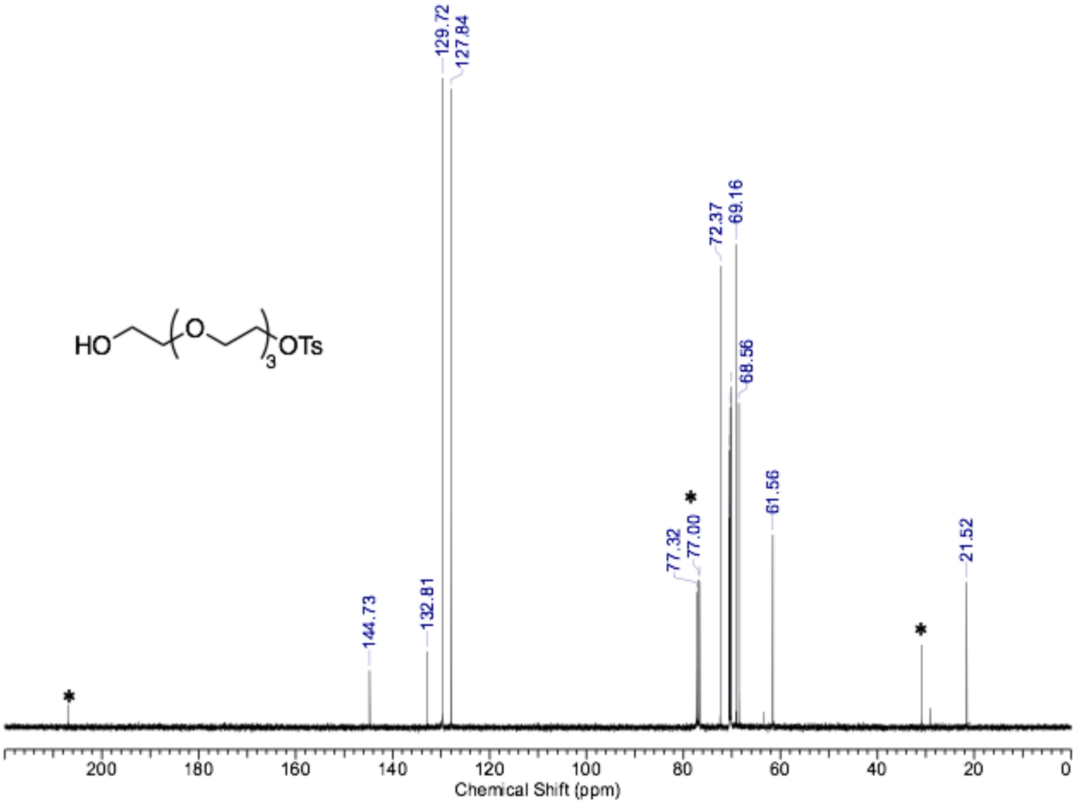

Figure 3.C2: ^{13}C{^{1}H} spectrum of TsO-EG$_4$-OH in CDCl$_3$. * denotes solvent signal(s).

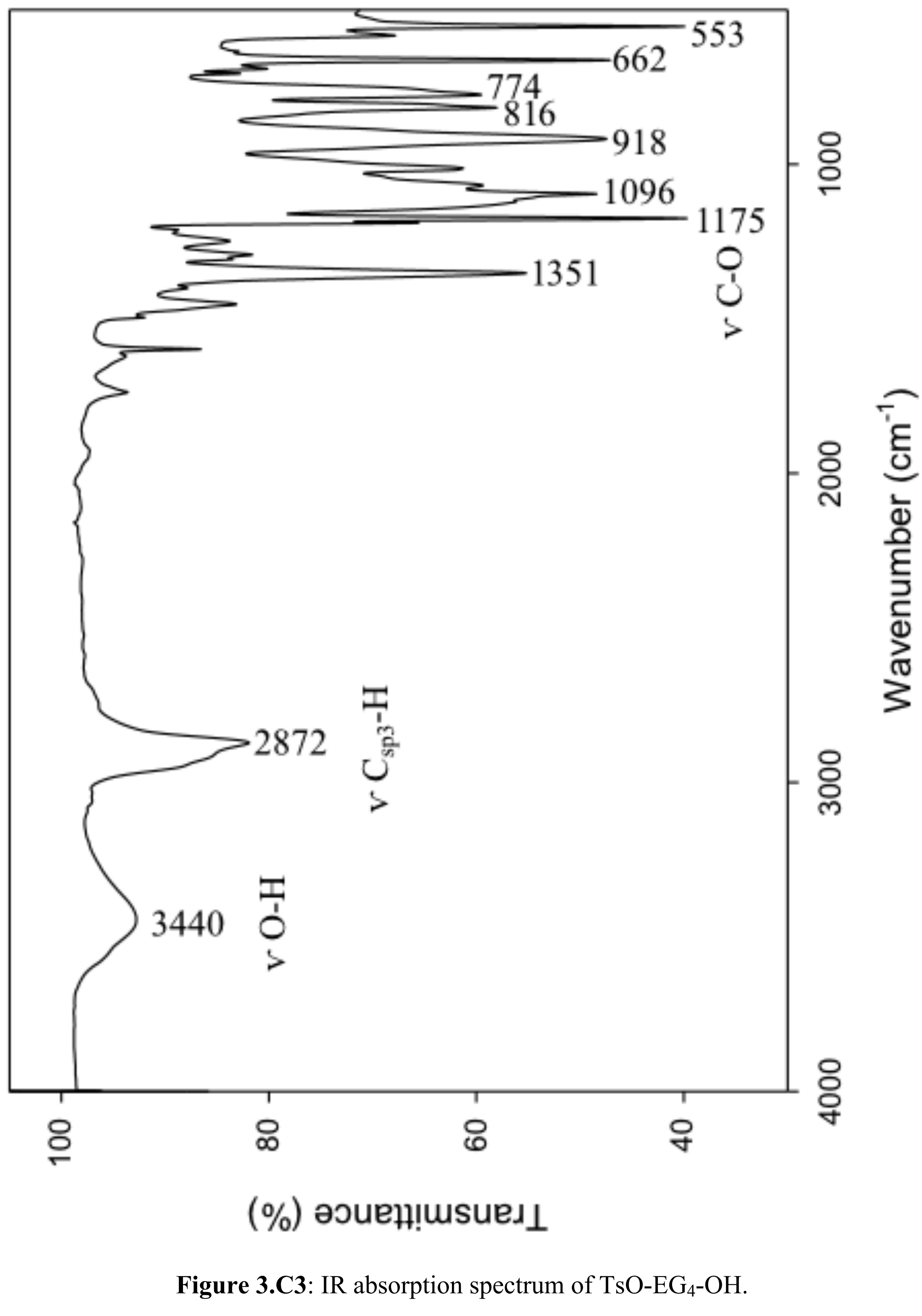

Figure 3.C3: IR absorption spectrum of TsO-EG$_4$-OH.

3.D Characterization of TsO-EG$_4$-COOMe

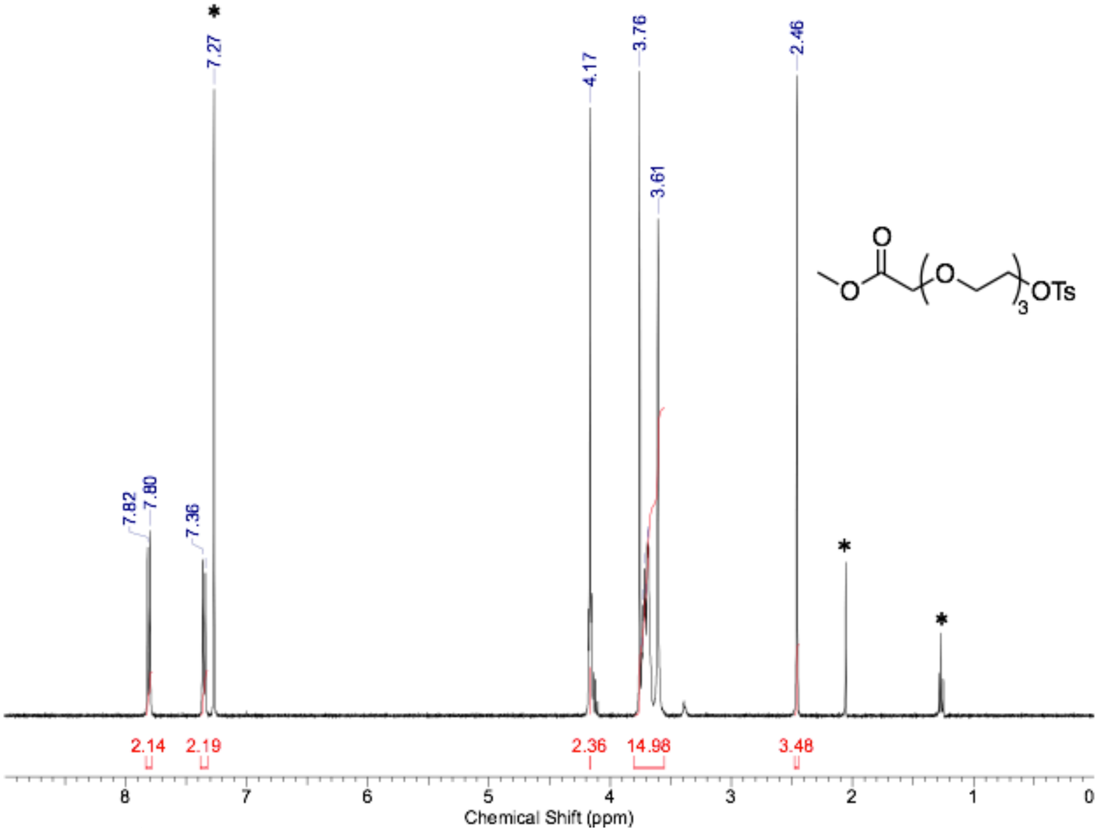

Figure 3.D1: ^{1}H NMR spectrum of TsO-EG$_4$-COOMe in $CDCl_3$. * denotes solvent signal(s).

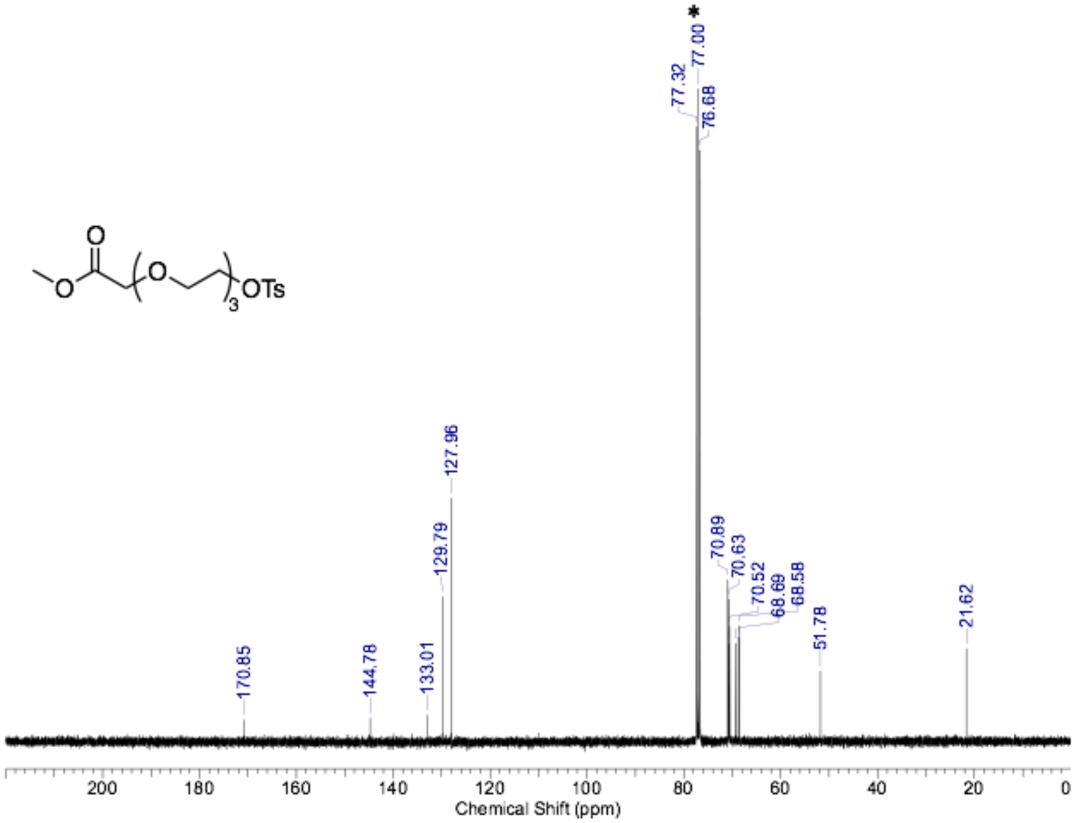

Figure 3.D2: $^{13}C\{^{1}H\}$ spectrum of TsO-EG$_4$-COOMe in $CDCl_3$. * denotes solvent signal(s).

3.E Characterization of N_3-EG_4-COOMe

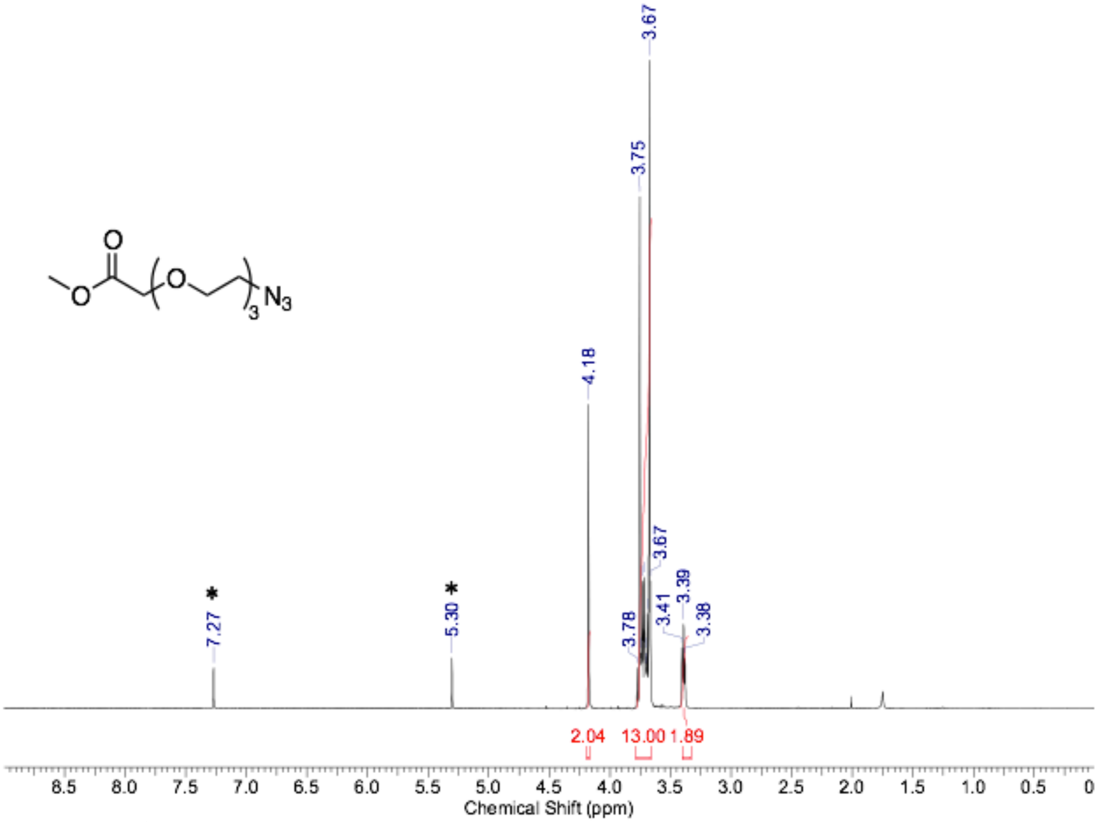

Figure 3.E1: ^{1}H NMR spectrum of N_3-EG_4-COOMe in $CDCl_3$. * denotes solvent signal(s).

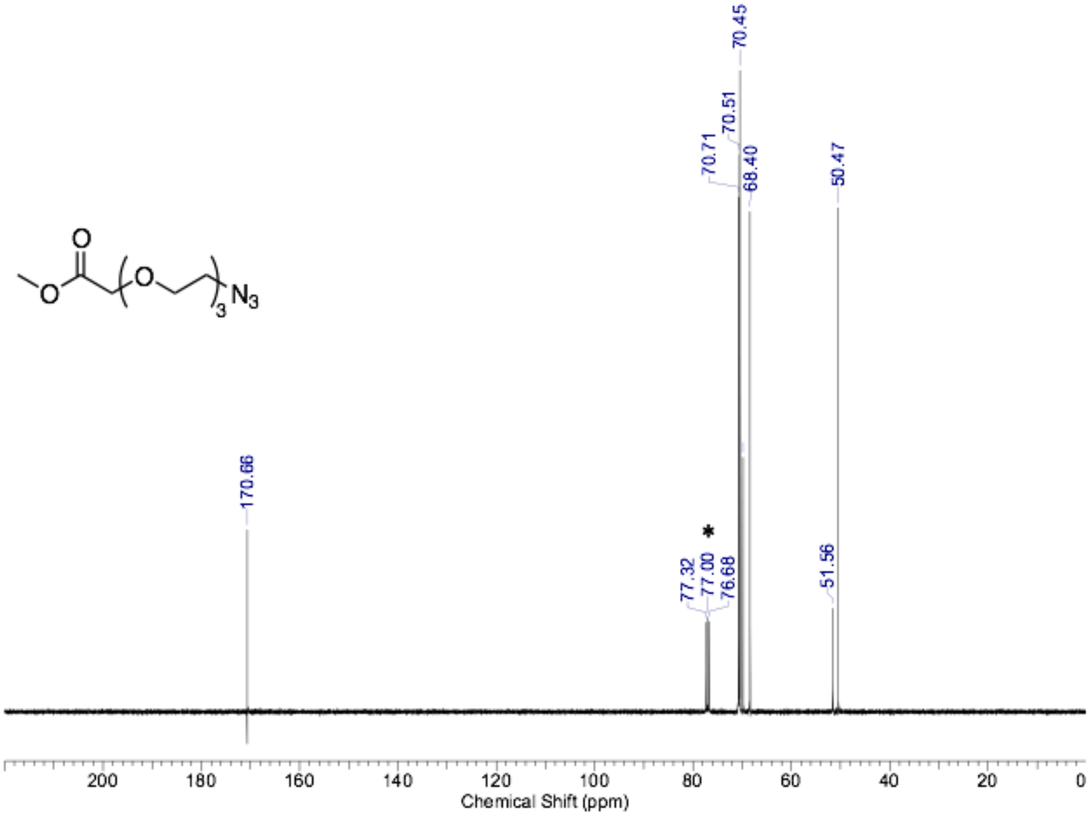

Figure 3.E2: $^{13}C\{^1H\}$ spectrum of N_3-EG_4-COOMe in $CDCl_3$. * denotes solvent signal(s).

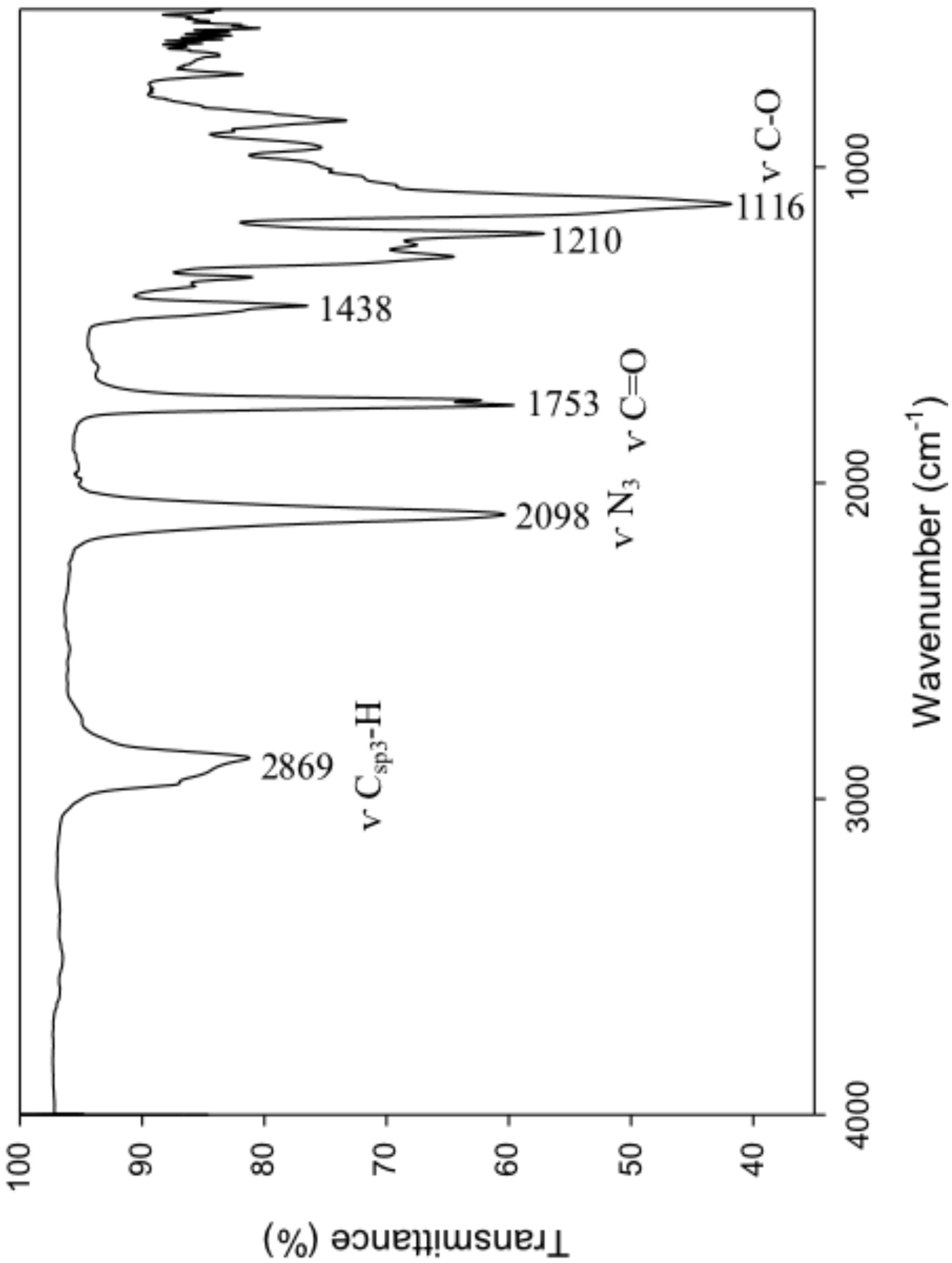

Figure 3.E3: IR absorption spectrum of N_3-EG_4-COOMe.

3.F Characterization of MeO-EG$_3$-OTs

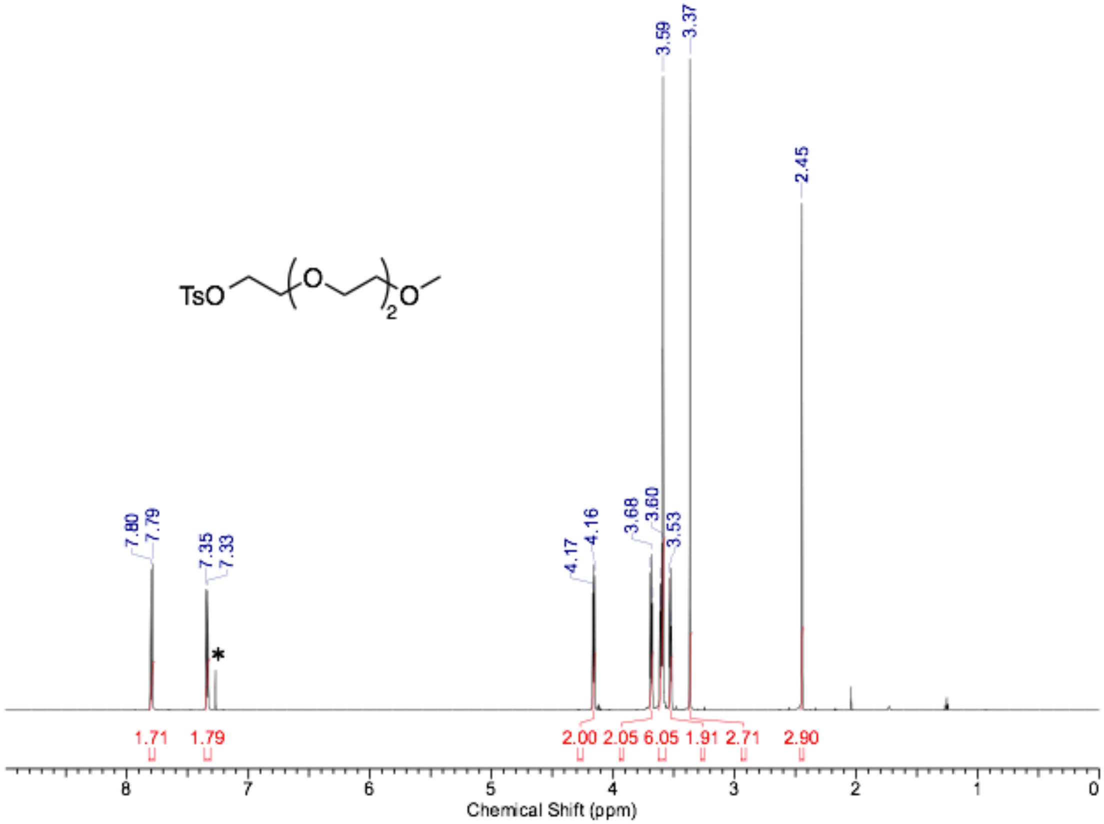

Figure 3.F1: ^{1}H NMR spectrum of MeO-EG$_3$-OTs in CDCl$_3$. * denotes solvent signal(s).

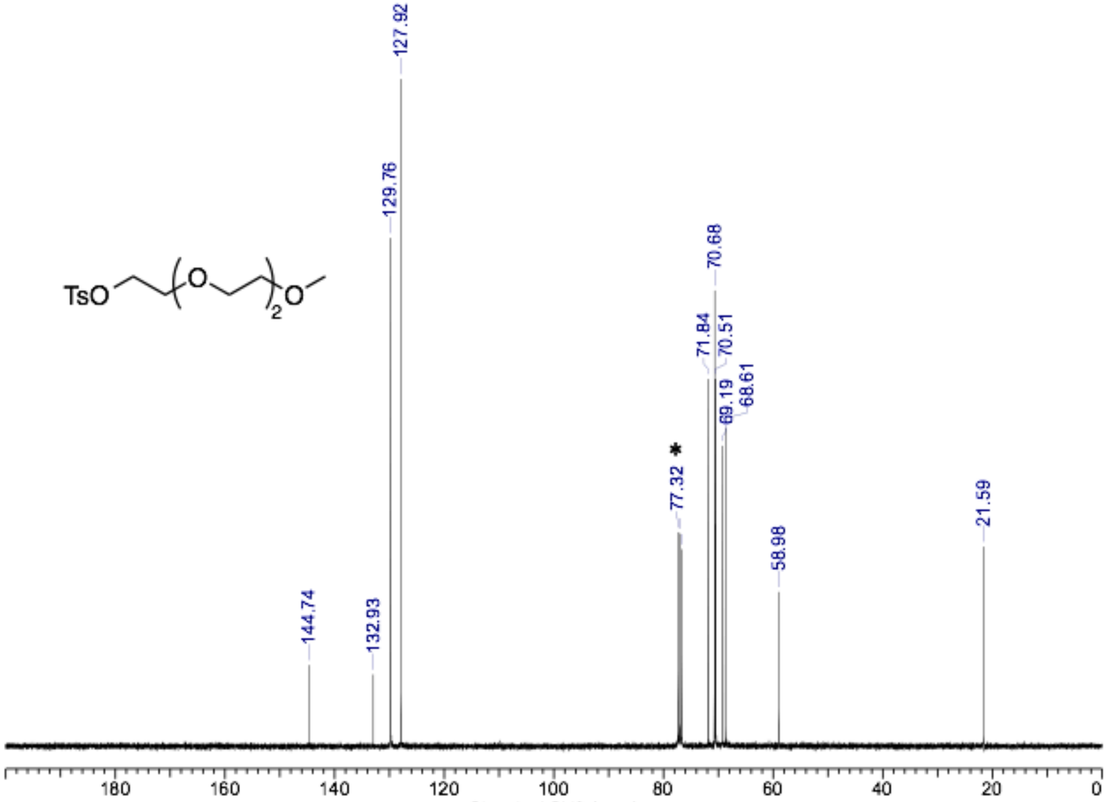

Figure 3.F2: ^{13}C {^{1}H} spectrum of MeO-EG$_3$-OTs in CDCl$_3$. * denotes solvent signal(s).

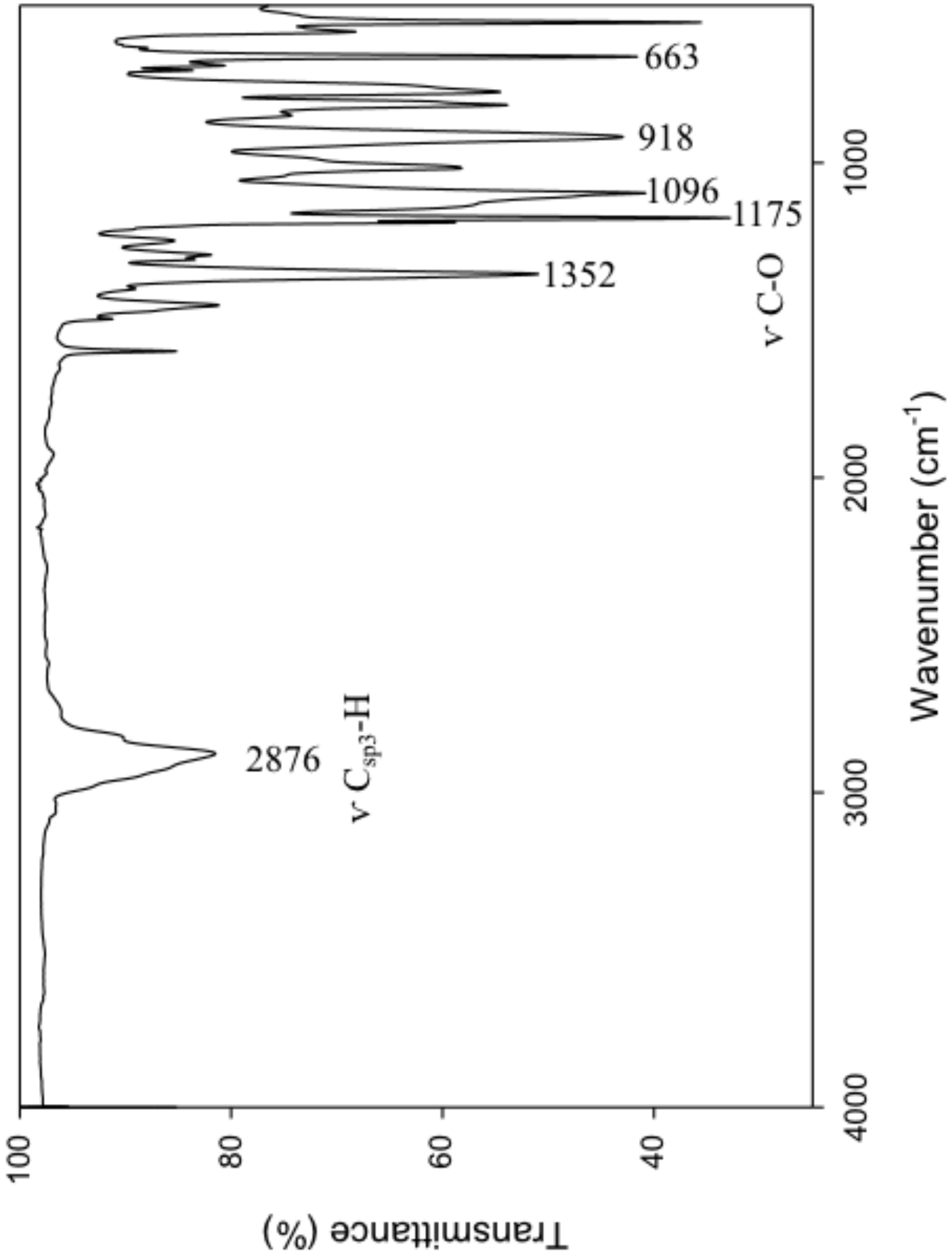

Figure 3.F3: IR absorption spectrum of MeO-EG_3-OTs.

3.G Characterization of MeO-EG$_3$-N$_3$

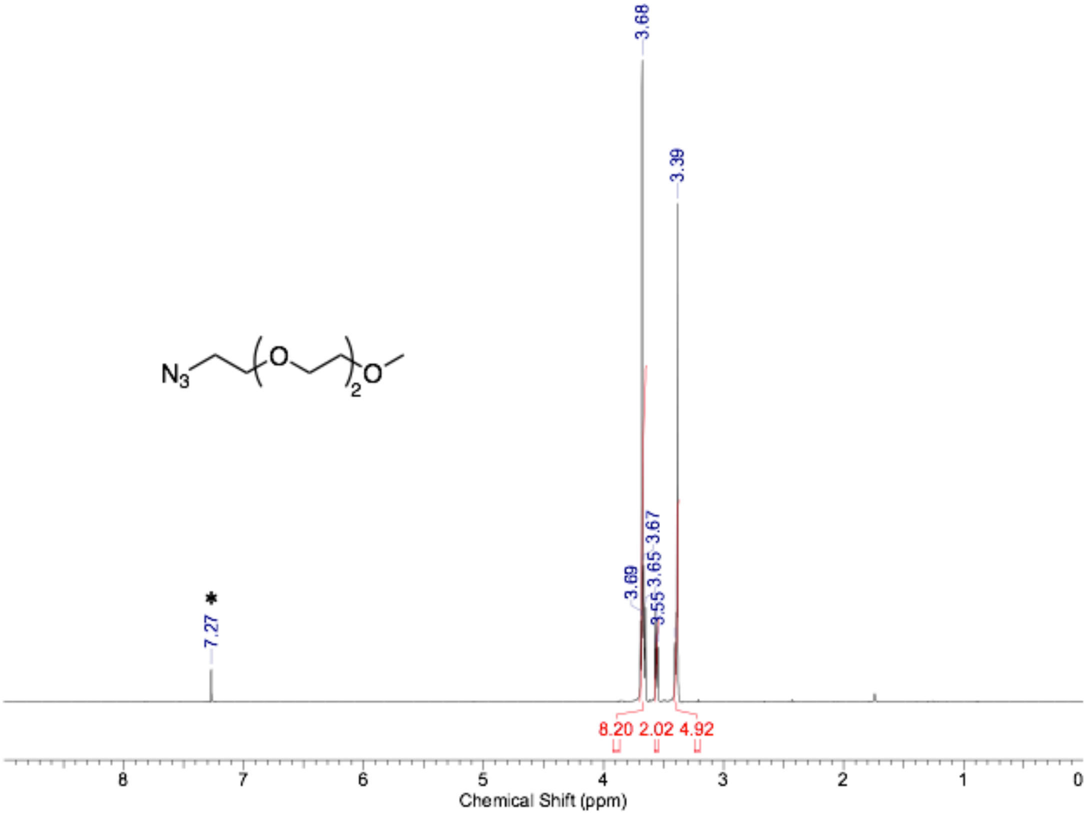

Figure 3.G1: ^{1}H NMR spectrum of MeO-EG$_3$-N$_3$ in CDCl$_3$. * denotes solvent signal(s).

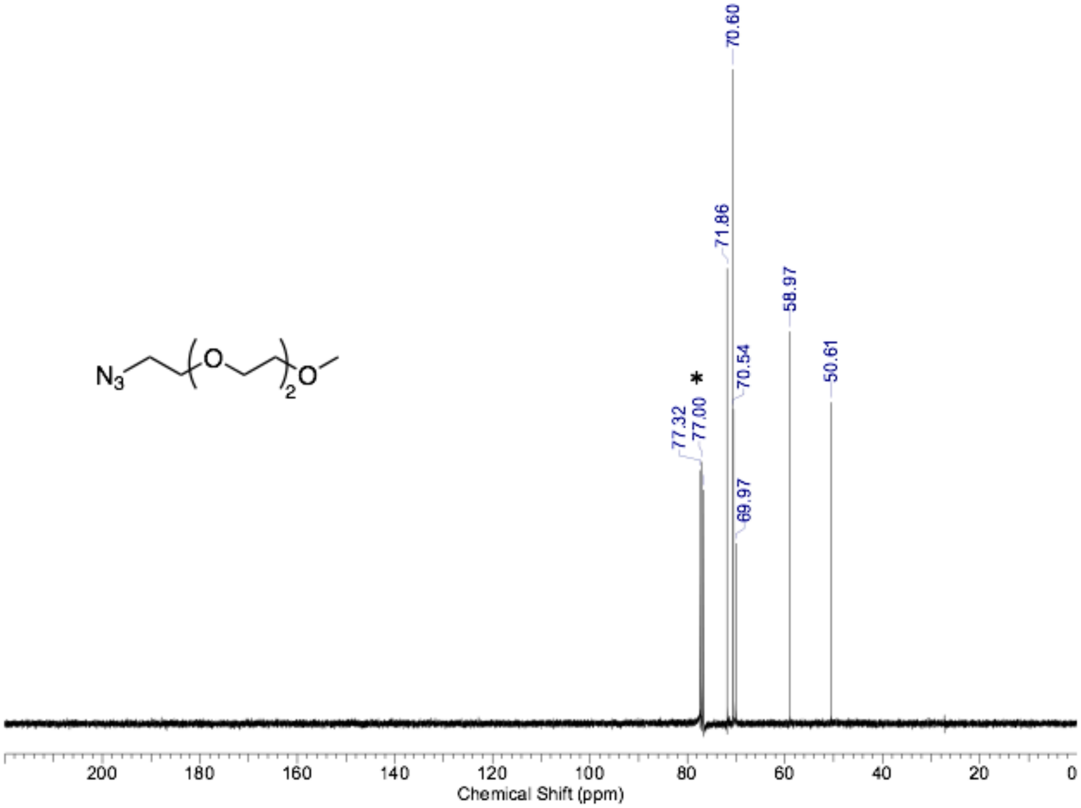

Figure 3.G2: ^{13}C{^{1}H} spectrum of MeO-EG$_3$-N$_3$ in CDCl$_3$. * denotes solvent signal(s).

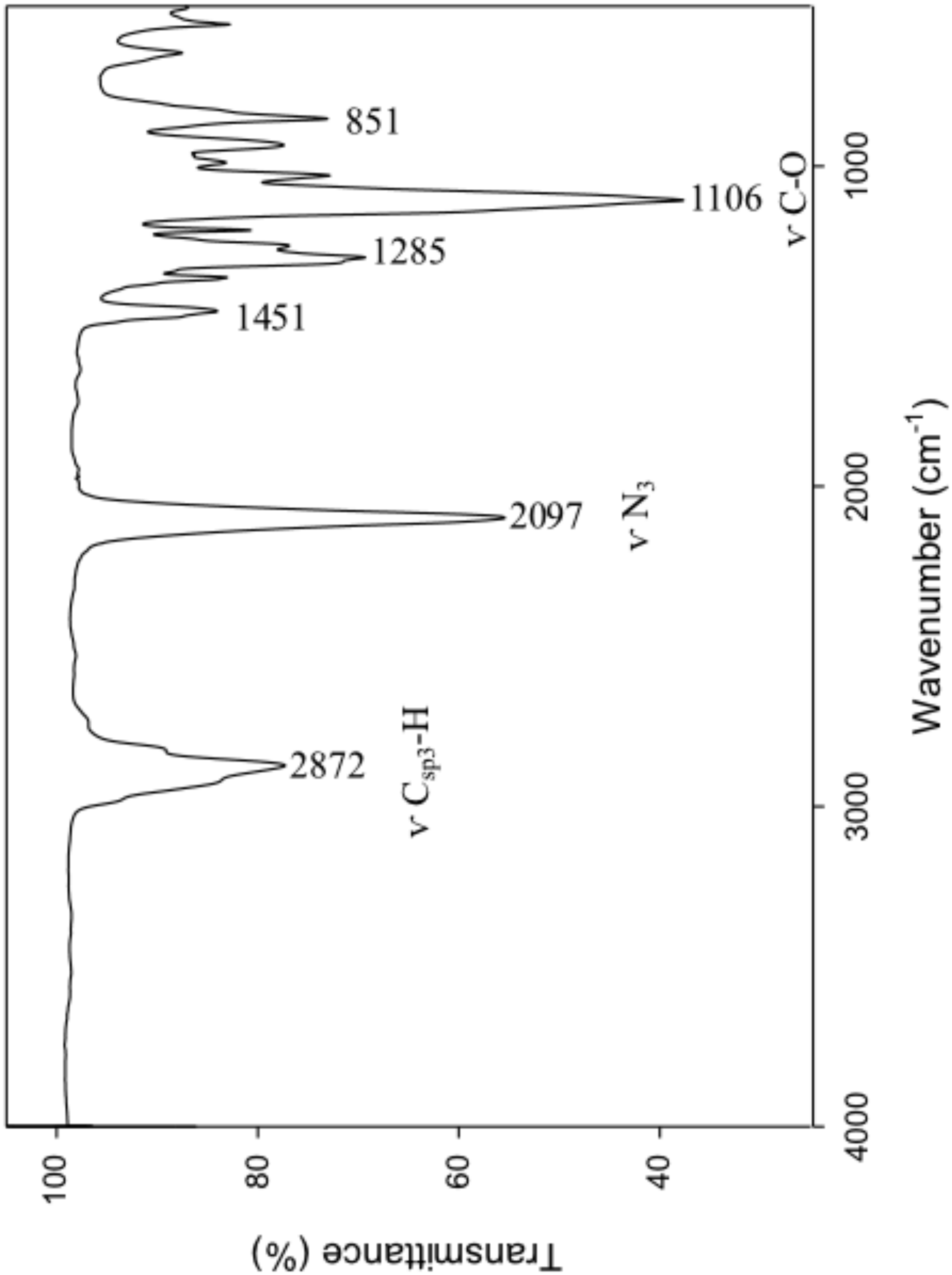

Figure 3.G3: IR absorption spectrum of MeO-EG_3-N_3.

3.H Characterization of MeO-EG$_3$-NH$_2$

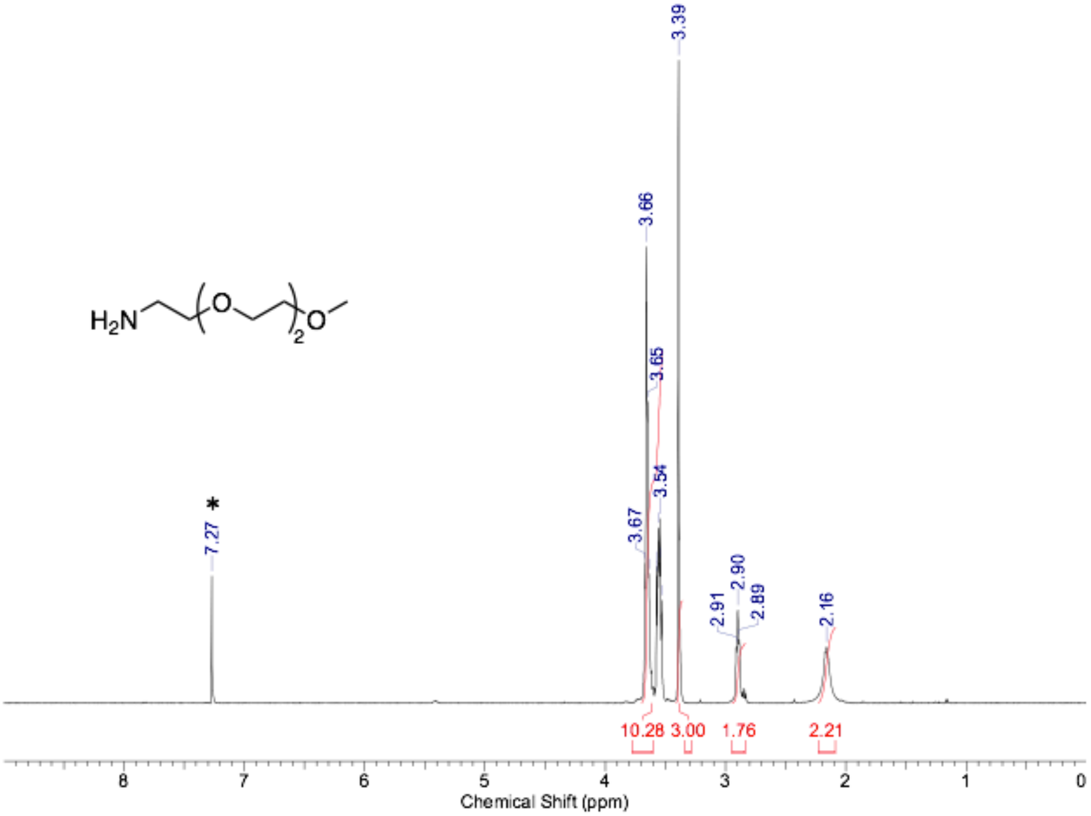

Figure 3.H1: ^{1}H NMR spectrum of MeO-EG$_3$-NH$_2$ in CDCl$_3$. * denotes solvent signal(s).

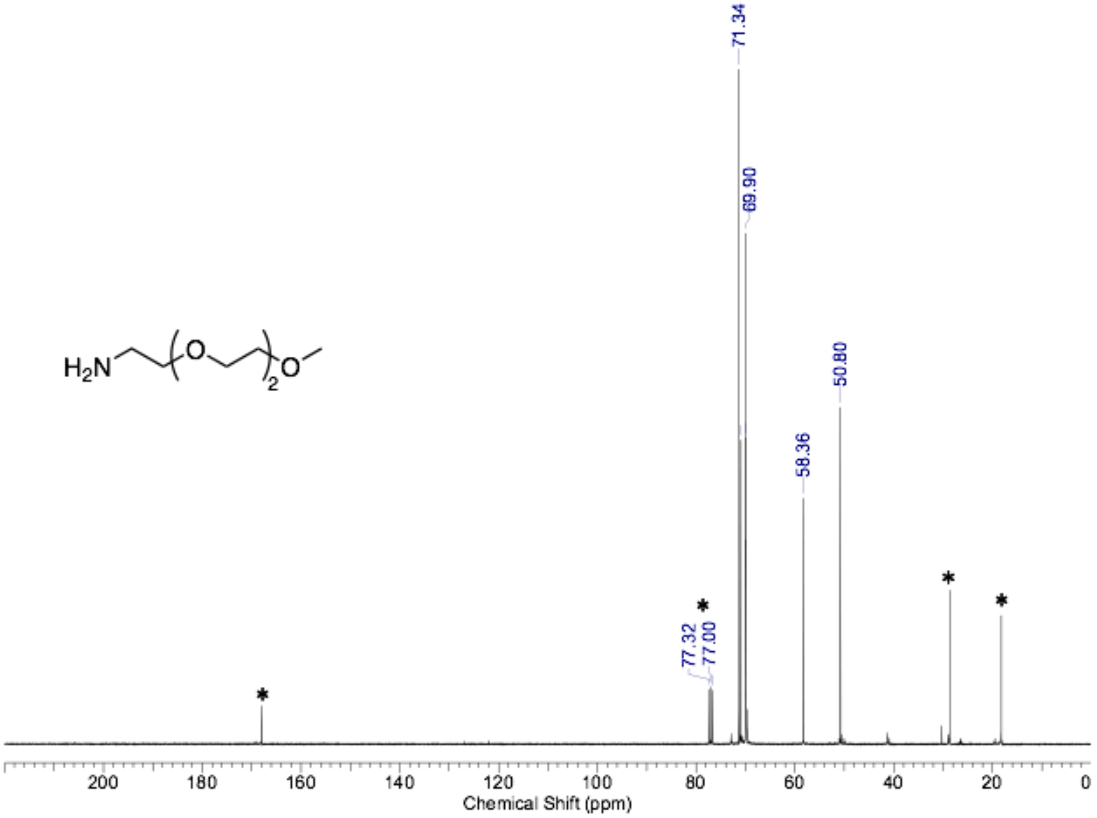

Figure 3.H2: ^{13}C{^{1}H} spectrum of MeO-EG$_3$-NH$_2$ in CDCl$_3$. * denotes solvent signal(s).

3.I Characterization of Ph_3CS-EG_3-OMe

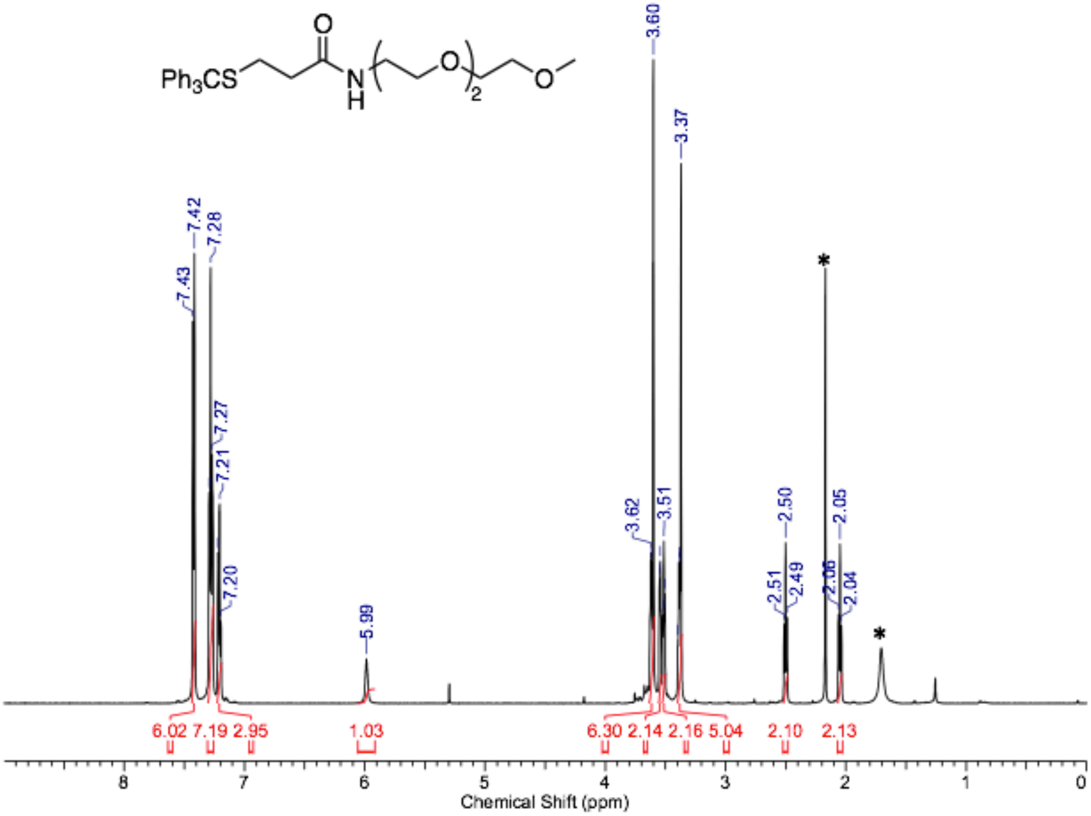

Figure 3.I1: ^{1}H NMR spectrum of Ph_3CS-EG_3-OMe in $CDCl_3$. * denotes solvent signal(s).

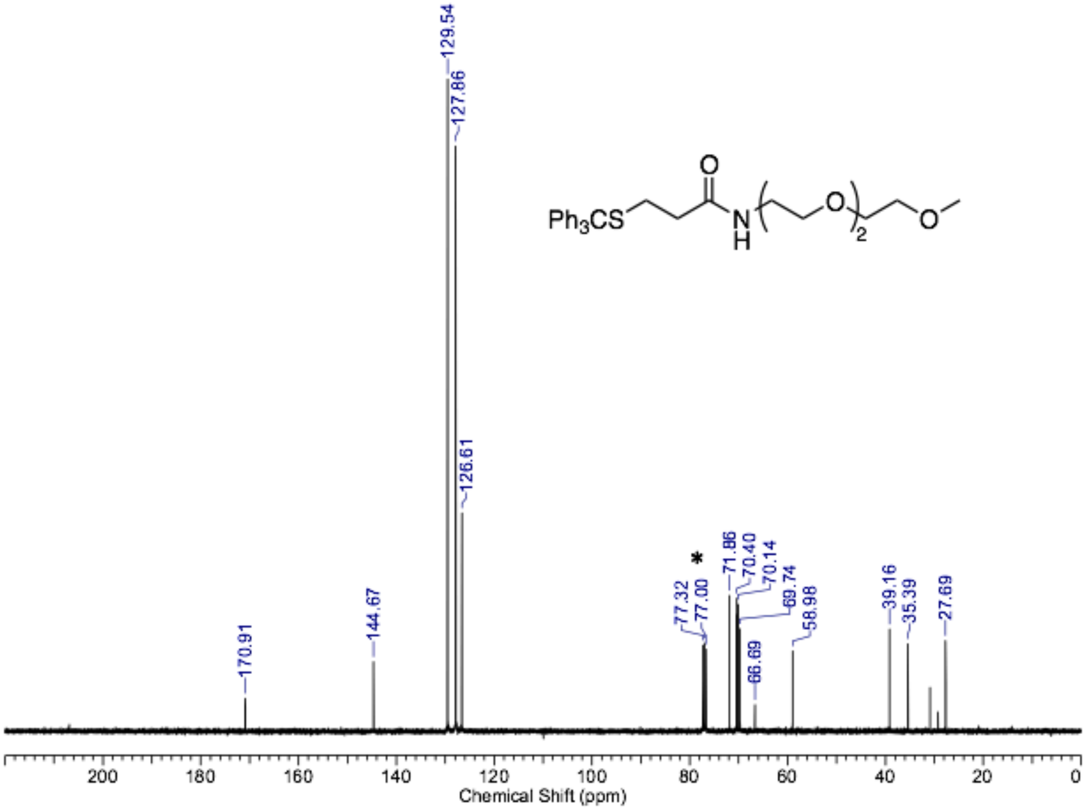

Figure 3.I2: $^{13}C\{^1H\}$ spectrum of Ph_3CS-EG_3-OMe in $CDCl_3$. * denotes solvent signal(s).

3.J Characterization of HS-EG$_3$-OMe

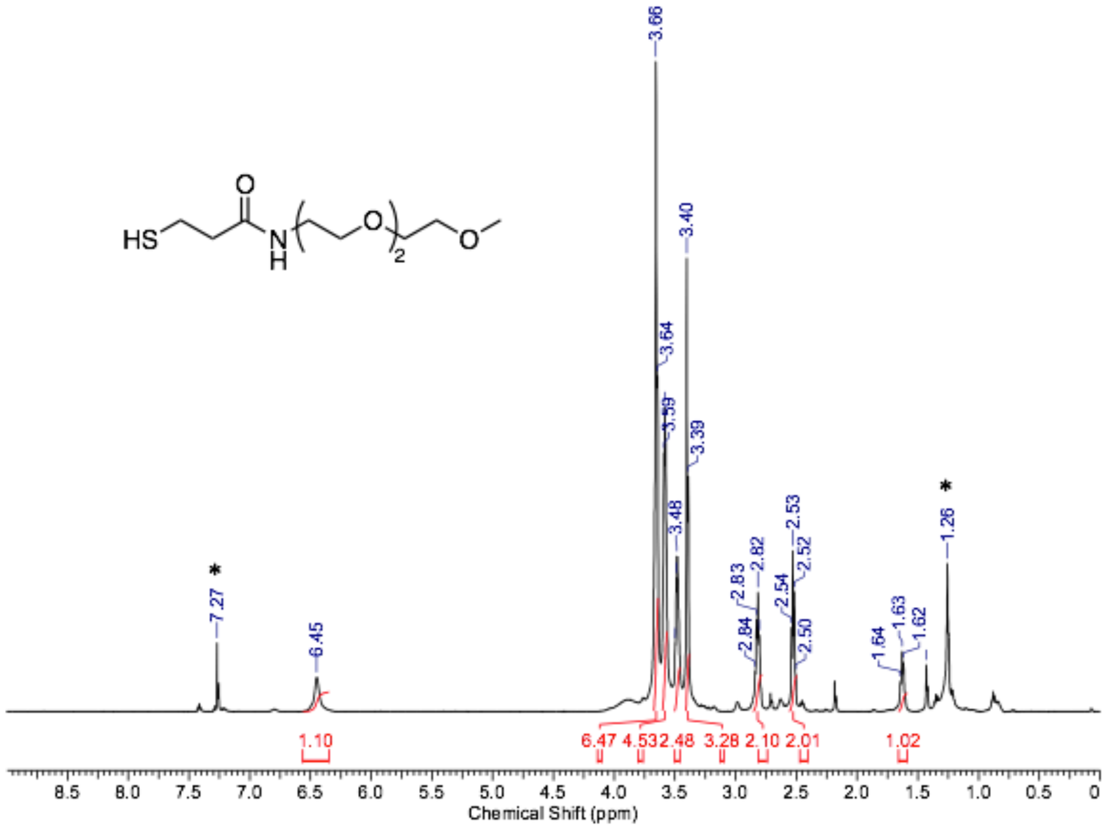

Figure 3.J1: ^{1}H NMR spectrum of HS-EG$_3$-OMe in CDCl$_3$. * denotes solvent signal(s).

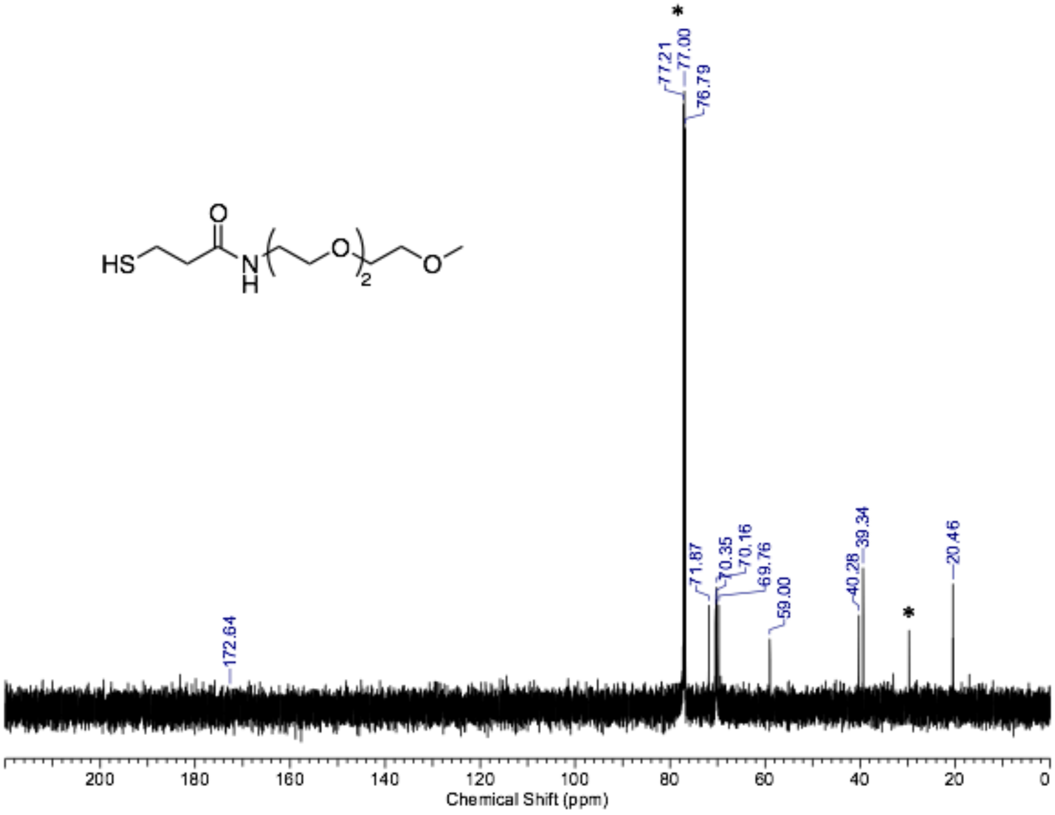

Figure 3.J2: ^{13}C{^{1}H} spectrum of HS-EG$_3$-OMe in CDCl$_3$. * denotes solvent signal(s).

3.K Characterization of Ph_3CS-EG_4-COOMe

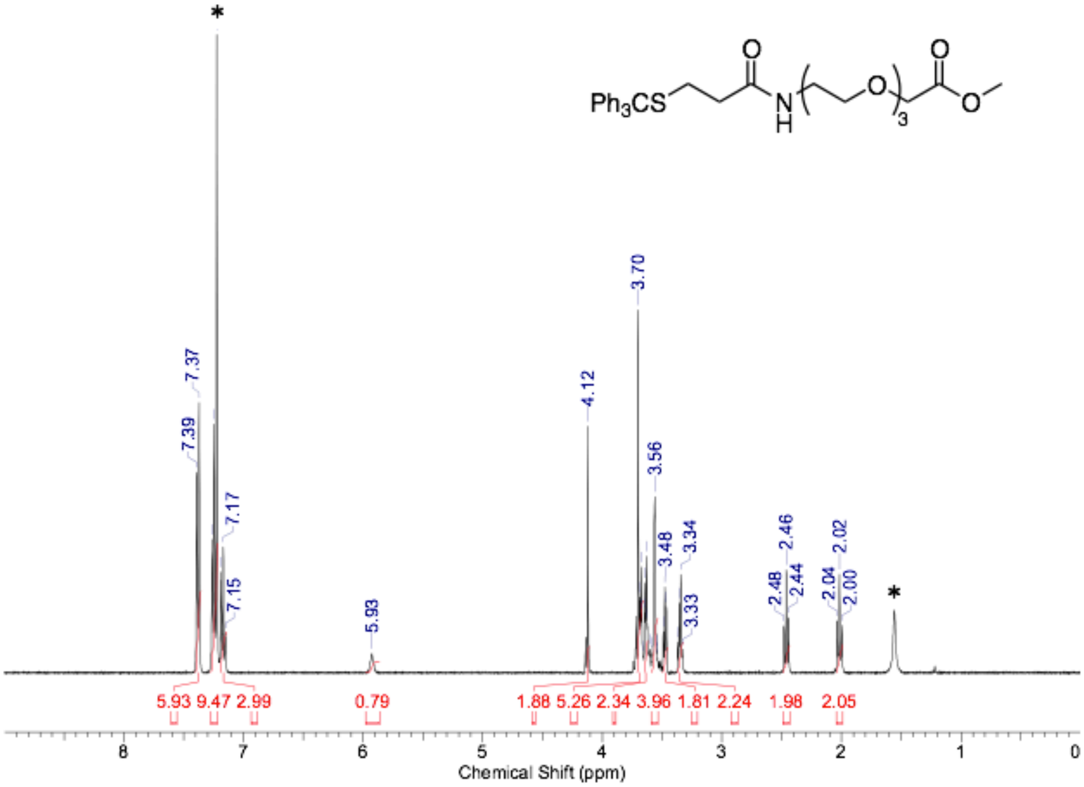

Figure 3.K1: ^1H NMR spectrum of Ph_3CS-EG_4-COOMe in $CDCl_3$. * denotes solvent signal(s).

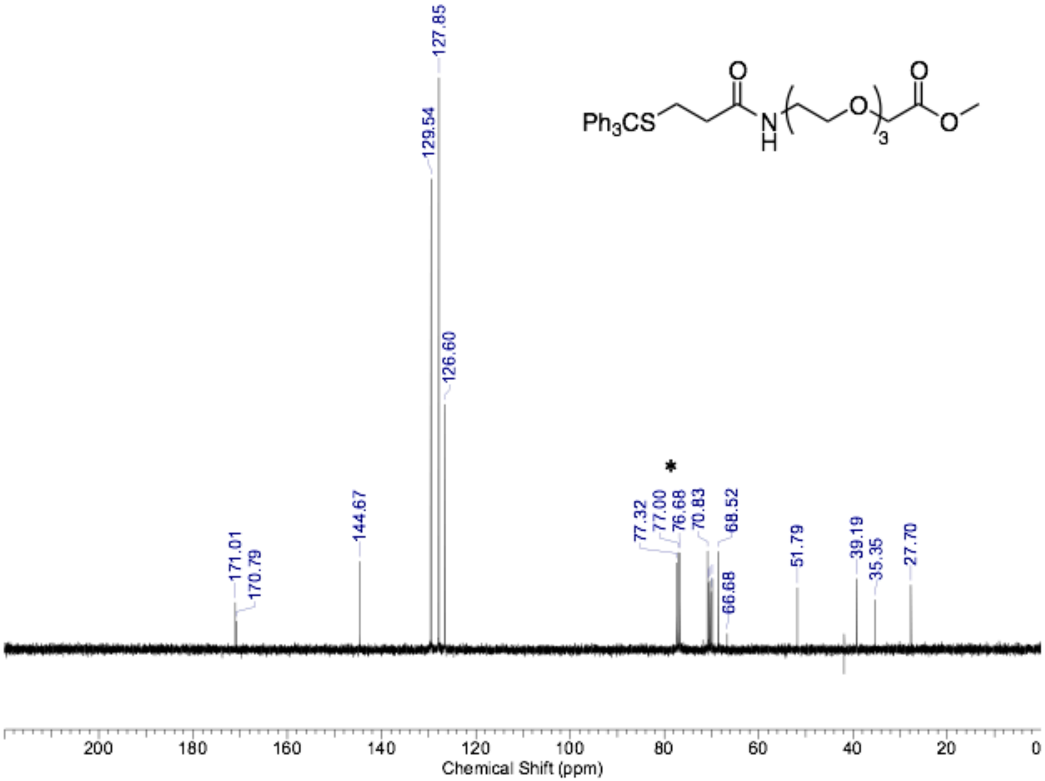

Figure 3.K2: $^{13}C\{^1H\}$ spectrum of Ph_3CS-EG_4-COOMe in $CDCl_3$. * denotes solvent signal(s).

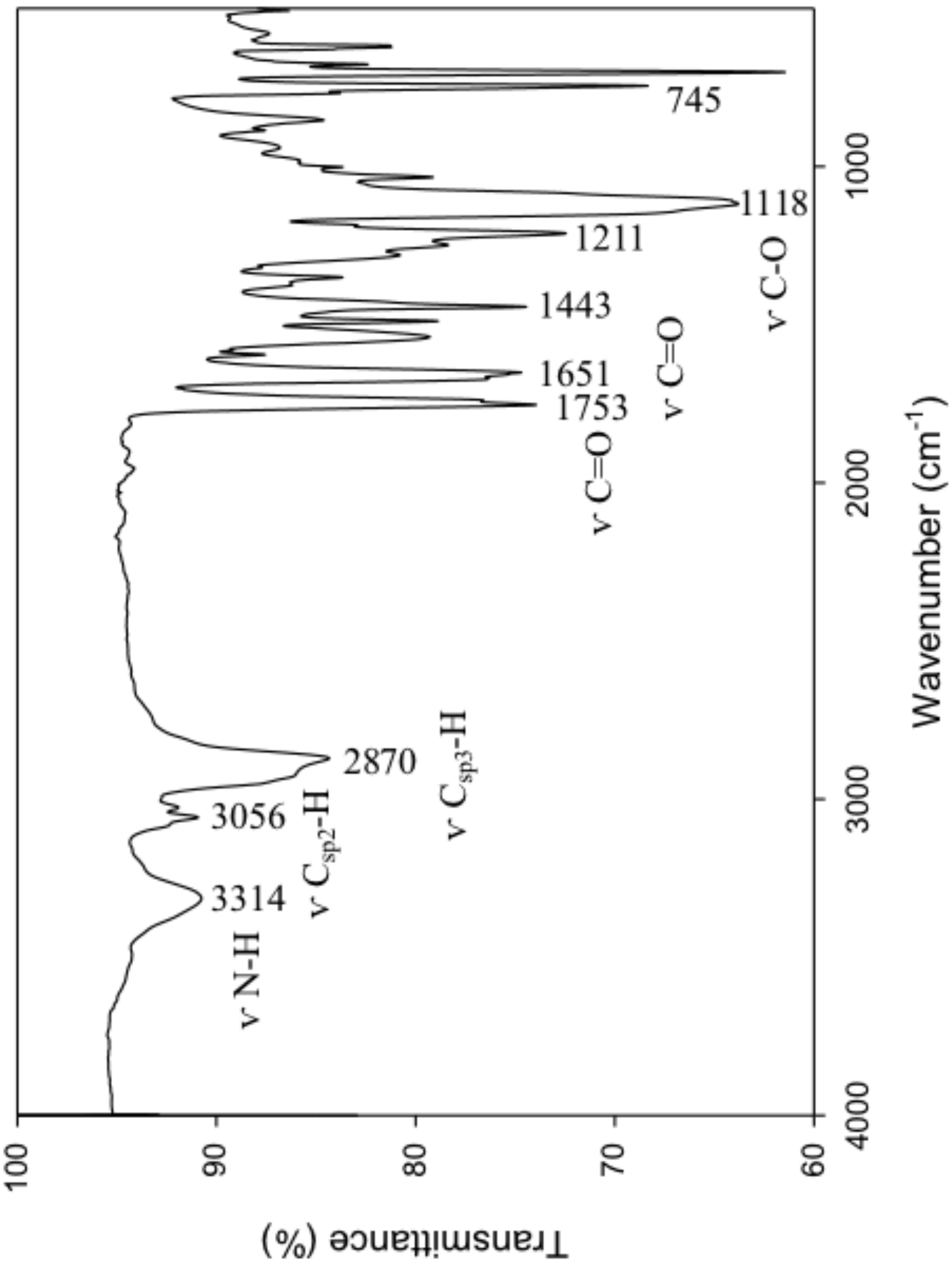

Figure 3.J3: IR absorption spectrum of Ph_3CS-EG_4-COOMe.

3.L Characterization of Ph_3CS-EG_4-COOH

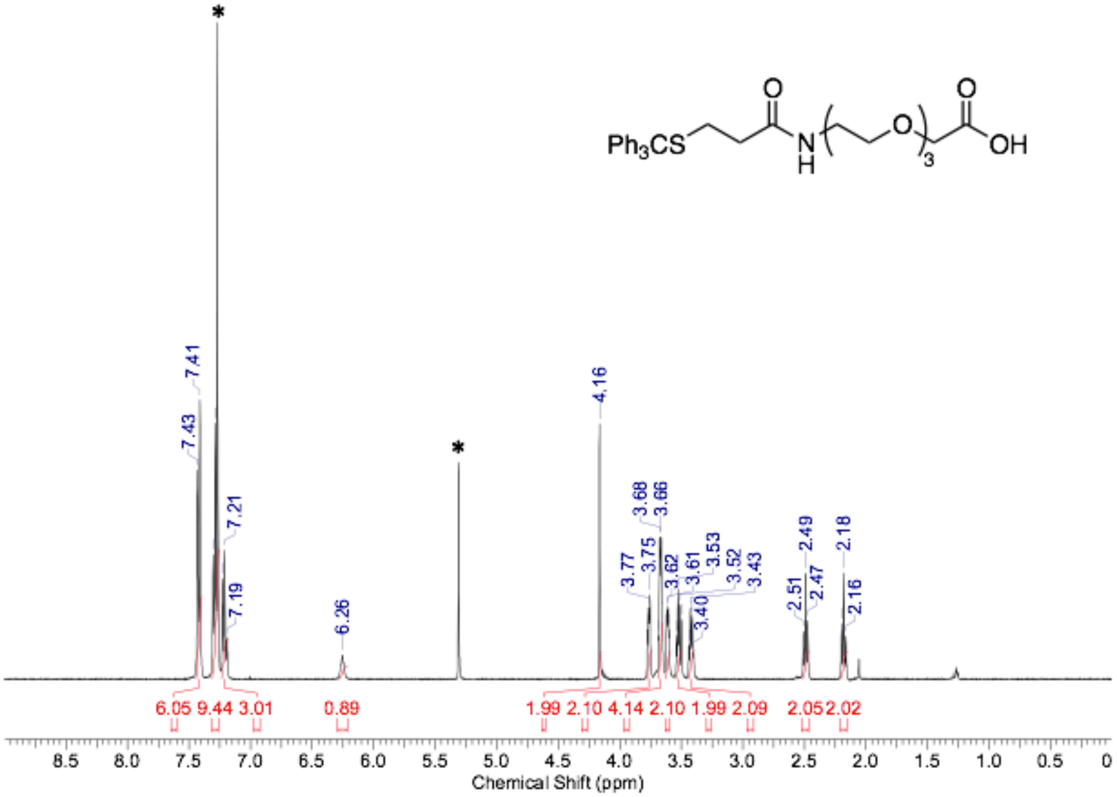

Figure 3.L1: ^1H NMR spectrum of Ph_3CS-EG_4-COOH in $CDCl_3$. * denotes solvent signal(s).

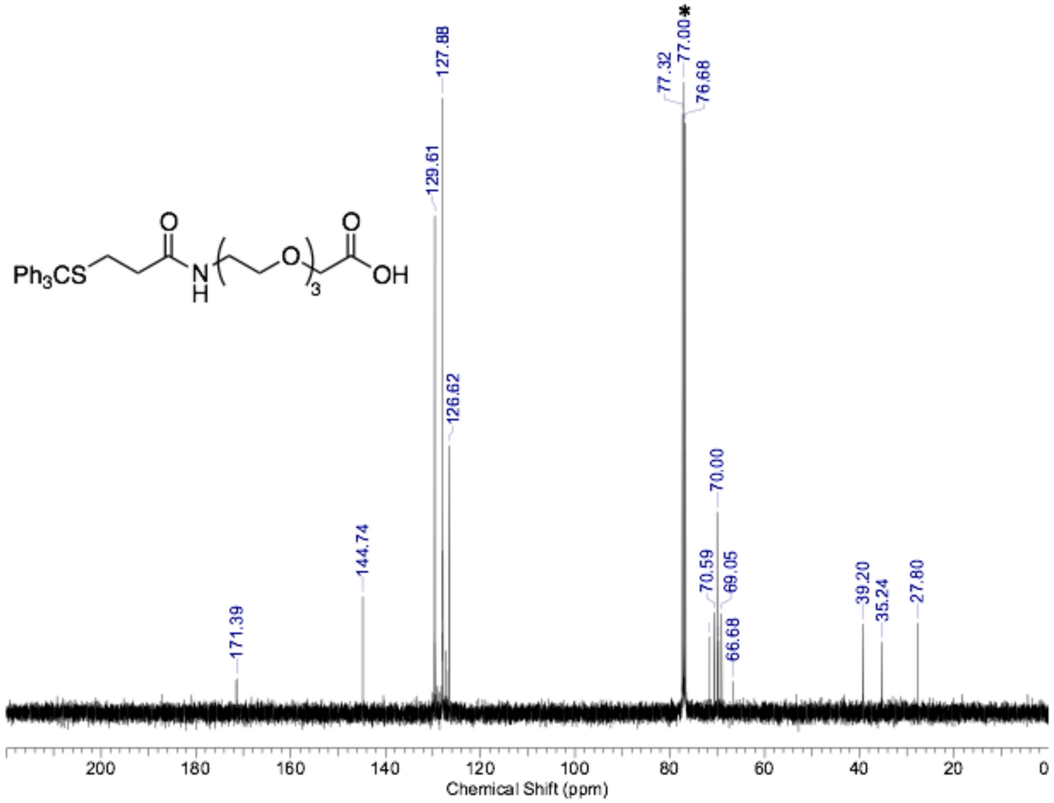

Figure 3.L2: $^{13}C\{^1H\}$ spectrum of Ph_3CS-EG_4-COOH in $CDCl_3$. * denotes solvent signal(s).

3.M Characterization of Ph_3CS-EG_4-EG_3-OMe

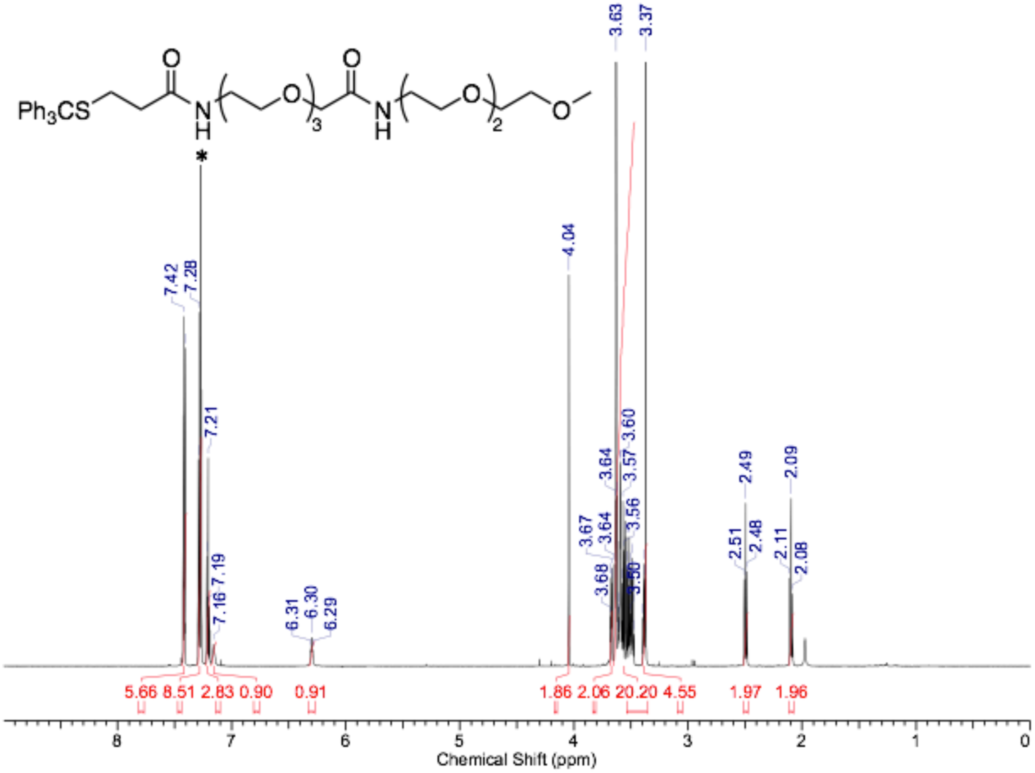

Figure 3.M1: ^{1}H NMR spectrum of Ph_3CS-EG_4-EG_3-OMe in $CDCl_3$. * denotes solvent signal(s).

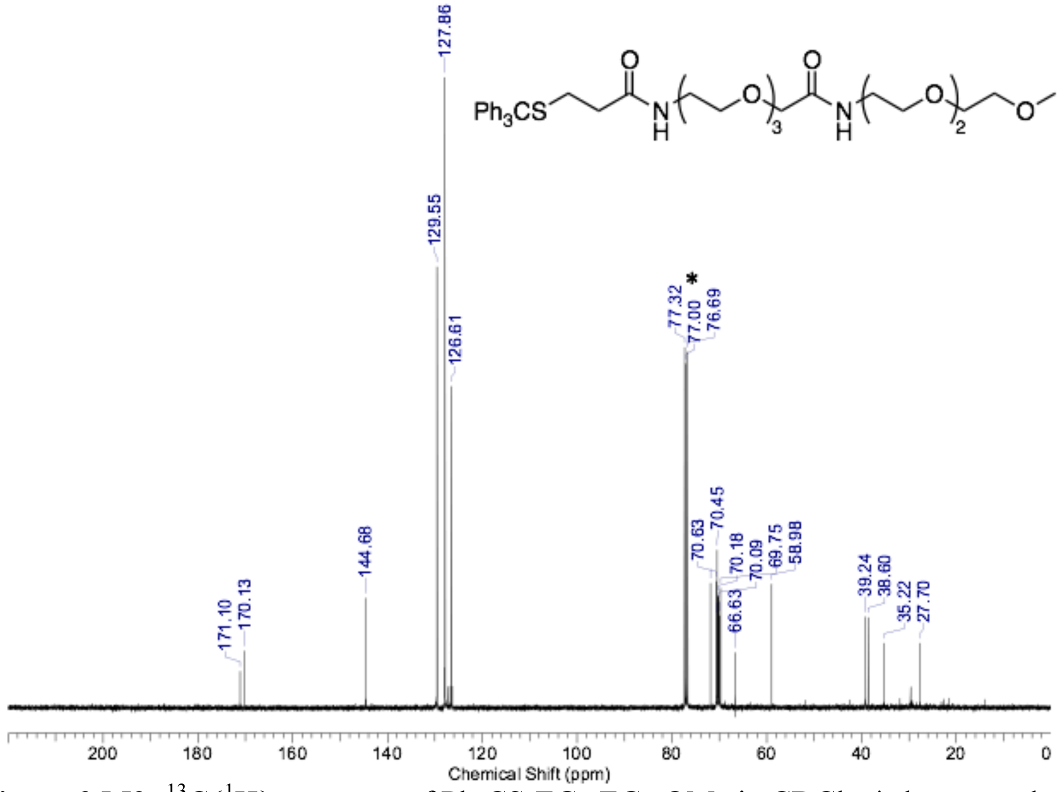

Figure 3.M2: $^{13}C\{^1H\}$ spectrum of Ph_3CS-EG_4-EG_3-OMe in $CDCl_3$. * denotes solvent signal(s).

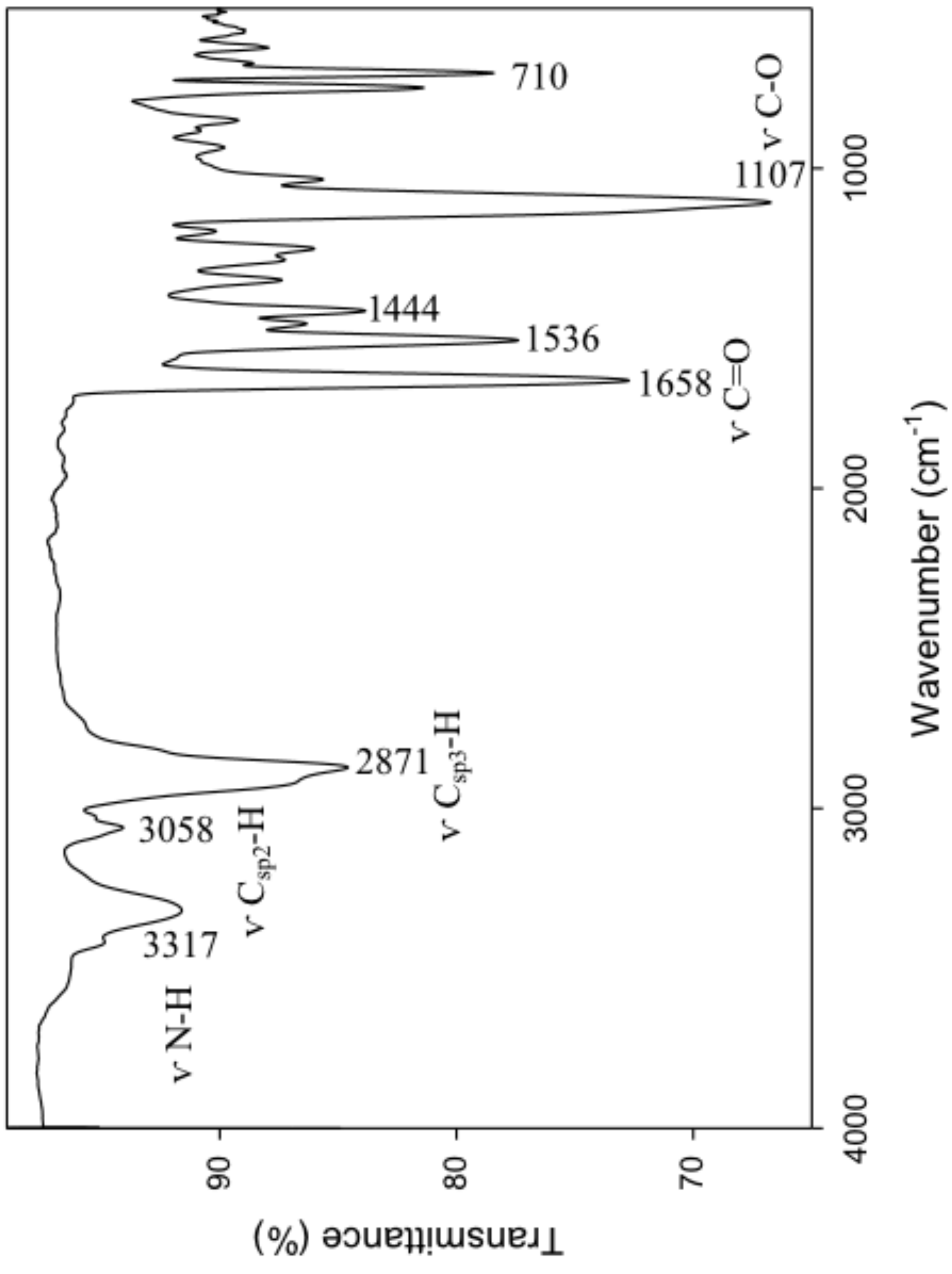

Figure 3.M3: IR absorption spectrum of Ph_3CS-EG_4-EG_3-OMe.

3.N Characterization of HS-EG$_4$-EG$_3$-OMe

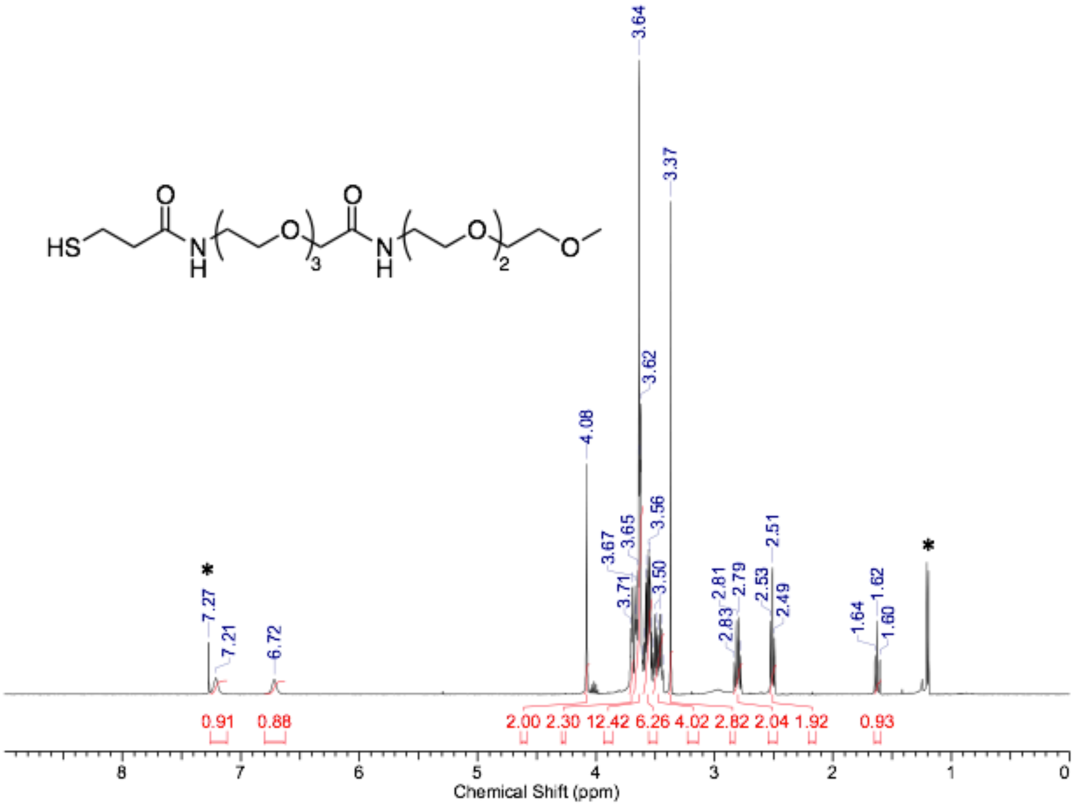

Figure 3.N1: ^{1}H NMR spectrum of HS-EG$_4$-EG$_3$-OMe in CDCl$_3$. * denotes solvent signal(s).

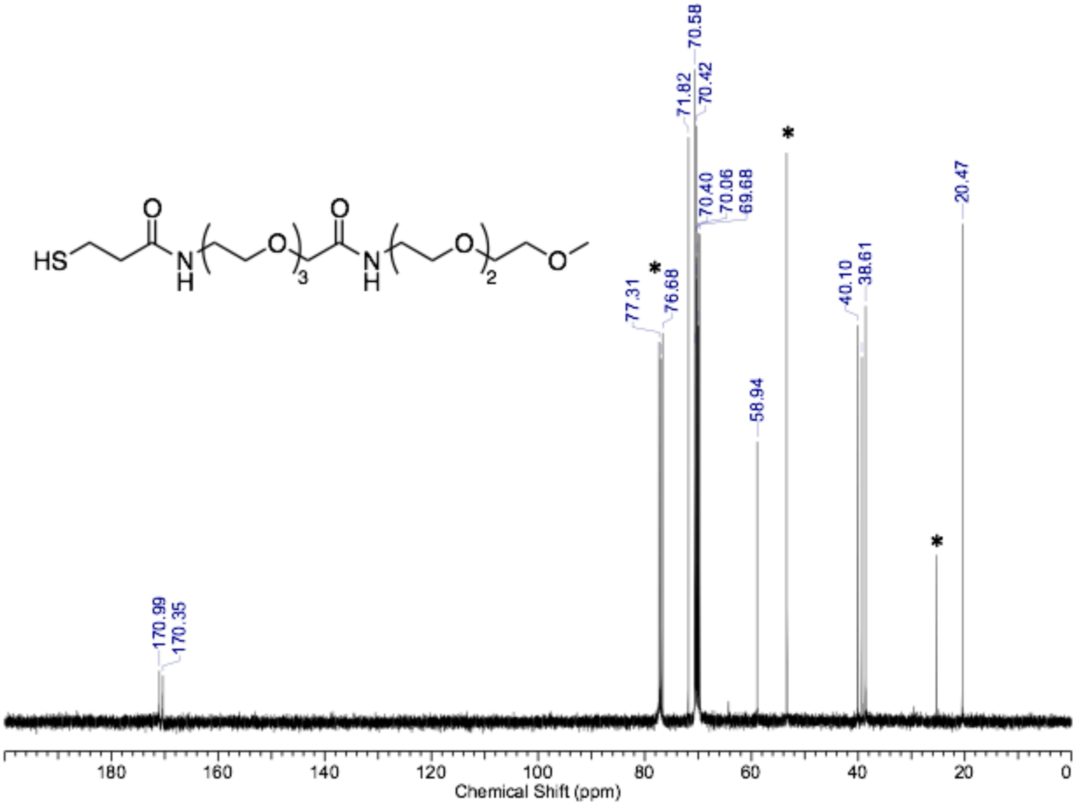

Figure 3.N2: ^{13}C{^{1}H} spectrum of HS-EG$_4$-EG$_3$-OMe in CDCl$_3$. * denotes solvent signal(s).

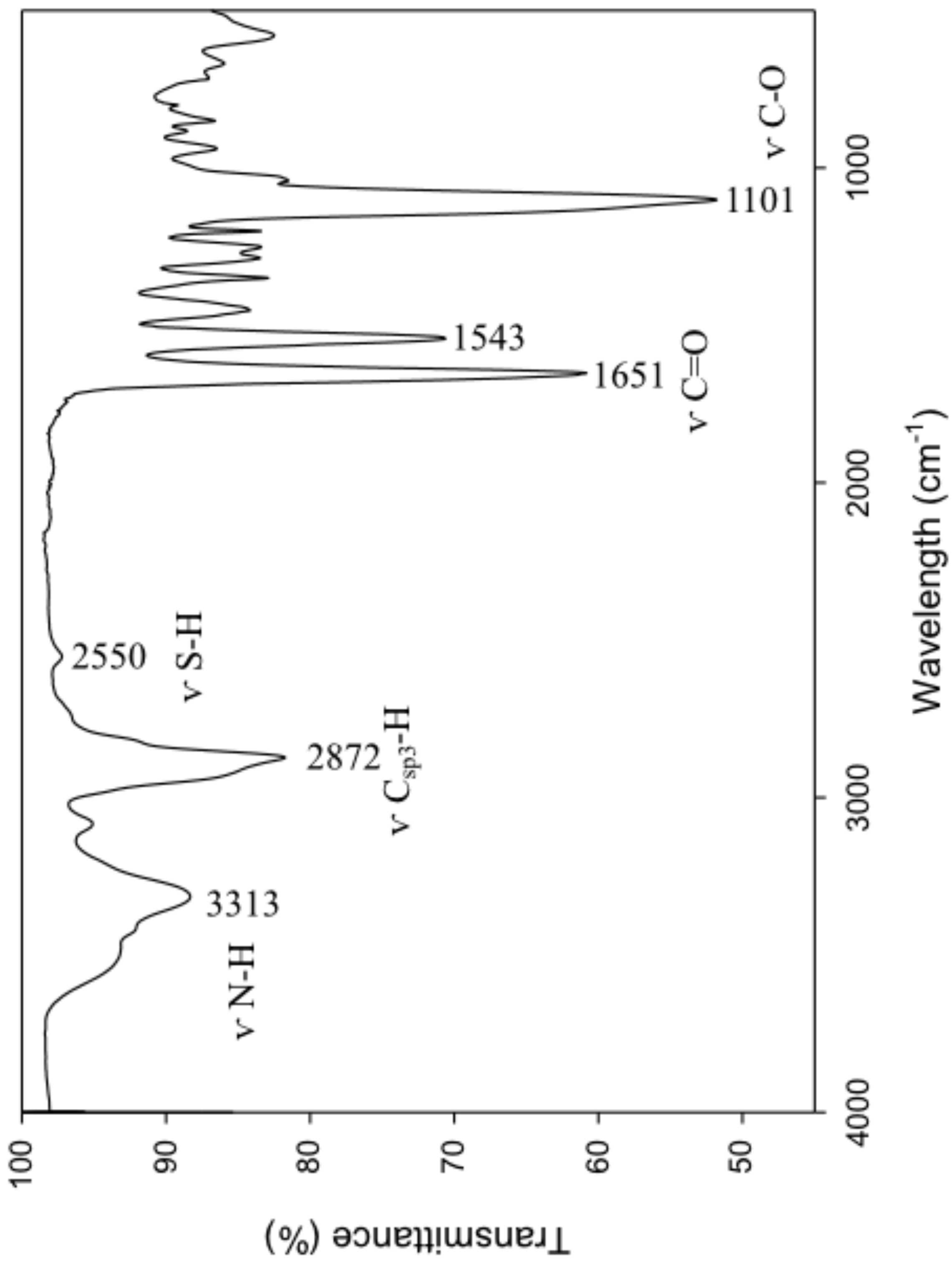

Figure 3.M3: IR absorption spectrum of HS-EG$_4$-EG$_3$-OMe.

5.3 List of Permissions

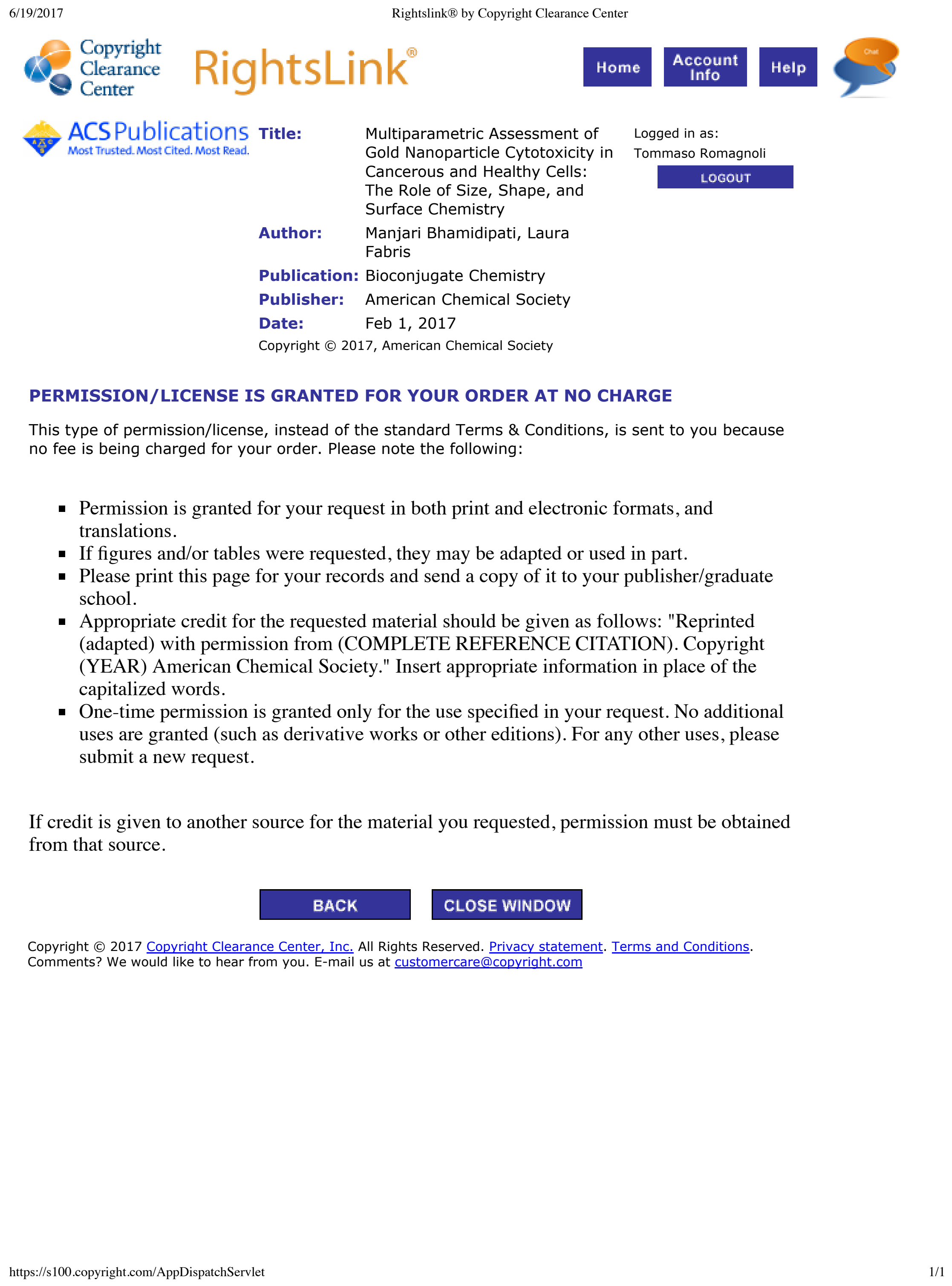

6/19/2017 Rightslink® by Copyright Clearance Center

Title: Multiparametric Assessment of Gold Nanoparticle Cytotoxicity in Cancerous and Healthy Cells: The Role of Size, Shape, and Surface Chemistry

Author: Manjari Bhamidipati, Laura Fabris

Publication: Bioconjugate Chemistry

Publisher: American Chemical Society

Date: Feb 1, 2017

Copyright © 2017, American Chemical Society

Logged in as:
Tommaso Romagnoli

PERMISSION/LICENSE IS GRANTED FOR YOUR ORDER AT NO CHARGE

This type of permission/license, instead of the standard Terms & Conditions, is sent to you because no fee is being charged for your order. Please note the following:

- Permission is granted for your request in both print and electronic formats, and translations.
- If figures and/or tables were requested, they may be adapted or used in part.
- Please print this page for your records and send a copy of it to your publisher/graduate school.
- Appropriate credit for the requested material should be given as follows: "Reprinted (adapted) with permission from (COMPLETE REFERENCE CITATION). Copyright (YEAR) American Chemical Society." Insert appropriate information in place of the capitalized words.
- One-time permission is granted only for the use specified in your request. No additional uses are granted (such as derivative works or other editions). For any other uses, please submit a new request.

If credit is given to another source for the material you requested, permission must be obtained from that source.

Copyright © 2017 Copyright Clearance Center, Inc. All Rights Reserved. Privacy statement. Terms and Conditions.
Comments? We would like to hear from you. E-mail us at customercare@copyright.com

https://s100.copyright.com/AppDispatchServlet 1/1

Western
Science

ACADEMIC CURRICULUM VITAE

Tommaso Romagnoli

UNIVERSITY EDUCATIONAL BACKGROUND

M.Sc.	Organic Chemistry The University of Western Ontario, London ON, Canada Supervised by Dr. Mark Workentin	2015/9 – 2017/6
B.Sc.	Honors Specialization in Chemistry (with Distinction) The University of Western Ontario, London ON, Canada Undergraduate thesis supervised by Dr. Joe Gilroy and Dr. Mark Workentin	2011/9 – 2015/5

RESEARCH SPECIFIC HONORS AND AWARDS

2016/9 – 2017/8	**Alexander Graham Bell Canada Graduate Scholarship – Master's (CGS-M) - $17,500** Awarded annually to excellent M.Sc. students across Canada. *Criteria: Academic excellence, outstanding research ability, and extracurricular involvement. Competition: 800 in Canada, 25 at Western University in all disciplines of science and engineering.*
2015/9 – 2016/8	**Ontario Graduate Scholarship (OGS) - $15,000** Awarded annually to excellent graduate students across Ontario. *Criteria: Academic excellence, research achievement and potential, communication skills and leadership abilities. Competition: 270 in Ontario.*

OTHER HONORS AND AWARDS

2017/5	**Lipson-Baines Award Winner – $500** Awarded annually to two full-time Masters or Doctoral students in Chemistry who have achieved the highest marks in the course Chemistry 9657/8 Seminar.
2011/9 – 2015/5	**Dean's Honor List** Named to the Dean's Honor List at Western University throughout all four years of undergraduate degree *Criteria: Academic excellence (> 80% average).*
2011/9 – 2012/5	**Western Scholarship of Excellence – $2,000** Awarded to incoming undergraduate students. *Criteria: Academic excellence (90-94.9% average).*

PUBLICATIONS

Journal Articles

1) P. Gobbo, **T. Romagnoli**, S. M. Barbon, J. T. Price, J. Keir, J. B. Gilroy and M. S. Workentin. “Expanding the Scope of Strained Alkyne Chemistry: A Protection-Deprotection Strategy via the Formation of a Dicobalt-Hexacarbonyl Complex.” *Chem. Commun*. **2015**, *51*: 6647-6650.

Conference Publications

2) D. Cool, H. Sadeghi Neshat , M. Bastian-Jordan, **T. Romagnoli**, J. Chedalavada, A. Fenster, N. Kakani. (**2013**). “Evaluation of Ablation Volume Stability to Non-parallel Placement of Multiple Microwave Probes in in vivo Porcine Liver Model.” Society of Interventional Radiology. Society of Interventional Radiology (SIR) Annual Meeting, New Orleans, LA, April 13, 2013 (S122-S123).

1) H. Sadeghi Neshat, D. Cool, A. Zaleski, **T. Romagnoli**, J. Chedalavada, A. Fenster, N. Kakani. (**2012**). “Intra-procedural Imaging for Radiofrequency (RF) and Microwave (MW) Ablation of Hepatocellular Carcinoma: A Pictorial Review.” Radiological Society of North America. Radiological Society of North America (RSNA) Annual Meeting, Chicago, IL, November 11, 2012.

PRESENTATIONS

2) A Solution to the PEG Dilemma: Efficient Bioconjugation of Large Gold Nanoparticles for Biodiagnostic Applications using Mixed Layers. Oral Presentation. Chemistry 9657/8 Seminar Series. London, ON Canada. Nov. 17, 2016.

1) Expanding the Scope of Strained Alkyne Chemistry: A Protection-Deprotection Strategy via the Formation of a Dicobalt-Hexacarbonyl Complex. Oral Presentation. 43rd Southern Ontario Undergraduate Student Chemistry Conference (SOUSCC). Mississauga, ON Canada. March 21, 2015.

TEACHING EXPERIENCE

2016/9 – 2016/12	Chemistry 2273a: Organic Chemistry I: Structure and Spectroscopy, Fall Term, University of Western Ontario. Laboratory Teaching Assistant Coordinator.
2015/9 – 2015/12	Chemistry 2273a: Organic Chemistry I: Structure and Spectroscopy, Fall Term, University of Western Ontario. Laboratory Teaching Assistant.
2015/9 – 2015/12	Chemistry 2213a: Organic Chemistry for Life Sciences, Fall Term, University of Western Ontario. Laboratory Teaching Assistant.